Robustness analysis with integral quadratic constraints, application to space launchers.

Julien Chaudenson

▶ **To cite this version:**

Julien Chaudenson. Robustness analysis with integral quadratic constraints, application to space launchers.. Other. Supélec, 2013. English. NNT : 2013SUPL0029 . tel-00988162

HAL Id: tel-00988162

https://theses.hal.science/tel-00988162

Submitted on 7 May 2014

HAL is a multi-disciplinary open access archive for the deposit and dissemination of scientific research documents, whether they are published or not. The documents may come from teaching and research institutions in France or abroad, or from public or private research centers.

L'archive ouverte pluridisciplinaire **HAL**, est destinée au dépôt et à la diffusion de documents scientifiques de niveau recherche, publiés ou non, émanant des établissements d'enseignement et de recherche français ou étrangers, des laboratoires publics ou privés.

N° d'ordre : 2013-29-TH

SUPELEC

ECOLE DOCTORALE STITS
« Sciences et Technologies de l'Information des Télécommunications et des Systèmes »

THÈSE DE DOCTORAT

DOMAINE : STIC
Spécialité : Automatique

Soutenue le
mercredi 4 décembre 2013

par :

Julien CHAUDENSON

Analyse de robustesse par contraintes intégrales quadratiques, application aux lanceurs spatiaux

Directeur de thèse :	Guillaume SANDOU	Professeur (Supélec, Gif-sur-Yvette)

Composition du jury :

Président du jury :	Olivier SENAME	Professeur (INP, Grenoble)
Rapporteurs :	Jean-Marc BIANNIC	Maître de recherches (ONERA, Toulouse)
	Matthew TURNER	Senior Lecturer (University of Leicester)
Examinateurs :	Iuliana BARA	Maître de conférences (Université de Strasbourg)
	Catherine BONNET	Directrice de recherche (INRIA, Saclay)
	Gilles DUC	Professeur (Supélec, Gif-sur-Yvette)
	Carsten SCHERER	Professeur (University of Stuttgart)
Membres invités :	Dominique BEAUVOIS (co-encadrant)	Professeur (Supélec, Gif-sur-Yvette)
	Samir BENNANI	Senior Expert (ESA/ESTEC, Noordwijk)
	Christophe FRECHIN	Ingénieur GNC (Astrium ST, Les Mureaux)
	Martine GANET	Expert GNC (Astrium ST, Les Mureaux)

Avant-propos

Le premier chapitre de ce manuscrit contient un résumé long en français du contenu du manuscrit. Les chapitres suivants sont rédigés en anglais.

Foreword

The first chapter of this thesis is a long summary of the main body written in French. The main body of the text is written in English.

Abstract

Robustness analysis with integral quadratic constraints,
application to space launchers

This thesis investigates stability and performance analysis of space launcher models. In the current context, the need for cost reduction and efficiency improvement of the verification and validation (V&V) industrial process leads toward the use of analytical techniques providing rigorous robustness guarantees. V&V tools based on Integral Quadratic Constraints (IQC) shall complement the stability and performance certificates yielded by the existing time-domain stochastic methods. The first study investigates the effect of the uncertain nonlinear equation for the rotating motion of a rigid launcher on the robust stability and robust performance of a representative three dimensional model. IQC are used to estimate the stability domain using a factorization of the equation of motion troublesome terms. The second contribution of this thesis addresses the stability analysis of pulse-modulated systems. Two a priori distinct IQC-based methods are implemented to obtain mathematical certificates on the stability of a space launcher model with a pulse-modulator used as a representative actuator.

À mes parents,
à mes frères.

Contents

List of Tables

List of Figures

Remerciements

En premier lieu, je souhaite exprimer toute ma gratitude à mes encadrants de Supélec Guillaume Sandou et Dominique Beauvois. Tout au long de ce projet, nos discussions auront été à la fois instructives et constructives et leurs questions m'ont toujours aidé à pousser ma réflexion le plus loin possible, pour le meilleur je l'espère. Je garderai longtemps le souvenir du temps passé à Supélec et de l'accueil qui m'a été fait au département Automatique, dirigé successivement par MM. Boucher et Dumur, de l'équipe enseignante, de Josiane et des innombrables services qu'elle m'a rendus, et de mes collègues doctorants avec qui il faisait bon vivre.

Mon passage à l'université de Stuttgart fut une grande expérience tant sur le plan scientifique que sur le plan humain. Je remercie sincèrement le professeur Carsten Scherer d'avoir mis à ma portée quelques un des pans de son immense savoir et de m'avoir permis de profiter au maximum de ce semestre de recherche au sein de son équipe. Aussi je remercie Ms. Schaettgen, Joost Veenman, Matthias Fetzer et Oussama Alaya d'y avoir également contribué.

Cette aventure n'aurait pas été possible sans la contribution d'Astrium ST en la personne de Martine Ganet. Sa connaissance profonde des problématiques industrielles posées pour la conception de lanceurs spatiaux m'a toujours obligé à garder comme ligne directrice la lisibilité de mes recherches et leur applicabilité. Je tiens aussi à remercier Christophe Frechin avec qui échanger m'a énormément appris, à tous points de vue. L'atmosphère amicale de l'équipe qui m'a reçu a contribué à faire de ce séjour sur le site des Mureaux une expérience réussie.

La dernière étape de mon tour d'Europe m'a fait poser ma valise sur les bords de la mer du Nord à l'ESTEC. J'y ai découvert la passion débordante, l'esprit visionnaire et la grande humanité de Samir Bennani envers qui je serai longtemps reconnaissant. J'ai eu le plaisir de vivre dans un groupe à l'ambiance chaleureuse, porté par son intérêt commun pour la recherche. Ainsi je remercie MM. Benoit et Ortega et toute l'équipe de l'accueil qui m'a été fait. Je remercie Guillaume Sabiron pour ses réponses à mes questionnements incessants et nos franches rigolades.

Côtoyer ces personnes et les nombreuses autres que j'ai eu la chance de rencontrer au cours de ces trois ans de thèse m'a permis de mener mes travaux dans les meilleures conditions.

Enfin je souhaite remercier comme il se doit mes parents dont l'exemple me pousse chaque jour à donner le meilleur de moi-même, au travail et dans la vie. Au terme de mes études, je ne peux mesurer ce que je leur dois tant leur contribution est immense. Je remercie mes frères dont je suis fier et dont la présence m'a toujours été d'un grand réconfort. Pour mes amis, de Paris et d'ailleurs, j'ai une pensée sincère en écrivant ces lignes. Je veux finalement témoigner de toute mon affection pour Julie, dont l'amour malgré la distance m'a permis d'en arriver ici aujourd'hui.

Chapter 1

Résumé

1.1 Introduction

Dans le contexte actuel, le développement et la production des lanceurs spatiaux européens est soumis à des objectifs d'efficacité et de réductions de coûts. En ce qui concerne la vérification et la validation des lois de commandes permettant le contrôle du lanceur au cours de la phase balistique de son vol, les marges sont grandes et les perspectives d'améliorations reposent sur un renouvellement des méthodes. Aujourd'hui, les outils de simulation fondés sur la théorie de Monte-Carlo sont au cœur du procédé, engendrant un coût financier que les acteurs du domaine souhaiteraient réduire. Une des solutions avancées repose sur l'utilisation de méthodes dites "analytiques" pour vérifier la satisfaction du cahier des charges en termes de critères de stabilité et de performance. A l'inverse des méthodes probabilistes utilisées actuellement, ces méthodes pourraient fournir des garanties formelles quant aux propriétés de robustesse du lanceur et permettraient de lever les incertitudes intrinsèques aux méthodes stochastiques. En effet, les avancées récentes de la théorie de l'automatique autorisent maintenant l'étude rigoureuse de systèmes de plus en plus grands et de plus en plus complexes. A cela s'ajoute l'augmentation des capacités de calcul qui permettent la résolution d'inégalités matricielles de plus en plus grandes. Il est donc très probable de voir à court terme ces méthodes analytiques venir étayer et/ou guider les analyses par simulations.
Une de ces méthodes recouvre la plupart des résultats venant des théories les plus connues que sont la théorie de Lyapunov, la théorie dite "entrée-sortie" et la théorie du contrôle robuste. Il s'agit de la théorie des Contraintes Intégrales Quadratiques (acronyme anglais : IQC). Cette théorie considérée comme unificatrice des différents courants de l'analyse des systèmes possède a priori les propriétés nécessaires à l'étude de systèmes aussi complexes que les lanceurs spatiaux. Tout d'abord, l'analyse IQC repose sur la modélisation classique en contrôle robuste qu'est la Représentation Linéaire Fractionnaire (acronyme anglais : LFR). Ce type de modélisation est connu pour sa flexibilité facilitant les modifications du modèle, chose à laquelle les IQC s'adaptent parfaitement bien. De plus, les IQC prennent rigoureusement en compte la structure des opérateurs de la LFR mais aussi leur nature ce qui limite le conservatisme des tests de stabilité et de performance au degré d'approximation de la description IQC. A ces propriétés avantageuses s'ajoute le fait que le test de stabilité du théorème classique des IQC peut être dans le cas général réécrit sous forme d'Inégalités Matricielles Linéaires (acronyme anglais : LMI) ce qui rend son implémentation aisée et les résultats obtenus fiables grâce aux algorithmes actuels de résolution. Au-delà de ces caractéristiques propres à l'analyse des systèmes, il est important de mentionner aussi les possibilités qu'offrent les IQC pour la synthèse de lois de commande. Ce pan de la théorie en constante progression promet des débouchés nombreux aux analyses faites au cours de ce projet ainsi qu'aux études futures.
C'est donc suite à ces premiers constats que le choix a été fait d'appliquer l'outil analytique IQC au problème de l'étude de la stabilité robuste et de la performance robuste d'un lanceur spatial en phase balistique. Les partenaires du projet souhaitant par cette étude éprouver la théorie sur des problèma-

tiques concrètes du domaine aérospatial, nous avons travaillé en particulier sur les conséquences pour la stabilité et la performance des équations de la dynamique et du mode de fonctionnement "tout-ou-rien" des tuyères dédiées au contrôle d'attitude. Cela a pu être fait en se concentrant essentiellement sur la modélisation du système et de ses éléments problématiques et sur l'application de la théorie puisqu'un outil d'analyse utilisant la théorie IQC, résultat d'un projet de l'Agence Spatiale Européenne (acronyme anglais : ESA), dénommé LPVMAD et implémenté sous Matlab® a été mis à notre disposition.
Dans ce cadre, après la phase de définition et de présentation du modèle à étudier, nous avons souhaité décrire de façon aussi concrète que possible, la théorie des IQC. Enfin, nous avons travaillé sur les deux problématiques susmentionnées. Tout d'abord, nous avons défini une représentation des équations de la dynamique pour un solide rigide en rotation permettant de procéder à une analyse prenant en compte les incertitudes de la matrice d'inertie de l'étage supérieur du lanceur ainsi que les couples gyroscopiques induits par ses asymétries et son mouvement de rotation. Cette modélisation pourra par la suite être réutilisée intégralement ou dans une version simplifiée pour d'autres études de stabilité d'un solide rigide en rotation. Dans un second temps, nous avons testé différentes méthodes visant à garantir la stabilité des systèmes à modulation d'impulsions. Les modulateurs d'impulsions de type PWM sont couramment utilisés pour représenter le mode de fonctionnement "tout-ou-rien" des tuyères du système de contrôle d'attitude. Cette étude a permis d'établir les bases d'une étude des systèmes à modulation d'impulsions avec la théorie des IQC.

Ces travaux ont été effectués dans le cadre du contrat ESA/NPI (European Space Agency / Network Partnering Initiative) numéro 4000103804 intitulé "Nonlinear multivariable analysis techniques for validation of launcher GNC systems" et établissant la collaboration entre le département Automatique de Supélec et Astrium Space Transportation.

Nous donnons dans les paragraphes suivants un résumé des différents chapitres de la thèse. Le chapitre 2 étant l'introduction générale, nous couvrirons les chapitres 3 à 6.

1.2 Chapitre 3 : Modélisation du lanceur

1.2.1 Introduction

Le premier chapitre de la thèse a pour but de décrire le modèle de lanceur spatial qui va être utilisé au cours des travaux pour en décliner nos différents modèles d'étude. Face à la complexité des modèles utilisés actuellement pour procéder à la validation des lois de commande dans le cadre d'analyses de Monte-Carlo, nous avons été dans l'obligation de produire un modèle plus simple. Toutefois, sa définition a été guidée puis validée par les ingénieurs des partenaires du projet : l'Agence Spatiale Européenne (ESA) et Astrium Space Transportation (Astrium ST). En effet, notre but étant de procéder à la validation analytique des lois de commande sur un modèle aussi représentatif que possible, nous avons conservé dans le modèle les éléments qui dictent son comportement à l'assemblage étage supérieur et charge(s) utile(s). Ces éléments sont le modèle dynamique décrit par les équations de Newton et le modulateur d'impulsions servant à représenter les tuyères du système de contrôle d'attitude.
Les paragraphes suivants décrivent les principaux éléments du modèle de référence utilisé pour les analyses.

1.2.2 Référentiels

Les référentiels utilisés au cours des travaux sont au nombre de trois. Tout d'abord, on définit un référentiel dit "de référence" $\mathcal{R}_{ref}$ par rapport auquel les mouvements du lanceur vont être décrits. Le système d'axes associé à $\mathcal{R}_{ref}$ est déterminé comme suit. $\mathcal{R}_{ref}$ est centré au centre de gravité G du lanceur. L'axe X_{ref}

pointe dans la direction du mouvement du centre de gravité autour de la terre. Dans l'hypothèse des lois de Képler pour une orbite circulaire, cet axe est tangent à la trajectoire du lanceur autour de la Terre. L'axe Y_{ref} pointe lui en direction du centre de la trajectoire i.e. le centre de la Terre. Ainsi il est orthogonal à X_{ref}. Enfin, Z_{ref} vient compléter le trièdre direct normé de référence. Pour l'étude, nous considérons $\mathcal{R}_{ref}$ comme Galiléen. Le second référentiel qui nous intéresse durant cette étude est un référentiel fixé au lanceur noté $\mathcal{R}_g$. Les trois axes de la base orthonormée liée à ce référentiel sont formés à partir de la géométrie générale du lanceur. Ainsi X_g correspond à l'axe longitudinal du lanceur et Y_g, Z_g à ses axes dits "transverses". Durant toutes les analyses, nous considérerons le mouvement et la position de $\mathcal{R}_g$ par rapport à $\mathcal{R}_{ref}$. Un dernier trièdre est défini afin de décrire le mouvement et la position désirés du lanceur, ce repère s'appellera $\mathcal{R}_{aimed}$ pour exprimer qu'il correspond à l'objectif de vitesse et de position de $\mathcal{R}_g$ par rapport à $\mathcal{R}_{ref}$.

1.2.3 Trajectoires commandées

Faisons un point sur ce qui est en général "demandé" au lanceur au cours d'une mission classique. Les deux principales manœuvres sont le "spin" et le "basculement". Le spin consiste en une rotation du lanceur autour d'un axe prédéfini (en général son axe longitudinal X_g). Cette manœuvre est intéressante lorsque la charge utile du lanceur doit être en rotation au moment du largage. Les vitesses de rotation couramment rencontrées sont de l'ordre de quelques dizaines de degrés par secondes. Le basculement est une manœuvre qui vise à positionner le lanceur d'une certaine façon par rapport au référentiel $\mathcal{R}_{ref}$ et donc par rapport à la Terre. On peut imaginer l'intérêt de cette manœuvre lorsqu'il s'agit de pointer l'antenne d'un satellite de télécommunication en direction de la Terre. En général, la mission du lanceur en phase balistique se résume, à de rares exceptions, à un enchaînement de ces deux manœuvres avec différents paramètres et différents critères de performance à satisfaire.

1.2.4 Modélisation du système

Équation de la dynamique

La dynamique du lanceur spatial en phase balistique est régie par la loi de Newton pour un solide rigide en rotation autour de son centre de gravité. L'équation de la dynamique détermine la vitesse angulaire ω de notre lanceur (i.e. de $\mathcal{R}_g$) par rapport au référentiel $\mathcal{R}_{ref}$ en fonction des couples qui sont appliqués sur chacun de ses axes. L'équation de Newton pour un solide rigide en rotation est donnée par :

$$\dot{\omega} = I_g^{-1}\left[\Gamma - \omega \times (I_g\omega)\right] \text{ avec } I_g = \begin{bmatrix} I_x & -I_{xy} & -I_{xz} \\ -I_{xy} & I_y & -I_{yz} \\ -I_{xz} & -I_{yz} & I_z \end{bmatrix}.$$

où Γ est la somme de tous les couples extérieurs appliqués au lanceur i.e. $\Gamma = \Gamma_{ACS} + \Gamma_{dist}$ où Γ_{ACS} est le couple produit par le système de contrôle d'attitude et Γ_{dist} la somme des couples perturbateurs internes ou externes.

Équation de la cinématique

Il est courant de considérer deux types de représentations de la position du lanceur par rapport au référentiel $\mathcal{R}_{ref}$. En effet, les angles d'Euler sont facilement compréhensibles et permettent de se représenter la position du lanceur aisément. Ils sont donc largement utilisés en analyse de données de vol ou de simulations. Toutefois, cette représentation possède une singularité entrainant une indétermination quant à la position réelle du lanceur. C'est pourquoi les ingénieurs en aérospatiale comme en aéronautique préfèrent

la représentation par quaternions. Bien qu'il soit difficile de visualiser la position d'un lanceur grâce à son quaternion d'attitude, cette représentation est la seule utilisée dans le domaine. Les équations gouvernant les variations des angles d'Euler (ϕ, θ, ψ) et du quaternion d'attitude q du lanceur en fonction de sa vitesse angulaire sont donnés ci-dessous :

$$\begin{cases} \dot{\phi} = & \omega_x + \tan\theta(\omega_y \sin\phi + \omega_z \cos\phi) \\ \dot{\theta} = & \omega_y \cos\phi - \omega_z \sin\phi \\ \dot{\psi} = & \frac{1}{\cos\theta}(\omega_y \sin\phi + \omega_z \cos\phi) \end{cases},$$

$$\dot{q} = \frac{1}{2} q \star \varpi \text{ avec } \varpi = \begin{bmatrix} 0 & \omega_x & \omega_y & \omega_z \end{bmatrix}^T,$$

où $\star$ désigne l'opérateur de multiplication des quaternions. Les quatre composantes du quaternion d'attitude définissent un vecteur et un angle permettant de décrire la position de $\mathcal{R}_g$ par rapport à $\mathcal{R}_{ref}$. L'équation de la dynamique et les équations régissant l'évolution des variables représentant l'attitude du lanceur constituent ce que l'on appellera généralement la "dynamique du lanceur". Elles viennent de la physique du problème et sont ce qui le caractérise. De plus, ces éléments sont parmi ceux que nos partenaires industriels souhaiteraient voir étudiés plus précisément. Nous allons maintenant présenter les autres éléments du modèle qui conduisent à l'application du couple Γ_{ACS} sur le lanceur à partir de son attitude α, en particulier le système de génération du couple Γ_{ACS} servant à réguler l'attitude.

Mesures d'attitude et estimation des états

Les trajectoires commandées comprennent en général des objectifs de position finale et de vitesse finale. Cependant, les outils de mesure embarqués ne permettent qu'une mesure de l'attitude du lanceur. Il est donc nécessaire d'estimer ce que sont les vitesses angulaires du lanceur avec un observateur afin d'effectuer le contrôle de celui-ci. Cette étape cruciale est en général effectuée en deux temps. Tout d'abord, les états du lanceur sont prédits à partir des estimations précédentes du vecteur d'état et de la mesure d'attitude courante. Ensuite, le vecteur d'état estimé est déterminé en combinant les mesures disponibles avec les prédictions. C'est ce vecteur d'état estimé que prendra en compte le régulateur dans son calcul du couple commandé Γ_c. La structure permettant l'élaboration de l'estimation peut avoir diverses formes. Dans notre cas, la prédiction se fait à partir d'un modèle linéaire à paramètres variants tandis que la combinaison est faite par de simples pondérations statiques.

Contrôle d'attitude

L'étape de détermination du couple commandé vise à calculer le couple correcteur Γ_c qu'il serait nécessaire d'appliquer au lanceur afin qu'il suive la trajectoire de référence. Pour cela, nos partenaires industriels nous ont proposé d'étudier une structure de régulation dite "Proportionnelle-Dérivée". Cette technique simple est très largement utilisée dans l'industrie. Ce type de régulateur prend en compte la différence entre l'attitude désirée et l'attitude estimée et la vitesse désirée et celle estimée en fonction de la manœuvre à réaliser. Bien entendu, les "erreurs" d'attitude sont définies différemment si l'attitude est représentée par les angles d'Euler ou par un quaternion. Dans le cas de l'utilisation des quaternions, le quaternion "d'erreur" paramétrant la rotation nécessaire pour superposer $\mathcal{R}_g$ et $\mathcal{R}_{aimed}$ est obtenu à partir d'un produit matriciel. Mise à part cette caractéristique, le régulateur a une structure relativement simple mais tout à fait représentative de la structure du régulateur d'un lanceur réel.

Actionneurs

Les actionneurs du lanceur sont chargés de lui appliquer un couple Γ_{ACS} correspondant au mieux à la commande Γ_c générée par le régulateur. La problématique posée par leur nature, leur complexité aux yeux d'un automaticien, est le second point considéré comme prioritaire par les partenaires du projet. Dans l'état actuel des choses, la production de couple se fait par la combustion d'un carburant dans des tuyères dont la résultante est la production d'une force. L'association de plusieurs de ces forces permet de produire un couple qui provoque la rotation du lanceur. Une des caractéristiques principales des tuyères du système de contrôle d'attitude est qu'elles ne peuvent être qu'ouvertes ou fermées. C'est-à-dire que la force qu'elles produisent ne peut être modulée et que l'on est dans le cas d'un contrôle dit "tout-ou-rien". Il est commun de modéliser ce comportement par un modulateur d'impulsions. Dans le cas des tuyères chargées du contrôle d'attitude, on choisit un modulateur de largeur d'impulsions (acronyme anglais : PWM). Cet opérateur produit à partir de Γ_c un signal Γ_{ACS} constitué d'une série de créneaux dont la largeur est définie à intervalles d'échantillonnage réguliers. Le calcul de la durée d'ouverture i.e. de la largeur d'impulsion, se fait de façon à ce que l'incrément de vitesse angulaire entre deux impulsions soit le même que celui requis par le régulateur.

1.2.5 Conclusion : Éléments à étudier

Le modèle de lanceur défini au cours de la première phase du projet et résumée ci-dessus n'a bien entendu pas toutes les caractéristiques des modèles utilisés lors des campagnes de validation par simulations de Monte-Carlo. Cependant, grand soin a été pris de représenter de façon fidèle le comportement général du lanceur. En effet, bien que les méthodes de validation analytique demandent certaines transformations et simplifications des modèles dans le but de les rendre "analysables", il était pour nous nécessaire de conserver une bonne représentativité des modèles afin que les résultats aient un réel sens physique. Ainsi les transformations du modèle d'étude ont été menées avec cet objectif mais aussi évidemment celui de rentrer dans le cadre théorique des analyses par IQC.

1.3 Chapitre 4 : État de l'art et potentiel des contraintes intégrales quadratiques (IQC)

1.3.1 Introduction

Le second chapitre de la thèse a pour but de décrire les principales méthodes d'analyse de robustesse, le contexte dans lequel elles s'exécutent et de présenter précisément l'outil d'analyse formel qu'est la théorie des IQC. Afin de faciliter sa compréhension, nous avons mis l'accent sur des exemples d'application concrets. Dans un premier temps, les outils les plus connus et la théorie sur laquelle ils se fondent sont brièvement introduits. La théorie la plus ancienne visant à établir la stabilité des systèmes est sans doute la théorie de V. Lyapunov. Ses travaux remontent à la fin du XIX$^{\text{ème}}$ siècle. Lyapunov a introduit une généralisation de la notion d'énergie qui permet d'établir la stabilité des systèmes décrits par des équations différentielles. Il fallut attendre la seconde partie du XX$^{\text{ème}}$ siècle pour que cette méthode soit utilisée et étendue. De nos jours, de très nombreux résultats sont fondés sur cette théorie, en particulier pour l'étude de la stabilité des systèmes non-linéaires. En effet, une étude de stabilité par recherche d'une fonction de Lyapunov peut être envisagée dès que le système considéré est régi par des équations différentielles ce qui confère à cette théorie un champ d'applications immense. En contrepartie de cet indéniable avantage, cela a mené les chercheurs à établir de nombreux résultats visant à étudier des systèmes très particuliers conférant peu de flexibilité à la technique. Ainsi, les méthodes fondées sur la théorie de Lyapunov sont peu adaptées à l'étude de grands systèmes complexes puisqu'elles s'incrivent mal dans le processus industriel habituel débutant d'un modèle simple que l'on complexifie au fur et à

mesure que l'étude progresse. La seconde méthode que nous avons considérée représente la théorie dite "entrée-sortie". Elle conduit au théorème du petit gain (ou théorème du gain faible). Cette méthode très simple consiste à s'assurer que le produit des normes des sous-systèmes d'un système bouclé est strictement inférieur à 1. Cette hypothèse vérifiée, il est ensuite possible de garantir que tout signal borné (au sens de la norme considérée) entrant dans le système produira d'autres signaux qui resteront bornés. Dans le cadre de cette théorie, très souvent, les sous-systèmes considérés sont au nombre de deux : l'un rassemblant les éléments nominaux du système, l'autre ses éléments perturbateurs. Cette représentation des systèmes très répandue est nommée Représentation Linéaire Fractionnaire (acronyme anglais : LFR). Des précisions à propos des LFR que nous considérerons seront données dans le paragraphe suivant. Le théorème du petit gain permet l'étude de n'importe quel système sous réserve que l'on puisse en calculer la norme. Il est donc, en particulier, adapté à l'étude de tous les systèmes physiques à de rares exceptions. Cependant, le fait de ne considérer que la norme des sous-systèmes lui confère en général un fort conservatisme que l'on ne peut se permettre lors de l'étude de systèmes complexes tels que les lanceurs spatiaux. Cette caractéristique de la méthode a conduit à l'utilisation de la dénomination "analyse de robustesse non structurée" pour décrire une étude par le théorème du petit gain. Cela est dû au fait que lors d'une telle étude, on ne considère pas du tout la nature des opérateurs, les relations entrée-sortie et les éventuels découplages entre chacune des composantes. Pour résoudre ce problème, le début des années 80 a vu l'apparition de la principale méthode d'analyse "structurée" : la μ-analyse. Précurseur du "contrôle robuste" avec le théorème du petit gain, cette méthode permet de prendre en compte la structure du sous-système perturbateur de la LFR. Prendre en compte la structure revient à considérer les éventuels découplages entre les entrées et sorties du bloc perturbateur de la LFR. Cette technique finalement similaire au théorème du petit gain dans le sens où elle établit elle aussi une "mesure" du système nominal a considérablement diminué le conservatisme des résultats d'analyse de robustesse par la théorie "entrée-sortie". Son inconvénient majeur vient du fait que la μ-analyse ne permet de considérer que des systèmes perturbateurs constitués de gains (éventuellement dynamiques) incertains. Cela réduit malheureusement considérablement son intérêt pour l'étude de systèmes non-linéaires complexes tels que les lanceurs où s'imbriquent incertitudes paramétriques et incertitudes dynamiques mais aussi non-linéarités, paramètres variant dans le temps, retards, etc.
À première vue, les avantages de chacun des outils évoqués ci-dessus sont ceux que l'on souhaiterait voir dans l'outil qui nous permettra d'étudier notre lanceur spatial. En effet, nous avons besoin d'étudier un système non-linéaire complexe, structuré et ce à partir d'un modèle d'analyse que l'on souhaite faire évoluer au cours des études afin de gagner en représentativité des résultats de stabilité et de performance. Il se trouve que la théorie des Contraintes Intégrales Quadratiques, en tant que théorie "unificatrice" des grandes théories d'analyse de stabilité et de performance robuste dispose des avantages de chacune des méthodes présentées. En effet, les résultats précédents peuvent être retrouvés dans des cas particuliers de la théorie IQC. Face à ce constat, l'outil IQC prend toute sa légitimité pour répondre au problème posé.

1.3.2 Contraintes intégrales quadratiques (IQC)

Il est maintenant temps d'introduire les IQC et la façon dont elles peuvent être utilisées pour procéder à une analyse de stabilité.

Cadre théorique

Le cadre théorique dans lequel s'appliquent les méthodes d'analyse de stabilité robuste et de performance robuste est commun avec toutes les autres méthodes d'analyse de robustesse (théorème du petit gain, μ-analyse). On considère que le système peut être représenté sous la forme d'une interconnection de deux opérateurs appelée LFR et schématisée figure 1.1. Le but premier de l'analyse par IQC est de montrer que tous les signaux transitant dans le système ont une norme $\mathcal{L}_2$ finie. En des termes plus familiers des ingénieurs, il s'agit de signaux dont l'énergie est finie.

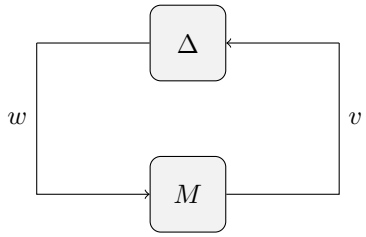

FIGURE 1.1 – Représentation linéaire fractionnelle pour l'analyse de stabilité

Pour commencer, on considèrera que les signaux entrant dans le système ont tous une norme $\mathcal{L}_2$ finie. Compte-tenu de ce que l'on cherche à montrer, cela reprend le contexte du théorème du petit gain. En effet, nous allons chercher à démontrer qu'aucun signal $\mathcal{L}_2$ ne peut "sortir" de son ensemble d'origine lorsqu'il passe dans la LFR (i.e. dans le système). Afin de pouvoir utiliser les IQC pour prouver la stabilité robuste de cette dernière, tous les systèmes de l'interconnection doivent être de norme $\mathcal{L}_2$-induite finie. Cela revient à dire que l'accroissement de la norme des signaux qui y passent ne peut et ne doit pas être infinie. Venons-en maintenant aux caractéristiques particulières que les opérateurs de la LFR doivent remplir pour qu'une analyse par IQC soit possible. Tout d'abord, la partie nominale M de la LFR doit être linéaire, invariante dans le temps et les pôles de sa fonction de transfert doivent avoir une partie réelle strictement négative. En ce qui concerne le second opérateur de la LFR i.e. la perturbation Δ, les seules contraintes à l'utilisation des IQC pour sa caractérisation sont qu'il doit être causal (non anticipatif) et borné au sens $\mathcal{L}_2$.
Ces quelques lignes nous ont permis de décrire les caractéristiques d'une LFR analysable par les contraintes intégrales quadratiques (IQC). De toute évidence, ces hypothèses sont tout à fait ordinaires et ne contraignent a priori pas les utilisateurs à de trop lourdes simplifications de leur modèle d'analyse. Cela est d'autant plus vrai que nous avons ici énuméré les hypothèses du théorème "classique" d'analyse de robustesse par IQC et qu'il existe des versions autrement plus générales.

Définitions

Les signaux et opérateurs typiques de l'analyse IQC ayant été définis, nous pouvons maintenant définir ce qu'est une IQC satisfaite par deux signaux.

Définition : Soit $\widehat{\Pi} : j\mathbb{R} \to \mathbb{C}^{(n_v+n_w)\times(n_v+n_w)}$ opérateur essentiellement borné sur l'axe imaginaire et Hermitien. Les signaux $v \in \mathcal{L}_2^{n_v}$ et $w \in \mathcal{L}_2^{n_w}$ satisfont l'IQC définie par $\widehat{\Pi}$ si

$$\int_{-\infty}^{+\infty} \begin{bmatrix} \widehat{v}(j\omega) \\ \widehat{w}(j\omega) \end{bmatrix}^* \widehat{\Pi}(j\omega) \begin{bmatrix} \widehat{v}(j\omega) \\ \widehat{w}(j\omega) \end{bmatrix} d\omega \geq 0 \tag{1.1}$$

est satisfaite. $\widehat{x}$ représente la transformée de Fourier de $x \in \mathcal{L}_2$.

On constate qu'une IQC est en effet une contrainte de signe sur l'intégrale d'une forme quadratique. De par sa définition et le théorème de Parseval, cette contrainte peut aussi être vue comme une contrainte sur les représentations temporelles de v, w et Π mais aussi comme une contrainte sur le produit scalaire pondéré par Π de $[v\ w]^T$ sur lui-même.
Dans le cadre d'une analyse de stabilité ou de performance robuste, les IQC servent à représenter les relations qui existent entre l'entrée et la sortie d'un opérateur. Ainsi, lorsqu'il existe une relation entre v et w du type $w = \Delta(v)$, on définit l'IQC décrivant un opérateur Δ comme suit.

Définition : Soit $\widehat{\Pi} : j\mathbb{R} \to \mathbb{C}^{(n_v+n_w)\times(n_v+n_w)}$ opérateur essentiellement borné sur l'axe imaginaire et Hermitien. On dit que l'opérateur $\Delta : \mathcal{L}_2^{n_v} \to \mathcal{L}_2^{n_w}$ satisfait l'IQC définie par $\widehat{\Pi}$ si pour tout signal $v \in \mathcal{L}_2^{n_v}$ on a

$$\int_{-\infty}^{+\infty} \begin{bmatrix} \widehat{v}(j\omega) \\ \widehat{\Delta(v)}(j\omega) \end{bmatrix}^* \widehat{\Pi}(j\omega) \begin{bmatrix} \widehat{v}(j\omega) \\ \widehat{\Delta(v)}(j\omega) \end{bmatrix} d\omega \geq 0 \tag{1.2}$$

.

On appelle Π le multiplicateur définissant l'IQC. Définie comme telle, l'IQC va permettre de représenter la façon dont Δ modifie son entrée v pour produire sa sortie $w = \Delta(v)$. De ce fait, lors d'une étude par IQC, les informations disponibles sur la manière dont Δ opère cette modification doivent être rassemblées dans l'opérateur Π. C'est à l'aide de ce dernier que la stabilité de l'association de Δ avec la partie nominale M de la LFR va être assurée. Nous allons voir tout de suite la forme que Π peut prendre dans un cas simple.

Description d'un opérateur non linéaire par une IQC

Afin de rendre les définitions ci-dessus plus concrètes, nous présentons brièvement un cas très simple permettant, à partir d'une propriété basique d'un opérateur non-linéaire Δ, de construire une IQC satisfaite par cet opérateur. D'autres exemples tout aussi pragmatiques peuvent être retrouvés dans le corps du manuscrit. Considérons un opérateur non-linéaire causal $\Delta : \mathcal{L}_2 \to \mathcal{L}_2$ satisfaisant la condition de secteur paramétrée par $\alpha \geq 0$ et $\beta > \alpha$. Cela signifie que pour tout $x \neq 0$,

$$\alpha \leq \frac{\Delta(x)}{x} \leq \beta \tag{1.3}$$

et $\Delta(0) = 0$. Cette condition très classique peut aisément être réécrite sous la forme d'une contrainte quadratique que l'on intègrera pour obtenir une IQC. On considérant $x = v(t)$ pour $t \geq 0$, on a :

$$\begin{aligned}
& \beta v(t)^2 \geq (\Delta v)(t) v(t) \geq \alpha v(t)^2, \\
\Leftrightarrow \quad & ((\Delta v)(t) - \alpha v(t)) \left(\beta v(t) - (\Delta v)(t)\right) \geq 0 \\
\Leftrightarrow \quad & (\alpha+\beta) v(t)(\Delta v)(t) - \alpha\beta v(t)^2 - (\Delta v)(t)^2 \geq 0 \\
\Leftrightarrow \quad & \begin{bmatrix} v(t) \\ (\Delta v)(t) \end{bmatrix}^T \underbrace{\begin{bmatrix} -\alpha\beta & \frac{\alpha+\beta}{2} \\ \frac{\alpha+\beta}{2} & -1 \end{bmatrix}}_{\Pi_{(\alpha,\beta)}} \begin{bmatrix} v(t) \\ (\Delta v)(t) \end{bmatrix} \geq 0
\end{aligned}$$

La contrainte quadratique obtenue peut, par intégration, servir à la définition d'une IQC décrivant Δ. Il est important de remarquer que la condition de secteur est seulement une condition suffisante de la validité de l'IQC définie par $\Pi_{(\alpha,\beta)}$. Cet exemple classique montre comment à partir de (α, β), les paramètres de la condition de secteur satisfaite par Δ, on peut déterminer un opérateur $\Pi_{(\alpha,\beta)}$, lui-même paramétré par (α, β), définissant une IQC satisfaite par Δ. Le théorème de stabilité qui suit utilise la représentation de Δ donnée par l'IQC définie par Π pour vérifier que les opérateurs M et Δ de la LFR sont compatibles.
Un autre point mérite d'être abordé ici. C'est la façon dont les IQC peuvent servir à décrire un opérateur Δ structuré. Nous avons mentionné auparavant le fait qu'il est très courant d'observer un découplage entre les entrées-sorties de l'opérateur Δ d'une LFR. Dans le but de procéder à une analyse de stabilité ou de performance dont le conservatisme est aussi réduit que possible, il est nécessaire que l'outil d'étude prenne en compte cette caractéristique de la structure de Δ. Cela est parfaitement réalisé par la description IQC puisque si l'on dispose de deux IQC définies par $\Pi^{(1)}$ et $\Pi^{(2)}$ décrivant deux opérateurs différents Δ_1 et

Δ_2, respectivement, il suffit de les concaténer pour obtenir une IQC satisfaite par l'opérateur structuré

$$\Delta = \begin{bmatrix} \Delta_1 & 0 \\ 0 & \Delta_2 \end{bmatrix} \tag{1.4}$$

dont le multiplicateur est

$$\Pi = \begin{bmatrix} \Pi_{11}^{(1)} & 0 & \Pi_{12}^{(1)} & 0 \\ 0 & \Pi_{11}^{(2)} & 0 & \Pi_{12}^{(2)} \\ \Pi_{21}^{(1)} & 0 & \Pi_{22}^{(1)} & 0 \\ 0 & \Pi_{21}^{(2)} & 0 & \Pi_{22}^{(2)} \end{bmatrix}. \tag{1.5}$$

Il est clair que d'une part la description IQC contient l'information dont on dispose à propos de la structure et que d'autre part, les opérateurs décrits par l'IQC structurée le seront aussi bien que quand ils constituent le seul bloc de perturbation.

1.3.3 Théorème classique de stabilité

Le théorème de stabilité utilisant les IQC rencontré le plus couramment dans la littérature s'énonce comme suit :

Théorème : Si

1. Pour tout $\tau \in [0;1]$, $I - \tau M\Delta$ est inversible et d'inverse causal ;
2. Pour tout $\tau \in [0;1]$, l'IQC définie par Π est satisfaite par $\tau\Delta$, c'est-à-dire pour tout $v \in \mathcal{L}_2$:

$$\int_{-\infty}^{+\infty} \begin{bmatrix} \hat{v}(j\omega) \\ \widehat{\tau\Delta(v)}(j\omega) \end{bmatrix}^* \Pi(j\omega) \begin{bmatrix} \hat{v}(j\omega) \\ \widehat{\tau\Delta(v)}(j\omega) \end{bmatrix} \mathrm{d}\omega \geq 0;$$

3. Il existe $\varepsilon > 0$ tel que

$$\forall \omega \in \mathbb{R}, \quad \begin{bmatrix} M(j\omega) \\ I \end{bmatrix}^* \Pi(j\omega) \begin{bmatrix} M(j\omega) \\ I \end{bmatrix} \preceq \varepsilon I_{n_w}. \tag{1.6}$$

Alors l'interconnection de (M, Δ) est stable i.e. l'opérateur $(I - M\Delta)^{-1}$ est borné au sens de la norme $\mathcal{L}_2$-induite.

Face aux trois hypothèses de ce théorème, plusieurs remarques sont importantes. Tout d'abord, la première hypothèse est, en général, valide pour les systèmes physiques. Il existe aussi des méthodes pour la tester dans certains cas non évidents. La seconde hypothèse est a priori satisfaite puisqu'elle correspond à l'obtention d'une description IQC de l'opérateur Δ et donc de l'opérateur Π définissant l'IQC satisfaite par Δ. Ceci est la base de toute étude de stabilité ou de performance par les IQC ; c'est ce que l'on cherche à déterminer en premier lieu lorsque l'on entreprend une analyse par IQC. Enfin, la troisième hypothèse constitue le test de stabilité en lui-même. C'est cette inégalité fréquentielle qui doit être vraie pour que l'interconnection de M et Δ soit stable au sens de la norme $\mathcal{L}_2$. Nous verrons par la suite que

cette inégalité peut être reformulée pour rendre sa vérification rapide et efficace.
Concrètement, l'idée de ce théorème est de ne pas utiliser directement l'opérateur Δ dans le test de stabilité. En effet, cet opérateur peut s'avérer particulièrement complexe et être composé de sous-opérateurs de différentes natures rendant l'analyse directe de l'association de M et Δ difficile. En effet, lors de la définition de la LFR on regroupe dans Δ tout ce qui est difficile à étudier avec les outils de l'automatique classique. Par exemple, Δ peut comporter des paramètres incertains, des paramètres variant au cours du temps, des paramètres variant à une certaine vitesse, des non linéarités (saturations, seuils, zone-mortes, etc.), des retards. De ce fait, il est plus simple de ne pas considérer Δ directement mais plutôt les informations que contient le multiplicateur Π définissant l'IQC satisfaite par Δ. Nous avons vu dans l'exemple ci-dessus que les paramètres de la condition de secteur satisfaite par l'opérateur Δ définissent le multiplicateur $\Pi_{(\alpha,\beta)}$ de l'IQC satisfaite par Δ. Cet exemple peut être généralisé à tout type d'opérateur Δ. Pour faire une analyse IQC, tous les paramètres caractérisant Δ doivent être rassemblés dans Π (gain énergétique, condition de secteur, gabarit fréquentiel de la sortie, retard maximal, etc.). Par la suite, c'est non pas l'association de M et Δ qui va être étudiée mais celle de M et Π. Dans l'inégalité fréquentielle du théorème, on vérifie la compatibilité entre M et Π pour s'assurer de la stabilité de l'interconnection entre M et Δ.

Implémentation

L'inégalité fréquentielle de l'hypothèse 3 est le test de stabilité à proprement parler. Il existe un résultat dit "Lemme de Kalman-Yakubotitch-Popov" (ou "lemme KYP") qui permet de reformuler ce nombre infini d'inégalités ($\omega \in \mathbb{R}$) en une Inégalité Matricielle Linéaire (LMI). Il devient alors facile d'implémenter le test de stabilité. Le lemme garantit l'équivalence entre les deux formulations ci-dessous :

Lemme KYP Étant données $A \in \mathbb{R}^{n\times n}$ Hurwitz, $B \in \mathbb{R}^{n\times n_w}$ telles que (A, B) est controlable, et $H = H^T \in \mathbb{R}^{(n+n_w)\times(n+n_w)}$, les propositions suivantes sont équivalentes :

- Pour tout $\omega \in \mathbb{R}_+$,

$$\begin{bmatrix} (j\omega I - A)^{-1}B \\ I \end{bmatrix}^* H \begin{bmatrix} (j\omega I - A)^{-1}B \\ I \end{bmatrix} \prec 0; \tag{1.7}$$

- Il existe une matrice symétrique $X = X^T \in \mathbb{R}^{n\times n}$ telle que la LMI

$$\begin{bmatrix} A & B \\ I & 0 \end{bmatrix}^T \begin{bmatrix} 0 & X \\ X & 0 \end{bmatrix} \begin{bmatrix} A & B \\ I & 0 \end{bmatrix} + H \prec 0, \tag{1.8}$$

  est valide.

1.3.4 Conclusion

Ce chapitre visait à introduire les IQC et la manière de les utiliser dans le contexte de l'analyse de stabilité et de performance d'un système complexe que nous devons mener. Nous avons constaté que les méthodes IQC tirent parti des avantages des méthodes dont elles sont une généralisation. De plus, elles semblent parfaitement adaptées à notre problématique car elles tiennent compte de la structure des systèmes. Il est important de remarquer que la stabilité obtenue par l'application du théorème IQC (norme $\mathcal{L}_2$-induite finie) n'est pas de la même nature que celle obtenue par les méthodes plus classiques (stabilité asymptotique, stabilité entrée-bornée/sortie-bornée). Des IQC décrivant différents opérateurs peuvent

être réutilisées lorsque ces opérateurs apparaissent plusieurs fois dans un même système ou dans d'autres systèmes et l'implémentation du test de stabilité sous forme de LMI est aisée. A cela nous ajouterons les propriétés décrites dans le corps du manuscrit telles que les combinaisons coniques de multiplicateurs et les différents degrés de liberté qu'offrent les multiplicateurs dynamiques. En contrepartie à cela, le problème principal lié à l'utilisation d'IQC pour la validation de critères de stabilité et de performance est que les LMI provenant de l'application du lemme KYP peuvent rapidement prendre de très grandes dimensions, rendant le test de stabilité très demandeur en capacité de calcul voire impossible à mener avec les capacités actuelles. Nous nous sommes heurtés à ce problème une fois au cours de cette thèse. Ce fut lors de l'étude de la stabilité et de la performance de notre modèle de lanceur spatial avec sa dynamique complète. Cette première application est présentée dans le chapitre suivant.

1.4 Chapitre 5 : Robustesse de la dynamique complète

1.4.1 Introduction

Le troisième chapitre de cette thèse est dédié à l'étude d'un modèle d'analyse du lanceur contenant les équations de la dynamique complètes, c'est-à-dire les équations obtenues avec une matrice d'inertie non-diagonale et en tenant compte des couplages gyroscopiques. Nous nous imposons de travailler dans le repère géométrique du lanceur car c'est dans ce repère que les consignes d'attitude et de vitesse sont données, que les tuyères produisent leur force et que la configuration de la charge utile est exprimée. Ces trois équations (une par axe de rotation) régissent l'évolution des vitesses angulaires du lanceur lors de l'application de couples extérieurs. On distingue trois couples appliqués : les couples délivrés sur chacun des axes du lanceur par les tuyères dédiées au contrôle d'attitude, les couples perturbateurs (vents solaires, atmosphère résiduelle, fuites d'ergols, etc.) et les couples gyroscopiques produits par les asymétries du lanceur et son mouvement de rotation. Ces derniers sont intrinsèques à la physique du lanceur mais on peut aussi se les représenter comme des perturbations de l'accélération angulaire du lanceur. La particularité de cette application par rapport à celle qui suivra est que c'est l'outil analytique disponible qui a guidé les transformations faites au modèle. En effet, l'outil LPVMAD étant mis à notre disposition, nous souhaitions l'exploiter au mieux. Ainsi, nous avons cherché à représenter le modèle d'analyse avec un bloc de perturbation Δ pour lequel il y avait des multiplicateurs dédiés déjà implémentés dans l'outil.

1.4.2 Modèle d'analyse

Dans un premier temps, nous définissons le modèle d'analyse sur lequel nous souhaitons mener notre étude de stabilité. Afin de procéder à une étude précise des équations de la dynamique, nous avons simplifié les autres parties du modèle afin de rendre possible la résolution des tests de stabilité robuste et de performance robuste mais aussi de simplifier l'analyse. En particulier, nous avons pris le parti de ne pas modéliser les équations de la cinématique. Du point de vue d'un automaticien, les équations de la cinématique liées aux angles d'Euler sont non-linéaires puisqu'elles font intervenir des fonctions rationnelles de cosinus et sinus appliquées aux états du système. En ce qui concerne les équations de la cinématique avec les quaternions, elles sont linéaires mais leurs paramètres varient au cours du temps. L'influence sur la stabilité de ces équations a été étudiée dans la littérature mais la question de l'influence réelle de la représentation de l'attitude sur la stabilité n'a pas encore été clairement résolue. Ici nous prenons le parti de ne pas choisir de représentation et de considérer l'attitude du lanceur comme l'intégrale de sa vitesse angulaire, une hypothèse valide pour les petits angles. Cela simplifie grandement le modèle d'analyse et permet de nous concentrer sur la dynamique. D'autre part, l'actionneur est modélisé par un opérateur de type saturation. Cette approximation est couramment utilisée dans l'industrie et elle nous fut conseillée dès le début du projet par nos partenaires industriels. Cette approximation a par la suite été confirmée par les études menées pendant cette thèse comme nous le verrons dans la seconde

application. Enfin, les étapes de mesure d'attitude, de reconstruction du vecteur d'état et de calcul du couple commandé sont simplifiées et la boucle de régulation est considérée comme continue et contrôlée par un régulateur proportionnel-dérivé $\mathcal{C}(s)$ dont la dérivée est filtrée. Ces hypothèses nous conduisent à la représentation du modèle d'analyse schématisée figure 1.2.

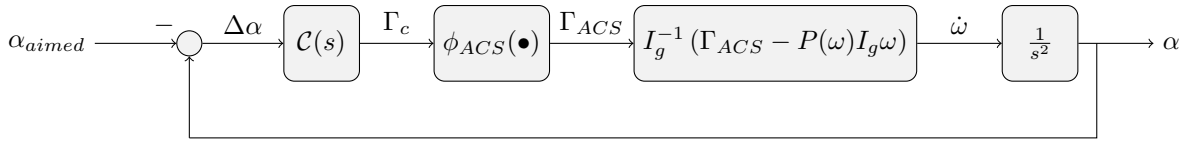

FIGURE 1.2 – Modèle d'analyse avec équations de la dynamique complètes

Il apparaît clairement sur ce schéma bloc que la difficulté de l'analyse de stabilité est causée par la dynamique non-linéaire du lanceur en rotation à laquelle nous ajouterons des incertitudes sur les termes de la matrice d'inertie. En écrivant l'équation de Newton sous forme matricielle, nous allons pouvoir décrire les travaux de transformation du système sur lesquels repose cette application.

$$\begin{bmatrix}\dot{\omega}_x\\ \dot{\omega}_y\\ \dot{\omega}_z\end{bmatrix} = \begin{bmatrix} I_x & -I_{xy} & -I_{xz}\\ -I_{xy} & I_y & -I_{yz}\\ -I_{xz} & -I_{yz} & I_z\end{bmatrix}^{-1} \left(\begin{bmatrix}\gamma_x\\ \gamma_y\\ \gamma_z\end{bmatrix} - \underbrace{\begin{bmatrix} 0 & -\omega_z & \omega_y\\ \omega_z & 0 & -\omega_x\\ -\omega_y & \omega_x & 0\end{bmatrix}}_{P(\omega(t))} \underbrace{\begin{bmatrix} I_x & -I_{xy} & -I_{xz}\\ -I_{xy} & I_y & -I_{yz}\\ -I_{xz} & -I_{yz} & I_z\end{bmatrix}}_{I_g} \begin{bmatrix}\omega_x\\ \omega_y\\ \omega_z\end{bmatrix} \right) \tag{1.9}$$

Dans l'équation ci-dessus, la dépendance en t des vitesses angulaires et des couples appliqués n'est pas représentée par souci de clarté. De plus, deux éléments sont problématiques pour un automaticien. Tout d'abord, il est ordinaire de considérer la matrice d'inertie du lanceur comme étant incertaine. En effet, cette matrice d'inertie représente la répartition des masses de l'étage supérieur du lanceur et de sa (ses) charge(s) utile(s). Cela représente un solide rigide de plusieurs mètres cubes dont l'inertie est très difficile à mesurer précisément. Il est donc absolument nécessaire de considérer ces incertitudes lors de la validation des lois de commande servant à la régulation d'attitude. Le second élément perturbateur empêchant l'analyse de la stabilité du système avec les méthodes d'analyse classique est la matrice de l'opérateur produit vectoriel $P(\omega(t))$. Cette matrice reprend les composantes de la vitesse angulaire du lanceur. Ses termes varient donc dans le temps.
A ces deux problèmes nous avons apporté la même solution, décrite dans le paragraphe suivant.

1.4.3 Factorisation de l'équation de la dynamique

Les deux problèmes susmentionnés peuvent être résolus de la même manière. Tout d'abord, nous avons considéré la matrice du produit vectoriel $P(\omega(t))$ comme une matrice de paramètres incertains variant dans le temps. Ainsi, nous changeons sa notation en $P(\hat{\omega}(t))$. Pour préparer la transformation du modèle en une LFR, nous avons considéré les paramètres de cette matrice comme affectés par des incertitudes additives. En ce qui concerne les termes de la matrice d'inertie, ils ont été considérés comme incertains, invariant dans le temps et affectés par des incertitudes multiplicatives. Ainsi pour la matrice du produit vectoriel nous avons 3 paramètres incertains apparaissant deux fois chacun et pour la matrice d'inertie nous avons 6 paramètres incertains. Les termes de la diagonale ne sont pas répétés mais ceux en dehors de la diagonale le sont deux fois.
Les incertitudes sur chacun des paramètres du modèle peuvent être quantifiées de manière spécifique. C'est-à-dire que nous savons quel degré d'incertitude affecte chacun des termes de la matrice I_g. Il est donc important de formuler le problème de façon à ce que chaque terme incertain soit affecté par "son"

incertitude. Pour cela, nous représentons les matrices incertaines de manière à ce que chacun de leurs termes soit accessible et que "son" incertitude lui soit attribuée. De plus, les matrices de produit vectoriel $P(\hat{\omega}(t))$ et d'inertie I_g ont des propriétés de symétrie particulières qu'il convient de prendre en compte pour ne pas augmenter le conservatisme du test de stabilité.
Nous avons donc recherché et obtenu des factorisations de ces deux matrices faisant intervenir une matrice diagonale rassemblant tous les termes des matrices incertaines répétés autant de fois qu'ils le sont dans leur matrice d'origine. Pour la matrice I_g nous définissons la matrice diagonale I_d et pour la matrice $P(\hat{\omega}(t))$ nous définissons $P_d(t)$:

$$I_d = \begin{bmatrix} I_x & 0 & 0 & 0 & 0 & 0 & 0 & 0 & 0 \\ 0 & I_y & 0 & 0 & 0 & 0 & 0 & 0 & 0 \\ 0 & 0 & I_z & 0 & 0 & 0 & 0 & 0 & 0 \\ 0 & 0 & 0 & I_{xy} & 0 & 0 & 0 & 0 & 0 \\ 0 & 0 & 0 & 0 & I_{xy} & 0 & 0 & 0 & 0 \\ 0 & 0 & 0 & 0 & 0 & I_{xz} & 0 & 0 & 0 \\ 0 & 0 & 0 & 0 & 0 & 0 & I_{xz} & 0 & 0 \\ 0 & 0 & 0 & 0 & 0 & 0 & 0 & I_{yz} & 0 \\ 0 & 0 & 0 & 0 & 0 & 0 & 0 & 0 & I_{yz} \end{bmatrix} \in \mathbb{R}^{9\times 9}, \tag{1.10}$$

$$\forall t \geq 0, \quad P_d(t) = \begin{bmatrix} \hat{\omega}_z(t) & 0 & 0 & 0 & 0 & 0 \\ 0 & \hat{\omega}_z(t) & 0 & 0 & 0 & 0 \\ 0 & 0 & \hat{\omega}_y(t) & 0 & 0 & 0 \\ 0 & 0 & 0 & \hat{\omega}_y(t) & 0 & 0 \\ 0 & 0 & 0 & 0 & \hat{\omega}_x(t) & 0 \\ 0 & 0 & 0 & 0 & 0 & \hat{\omega}_x(t) \end{bmatrix} \in \mathbb{R}^{6\times 6}. \tag{1.11}$$

Par suite, nous définissons I_d^0 et P_d^0 les matrices diagonales nominales correspondant à I_d et $P_d(t)$ et contenant les valeurs nominales des paramètres d'inertie et de vitesse angulaire, respectivement. A partir de ces matrices diagonales, deux manipulations successives vont permettre leur utilisation dans la LFR du modèle. Premièrement, on applique à ces matrices les incertitudes décrites auparavant en définissant les matrices de paramètres incertains Δ_I et $\Delta_\omega(t)$ dont la structure correspond à I_d et $P_d(t)$, respectivement :

$$\Delta_I = \begin{bmatrix} \delta_x & 0 & 0 & 0 & 0 & 0 & 0 & 0 & 0 \\ 0 & \delta_y & 0 & 0 & 0 & 0 & 0 & 0 & 0 \\ 0 & 0 & \delta_z & 0 & 0 & 0 & 0 & 0 & 0 \\ 0 & 0 & 0 & \delta_{xy} & 0 & 0 & 0 & 0 & 0 \\ 0 & 0 & 0 & 0 & \delta_{xy} & 0 & 0 & 0 & 0 \\ 0 & 0 & 0 & 0 & 0 & \delta_{xz} & 0 & 0 & 0 \\ 0 & 0 & 0 & 0 & 0 & 0 & \delta_{xz} & 0 & 0 \\ 0 & 0 & 0 & 0 & 0 & 0 & 0 & \delta_{yz} & 0 \\ 0 & 0 & 0 & 0 & 0 & 0 & 0 & 0 & \delta_{yz} \end{bmatrix} \in \mathbb{R}^{9\times 9}, \tag{1.12}$$

$$\forall t \geq 0, \quad \Delta_\omega(t) = \begin{bmatrix} \delta\omega_z(t) & 0 & 0 & 0 & 0 & 0 \\ 0 & \delta\omega_z(t) & 0 & 0 & 0 & 0 \\ 0 & 0 & \delta\omega_y(t) & 0 & 0 & 0 \\ 0 & 0 & 0 & \delta\omega_y(t) & 0 & 0 \\ 0 & 0 & 0 & 0 & \delta\omega_x(t) & 0 \\ 0 & 0 & 0 & 0 & 0 & \delta\omega_x(t) \end{bmatrix} \in \mathbb{R}^{6\times 6}. \tag{1.13}$$

Ainsi nous pouvons définir les matrices I_d et $P_d(t)$ par :

$$I_d = I_d^{(0)}(I_9 + \Delta_I) \text{ et } \forall t \geq 0, \quad P_d(t) = P_d^{(0)} + \Delta_\omega(t). \tag{1.14}$$

Les équations ci-dessus expriment les incertitudes multiplicatives sur les inerties et additives sur les vitesses.
Dans un second temps, nous pouvons reconstruire les matrices originales I_g et $P(\hat{\omega}(t))$ avec les matrices de factorisation ci-dessous :

$$M_1 = \begin{bmatrix} 1 & 0 & 0 & 1 & 0 & 1 & 0 & 0 & 0 \\ 0 & 1 & 0 & 0 & 1 & 0 & 0 & 1 & 0 \\ 0 & 0 & 1 & 0 & 0 & 0 & 1 & 0 & 1 \end{bmatrix} \tag{1.15}$$

et

$$M_2 = \begin{bmatrix} 1 & 0 & 0 & 0 & -1 & 0 & -1 & 0 & 0 \\ 0 & 1 & 0 & -1 & 0 & 0 & 0 & 0 & -1 \\ 0 & 0 & 1 & 0 & 0 & -1 & 0 & -1 & 0 \end{bmatrix}^T. \tag{1.16}$$

pour la matrice d'inertie et

$$T_1 = \begin{bmatrix} 1 & 0 & 1 & 0 & 0 & 0 \\ 0 & 1 & 0 & 0 & 1 & 0 \\ 0 & 0 & 0 & 1 & 0 & 1 \end{bmatrix} \tag{1.17}$$

et

$$T_2 = \begin{bmatrix} 0 & 1 & 0 & -1 & 0 & 0 \\ -1 & 0 & 0 & 0 & 0 & 1 \\ 0 & 0 & 1 & 0 & -1 & 0 \end{bmatrix}^T . \tag{1.18}$$

pour la matrice de produit vectoriel. En effet, on retrouve les matrices grâce aux expressions

$$I_g = M_1 I_d M_2 \text{ et } P(\hat{\omega}) = T_1 P_d(t) T_2. \tag{1.19}$$

Ces factorisations vont être au cœur de la transformation du modèle d'analyse en LFR. Après introduction des matrices d'incertitudes, des matrices nominales et des matrices de factorisation dans les équations de la dynamique, la structure de l'opérateur définissant α à partir de Γ_{ACS} peut être représentée sous forme du schéma bloc de la figure 1.3.

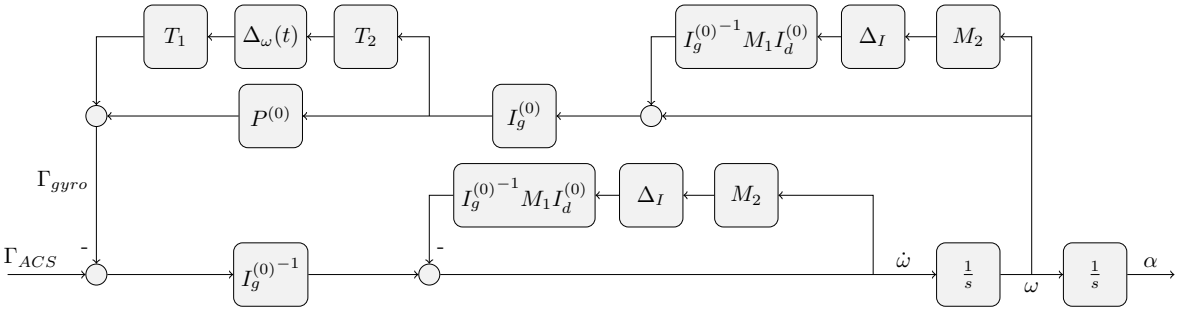

FIGURE 1.3 – Schéma bloc des équations de la dynamique factorisées

Cette structure est parfaitement appropriée à la définition d'une LFR du modèle d'analyse, elle sépare un modèle nominal des perturbations Δ_I et $\Delta_\omega(t)$ qui permettent une représentation complète des équations de Newton. On remarque que comme la matrice d'inertie I_g et son inverse sont utilisées pour la description du mouvement, la matrice d'incertitude Δ_I apparaît deux fois dans cette schématisation. Cette nouvelle représentation des équations du mouvement associée à la représentation classique de l'opérateur saturation avec un opérateur zone-morte permet la définition de la LFR du modèle d'analyse. Le bloc de perturbation Δ de cette LFR est de taille 27. Le bloc Δ_I y apparaît deux fois en raison de la présence de I_g et I_g^{-1} dans l'équation de Newton, le bloc $\Delta_\omega(t)$ une fois et l'opérateur zone-morte entrant dans la représentation de la saturation a trois entrées et trois sorties. Le but est maintenant d'étudier la stabilité du modèle. A minima, nous souhaitons prouver la stabilité pour les incertitudes "nominales" de l'inertie. On considère généralement que les termes de la diagonale de I_g sont incertains à $\pm 10\%$ tandis que ceux en dehors de la diagonale peuvent avoir une valeur entre -100% et $+900\%$ de leur grandeur nominale. En ce qui concerne les paramètres incertains se trouvant dans la matrice du produit vectoriel déterminant les couples gyroscopiques, ils doivent représenter les composantes du vecteur vitesse angulaire, c'est-à-dire toutes les valeurs que celles-ci peuvent prendre au cours d'un vol. Pour paramétrer l'ensemble de leurs variations possibles nous définissons délibérément un domaine de valeurs extrêmement grand par rapport

aux vitesses rencontrées lors d'une mission type. Nous faisons cela pour être sûr que toutes les trajectoires physiquement réalisables par le lanceur sont couvertes par la modélisation choisie. Par conséquent, les domaines de variations de chacun des paramètres de vitesse sont les suivants pour tout $t \geq 0$:

$$\hat{\omega}_x(t) \in [-100 \text{ deg.s}^{-1}, +100 \text{ deg.s}^{-1}],$$

$$\hat{\omega}_y(t), \hat{\omega}_z(t) \in [-50 \text{ deg.s}^{-1}, +50 \text{ deg.s}^{-1}].$$

Une autre information à propos des paramètres représentant les composantes de la vitesse angulaire a son importance lors de l'étude de stabilité robuste avec les IQC de l'outil LPVMAD. En effet, compte tenu de la conception du lanceur, nous pouvons majorer les valeurs que peuvent prendre les dérivées par rapport au temps de chacune des composantes de la vitesse angulaire du lanceur i.e. les accélérations angulaires. En effet, par une simple approximation monodimensionnelle de la dynamique et compte tenu de la saturation appliquée au couple commandé Γ_c pour produire Γ_{ACS}, nous pouvons majorer l'accélération maximale par axe. Cette information peut être introduite dans le multiplicateur définissant l'IQC satisfaite par les paramètres variant dans le temps du bloc de perturbation $\Delta_\omega(t)$, nous établissons le maximum de sa valeur absolue à 1deg.s^{-1} et allons la prendre en compte dans l'étude. Cela a pour but de réduire le conservatisme en décrivant plus précisément les caractéristiques de ces paramètres incertains.

1.4.4 Analyse de stabilité robuste

L'outil IQC LPVMAD mis à disposition du projet par l'ESA permet d'analyser facilement la stabilité robuste de la LFR définie au paragraphe précédent. On cherche à établir une estimation du domaine de stabilité du modèle de lanceur. Pour représenter ce domaine, nous considérons que l'incertitude relative affectant les termes diagonaux de la matrice d'inertie δ_d exprimée en pourcentage. De façon similaire, nous définissons δ_{od} l'incertitude relative maximale affectant les termes en dehors de la diagonale de I_g. Pour faciliter la lecture des résultats et la représentation du domaine de stabilité, δ_{od} n'est pas exprimé en pourcentage. Ainsi, nous définissons le plan (δ_d, δ_{od}) dans lequel le domaine de stabilité va être évalué. Dans ce plan, les incertitudes "nominales" de l'inertie définies à la fin du paragraphe précédent sont représentées par le point $(10\%, 10)$. Cela correspond à une incertitude de $\pm 10\%$ sur les termes de la diagonale et à une incertitude entre -100% et $+900\%$ sur les termes hors-diagonaux. Pour déterminer le domaine de stabilité, nous commencons par fixer la valeur de l'incertitude des termes diagonaux δ_d. Ensuite, nous essayons de résoudre le test de stabilité pour δ_{od} aussi grand que possible jusqu'à trouver la valeur limite. Nous reproduisons ensuite cela pour différentes valeurs de δ_d. Le domaine de stabilité obtenu par analyse IQC est représenté figure 1.4.
Le domaine de stabilité obtenu contient le point $(10\%, 10)$ ce qui indique que notre représentation des équations du mouvement associée à l'outil IQC permet de prouver la stabilité robuste du modèle dans le cas d'étude défini par les partenaires industriels. De plus, l'estimation du domaine de stabilité est très satisfaisante dans la mesure où les marges vis-à-vis des incertitudes "nominales" sont grandes. Il faut toutefois prendre en compte le fait que le modèle est simplifié et donc que ces marges sont certainement réduites pour des modèles d'analyse plus représentatifs. Cependant, notre but premier était de trouver comment représenter l'équation de Newton dans le cadre d'une analyse de robustesse ce qui a été fait. A cela s'ajoute le fait que nous pouvons espérer augmenter la représentativité de ce système tout en restant capable de résoudre le test de stabilité robuste avec les IQC.
Afin de compléter cette analyse de robustesse, nous avons mis en place une extension du modèle d'analyse permettant de déterminer la robustesse en performance du lanceur face aux incertitudes de la matrice d'inertie. Nous avons choisi de traiter le problème de performance robuste comme un problème de stabilité robuste. Cela nous a conduit à compléter notre LFR en y ajoutant un nouvel opérateur incertain Δ_P de taille 3 et de norme $\mathcal{L}_2$ bornée reliant la sortie correspondant l'erreur d'attitude à une entrée correspondant à un couple perturbateur. Il est représenté sur le schéma bloc figure 1.5.

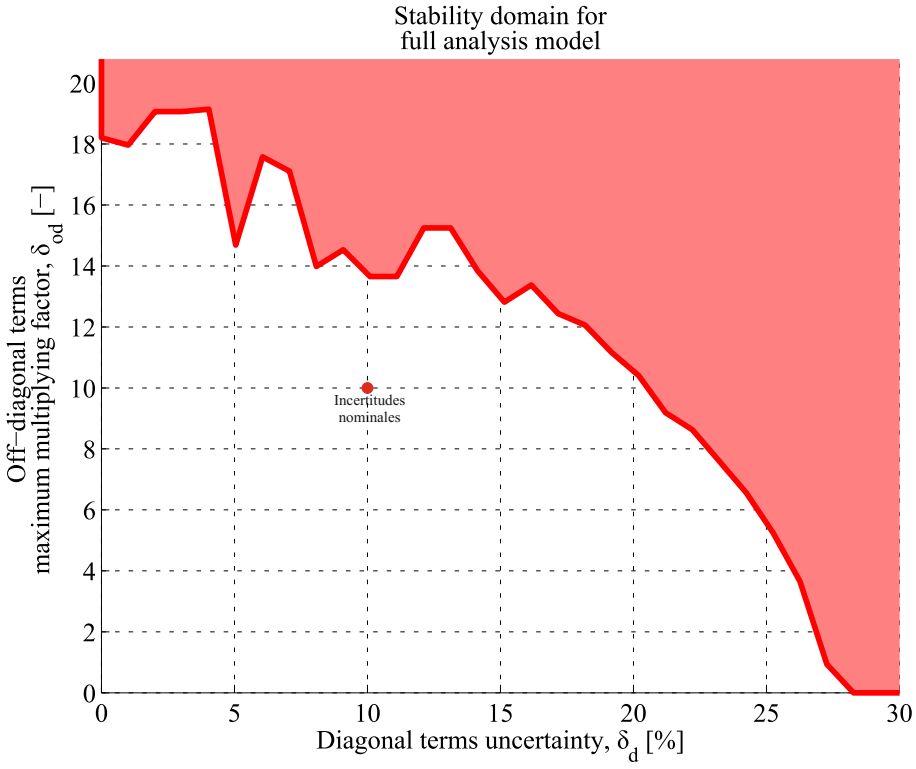

FIGURE 1.4 – Estimation de la région de stabilité

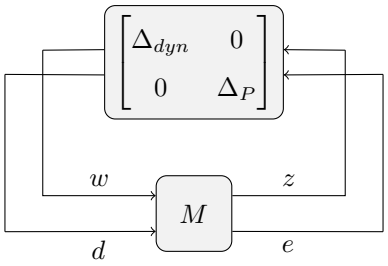

FIGURE 1.5 – LFR pour l'analyse de performance robuste

La taille de la LFR obtenue ne nous a malheureusement pas permis de faire l'étude de sa version complète et le modèle d'actionneur utilisant l'opérateur zone-morte a dû en être retiré. Toutefois, notre ambition première dans cette étude était de poser le problème de validation de la performance robuste et de proposer une méthode pour le résoudre ce que nous avons fait. L'étude du modèle simplifié a donné lieu au tracé de courbes dites "iso-performance" permettant de visualiser les variations de performance à l'intérieur d'une estimation du domaine de stabilité en fonction du degré d'incertitude sur les paramètres du modèle. Un exemple de tracé est donné figure 1.6.

1.4.5 Conclusions

Cette première application nous a permis de déterminer un mode opératoire pour traiter la stabilité et la performance robuste d'un modèle de lanceur comportant les équations de la dynamique complètes. Par une factorisation des matrices I_g et $P(\hat{\omega})$, nous avons obtenu une représentation linéaire fractionnaire du modèle couvrant toutes ses trajectoires possibles. Nous avons aussi été en mesure d'appliquer à chaque

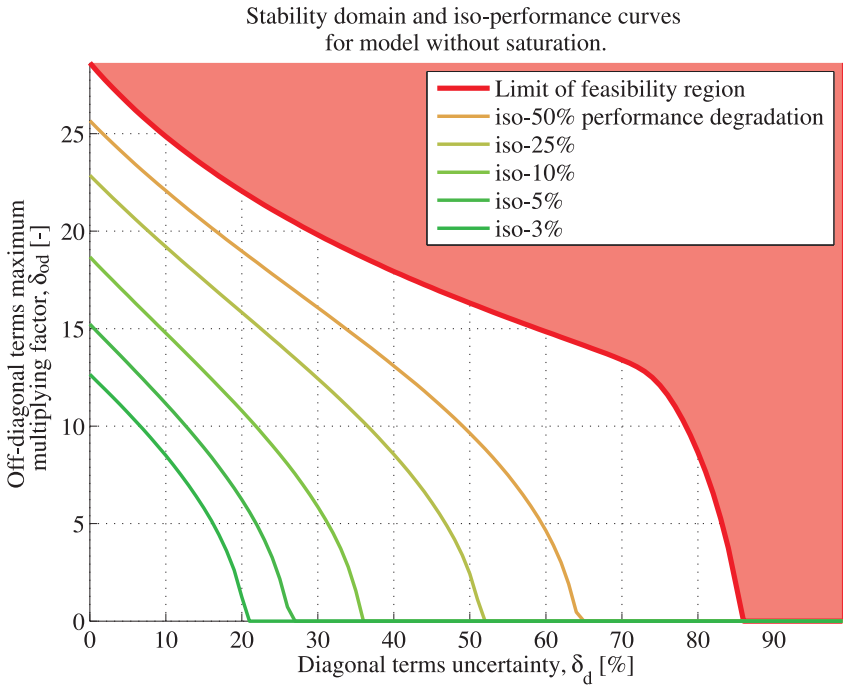

FIGURE 1.6 – Estimation de la région de stabilité et courbes iso-performance

terme incertain sa propre incertitude évitant ainsi d'ajouter du conservatisme au test de stabilité. Enfin, l'outil IQC LPVMAD a permis la détermination du domaine de stabilité robuste du modèle, celui-ci dépassant les objectifs fixés initialement. L'analyse de performance robuste du système est venue confirmer indirectement les hypothèses émises après des simulations temporelles. Celles-ci avaient mis en évidence le non-respect des critères de performance en précision de pointage et ce malgré la réduction de la taille du problème en raison des capacités de calcul disponibles.
Pour ce qui est des perspectives, il est évident qu'une analyse de sensibilité du système en les différents paramètres incertains permettrait certainement de réduire la taille du problème tout en conservant la représentativité du modèle. Pour répondre à ce même objectif de réduction de la taille du problème, on peut éventuellement envisager de trouver une autre forme de factorisation du problème permettant d'augmenter la compacité de l'opérateur Δ. Enfin, le but final de ces études serait d'associer les travaux de cette application avec ceux de la seconde application décrite dans le chapitre suivant.

1.5 Chapitre 6 : Analyse de stabilité des systèmes à modulation d'impulsions

1.5.1 Introduction

Une seconde application de la théorie des IQC à la validation de lois de commande est présentée dans le quatrième et dernier chapitre de la thèse. Cette application vise à utiliser les IQC pour étudier la stabilité des systèmes comportant le modulateur d'impulsions PWM décrit dans le premier chapitre. Cet opérateur classique dans d'autres domaines convient parfaitement à la représentation du mode de fonctionnement "tout-ou-rien" des tuyères exerçant le contrôle d'attitude d'un lanceur. Cependant, il possède des propriétés particulièrement délicates à traiter dans le cadre d'une analyse de stabilité ou de performance robuste. Concrètement, le modulateur de largeur d'impulsions (acronyme anglais : PWM) a l'effet d'un échantillonneur, son signal de sortie est constant par morceaux et prend des valeurs dans un ensemble

fini. S'ajoute à cela qu'avec la définition de la durée d'impulsion utilisée pour les lanceurs que nous étudions, nous n'avons aucune garantie quant au caractère fini du gain énergétique de l'opérateur. Cela viole l'hypothèse principale faite sur les opérateurs composant la LFR du modèle en vue de l'application du théorème de stabilité IQC. Ainsi, ces propriétés nous ont conduits à pratiquer des transformations du modèle d'analyse afin de le représenter avec des opérateurs de gain énergétique fini qui puissent être analysés avec la théorie IQC.
L'étude de la stabilité du modèle de lanceur avec un PWM a été faite en deux temps. Nous avons au début de la thèse travaillé de façon pragmatique sur la quantification de la différence entre la vitesse angulaire du modèle avec PWM et celle d'un modèle où le PWM est remplacé par un actionneur "nominal". Plus tard dans nos travaux, en travaillant de nouveau sur ce problème, nous avons trouvé dans la littérature une modélisation du PWM en tous points similaire à la nôtre conduisant à une étude de la stabilité par la théorie des IQC. Bien que différentes sur le plan théorique, ces deux études menées indépendamment s'avèrent finalement très semblables sur le plan de la modélisation et laissent aisément concevoir les très encourageantes perspectives de combinaison des résultats obtenus.

1.5.2 Modèle d'analyse

Pour se concentrer sur l'étude de l'effet de l'actionneur "tout-ou-rien" sur la stabilité du modèle de lanceur, nous avons simplifié les autres éléments du modèle à commencer par le modèle dynamique. Nous avons en effet considéré un modèle dynamique monodimensionnel constitué d'un gain et d'un double intégrateur permettant de déterminer l'attitude à partir du couple délivré par les tuyères Γ_{ACS}. Afin de se soumettre aux hypothèses parfois restrictives des résultats utilisés, les intégrateurs pourront être approchés par des filtres passe-bas du second ordre à pôle double strictement négatif. De la même façon que pour l'application précédente, nous nous contentons d'un correcteur proportionnel-dérivé (PD) à dérivée filtrée pour modéliser la reconstruction de la vitesse angulaire à partir de la mesure d'attitude et de régulateur. Finalement, le modèle PWM de l'actionneur est défini par son signal de sortie $\Gamma_{ACS} = w$ en fonction de son entrée $\Gamma_c = z$ comme suit :

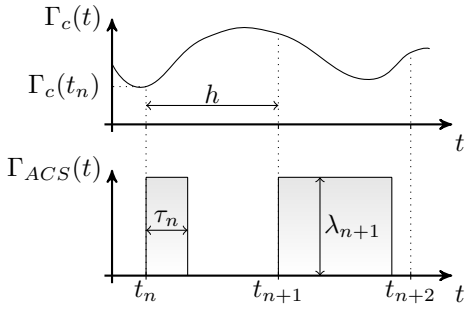

FIGURE 1.7 – Schéma de l'entrée et de la sortie de l'opérateur PWM

$$\forall \Gamma_c \in \mathcal{L}^1, \quad \mathcal{P}(\Gamma_c)(t) = \Gamma_{ACS}(t) = \begin{cases} \lambda_n, & t \in [t_n, t_n + \tau_n), \\ 0, & t \in [t_n + \tau_n, t_{n+1}); \end{cases} \tag{1.20}$$

avec

$$\lambda_n = \quad sign\left(\Gamma_c(t_n)\right)\Gamma_{av},$$

$$\tau_n = \begin{cases} 0, & \text{si } |\Gamma_c(t_n)| < \Gamma_{min} \\ \frac{|\Gamma_c(t_n)|}{\Gamma_{av}} h, & \text{si } \Gamma_{min} \leq |\Gamma_c(t_n)| < \Gamma_{av} \\ h, & \text{si } |\Gamma_c(t_n)| \geq \Gamma_{av} \end{cases} . \tag{1.21}$$

Cette définition prend en compte la durée d'ouverture maximale des tuyères et leur durée d'ouverture minimale. Pour augmenter la représentativité de la modélisation du fonctionnement des tuyères, nous voudrions dans cette application considérer la hauteur des impulsions comme une donnée incertaine du problème. Dans les faits, le couple dispensé par les tuyères peut diminuer jusqu'à 50% au cours du vol en raison notamment, des variations des propriétés des ergols au cours de la mission. Cette caractéristique sera prise en compte dans une des deux analyses seulement par l'introduction d'un paramètre δ_Γ modélisant l'incertitude relative sur la hauteur des impulsions du PWM. Enfin, la valeur de la période d'échantillonnage pour laquelle nous souhaiterions être en mesure de prouver la stabilité est de 1 seconde. Plus généralement, nous souhaiterions être en mesure de prouver la stabilité du modèle pour une période d'échantillonnage aussi grande que possible.
Le modèle d'analyse défini ainsi, notre raisonnement lors de la première étude a été le suivant.

1.5.3 Modélisation du PWM par étude de la vitesse angulaire

Transformations de la boucle fermée

La simplicité du modèle d'analyse nous permet de déterminer exactement l'expression analytique de la vitesse angulaire ω_{pwm} du lanceur monodimensionnel lorsque le signal de couple Γ_{ACS} est produit par un opérateur PWM. L'étude de l'expression analytique du signal ainsi que de la forme de sa représentation temporelle nous a conduits à exprimer la vitesse angulaire ω_{pwm} comme la somme de deux composantes. En effet, compte tenu de la définition de Γ_{ACS}, la vitesse angulaire ω_{pwm} est affine par morceaux par rapport au temps. Plus précisément elle alterne sur chaque période d'échantillonnage une phase affine et une phase constante comme l'indique la figure 1.8. Venons-en à la décomposition de la vitesse angulaire en deux composantes dont l'addition produit ω_{pwm}. La première serait générée par un actionneur dit "nominal" comportant une saturation et un échantillonneur-bloqueur cadencé à la période d'échantillonnage h (représentation sur la figure 1.8). La seconde vitesse angulaire viendrait compléter la vitesse produite par l'actionneur nominal pour que la somme des deux soit égale à celle produite par l'actionneur réel modélisé. Nous avons défini que ce "complément" serait généré par un opérateur non-linéaire Δ_{PWM}. L'intérêt des différents opérateurs susmentionnés est qu'ils sont facilement représentables sous forme LFR. De la même façon que pour la première application, les multiplicateurs de LPVMAD ont guidé nos recherches pour faciliter l'implémentation du test de stabilité.
A la suite de cette phase de transformation du modèle d'analyse initial, nous le reformulons de la façon représentée figure 1.9 pour que sa LFR soit facilement accessible.

Analyse de stabilité robuste

Comme indiqué précédemment, l'analyse du modèle transformé est aisée puisque les transformations conduisent à une LFR du modèle d'analyse dont le bloc perturbateur peut être décrit avec les multiplicateurs disponibles dans la toolbox LPVMAD mise à notre disposition. Nous avons présenté les résultats de l'étude dans le plan (δ_Γ, h). En effet, nous souhaitons être en mesure de prouver la stabilité du sys-

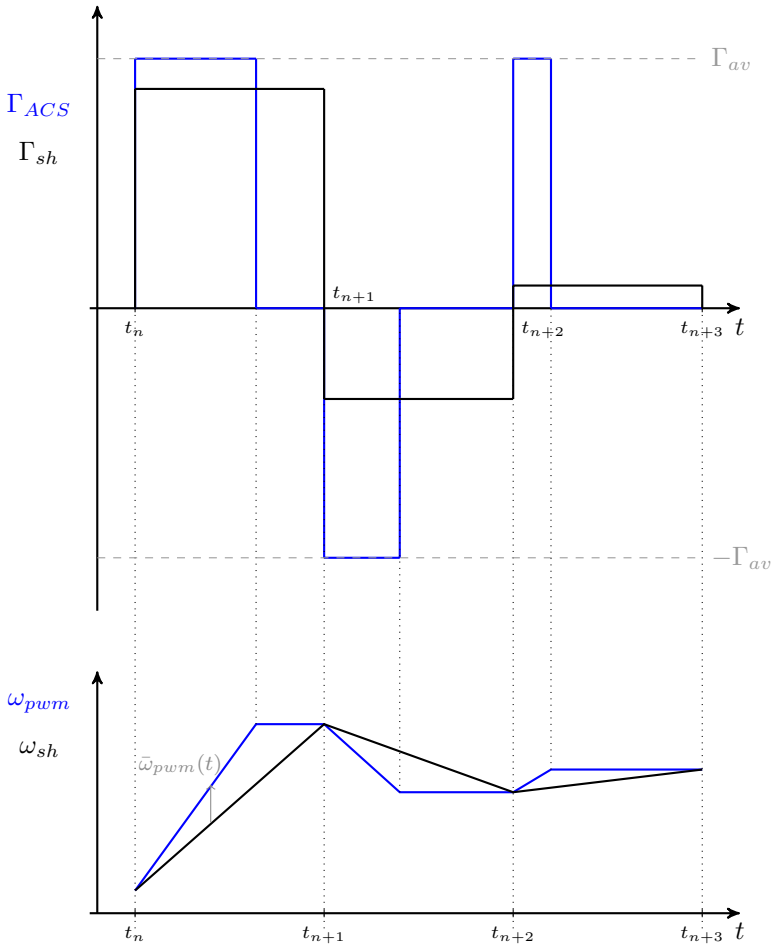

FIGURE 1.8 – Comparaison des couples et vitesses angulaires, $\omega = \int \Gamma / J dt$

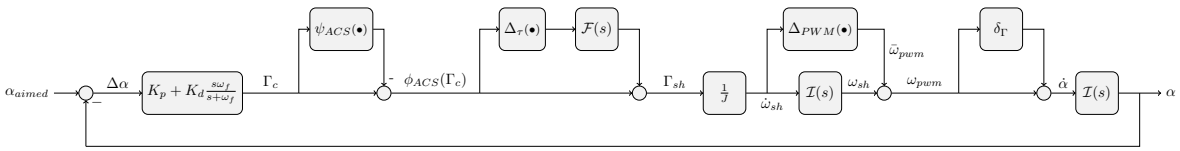

FIGURE 1.9 – Boucle fermée du modèle d'analyse avant LFR

tème pour une période d'échantillonnage h aussi grande que possible car peu d'activations des tuyères implique peu de consommation d'ergols et une plus faible usure des valves d'activation. Cela permettrait aussi aux missions d'être plus longues. Cependant, nous souhaitons aussi prouver la stabilité pour de fortes incertitudes sur le couple disponible δ_Γ afin de parer à tout problème de fuite ou de panne. Ainsi, voir comment évoluent les valeurs de δ_Γ et h pour lesquelles la stabilité peut être prouvée est primordial. Les résultats de l'étude sous forme d'estimation du domaine de stabilité sont présentés en figure 1.10. Ils montrent que malgré un relativement vaste domaine où la stabilité est prouvée, notamment vis-à-vis de l'incertitude sur le couple disponible δ_Γ, nous ne pouvons pas garantir la stabilité du modèle pour la période d'échantillonnage souhaitée (1 seconde). Cependant, la relative simplicité du modèle permet une bonne compréhension de la problématique et de l'effet du PWM par rapport à un actionneur plus simple. De plus, même si l'utilisation de cette modélisation pour un modèle tridimensionnel ne semble pas évidente, on peut envisager l'extension de ces travaux vers le cas 3-axes.

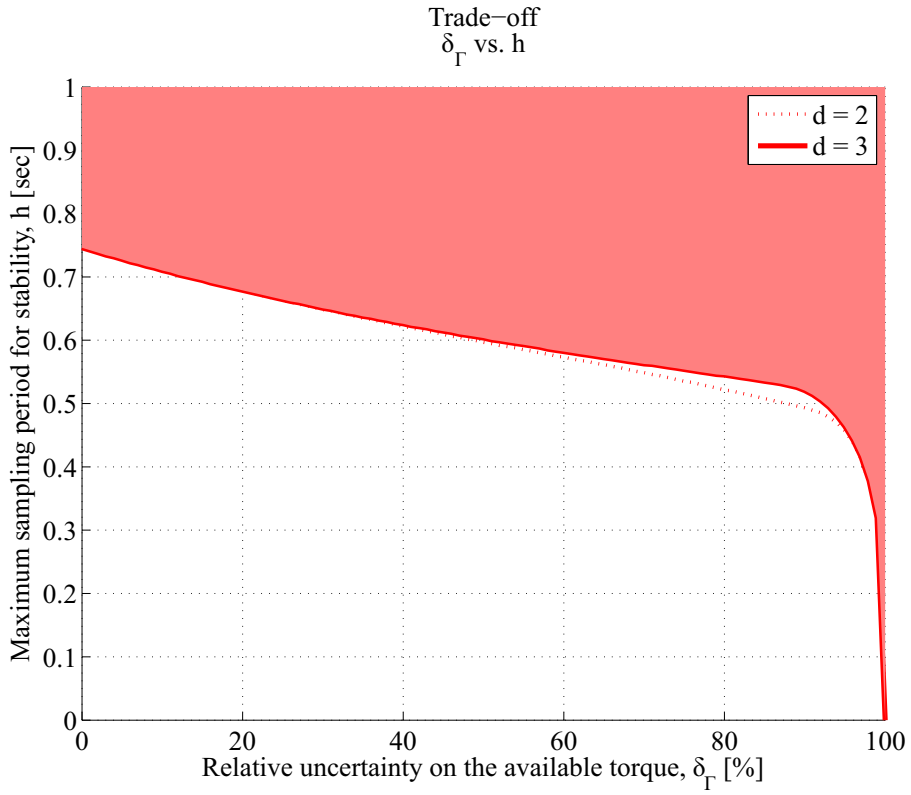

FIGURE 1.10 – Estimation du domaine de stabilité

1.5.4 Transformation de la boucle par introduction de la non-linéarité équivalente

Transformations de la boucle

La seconde méthode utilisée pour faire l'analyse du modèle comportant le PWM est en réalité parfaitement semblable à l'approche pragmatique de la section précédente. Toutefois, elle fait appel à des arguments plus pragmatiques du point de vue de la théorie des IQC pour justifier de la transformation du modèle du système en boucle fermée. Le résultat de stabilité obtenu repose sur des IQC et un théorème de stabilité différents de la théorie classique utilisée lors de la première étude. Cependant, la poursuite de ces études montrera probablement que les deux méthodes sont en réalité très complémentaires.
Les transformations que nous allons faire ici sont basées sur un fait simple. Pour tout modulateur d'impulsions on peut définir une non-linéarité équivalente dont la sortie reproduit la valeur moyenne de la sortie du modulateur sur chaque période d'échantillonnage. Concrètement, cette non-linéarité, aussi appelée caractéristique statique, reproduit en partie les composantes basse-fréquence du signal modulé. Selon les propriétés du modulateur étudié, cette non-linéarité peut en général être réduite à l'association en série d'opérateurs courants en automatique. C'est le cas pour le modulateur que nous avons utilisé pour l'étude dont on définit la non-linéarité équivalente par l'opérateur Φ défini ci-dessous :

$$\forall z \in \mathcal{L}, \quad \Phi(z) = \begin{cases} 0, & \text{si } |z| < \Gamma_{min} \\ z, & \text{si } \Gamma_{min} \leq |z| < \Gamma_{av} \\ sign(z)\Gamma_{av}, & \text{si } |z| \geq \Gamma_{av} \end{cases} . \tag{1.22}$$

Comme indiqué par sa définition, Φ est défini par l'association d'un opérateur saturation et d'un opérateur zone-morte en série. Pour l'étude, Φ est associée à un échantillonneur-bloqueur, synchronisé à la fréquence d'échantillonnage du modulateur, pour modéliser le caractère discret du PWM. On remarque immédiatement la similitude entre le modèle d'actionneur "nominal" introduit dans la section précédente et la caractéristique statique introduite ici. Ces deux opérateurs peuvent être considérés comme ceux dont l'effet sur le système est le plus proche de l'effet du modulateur. Ainsi les autres opérateurs venant compléter la représentation du système modulé peuvent être considérés comme ayant une influence mineure sur le système complet. L'avantage de la caractéristique statique que nous venons de définir est qu'elle peut être entièrement caractérisée de façon analytique et donc qu'elle se prête très bien à l'analyse IQC. Il va donc de soi de l'introduire dans le modèle d'analyse afin de représenter partiellement l'opérateur PWM dont la description IQC est impossible. Afin de représenter le modèle d'analyse de façon précise, l'introduction de la non-linéarité équivalente en remplacement du PWM implique de compléter le modèle avec un autre opérateur dont la sortie permet de couvrir totalement les trajectoires du modèle d'analyse initial. Ces dernières modifications se font sous des hypothèses sur l'ordre relatif du système nominal initial relativement lourdes dans le cas général mais souvent satisfaites dans le cas des systèmes spatiaux. Finalement, suite à ces transformations le modèle d'analyse final contient un opérateur de perturbation Δ comportant deux entrées et deux sorties. L'effet additionné de ces deux sorties (dont une est produite par l'association Φ/échantillonneur-bloqueur) sur le système nominal reproduit exactement l'effet d'un signal modulé par un PWM. La partie nominale est une extension de la partie nominale de la LFR obtenue initialement en considérant le PWM comme bloc perturbateur. Cette LFR est présentée figure 1.11. Bien qu'apparemment très différente de la LFR de la première étude, il s'agit bien d'un système équivalent à celui représenté figure 1.9. L'analyse de stabilité de la LFR du modèle d'analyse par la théorie des

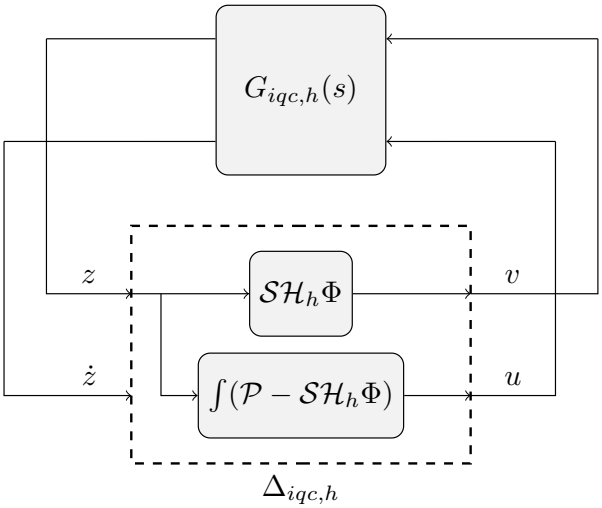

FIGURE 1.11 – LFR of the model for analysis as a pulse-modulated system after coordinate change

IQC est faite en utilisant un test de stabilité similaire au critère de Popov. Il diffère de celui-ci car des modification ont dû être apportées pour prendre en compte l'échantillonneur-bloqueur du modèle. La méthode utilise aussi une contrainte sur l'énergie des sorties de $\Delta_{iqc,h}$. Celle-ci traduit le fait que la sortie de la non-linéarité équivalente a une plus grande énergie que la seconde sortie, exprimant le fait que son influence sur les sorties du système nominal est plus grande. Au cours de l'étude, une contrainte sur le signe des sorties de l'opérateur $\Delta_{iqc,h}$ a été déterminée et utilisée, occasionnant une baisse significative du conservatisme du test de stabilité.

Analyse de stabilité

L'analyse de stabilité par cette seconde méthode a été grandement simplifiée par la modification de l'hypothèse d'utilisation du théorème. En effet, le résultat de la littérature sur lequel nous avons fondé nos recherches utilisait une condition non linéaire d'application du test de stabilité. En transformant cette condition en une inégalité matricielle linéaire (acronyme anglais : LMI), nous avons rendu l'application du théorème aisée. De plus, l'amélioration de la description de Δ par l'ajout d'une nouvelle IQC a permis l'obtention des résultats de la figure 1.12. Sur cette figure apparaît un paramètre du problème non évoqué jusqu'ici. Il s'agit de la constante de Lipschitz de la non-linéarité équivalente que nous sommes contraints de définir comme étant finie ($L_{max} < \infty$) en dépit du fait que la pente de la caracatéristique de notre non-linéarité équivalente soit infinie. C'est pourquoi cette méthode contraint à faire une approximation de la non-linéarité équivalente que l'on peut lier à certaines hypothèses faites lors de l'étude avec la première méthode. Toutefois, les travaux de cette étude ont permis d'améliorer significativement la facilité d'implémentation ainsi que le conservatisme du test de stabilité.

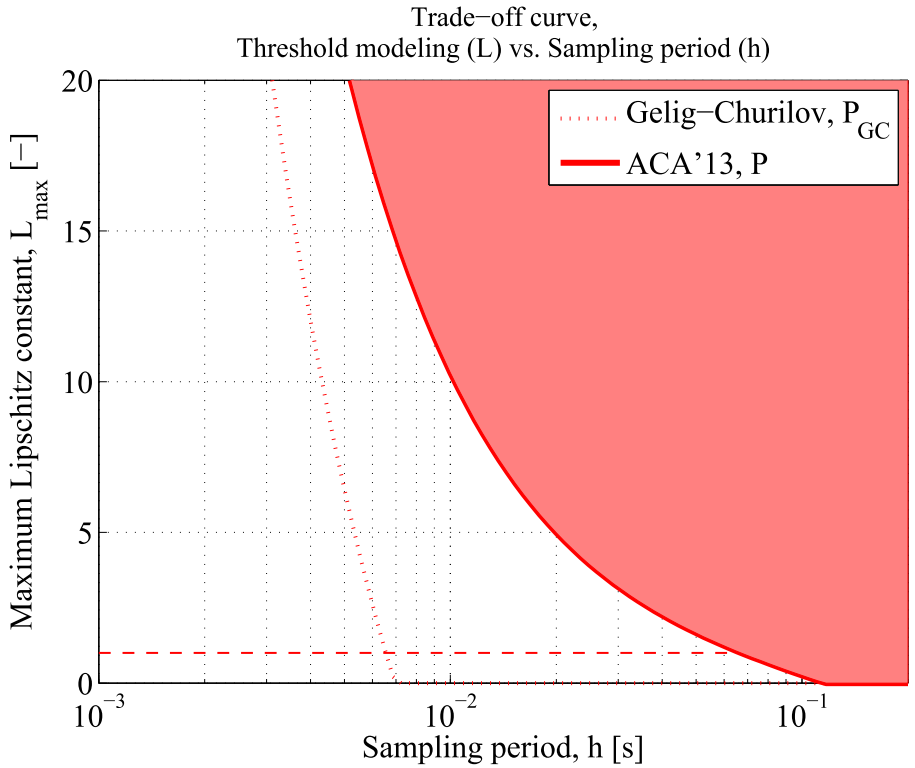

FIGURE 1.12 – Compromis entre la fréquence d'échantillonnage et la représentativité du modèle, les combinaisons (h, L_{max}) sous les courbes sont stables.

1.5.5 Conclusions

Nous avons pu lier deux études du PWM a priori complètement différentes et constater la grande similitude de notre approche pragmatique avec l'approche rigoureuse sur le plan mathématique. Etant donné le fait que les études analytiques de ces systèmes pourtant répandus dans le domaine spatial sont très rares, celles-ci ouvrent des perspectives intéressantes pour de nouvelles études.
D'autre part, les résultats ont montré que l'étude des systèmes à modulation d'impulsion via la description IQC passe par une transformation du modèle et une séparation du PWM en deux opérateurs compatibles avec la théorie et représentatifs de l'effet réel d'un train d'impulsions sur la dynamique passe-bas d'un

lanceur. Une fois ces modifications faites et la stabilité vérifée, deux problèmes majeurs apparaissent. Le premier est le conservatisme encore trop important des tests de stabilité utilisés. Malgré l'augmentation de l'ordre des multiplicateurs utilisés dans la première étude et l'ajout de nouvelles IQC à la description de la seconde étude, il nous a été impossible de prouver la stabilité du système "nominal" cadencé à 1 Hz. Le second problème vient du fait que le traitement de l'effet de zone-morte induit par la durée d'ouverture minimale des tuyères est un élément complexe à traiter duquel résulte nécessairement des approximations du modèle.
Toutefois, les résultats permettent d'envisager de nouveaux développements pour les deux méthodes, voire même une fusion des meilleurs points des deux techniques qui pourraient conduire à des études simples et peu conservatives des systèmes avec PWM.

1.6 Conclusion

Cette thèse intitulée "Analyse de robustesse par Contraintes Intégrales Quadratiques, application aux lanceurs spatiaux" avait pour objectif de préparer l'introduction d'outils analytiques reposant sur les Contraintes Intégrales Quadratiques dans le processus de vérification et validation des lois de commande en phase balistique des lanceurs spatiaux Européens. L'application de ces méthodes aux problématiques d'évaluation de domaines de stabilité et de performance robuste de modèles représentatifs de l'étage supérieur du lanceur et de sa (ses) charge(s) utile(s) permettra à court terme de rendre le processus plus efficace et plus rigoureux. À plus long terme, les perspectives sont très nombreuses et vont de la synthèse de régulateurs robustes à la recherche de pires cas.
Avant cela, il est nécessaire d'évaluer les avantages et inconvénients de l'utilisation d'une telle technique dans le cadre de l'analyse des systèmes spatiaux. De plus, il existe encore des points à améliorer avant une plus large diffusion de ces techniques.
Les ingénieurs en contrôle se heurtent en règle générale à deux problèmes lors de l'étude des marges de stabilité du lanceur dans le domaine fréquentiel. Le premier est le caractère non-linéaire intrinsèque à la physique du mouvement de rotation d'un solide rigide. Le second est le fonctionnement en mode "tout-ou-rien" des actionneurs dédiés au contrôle d'attitude introduisant lui aussi une forte non-linéarité dans le système. Dans ces deux cas les méthodes de l'automatique classique sont inadaptées ou inexactes. Avec la théorie des IQC, il est possible de prendre en compte un modèle d'analyse représentatif du système de façon parfaitement rigoureuse, sans approximation. C'est là tout l'intérêt de la méthode. De plus, de nombreux résultats tels que la μ-analyse, le théorème du petit gain ou le critère de Popov se trouvent être des cas particuliers du principal théorème de stabilité de la théorie des IQC. Cela implique qu'en règle générale, une analyse IQC d'un système ne peut qu'être moins conservative qu'une analyse avec ces méthodes plus classiques. A ces avantages s'ajoutent une grande modularité ainsi qu'une implémentation aisée du test de stabilité sous forme de LMI dans le cas où LPVMAD ne suffit pas.
Il existe deux principales contreparties à ces nombreux avantages. Tout d'abord, la théorie en elle-même n'est pas très lisible pour les ingénieurs qui pourraient l'utiliser. Bien qu'il soit possible d'interpréter cette théorie par des arguments énergétiques, cela freine l'adoption de cette technique au détriment des méthodes $\mathcal{H}_\infty$ ou de la μ-analyse, plus lisibles et plus en correspondance avec la formation des ingénieurs en exercice actuellement. Le second problème rencontré par la théorie des IQC est lié au fait que l'implémentation du test de stabilité repose sur des LMI dont la taille devient très vite trop grande pour que le problème puisse être résolu sur une machine de laboratoire classique. Ce problème a été rencontré lors des travaux de la première application où la représentativité du modèle a dû être diminuée lors du test de performance robuste. C'est pourquoi la compacité de la modélisation sous forme LFR a une importance cruciale. Bien entendu, les avancées en capacité de calcul devraient permettre de progresser en termes de représentativité des modèles d'analyse mais on attend aussi des progressions quant à l'exploitation de la structure des problèmes LMI posés avec la théorie des IQC.

La première application a permis de définir une représentation sous forme de LFR des équations régissant le mouvement de rotation d'un solide rigide autour de son centre de gravité. Bien que conséquente, la taille de cette LFR ne semble pas être réductible en conservant le type de factorisation utilisé. Toutefois, des études de sensibilité ou de nouvelles factorisations devraient rendre possible la réduction de cette taille sans conduire à des pertes de représentativité. L'étude de stabilité robuste a permis de montrer la stabilité du modèle pour un vaste domaine d'incertitudes sur les termes de la matrice d'inertie. De plus, l'étude de performance dans les domaines temporel et fréquentiel a mis en évidence la forte influence d'un actionneur de type saturation sur la performance robuste du système. Les limites des capacités de résolution de problèmes LMI ont été atteintes obligeant à des simplifications du modèle d'analyse.
La seconde application était dédiée à la seconde problématique soulevée par les partenaires du projet. Il s'agissait d'étudier l'influence de l'actionneur "tout-ou-rien" sur la stabilité robuste du modèle de lanceur. Plusieurs méthodes a priori différentes ont été utilisées. La première reposait sur une modélisation pragmatique de l'effet du PWM sur la vitesse angulaire d'un modèle simple de lanceur et l'utilisation de la toolbox Matlab® LPVMAD. La seconde comportait des transformations du système motivées par des arguments pratiques sur la représentation d'opérateurs par des IQC. Au final, il est apparu que les méthodes utilisées étaient en réalité très similaires sur le plan de la modélisation. Au cœur de cette dernière, l'hypothèse que ce sont les harmoniques basse-fréquence du signal modulé qui dirigent le système et non les harmoniques de haute-fréquence. Les résultats produits à partir de cette représentation du système semblent prometteurs et offrent de nombreuses perspectives d'extensions.
Cette thèse a permis de mesurer le grand potentiel de la théorie des IQC pour l'analyse de systèmes non-linéaires complexes. Les méthodes fondées sur la théorie de Lyapunov qui ont été comparées aux techniques IQC ont à chaque fois donné des résultats plus conservatifs. Sur le plan de l'analyse, de nombreuses questions restent encore ouvertes : le traitement des équations de la cinématique, la modélisation de l'effet du PWM sur un modèle tridimensionnel, la prise en compte rigoureuse des couples gyroscopiques, etc. Poursuivre les études sur ces sujets permettra certainement de traiter le problème de la dynamique complète associée à un actionneur de type modulateur d'impulsions. A plus long terme, les analyses de stabilité et de performance avec des outils analytiques auront des répercutions directes sur la synthèse de correcteurs robustes. En effet, la plupart des résultats d'analyse évoqués dans cette thèse peuvent être utilisés pour la synthèse de correcteurs. Ainsi, utiliser ces méthodes pour systématiser le réglage des gains des correcteurs permettra de produire plus efficacement et plus rapidement des lois de commande à même de satisfaire le processus de validation conduisant à des économies de moyens et des garanties plus rigoureuses sur le comportement du lanceur.

Chapter 2

Introduction

In the aerospace field, the Validation and Verification (V&V) process is a crucial phase of the construction of space launchers. This stage usually takes place between development and production of the rocket but it influences both upstream and downstream works. In the course of the V&V process, the goal of the engineers is to establish whether a given design of the launcher is going to fulfill the technical specifications of the mission or not. These technical specifications concern the physical limitations of the launcher structure but also the fact that the launcher has to cruise along a trajectory with the aim to deliver its payload at the right orbital position and in a specific attitude and angular speed setup. The setting and tracking of this flight path is realized by on-board Guidance Navigation and Control (GNC) systems. The function of the GNC systems is to make the vehicle follow the trajectory it sets to achieve the mission while satisfying the numerous requirements of payload release. In addition to these intrinsic constraints, the environmental conditions are changing dramatically over the mission and the launcher also has to face these perturbations without compromising its flight. In such a framework, robust V&V of control laws and the associated Attitude Control System (ACS) allows assessing the ability of the launcher to fulfill its mission. Consequently, it is a key phase since GNC systems are both mission critical and safety critical. Not only it is required that the launcher flies, but it has to fly according to the flight plan within a tight flight envelope and without putting at risk the surroundings, the payload or itself. In the case when the V&V process fails because the requirements are not fulfilled, expensive modifications of the launcher are planned and months of development can be reconsidered in order to obtain the flight certification.

Today, in the industry, V&V relies essentially on time-domain analysis techniques. Methods based on Monte-Carlo simulations are extensively used in all space programs over the globe, see as examples [Hanson and Beard, 2010], [Jang et al., 2008] or [Falcoz et al., 2010]. The setup of such validation techniques is rather simple, based on a highly accurate and representative simulation model, thousands of flight simulations are run. The differences between each run are in the value of the launcher parameters and the flight conditions. These characteristics are chosen over a set of predefined feasible values. The range of feasible values are set such that all possible flight conditions are covered. For instance, the parameters can be the initial mass repartitions, the force delivered by the thrusters, the propellant pressure. Concerning the flight conditions, it can be wind gusts or atmospheric parameters. After a batch of simulations, a verification of the technical specifications and of all the flight parameters is done to assess if no constraint is violated and to check that all requirements are met. As an example, we verify that the angular speed remains in a given domain, that the thrusters are set to ON less than given duration during the flight, etc. When one of the technical specifications is not achieved or when a constraint is violated, the simulated mission is considered to be failed. Then from the ratio of failures to successes, a probabilistic guarantee of "good" behavior of the launcher is obtained. After this, certification is given

when a certain level of confidence is reached.

In this context, the requirements are so stringent that V&V is costly and very time consuming with this so-called time-domain method. In addition to the duration issue, the main drawback of this method is that the random choice of the parameters over their predefined range of feasible values does not guarantee that all the possible parameter combinations are investigated. The same thing can also be said about flight conditions or other external perturbations. Indeed, it is possible that the "worst" parameter combination does not lie in the randomly sampled parameter combinations of the parameter ranges. Formally, we have a continuous set of flight conditions for the space launcher and we only obverse discretely sampled parameter combinations within this set. After, from this data only, some conclusions about the behavior over the whole set of flight conditions are drawn. It can cause some reliability issues for systems which are highly nonlinear as space launchers. Indeed, such methods give no rigorous guarantee concerning the stability and performance due to the observation of discrete operating points. The "certificate" that is obtained solely consists in a probability of success of the mission. Thanks to the supposed accuracy of the simulation model, this "certificate" ensures that in a very large majority of cases, the flight will be a success. However, no rigorous guarantee can be obtained about the behavior of the launcher over the whole set of parameters and flight conditions. This is prejudicial for our industrial partners as it can lead to late and costly redesigns when a trouble making parameter combination is found at the end of the V&V process. From a more pragmatic point of view, a certificate of stability and performance of the launcher over a vast flight envelope would be a strong argument during negotiations with customers.
These are some of the reasons why our industrial partners aim to use and adapt new techniques for control law validation that would provide more guarantees about the mission success through a more rigorous V&V.

The methods that give a mathematically rigorous certificate of "good" behavior are called analytical methods. They are tools that can be used to prove stability and performance of systems through an appropriate mathematical modeling. The model, in our case a space launcher model, depends on the method to be used and has to "fit" in the framework of the tool. This is why before starting the analysis, it is needed to determine the system we want to analyze and to define a model of it. To carry out analytical validation, the recommended approach is different from the approach for time-domain V&V. The main consequence of the use of analytical methods is on the level of accuracy of the models we will be able to analyze. Therefore, the analysis will be done on models that are not as representative of the system as those used for Monte-Carlo validation. Hence, we will rely on simplified models that can fall into the mathematical framework of the method to be used. In order to simplify the models without loss of representativeness, the first step should be to answer the questions: *what is the phenomenon to be studied? what behavior the system is expected to have in this situation? what element in the loop is the cause of such behavior? what part of the system is not influencing the behavior so much?* In our case, answering to these questions will allow specifying a model of the space launcher whose trajectories cover representatively the trajectories of the actual launcher, with eventually as side-effects, approximations or conservatism. At this point, the knowledge that the system engineers have about the behavior of the launcher is crucial to guide the simplification process and chose approximations that do not erase the subsystems and parameters which influence most the operation of the launcher. This step done cautiously, it should result in an analysis model that is representative of what we want to study but that is simple enough to be assessed with analytical tool. After the modeling step, considering the characteristics of the analysis model and with good knowledge of the available analytical tools, we should be able to select the formal method that is most suitable to assess the analysis model in terms of robust stability and robust performance. Robustness analysis has exactly the same purpose as V&V. Its goal is to address the consequences of the presence of "trouble making" elements in a system on stability and more importantly

on performance. From a control system engineer point of view, by "trouble making", we understand elements that cannot be taken into account by classical linear stability and performance analysis. For instance, these elements are the flight parameters we select randomly for Monte-Carlo simulation such as uncertain inertia parameters, variations of propellant mass, etc. It also relates to nonlinear perturbations such as saturation phenomena or transmission delays.
Finally, in a setup that may seem more restrictive than Monte-Carlo framework, various tools allow to perform robust reliable V&V of representative models.

Based on these considerations, a robust stability and performance certificate on a sufficiently representative model of a launcher should allow our industrial partners to strengthen their Monte-Carlo simulation results by giving a confirmation of the results obtained with the time-domain approach. Of course, the aerospace domain has specific needs and developing dedicated analytical V&V tools may, in the future, give them more and more influence as they might not remain limited to stability analysis. Firstly, we can think of improved Monte-Carlo simulations where the parameter selection is not random anymore but driven by an analytical tool which looks for worst cases in its framework. Such worst case search is done with μ-analysis in [Balas et al., 2005] for systems with time-invariant uncertainties with encouraging outcomes. Secondly, we can also think of using the tools upstream during control law synthesis in order to reduce the number of controller re-tunings. Here again, structured singular value based tools have already been used, see e.g. [Fujita et al., 1995]. The advanced tools we aim to use are not ready yet for direct applications to design but a first step in this direction is to use the methods for complex robust stability analyzes in order to point out and understand the lacks in the theory and to continue their development for further applications. Indeed, these methods are also powerful when dealing with robust performance or controller synthesis but only a solid stability analysis framework will enable us to go further.

Despite these encouraging facts and promising outlooks, we observed in the industry that the analytical tools in use are not always used in the most fruitful way. Most of them are suitable for V&V of complex systems such as space launchers but the results they give are not understood well enough. As mentioned above, the mathematical tools available for control law V&V are all based on a model of the system of interest. Depending on the tool, the model has to fulfill certain constraints. Since these constraints can be quite strong e.g. linearity, time-invariance, nominal stability, etc; they can lead to very rough approximations of the system at the price of a loss of representativeness of the analysis model. To avoid this drawback, two key factors must be taken into account. First, the tool needs to be appropriate with regard to the analysis model. For instance, if one of the fundamental property of the system is to be time-varying, only the use of certain tools is relevant. They will allow to represent that property in the analysis model and will account for it during the analysis. Such methods will give meaningful stability results. On the contrary, some analytical techniques are not suited for time-varying systems analysis and the results they will eventually give will make no sense. As an example, the μ-analysis cannot be used for validation of time-varying systems. Secondly, as a repetition from previous paragraphs and as a consequence of the first remark, the modeling has to be done with care for the representativeness of the model. Please notice that we make a difference between representativeness and accuracy. Indeed, since state-of-the-art formal tools are not ready yet to handle highly complex space systems, we have to rely on simplified representations of them. Fortunately, these simplifications are not always deleterious but they must be done with a good idea of their outcomes on the representativeness of the model and the consequences on the interpretation we can make of the stability or performance result. Although the framework can be seen as restrictive, it should be exploited at best.

Currently, the main gap between analytical tools and industrial applications is the theory. It manifests through the issues we alluded to in the previous paragraph. In facts, the theoretical building blocks

of the analytical techniques are not always readable enough for an efficient implementation and industrial use. It causes the integration of the tool to be arduous and slow. ESA projects as the one resulting in the delivery of the LPVMAD tool [Köroglu et al., 2008] aimed to provide a wider access to these tools for research and industry. They give a mean to engineers to investigate the properties of their systems with advanced tools and to get an overview of the underlying theoretical results.

Following this path, the ESA NPI sponsored PhD for *Nonlinear multivariable analysis techniques for validation of launcher GNC systems*, contract number 4000103804 led during these three years by the European Space Agency (ESA) and Astrium Space Transportation (Astrium ST) aimed to make use of the IQC theory and the LPVMAD tool in the context of robust V&V of control laws for ballistic flight of space launchers. To do so, the work was structured according to a classical robustness analysis. First, the main features and characteristics of a space launcher in ballistic flight are enumerated. Followed immediately a precise definition of a so-called pre-analysis model. This modeling stage allowed us to spot the key subsystems of the model under the supervision of our industrial partners i.e. those affecting most the launcher on a behavioral point of view. We were also guided by their need for better knowledge and better representation of the subsystems in an analytical validation framework. Here our industrial partners had precise needs corresponding to issues met in the past while attempting to provide rigorous robust stability certificates. Two key components were defined. They are the dynamic model based on the equation of motion and kinematic equation, and the ACS actuator with particular modeling of the thrusters. From the pre-analysis model, analysis models were built to address the robust stability of models involving the main problems with Integral Quadratic Constraints (IQC) based analytical results. This work has been done keeping in mind that the representativeness of the analysis models was crucial and that the pre-defined key features should be preserved. After these preparation steps we looked inside the toolbox and in the literature in order to analyze our models. The implementation of these studies were made easier by the tool LPVMAD since it is well suited for analysis in the classical IQC framework. Nevertheless, the specificity of space launchers subsystem drove us outside the classical IQC framework for the analysis of pulse-modulated systems leading to ad-hoc implementations needed to perform the stability analysis. Finally, the IQC analysis techniques but also others analytical results have been involved in the assessment of the robust stability and robust performance of the widely unknown, uncertain, highly nonlinear and time-varying space launcher analysis models.

This thesis contains four main chapters. In chapter 3, we present the space launcher model that is to be studied. It is the "pre-analysis" model mentioned in the above paragraphs. Even though it is already simplified, it contains the most important features of a real launcher and describes its motion in a representative fashion. The controlled closed-loop has a very classic structure and we describe the subsystems independently in accordance to the data given by our industrial partners. This structure and the components in the pre-analysis system led to the choice of the formal tool described along the lines of chapter 4. In this chapter, we define the framework in which we can perform IQC based robust stability analysis. From control system basic definitions and properties, we introduce the IQC analysis context. It is emphasized that IQC are a mean of representation of operators. Simple examples are presented for the reader to get used to the notations and the methods generally employed to derive valid IQC descriptions of operators. These definitions set up the conditions for IQC stability theorems. We present two theorems relying on different kinds of IQC with the aim to remind to the reader that IQC must, in the first place, be seen as a tool for operator description and that afterward this representation can be useful to reach different kinds of stability results. Finally, we dwell on particular widely used multipliers implemented in LPVMAD. Their mathematical construction is given for simple cases, still with the will to show how multipliers can be built. The chapters 5 and 6 are dedicated to the application of the theory and the presentation new results obtained during the project. The general outline of the applications studied during this thesis follows the steps described in the previous paragraph. Chapter 5 deals

with the first key feature of the model: the nonlinear uncertain equation of motion is studied. Driven by the IQC multipliers available in LPVMAD, a factorized expression of Newton's equation is defined. For this analysis model we intend to address the robustness issues in the face of inertia uncertainties and constrained control inputs. We perform the corresponding robust stability and robust performance analyzes. Finally, in chapter 6 we present our works done on the second key problem pointed out by our industrial partners which is the ACS involving thrusters modeled as pulse-modulators. In order to perform the stability analysis of this pulse-modulated system, three different results have been used to face the issues caused by pulse-width modulation on robust stability. First, an approach relying on the description of the pulse-modulator with multipliers from the literature leads to a new representation of the PWM and promising results obtained with LPVMAD in the classical IQC framework. The results are then compared to the ones obtained for a Lyapunov based method. Finally, we established a link between our works and a promising approach relying on loop transformations and hard-IQC description of pulse-modulated systems. Further works in this direction gave promising stability results that are presented there. It is also emphasized that this framework could be at the basis of new improvements in the analysis of pulse-modulated system. The last chapter contains the conclusions and outlooks while two appendices are dedicated to the description of classical IQC multipliers and other perspectives for the improvement of the analysis of pulse-modulated systems.

This PhD was performed in the frame of an ESA/NPI sponsored project for "Nonlinear multivariable analysis techniques for validation of launcher GNC systems", contract number 4000103804.

Chapter 3

Space launcher description

3.1 Introduction

The goal of this first chapter is to define the system we are going to analyze. The system we study is the upper-stage of a space launcher with its payload during exo-atmospheric flight. We will refer to the upper-stage with its payload as "the launcher", "the space vehicle" or simply "the vehicle". As mentioned in the introduction, the project aims to use and develop advanced analytical methods to analyze the behavior of space vehicles. Such a study was considered in order to complement and improve the time-domain tools and methods currently in use in the industry for control law validation.
Indeed, current V&V essentially relies on simulations due to the complexity of the system. It is also the reason why analytical tools are not easy to use for the validation process. The model of the space launcher that we are going to define exhibits features which are known to be trouble making for a control system engineer willing to perform analytical control law validation. It has been defined with the knowledge of the industrial partners of the project who had already determined some issues to be addressed before being able to perform analytical control law validation. As a consequence, the model is simplified and does not have all of the real launcher features. However, it was built with the know-how of ESA and EADS Astrium GNC engineers. Consequently, it captures the main characteristics of the behavior of an actual space launcher and so it is considered representative of its behavior. For a better understanding of the studies to come, we will focus only on the model of the launcher that has been defined and used for the analysis.
In the sections to come, we define each part of the model separately.

3.2 Dynamics of a space launcher

3.2.1 Introduction

The following section aims to setup the dynamic model. The motion of the space launcher is defined with respect to a reference frame using Newton's equation of motion of a three degree-of-freedom rigid body. Some of the features of the equation are investigated to give a first overview of the characteristics of the vehicle and of the properties that may cause troubles in the course of the V&V process.

3.2.2 Frames definition

The first step of the model description is to define the frames that are going to be used during the study. These frames will allow describing the motion of the launcher in space. Indeed, to describe the motion, it is required to establish the frames with respect to which we want to observe and analyze the motion.

Four frames will be considered for this study.
The physical system we observe is a space vehicle orbiting around the Earth during the so-called ballistic phase of its mission. The ballistic phase is a phase for which we assume the vehicle does not change its translational speed and so keeps the same orbit. The absence of change in the translational motion is due to the fact that we consider that no forces are applied to the vehicle as the residual friction of the atmosphere is negligible. Hence the translation of the vehicle around the Earth is not taken into account during these works. As a consequence of that, the motion we will be interested in will be the rotation of a rigid body around its center of gravity. In our case, it will be the rotational motion of a rigid space launcher around its center of mass denoted by G. This is the reason why we first define the reference frame $\mathcal{R}_{ref}$ centered at G. $\mathcal{R}_{ref}$ moves with the vehicle center of gravity i.e. with G, along the orbit trajectory. For convenience, we assume that the orbit is circular. The first axis X_{ref} is collinear with the translational velocity vector that is tangent to the orbit. The second axis is denoted Y_{ref} and points toward the center of the trajectory i.e. the center of the Earth. As we consider a Keplerian circular orbit, Y_{ref} is perpendicular to X_{ref}. The third vector Z_{ref} completes the orthogonal direct basis. Finally we assume that $X_{ref}, Y_{ref}, Z_{ref}$ are unitary vectors to make the basis unitary.
The second frame is the geometrical frame of the launcher $\mathcal{R}_g$. The center of $\mathcal{R}_g$ is defined to be G. This frame is defined by the geometry of the vehicle and its symmetry axes. Even though a space launcher is almost never symmetric, the axes of $\mathcal{R}_g$ are defined by the general shape of the launcher as in figure 3.1. $\mathcal{R}_g$ is fixed with respect to the launcher. The first axis X_g corresponds to the longitudinal axis of the launcher. Again, even though it is not symmetric at all, the vehicle formed by the upper-stage and the payloads is usually longer than it is deep or wide. We will say that generally this is the axis pointing upward when the launcher is on the launch pad, or pointing toward the direction of the orbital motion in space. Axes Y_g and Z_g are defined the same way and define an orthonormal basis. We refer to X_g as the longitudinal axis while Y_g and Z_g are called transverse axes. Figure 3.1 represents how $\mathcal{R}_g$ is defined with respect to the vehicle geometry. As it is defined and since it is fixed to the vehicle, $\mathcal{R}_g$ represents the attitude of the vehicle. Hence the position of $\mathcal{R}_g$ with respect to $\mathcal{R}_{ref}$ is the one that matters to us as we will see later on.

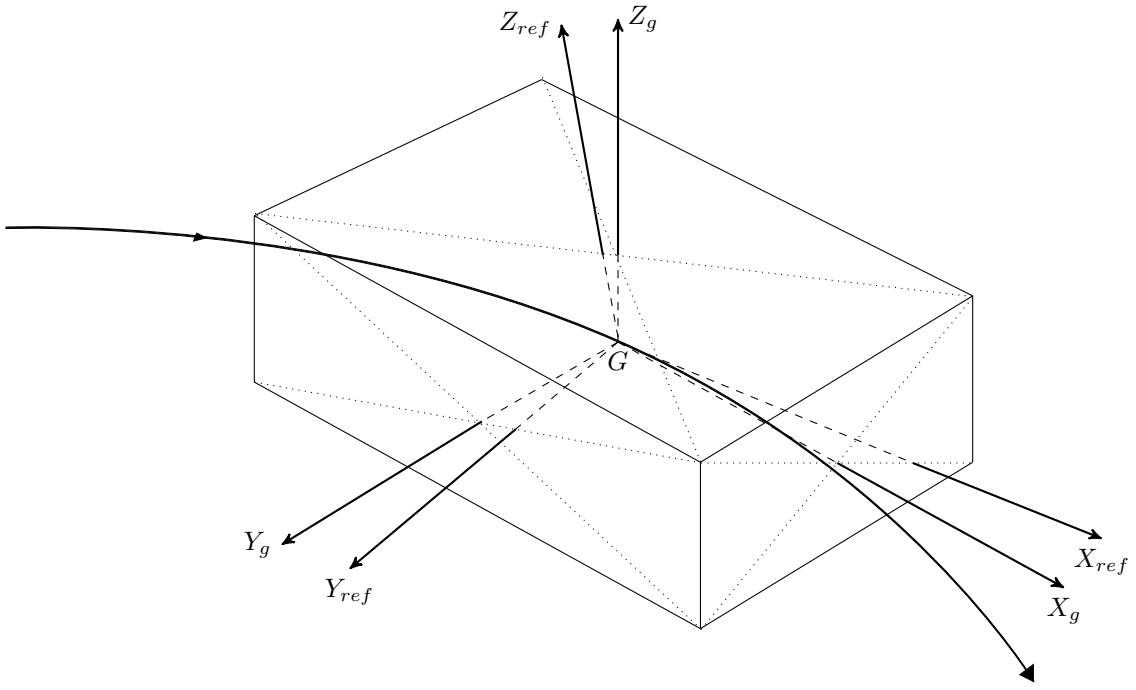

Figure 3.1: Frames $\mathcal{R}_{ref}$ and $\mathcal{R}_g$

Another frame is linked to the vehicle and is centered at G. It is the inertial frame $\mathcal{R}_p$. This frame (X_p, Y_p, Z_p) is the principal frame of inertia of the launcher. By definition, the inertia matrix of the launcher expressed in this frame is diagonal as in (3.2). Moreover, since $\mathcal{R}_p$ is fixed with respect to the launcher it results from a fixed rotation of $\mathcal{R}_g$.
Finally, the last frame to be defined is the aimed frame $\mathcal{R}_{aimed}$. This frame is also centered at G and represents the aimed position of $\mathcal{R}_g$. During a maneuver, the aimed frame sets the ideal trajectory that the geometrical frame $\mathcal{R}_g$ is supposed to follow. During the flight, the Attitude Control System (ACS) aims to superimpose $\mathcal{R}_g$ and $\mathcal{R}_{aimed}$ at all time.
To summarize, the motion of the vehicle is expressed with respect to $\mathcal{R}_{ref}$. The role of attitude control is to make $\mathcal{R}_g$ overlap $\mathcal{R}_{aimed}$ since the latter represents the position we want $\mathcal{R}_g$ to have with respect to $\mathcal{R}_{ref}$.

3.2.3 Equation of motion for a rotating rigid body

The physical dynamic system to be considered during this study is made of the upper-stage of the launcher and the payload (satellite(s), transfer vehicle, etc.) in ballistic flight. Since at that moment of the mission, this assembly is rather stocky as it has no solar panels, we can assume that it is rigid and so that there is no torsion of the body exciting flexible modes. This assumption also covers the fact that we do not consider the possible motion of the liquid propellant in the tanks since they would also manifest similarly to flexible modes. This phenomenon called sloshing does not enter the scope of our study. Furthermore, as mentioned before, the exo-atmospheric flight allows considering rotational motion only as there is no residual atmosphere and no "boost phase" which would need to take into account the application of forces to the launcher. As a consequence, the equations representing the rotational motion of the rigid space launcher are based on angular momentum theorem (3.6) and describes the effect of the application of external torques on the angular accelerations of the launcher. This theorem requires to choose the frame to be used in order to define the associated inertia matrix, angular speed and external torque. We represent the motion of the vehicle in the geometrical frame $\mathcal{R}_g$ as it represents the geometry of the launcher. This is important since the antennas or tanks for propellants have their position expressed in this frame.
Firstly, the inertia matrix of the vehicle in the geometrical frame $\mathcal{R}_g$ is:

$$I_g = \begin{bmatrix} I_x & -I_{xy} & -I_{xz} \\ -I_{xy} & I_y & -I_{yz} \\ -I_{xz} & -I_{yz} & I_z \end{bmatrix} \text{ with } I_x, I_y, I_z > 0 \text{ and } I_{xy}, I_{xz}, I_{yz} \geq 0. \tag{3.1}$$

This matrix results from the change of coordinates applied to the inertial frame $\mathcal{R}_p$ inertia matrix

$$I_p = \begin{bmatrix} I_1 & 0 & 0 \\ 0 & I_2 & 0 \\ 0 & 0 & I_3 \end{bmatrix}, \tag{3.2}$$

and can be expressed as a function of I_p and the rotation matrix $R \in \mathbb{R}^{3\times3}$ as $I_g = RI_pR^{-1}$. In the case when the launcher is axisymmetric with respect to the axes of $\mathcal{R}_p$, the inertia matrices I_p and I_g are diagonal and equal. All the terms in the inertia matrices are homogeneous to kg.m^2. The terms of the

inertia matrix I_g can be obtained using the formulas:

$$\begin{cases} I_x = & \int_{sv}(y^2+z^2)dm \\ I_y = & \int_{sv}(x^2+z^2)dm \\ I_z = & \int_{sv}(x^2+y^2)dm \end{cases} \text{ and } \begin{cases} I_{xy} = & \int_{sv} xy\, dm \\ I_{xz} = & \int_{sv} xz\, dm \\ I_{yz} = & \int_{sv} yz\, dm \end{cases}, \tag{3.3}$$

where (x, y, z) is the position of the infinitesimal mass element dm of the space vehicle sv with respect to the center of $\mathcal{R}_g$. To express the angular momentum theorem, we also define two vectors: the angular speed of the vehicle $\omega \in \mathbb{R}^3$ expressed in $\mathcal{R}_g$ by

$$\omega = \begin{bmatrix} \omega_x \\ \omega_y \\ \omega_z \end{bmatrix} \text{ in rad.s}^{-1}, \tag{3.4}$$

and the torque applied to the vehicle $\Gamma \in \mathbb{R}^3$ expressed in $\mathcal{R}_g$ by

$$\Gamma = \begin{bmatrix} \gamma_x \\ \gamma_y \\ \gamma_z \end{bmatrix} \text{ in Nm.} \tag{3.5}$$

Finally, using the above definitions (3.1), (3.4) and (3.5), we can write the equation of motion of a rotating rigid body in the geometrical frame $\mathcal{R}_g$ as:

$$\dot{\omega} = I_g^{-1}\left[\Gamma - \omega \times (I_g\omega)\right]. \tag{3.6}$$

(3.6) is expressed in the geometrical frame $\mathcal{R}_g$ with I_g being in general a full 3×3 matrix. However, it is worth noticing that (3.6) expressed in the inertial frame $\mathcal{R}_p$ leads to the famous Euler equation for a rotating rigid body which can be found in [Sidi, 1997] or in [Hughes, 1986].

To get another mathematical expression for (3.6), we introduce the matrix representation of the cross-product.

3.2.4 Cross-product expression

It is convenient to rewrite the cross-product $\omega \times I_g\omega$ from (3.6) as a matrix product. For this we need to introduce the skew-symmetric ω dependent matrix P:

$$P = \begin{bmatrix} 0 & -\omega_z & \omega_y \\ \omega_z & 0 & -\omega_x \\ -\omega_y & \omega_x & 0 \end{bmatrix}. \tag{3.7}$$

P depends on the components of the angular speed vector that are ω_x, ω_y and ω_z from (3.4). Using the matrix expression of the cross-product, (3.6) can be recast into

$$\dot{\omega} = I_g^{-1}\left(\Gamma - P(\omega)I_g\omega\right), \tag{3.8}$$

where the dependence of P in the angular speed is denoted by $P(\omega)$. This notation of the gyroscopic coupling term as a matrix product is more convenient for building the simulator. We will see later on in chapter 5 that this representation of the cross-product can be exploited to perform the stability analysis.

3.2.5 Acceleration expression

From (3.8), we observe that the angular acceleration of the vehicle is generated by two distinct terms which are Γ and $P(\omega)I_g\omega$. Both of them are homogeneous to torques expressed in Nm. The first one is the external torque applied to the system. It is denoted by Γ. Γ is partly produced by the thrusters of the ACS that generate the component Γ_{ACS}. Other external perturbations are gathered in Γ_{dist}. Mainly, Γ_{dist} is caused by solar wind, solar radiations, residual atmosphere, earth oblateness, surrounding bodies attraction, etc. Hence Γ can be written as:

$$\Gamma = \Gamma_{ACS} + \Gamma_{dist}. \tag{3.9}$$

The second "torque" applied to the launcher according to (3.8) is

$$\Gamma_{gyro} = -P(\omega)I_g\omega. \tag{3.10}$$

It is referred to as gyroscopic coupling torque in Nm. The definition in (3.10) shows that $\Gamma_{gyro} \neq 0$ as soon as the angular velocity vector is non zero. Thus contributors to Γ_{gyro} are rotational motion ($\omega \neq 0$) and the asymmetry of the launcher i.e. when any of the off-diagonal terms in the inertia matrix I_g (3.1) is non-zero.

3.2.6 Torque for control

From the previous paragraphs, we can recast the equation of motion (3.8) into

$$\dot{\omega} = I_g^{-1}\left(\Gamma_{ACS} + \Gamma_{dist} + \Gamma_{gyro}\right), \tag{3.11}$$

where the torque delivered by the ACS is Γ_{ACS}, Γ_{dist} represents external disturbing torques and Γ_{gyro} represents internal disturbing torques. Since the total disturbing torque $\Gamma_{dist} + \Gamma_{gyro}$ can be evaluated a priori, we can determine the needs in ACS torque for attitude control. Basically, Γ_{ACS} needs to be at least as large as $\Gamma_{dist} + \Gamma_{gyro}$ to keep control of the vehicle. For the case we are interested in, we consider the disturbing torque Γ_{dist} to have components which are constant or with sinusoidal variations of known magnitude.
As a preliminary study, we can compute Γ_{gyro} for angular velocity vectors ω within the usual flight envelope of space launchers during ballistic flight and compare it with the feasible values of Γ_{ACS} to define the region of the flight envelope where $\Gamma_{gyro} < \Gamma_{ACS}$.

Example 1 (Amplitude of gyroscopic couplings) *To perform this preliminary study, we choose two different inertia matrices $I_g^{(1)}$ and $I_g^{(2)}$ to evaluate the norm of the torques resulting from gyroscopic couplings. The goal is to evaluate what are the values of ω_y and ω_z that produce a vector Γ_{gyro} with all of its components below Γ_{ACS} feasible values for a given range of longitudinal angular rate $\omega_x \in [-\omega_x^{max}, \omega_x^{max}]$ and $\omega_x^{max} \in \{\omega_1^{max}, ..., \omega_n^{max}\}$. We set:*

$$I_g^{(1)} = \begin{bmatrix} 22500 & 0 & 0 \\ 0 & 42000 & 0 \\ 0 & 0 & 44000 \end{bmatrix} \text{ and } I_g^{(2)} = \begin{bmatrix} 22500 & -50 & -1100 \\ -50 & 42000 & -250 \\ -1100 & -250 & 44000 \end{bmatrix}$$

for the inertia matrices and we consider that the components of Γ_{ACS} *range in:*

$$\Gamma_{ACS}^{(min)} = -\Gamma_{ACS}^{(max)} = \begin{bmatrix} -400 \\ -200 \\ -100 \end{bmatrix} \leq \Gamma_{ACS} \leq \begin{bmatrix} 400 \\ 200 \\ 100 \end{bmatrix} = \Gamma_{ACS}^{(max)}. \tag{3.12}$$

We will see later on how Γ_{ACS} *varies within this range. The subsets of* $\mathbb{R}^2$ *presented in figures 3.2 and 3.3 show the values of the transverse angular speeds* (ω_y, ω_z) *for which* Γ_{gyro} *can get larger than those of* Γ_{ACS} *presented in equation (3.12) even for small transverse angular speeds when the launcher is spinning at a given angular rate* ω_x*. The regions are also getting smaller and change shape when the vehicle is asymmetric. For instance on figure 3.3, the large coupling term* I_{xz} *severely reduces the size of the region in which the available torque is large enough in the vertical direction. Hence, the maneuvers that the vehicle is expected to do will have to account for control capabilities and avoid too large transverse angular speeds. In particular, ACS dimensions and also acceleration requirements will be chosen such that* Γ_{ACS} *is always large enough to keep control of the vehicle. The notion of available torque will be defined in section 3.7.*

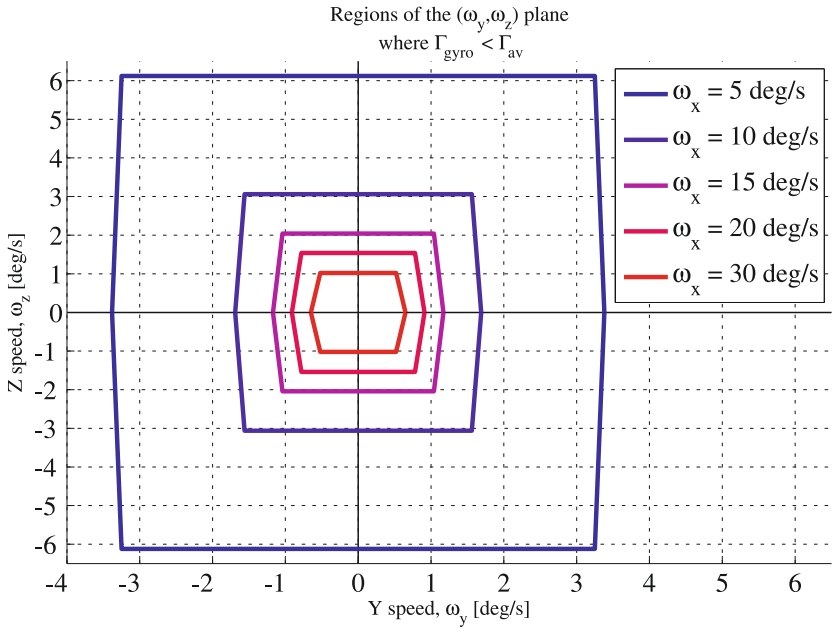

Figure 3.2: Regions where $\Gamma_{gyro} < \Gamma_{ACS}$ in the (ω_y, ω_z) plane, diagonal inertia matrix $I_g^{(1)}$.

3.2.7 Block diagrams

Finally, to give a clearer representation of the dynamic equation for rotational motion of a three-dimensional rigid body whose different expressions are defined in (3.6-3.8-3.11), we give a block diagram in figure 3.4. It shows how the gyroscopic couplings Γ_{gyro} have the effect of disturbing torques generated by the angular speed of the vehicle and asymmetries in the masses repartitions.
Later on in the overall system representation, the "feedback" path generating Γ_{gyro} will be merged into a single block leading to the representation figure 3.5. The state variable of this block is $\omega \in \mathbb{R}^3$. Hence figure 3.4 will be presented in a more compact way which will be more convenient for future representations of the closed-loop system, especially the final block diagram in figure 3.29.

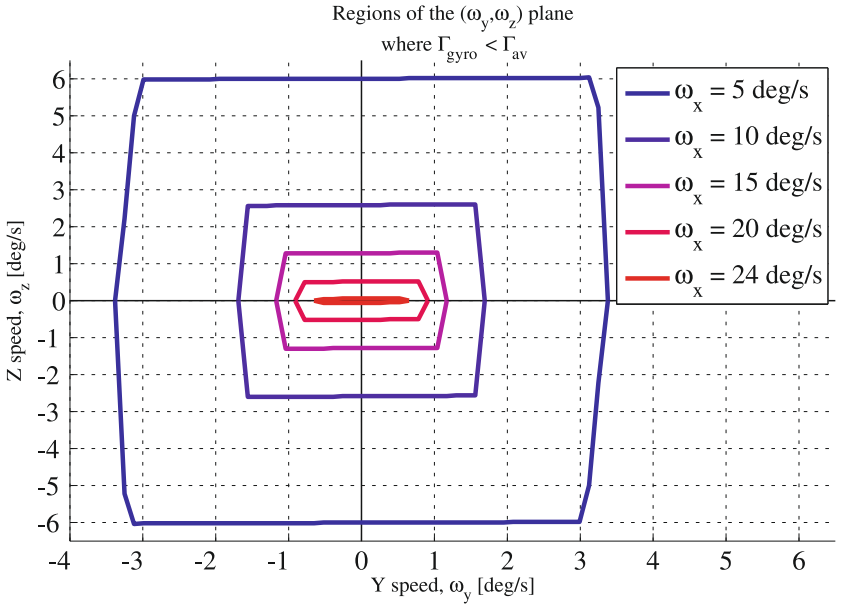

Figure 3.3: Regions where $\Gamma_{gyro} < \Gamma_{ACS}$ in the (ω_y, ω_z) plane, full inertia matrix $I_g^{(2)}$.

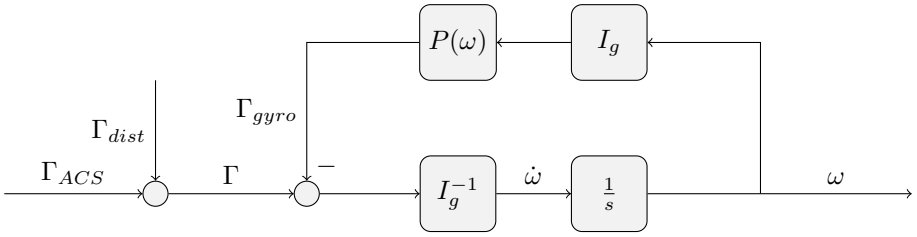

Figure 3.4: Block diagram for Newton's equation of rotational motion

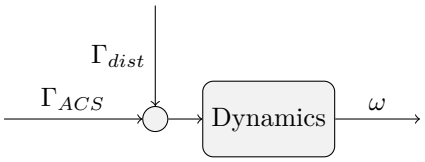

Figure 3.5: Simplified block diagram for the equations of motion

The way external and internal torques influence the vehicle motion has been described. Some trouble making features of the equation of motion (3.6) have already been shown. We are now going to introduce the means of representation of the attitude of the vehicle.

3.3 Kinematics, how to represent the attitude of the launcher?

The attitude of a body is its position i.e. its orientation, with respect to a reference frame. In our case, most of the time we would like to represent the attitude of $\mathcal{R}_g$ with respect to $\mathcal{R}_{ref}$. There exist two main ways to express the attitude of a body in space. One uses the so-called Euler angles. It is the easiest to read and to visualize since these angles parameterize three successive rotations of the body. It has one main drawback due to the existence of a singularity in its definition. It is that for one position of the body, the Euler angles are not enough to determine what is the actual position of the launcher. This is why, on board software and so all accurate simulation models will rely on the quaternion representation

which is the second way to parameterize the attitude of a body. This way of representing the attitude of the launcher is more abstract but very widely used since it gives a different representation for every possible position and so does not have the singularity of the Euler angles. However, the Euler angles representation will be used frequently for representation of the attitude of the launcher in the plots resulting of simulations (see e.g. section 3.8) since it is more readable than the quaternion representation. Basically, the attitude coordinates of the launcher are the parameters of the rotation which transforms $\mathcal{R}_{ref}$ into $\mathcal{R}_g$. As mentioned in the introduction, the position of $\mathcal{R}_g$ tells about the position of the vehicle with respect to $\mathcal{R}_{ref}$ and so with respect to Earth and is meaningful for all communication devices and sensors. For instance, we would like communication devices such as antennas to point toward a certain region of Earth for data transmission. Hence we measure the position of the vehicle (of $\mathcal{R}_g$) with respect to the reference frame (of $\mathcal{R}_{ref}$). The Euler angles representation considers this rotation as the result of three successive rotations done respecting a certain convention that will be described soon. These three rotations are combined into one single rotation parameterized with the three Euler angles of the aforementioned rotations. On the contrary, the quaternion representation is based on the fact that the transformation from $\mathcal{R}_{ref}$ to $\mathcal{R}_g$ can be defined as one single rotation around a certain axis to be determined.
The following section aims to define the attitude representations that are the Euler angles and the quaternions more precisely. For a thorough description of the kinematics of bodies in space we recommend [Sidi, 1997] and [Hughes, 1986].

3.3.1 Rotation conventions

The first step before defining the Euler angles representing the attitude of a launcher is to introduce the rotation convention that we will use to define those angles. To go from $\mathcal{R}_{ref} = (G, X_{ref}, Y_{ref}, Z_{ref})$ to $\mathcal{R}_g = (G, X_g, Y_g, Z_g)$, we proceed to three successive rotations of the reference triad $(X_{ref}, Y_{ref}, Z_{ref})$, that are described in table 3.1.

Rotation	Rotation axis	Rotation angle
1^{st}	Z_{ref} $(\mathcal{R}_{ref} \Rightarrow \mathcal{R}_g^{'})$	Yaw angle, $\psi \in (-\pi, \pi]$
2^{nd}	$Y_g^{'}$ $(\mathcal{R}_g^{'} \Rightarrow \mathcal{R}_g^{''})$	Pitch angle, $\theta \in [-\pi/2, \pi/2]$
3^{rd}	X_g $(\mathcal{R}_g^{''} \Rightarrow \mathcal{R}_g)$	Roll angle, $\phi \in (-\pi, \pi]$

Table 3.1: Successive rotations from $\mathcal{R}_{ref}$ to $\mathcal{R}_g$

The rotations angles ψ, θ and ϕ change if we represent the attitude using another rotation convention i.e. if we change the order of the rotations. The convention we will use is referred to as "yaw-pitch-roll" or "3-2-1" or "Z-Y-X" or "ψ-θ-ϕ". Figures 3.6, 3.7 and 3.8 show the successive rotations of the reference frame $\mathcal{R}_{ref}$ to obtain $\mathcal{R}_g$.

Using the angles of the three rotations from table 3.1 and the associated rotation matrices, we can define

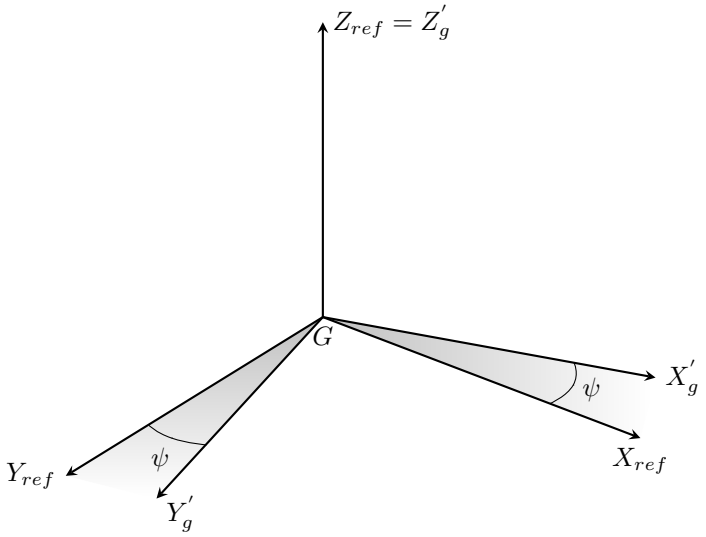

Figure 3.6: Axes after first rotation

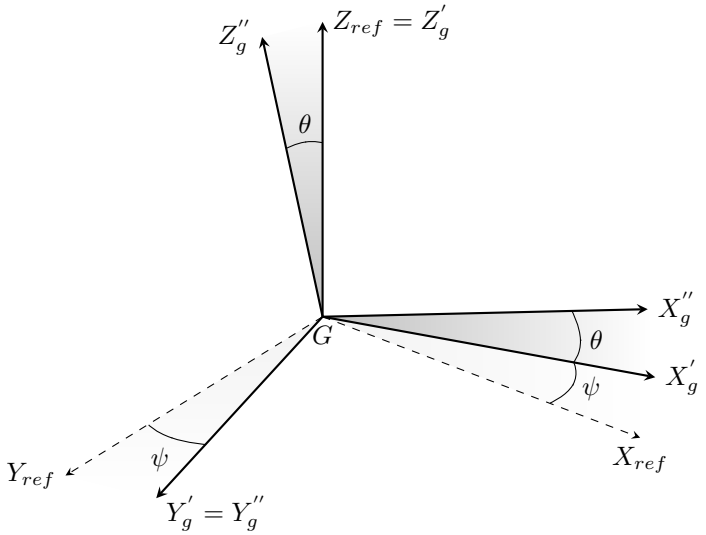

Figure 3.7: Axes after second rotation

the transformation matrix that allows going from $\mathcal{R}_{ref}$ to $\mathcal{R}_g$,

$$
\begin{aligned}
M_{ref\to g} = & \underbrace{\begin{bmatrix} 1 & 0 & 0 \\ 0 & \cos\phi & \sin\phi \\ 0 & -\sin\phi & \cos\phi \end{bmatrix}}_{A_\phi} \underbrace{\begin{bmatrix} \cos\theta & 0 & -\sin\theta \\ 0 & 1 & 0 \\ \sin\theta & 0 & \cos\theta \end{bmatrix}}_{A_\theta} \underbrace{\begin{bmatrix} \cos\psi & \sin\psi & 0 \\ -\sin\psi & \cos\psi & 0 \\ 0 & 0 & 1 \end{bmatrix}}_{A_\psi}, \\
= & \begin{bmatrix} \cos\theta\cos\psi & \cos\theta\sin\psi & -\sin\theta \\ \sin\phi\sin\theta\cos\psi - \cos\phi\sin\psi & \cos\phi\cos\psi + \sin\phi\sin\theta\sin\psi & \sin\phi\cos\theta \\ \sin\phi\sin\psi + \cos\phi\sin\theta\cos\psi & \cos\phi\sin\theta\sin\psi - \sin\phi\cos\psi & \cos\phi\cos\theta \end{bmatrix}.
\end{aligned}
\tag{3.13}
$$

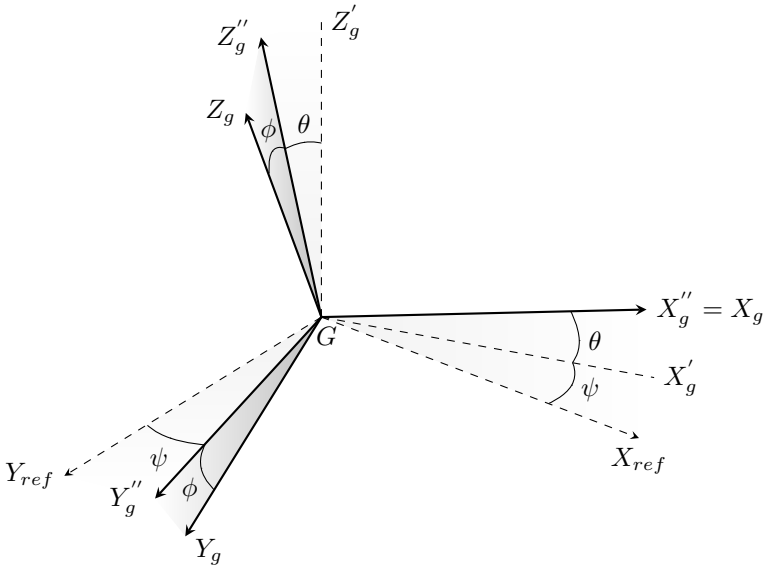

Figure 3.8: Axes after third and last rotation

The above matrix is the matrix product of the three rotation matrices of the "Z-Y-X" rotations. With (3.13), a vector a defined in $\mathcal{R}_{ref}$ by a_{ref} can be expressed in the frame $\mathcal{R}_g$ by:

$$a_g = M_{ref\to g} a_{ref}. \tag{3.14}$$

Similarly, a matrix expressed in $\mathcal{R}_{ref}$ by N_{ref} has its value in $\mathcal{R}_g$ determined using $M_{g\to ref}$ in the relationship:

$$N_g = M_{ref\to g} N_{ref} M_{ref\to g}^{-1}. \tag{3.15}$$

Finally, we claim that $M_{ref\to g}$ has the property: $M_{ref\to g}^{-1} = M_{ref\to g}^{T}$.

3.3.2 Euler angles

The angles describing the rotations presented in table 3.1 are called the Euler angles. They are usually given in the vector

$$E = [\phi, \theta, \psi] \in \mathbb{R}^3. \tag{3.16}$$

Notice that they are given in a different order than the order of the rotations defined in table 3.1. The speed of rotation about the three axes can be set as the derivative with respect to time of each one of the rotation angles. If we set the angular speed vector of the launcher ω to be

$$\omega = \begin{bmatrix} \omega_x \\ \omega_y \\ \omega_z \end{bmatrix}$$

as in section 3.2, we can define its components using the derivatives of the components of E:

$$\begin{bmatrix} \omega_x \\ \omega_y \\ \omega_z \end{bmatrix} = A_\phi A_\theta A_\psi \begin{bmatrix} 0 \\ 0 \\ \dot{\psi} \end{bmatrix} + A_\phi A_\theta \begin{bmatrix} 0 \\ \dot{\theta} \\ 0 \end{bmatrix} + A_\phi \begin{bmatrix} \dot{\phi} \\ 0 \\ 0 \end{bmatrix}. \tag{3.17}$$

Equation (3.17) can be solved for the Euler angles derivatives and leads to the kinematic equation:

$$\begin{cases} \dot{\phi} = & \omega_x + \tan\theta(\omega_y \sin\phi + \omega_z \cos\phi) \\ \dot{\theta} = & \omega_y \cos\phi - \omega_z \sin\phi \\ \dot{\psi} = & \frac{1}{\cos\theta}(\omega_y \sin\phi + \omega_z \cos\phi) \end{cases} \tag{3.18}$$

The singularity of the Euler representation appears clearly here for $\theta = \pm\frac{\pi}{2}$ where $\dot{\psi}$ and $\dot{\phi}$ are undefined. Otherwise, equations in (3.18) are nonlinear. A well-known first order approximation can be given for $\psi \ll 1$, $\theta \ll 1$, $\phi \ll 1$ using Taylor expansion of cos and sin functions about zero:

$$\begin{cases} \dot{\phi} & \simeq & \omega_x \\ \dot{\theta} & \simeq & \omega_y \\ \dot{\psi} & \simeq & \omega_z \end{cases} \tag{3.19}$$

The block diagram representation of the kinematic equation with Euler angles is given in figure 3.9. This figure shows the influence of the current attitude on the time derivative of the attitude.

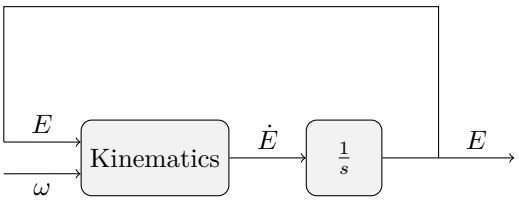

Figure 3.9: Block diagram for kinematic equations with Euler angles

Since the Euler representation of the attitude has a singularity, it is not reliable enough to be used in an ACS for space launcher where there is a crucial need for very high reliability. This is why space vehicles and also airplanes have their attitude measurements and control laws based on quaternion representation.

3.3.3 Quaternions

In this paragraph we describe the quaternions representation of the attitude. For a full presentation, the reader may refer to [Sidi, 1997] or [Hughes, 1986].
We saw in section 3.3.1 that the attitude of a body e.g. of the geometrical frame of a body $\mathcal{R}_g$, with respect to some reference frame e.g. $\mathcal{R}_{ref}$, can be expressed as the result of three successive rotations of $\mathcal{R}_{ref}$. The quaternion representation is based on the fact that the overall rotation resulting from the three successive rotations can be expressed as a single rotation whose axis and angle will be defined later on. A quaternion is a vector from $\mathbb{R}^4$ containing a description of this axis of rotation together with the rotation angle. To introduce the quaternions we again use the two frames $\mathcal{R}_{ref}$ and $\mathcal{R}_g$ since they are the frames whose position with respect to one another is interesting to us. Nevertheless, we could have

generalized these notations to other frames.
As said before, we can obtain $\mathcal{R}_g$ from $\mathcal{R}_{ref}$ with one rotation of angle σ around a unitary vector u. Obviously, u is invariant when applying any rotation of axis u to it. Hence it has the same coordinates in $\mathcal{R}_{ref}$ and $\mathcal{R}_g$. This particularity can be expressed as

$$u = \begin{bmatrix} u_1 \\ u_2 \\ u_3 \end{bmatrix}_{ref} = \begin{bmatrix} u_1 \\ u_2 \\ u_3 \end{bmatrix}_{g}. \tag{3.20}$$

Now assuming that $\mathcal{R}_g$ results from a rotation of the frame $\mathcal{R}_{ref}$ of σ around u, the quaternion to go from $\mathcal{R}_{ref}$ to $\mathcal{R}_g$ is defined by

$$q_{ref\to g} = \begin{bmatrix} \cos(\frac{\sigma}{2}) \\ u_1 \sin(\frac{\sigma}{2}) \\ u_2 \sin(\frac{\sigma}{2}) \\ u_3 \sin(\frac{\sigma}{2}) \end{bmatrix}. \tag{3.21}$$

To simplify the notations and as the attitude of the frames to be considered are always defined with respect to $\mathcal{R}_{ref}$, we will use the shorthand notation $q_{ref\to g} = q_g$. More generally when we will discuss about the attitude of the launcher, we will use $q = q_g$. The first component of $q_{ref\to g}$ in (3.21) is called the scalar component. It is the one from which σ can be immediately recovered. The last three components are called vector components. They define the axis of rotation. Defined as in (3.21), the quaternion $q_{ref\to g}$ has a Euclidean norm of 1 and represents the rotation needed to go from $\mathcal{R}_{ref}$ to $\mathcal{R}_g$ in a unique fashion. For any position of the geometrical frame $\mathcal{R}_g$, we can give the corresponding quaternion i.e. the rotation that is needed to go from $\mathcal{R}_{ref}$ to $\mathcal{R}_g$.

Let us now describe how the quaternions change when the space launcher has non zero angular speed by defining the kinematic equation with the quaternion representation as we did for the Euler angles (3.18). To do so, we need some definitions that will help us to manipulate quaternions. Consider we have a quaternion q describing the rotation from $\mathcal{R}_1$ to $\mathcal{R}_2$. First of all, the quaternion $-q$ describes the same rotation. Indeed, with the notation from (3.21), $-q$ corresponds to a rotation of $-\alpha$ around $-u$. Secondly, the rotation from $\mathcal{R}_2$ to $\mathcal{R}_1$ can be expressed by the inverse of q denoted q^{-1} and defined by:

$$q^{-1} = q_{1\to 2}^{-1} = \begin{bmatrix} q_0 \\ -q_1 \\ -q_2 \\ -q_3 \end{bmatrix} = q_{2\to 1}. \tag{3.22}$$

Looking again at definition (3.21), the inverse quaternion can be seen as describing a rotation of $-\alpha$ around u or a rotation of α around $-u$. Finally, let us consider that we also have q' describing the rotation from $\mathcal{R}_2$ to $\mathcal{R}_3$. The quaternion of the rotation from $\mathcal{R}_1$ to $\mathcal{R}_3$ is the quaternion product of q

and q'. The quaternion product is defined by the matrix product

$$q \star q' = \begin{bmatrix} q_0 & -q_1 & -q_2 & -q_3 \\ q_1 & q_0 & -q_3 & q_2 \\ q_2 & q_3 & q_0 & -q_1 \\ q_3 & -q_2 & q_1 & q_0 \end{bmatrix} \begin{bmatrix} q_0^{'} \\ q_1^{'} \\ q_2^{'} \\ q_3^{'} \end{bmatrix}. \tag{3.23}$$

Now we can define how the attitude quaternion of the launcher varies with respect to the attitude and angular speed during the motion. As for the Euler angles, the expression of the quaternion derivative by the kinematic equation is calculated from current attitude quaternion and current angular speed. This equation involves a particular quaternion defined with the angular velocity vector ω that is

$$\varpi = \begin{bmatrix} 0 \\ \omega_x \\ \omega_y \\ \omega_z \end{bmatrix}. \tag{3.24}$$

We have the following relationship between ω denoting the angular velocity vector of $\mathcal{R}_g$ with respect to $\mathcal{R}_{ref}$ and q ($= q_g = q_{ref \to g}$), and the time-derivative of the attitude quaternion denoted by $\dot{q}$:

$$\dot{q} = \frac{1}{2} q \star \varpi = \frac{1}{2} \begin{bmatrix} -q_1 & -q_2 & -q_3 \\ q_0 & -q_3 & q_2 \\ q_3 & q_0 & -q_1 \\ -q_2 & q_1 & q_0 \end{bmatrix} \begin{bmatrix} \omega_x \\ \omega_y \\ \omega_z \end{bmatrix}. \tag{3.25}$$

According to the above equality, the kinematic equation for the space launcher with quaternion representation is a matrix product. To represent the kinematic equation, we can build the block diagram showed in figure 3.10.

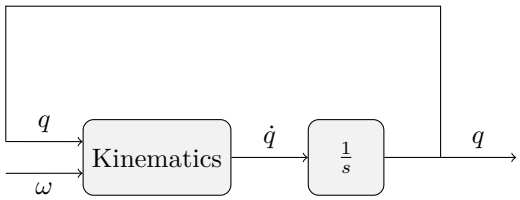

Figure 3.10: Block diagram for kinematic equations with quaternions

The quaternion representation of the attitude of the launcher is at first sight far from Euler representation and is rather hard to visualize. However, it has a crucial feature for small angles which will be exploited later on for the design of the control law. In facts, the vector components of the quaternion can be assumed to be proportional to the Euler angles for small deviations of $\mathcal{R}_g$ from $\mathcal{R}_{ref}$. It occurs if $\psi \ll 1$,

$\theta \ll 1$, $\phi \ll 1$, then we can write:

$$\begin{bmatrix} q_0 \\ q_1 \\ q_2 \\ q_3 \end{bmatrix} \simeq \begin{bmatrix} 1 \\ \phi/2 \\ \theta/2 \\ \psi/2 \end{bmatrix}. \tag{3.26}$$

Later on in section 3.6, we will see how this approximation can be used for attitude control. We also remark that the "small-angles" approximation is used to express the small angles variations in (3.19). Thus:

$$\begin{cases} \dot{\phi} \simeq \omega_x \simeq 2\dot{q}_1 \\ \dot{\theta} \simeq \omega_y \simeq 2\dot{q}_2 \\ \dot{\psi} \simeq \omega_z \simeq 2\dot{q}_3 \end{cases} \tag{3.27}$$

Finally, the identity operator can be expressed as the quaternion:

$$q = \begin{bmatrix} 1 \\ 0 \\ 0 \\ 0 \end{bmatrix}. \tag{3.28}$$

It is the quaternion of a rotation of angle zero around any unitary vector u. This is another feature of the quaternion notation that will be useful for the definition of a quaternion based attitude control law. Indeed, (3.28) means that the quaternion from $\mathcal{R}_{ref}$ to $\mathcal{R}_g$ has its vector components that tend to zero when the geometrical frame $\mathcal{R}_g$ tend to the reference frame $\mathcal{R}_{ref}$. In a more general formulation, we can say that when the rotation tends to the identity, the vector component tends to zero.
The mathematical framework of the quaternions and their applications are much broader than presented here. However, we presented the basics for space applications. Good reviews of their properties and uses are given in [Sidi, 1997] and [Hughes, 1986].

3.3.4 Block diagram

To conclude on a general block diagram representing the kinematic equation, we introduce a generalized attitude variable α denoting the attitude of the launcher. It can be either the Euler angles vector E or the quaternion q. Figure 3.11 is a shortened notation for the kinematic block with its inputs and outputs. The state variable of this block is $\alpha \in \mathbb{R}^3$ or $\mathbb{R}^4$.

Figure 3.11: Shortened block diagram for kinematic equations

3.4 Typical trajectories of the geometrical frame

The space vehicle dynamics and kinematics have now been defined so we know how to determine the position of the launcher with respect to a reference but also how this position is changed by the application of torques to the vehicle or non zero angular speeds. The question to be answered now is: what kind of maneuver (of position change) do we expect the launcher to perform?
The flight is split into the atmospheric phase and the ballistic phase. The atmospheric phase covers all the time when the main engine is ON and produces a force in order to reach a given orbit. During the ballistic phase, the main engine is OFF and the launcher has to control its attitude and speed with respect to $\mathcal{R}_{ref}$ to fulfill the designated payload release attitude and speed or to prepare the boosts or for de-orbitation. To achieve that, some predefined maneuvers are performed successively. The following paragraphs are defining the typical aimed trajectories of the states during these maneuvers. Depending on the mission, these have to be done with a certain accuracy and certain performance requirements. We will also see that the trajectories also depend on the system itself and the available control input throughout this brief overview of guidance typical requests.
To define the maneuvers, we will use the generalized attitude variable α without omitting that for a real space launcher the maneuvers are defined as a function of the quaternion attitude representation.

3.4.1 Slew maneuver

The first maneuver we describe is the slew maneuver. It consists in changing the attitude from initial attitude to aimed attitude through torque inputs. The slew maneuver can be realized from any initial conditions. In terms of the generalized attitude variable α that we defined, the slew maneuver can be presented as a transformation that will change the attitude of $\mathcal{R}_g$ with respect to $\mathcal{R}_{ref}$ from $\alpha^{(init)}$ to $\alpha^{(final)}$. In this context, the main goal is to compute a reference trajectory for the aimed frame $\mathcal{R}_{aimed}$ that the vehicle and so $\mathcal{R}_g$ can track with errors that are small enough to keep the small angle approximation in (3.26) and (3.19) valid. Hence the guidance module generates a trajectory which is not too demanding for the vehicle in terms of angular accelerations and decelerations such that the tracking performance can be good with the built-in ACS. Since the mission duration is usually not an issue, the launcher can perform slow maneuvers. As an example, a typical attitude reference trajectory is sketched in figure 3.12. This trajectory represents the track to be followed by one of the component of the Euler angles vector E or one of the vector component of the quaternion q.

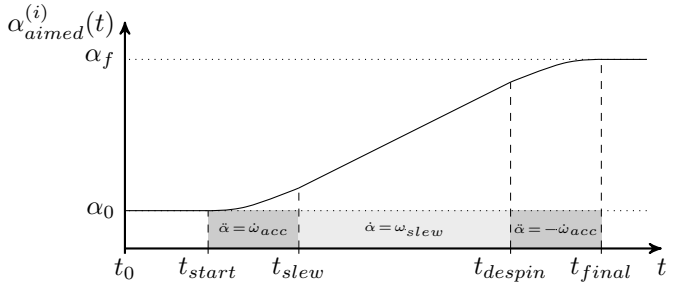

Figure 3.12: Typical attitude trajectory for a slew maneuver

The trajectory figure 3.12 has several parameters. For generality, we represents the trajectory that we want α to follow. It is split in several time periods delimited by particular time instants defined below:

- t_0, it is the time instant when simulation starts. At $t = t_0$, the actual attitude and angular speed of the launcher can be arbitrarily far from $E^{(init)}$ or $q^{(init)}$ as the previous maneuver may have caused large deviation from the aimed speed. However, preparing maneuvers aiming to recover the

previously aimed attitude $\alpha^{(init)}$ are generally performed before starting the actual slew maneuver if large perturbations are measured. We will assume that at the beginning of the simulation, the state variables of the controller, if the controller has state variables, are set to zero.

- t_{start}, it is the initial time of the slew maneuver. From that time on, the vehicle should slew to the final attitude. To do so, the aimed trajectory has constant acceleration. Ideally, double integration of a constant acceleration implies a trajectory that is quadratic in time for the aimed attitude α_{aimed} as in figure 3.12. The acceleration phase is done at a given acceleration $\dot{\omega}_{acc}$. $\dot{\omega}_{acc}$ is a function of the available torque around the axis of rotation. Usually, since the aimed speeds for slew are low, we only use a fraction of the available torque to limit propellant consumption. The notion of available torque will be defined in section 3.7 in this chapter.

- t_{slew}, it is the time when the constant speed slew starts i.e. the time when the acceleration goes back to zero. The aimed velocity is ω_{slew} around the axis of rotation. This speed is defined from the characteristics of the system and generally is about 1 or 2 degrees per second.

- t_{despin}, it is the time when the deceleration starts and the rotational motion of the vehicle slows. Since by assumption the available torque around an axis is the same for positive and negative torque, the deceleration is $-\dot{\omega}_{acc}$ so as for the acceleration phase the aimed attitude is quadratic in time.

- t_{final}, it is the end time of the maneuver. At this time instant, the system must have reached its aimed final attitude $\alpha^{(final)}$ and the aimed angular speed should be around zero to fulfill the performance requirements. Hence only attitude adjustments are done to stabilize the vehicle at its aimed value α_{aimed}.

When proceeding to a slew maneuver, the main goal is to achieve the required pointing precision while limiting propellant consumption and thrusters activations. This is why the rotation rate ω_{slew} is low and the duration of the slew can be long for large amplitude maneuvers. Concerning pointing accuracy, it is generally not prescribed that the vehicle follows precisely the trajectory during the slew. However, final attitude precision requirement can be very demanding e.g. less than $0.1°$.

3.4.2 Spin maneuver

The second main maneuver is the spin maneuver. It consists in rotating the vehicle about one axis at constant speed while pointing toward a given constant direction. This must be realized in spite of the gyroscopic couplings developing with the rotational motion (see their description in paragraph 3.2.6). This maneuver occurs when the payload must be released with initial angular speed. For instance, such requirement can be enforced to avoid heavy shielding and insulation for satellites whose attitude is fixed and so which expose one of their side to the sunlight for longer durations. As before, the spin maneuver can be realized from any initial conditions but preparing maneuvers can be performed in case of large deviations from the initial aimed states. To perform the rotation, we compute an aimed velocity profile that includes an acceleration phase and a constant rotation rate phase. Figure 3.13 depicts the typical angular speed trajectory around the desired axis of rotation. In most cases, this axis is an axis of the geometrical frame $\mathcal{R}_g$ and more particularly the longitudinal axis X_g.
According to figure 3.13, the trajectory can be compared to the slew maneuver trajectory, especially in the case we consider that the despin maneuver is done before pursuing the mission. Nevertheless, for a spin maneuver the orders of magnitude in the acceleration and speed but also the performance requirements are completely different. The aim of this maneuver is to reach a certain rotation rate around the desired axis of rotation and not a particular attitude. However, since the spinning generally occurs around the longitudinal axis X_g, it requires the stabilization of transverse axes (Y_g and Z_g) in terms of speed and position. The figure introduces several characteristic values which are described hereunder.

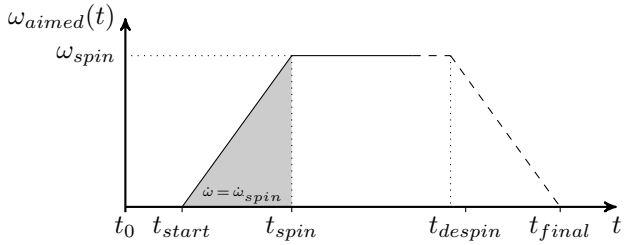

Figure 3.13: Typical speed trajectory for a spin maneuver

- t_0, it is the initial time. At this time instant, the actual angular speed of the launcher can be arbitrarily far from $(\omega_x, \omega_y, \omega_z)^{(init)}_{aimed}$ as the previous maneuver may have caused large deviation from the aimed speed. The same applies to the initial attitude. Yet, preparing maneuvers can be done to stabilize the vehicle before starting the rotation.

- t_{start}, it is the starting time instant of the maneuver. From that time on, the vehicle starts to rotate around the chosen axis. A very stringent requirement is to keep angular speed around the other axes e.g. the transverse axes Y_g, Z_g in the case the rotation is about X_g, as low as possible. The acceleration has a constant aimed value defined from the available torque about the desired axis of rotation and denoted as $\dot{\omega}_{spin}$. The acceleration can correspond to torque commands up to 90% of the available torque. For now, we consider that the available torque is the torque that we are able to apply about the axis of rotation thanks to the ACS.

- t_{spin} is the time when the aimed rotation speed is reached. The velocity must then be close to ω_{spin}. It can have values from a few degrees per second up to $30°s^{-1}$. Although the requirements for the tracking of the aimed angular speed was not too tight during the acceleration, keeping the aimed angular speed after t_{spin} is mission critical. Furthermore, transverse axes have to be stabilized as well. A special spin maneuver which is the de-orbitation maneuver can require higher speeds but with less stringent precision requirements.

To summarize, when performing a spin maneuver about the longitudinal axis X_g, the main goal is to achieve the required angular speed about X_g while keeping X_g pointing in the right direction so the transverse angles and transverse speeds should be maintained to their aimed values. This must be done despite large gyroscopic couplings induced by the rotating motion and the asymmetry of the launcher. Their value has been investigated in paragraph 3.2.6. The requirements on the deviation of the rotation axis can be very demanding e.g. less than 0.25°.

The two typical maneuvers described above are generally the building blocks of the proceedings of the mission. Indeed, once the exo-atmospheric flight starts, the mission consists in successively performing different maneuvers based mainly on slews and spins with different parameters. The drift mode is also widely used but we decided to focus on slew and spin only. The role of the controller is to compute the torque commands that will allow the vehicle to track the desired trajectories while satisfying the performance requirements such as reference tracking, propellant consumption, thrusters activations, etc. For that the controller needs to have access to the current attitude and angular speed of the launcher. These measures are obtained from the navigation unit which role is to ensure states measurements.

3.5 Attitude measurements and states reconstruction

In the first two paragraphs of this section, the dynamics of the system i.e. the way external torques are influencing the motion of the system, and the kinematics of the system i.e. the way to represent the

attitude of the system relatively to some reference and how it varies during the flight, were presented. These two equations correspond to the state-space description of the physical system that we study and that we have to control. A representation of it looks like figure 3.14.

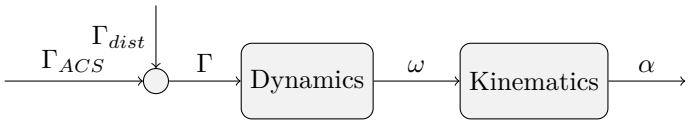

Figure 3.14: Compact block diagram for the space vehicle

Defined in such way, the space vector of the launcher can be defined in the geometrical frame $\mathcal{R}_g$ with respect to the reference frame $\mathcal{R}_{ref}$ as

$$X = \begin{bmatrix} \omega \\ \alpha \end{bmatrix}. \tag{3.29}$$

X belongs to $\mathbb{R}^6$ or $\mathbb{R}^7$ depending on the choice of variable for attitude representation. In most cases, the hardware available on board only allows measuring the vehicle attitude α. We saw in section 3.4 that some maneuvers require angular speed control. Since the measurement of ω is not accessible, an algorithm is implemented to reconstruct the angular speeds from the attitude measurements. The measurement step and speed reconstruction step are described in the two paragraphs to come.

3.5.1 Measurements

It is very common to consider that measured signals result from the addition of the signal to be measured to some perturbations which can be modeled by a noise signal with normal distribution of given mean and standard deviation. Hence, we simply consider that the measured attitude α' can be decomposed as in (3.30):

$$\alpha' = \alpha + \alpha_{dist}. \tag{3.30}$$

Here α_{dist} represents a noise input signal describing how the measurement step deteriorates the attitude signal. In addition to that, it is also common to complete the model of the measurement process with a time-delay denoted by τ_{meas}. We can introduce the measurement delay after the noise input to get the actual measured attitude α_{meas} as in figure 3.15.

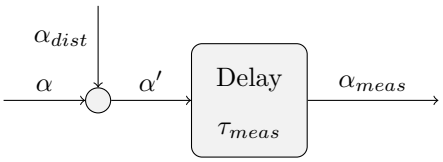

Figure 3.15: Block diagram of the measurement step

Later on, we will need a simple representation of the measurement step and so we will rely on the one-block representation of the diagram figure 3.16. We see on this figure that we put aside one of the main characteristic of the measurement process during the description. This feature is the sampling of the measured signal. Attitude control of space launcher is realized by a computer and so discrete signals are needed as inputs of the controller. This is why we introduce a sampling device $\mathcal{S}_h$ at the output of the measurement unit. The sampling period of the system will be denoted by h.

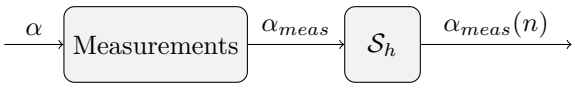

Figure 3.16: Compact block diagram of the measurement step

3.5.2 States reconstruction

The state reconstruction step aims to produce an estimation X_{estim} of the state vector X. The problem is that at each sample-time $t_n = nh$, we only know the measured attitude of the vehicle $Y_{meas}(n) = \alpha_{meas}(n)$ and the previous state vector estimation $X_{estim}(n-1)$. Moreover we need to define $X_{estim}(n)$ by computation of an estimation of the actual attitude $\alpha(n)$ and the actual angular speed $\omega(n)$. These estimations are necessary to control the spacecraft and to allow reference tracking. To determine them, an estimator relying on a mathematical model of the vehicle is used to find an estimate of the state vector $X_{estim}(n)$. The mathematical model allows predicting the future value of the state vector considering its last estimation $X_{estim}(n-1)$. A basic relationship for the prediction step is given by

$$\begin{cases} X_{pred}(n) = & f(X_{estim}(n-1)), \\ Y_{pred}(n) = & h(X_{estim}(n-1)). \end{cases} \tag{3.31}$$

where f and h can be any nonlinear function expressing the relationship between $X_{estim}(n-1)$ and $X_{pred}(n)$ and $Y_{pred}(n)$, respectively. To determine the estimated state vector $X_{estim}(n)$, we adjust the prediction $X_{pred}(n)$ by adding the information contained in the measurement $Y_{meas}(n)$. The so-called readjusting step can be described as below:

$$X_{estim}(n) = X_{pred}(n) + R\left(Y_{meas}(n) - Y_{pred}(n)\right). \tag{3.32}$$

In (3.32), the matrix R is used to introduce the measurement into the estimated vector. Depending on how confident we can be about the measured data, we can increase or decrease the values in R. This reconstruction step can be done with various prediction models f and readjusting steps (3.32). This is the reason why we only give a basic description of the process and in particular we do not give the prediction model even though it can be a rather simple linear one.
Finally, the output is the estimated state vector at time t_n denoted by $X_{estim}(n)$. This estimation will be used by the controller to compute the torques needed for attitude and speed control. The estimated state vector X_{estim} with structure defined by (3.29) corresponds to the general case. X_{estim} contains the estimated attitude α_{estim} as well as the estimated angular speed ω_{estim} in this simplified framework. However, other variables can be accessed through the prediction and estimation steps such as disturbing torques, dynamics unbalances, etc. A schematic representation is given figure 3.17 where all the signals are discrete-time signals. This block generally has a state vector but we will omit it for simplicity.

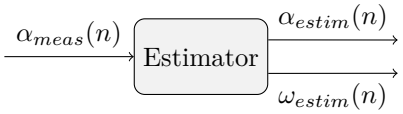

Figure 3.17: Block diagram of the estimation step

3.6 Controller, how to track attitude and speed references?

The previous section aimed to show how the attitude measurements α_{meas} are used to access the estimation of the actual attitude α_{estim} and to reconstruct and estimate the true angular speed ω by computing ω_{estim}. These signals will allow the controller to perform reference tracking and maneuvering through calculation of the tracking error and computation of the torque command.
The estimated state vector X_{estim} with components as in (3.29) is used by the controller in a simple proportional-derivative structure after determining the error between X_{estim} and X_{aimed}. We mentioned in paragraph 3.5.2 that X_{estim} can contain estimations of other states of the space vehicle but the controller we consider is only concerned with ω_{estim} and estimated attitude quaternion q_{estim}. From these two inputs and the aimed states ω_{aimed} and q_{aimed}, it determines the control torque vector Γ_c. Ideally, applying Γ_c to the launcher would allow the geometrical frame $\mathcal{R}_g$ to follow the aimed frame $\mathcal{R}_{aimed}$.
From ω_{estim} and q_{estim}, the computation of Γ_c goes as follow. First, the angular speed error is determined. It is simply the difference between estimated angular speed ω_{estim} and aimed angular speed ω_{aimed}:

$$\Delta\omega = \omega_{estim} - \omega_{aimed}. \tag{3.33}$$

Secondly, the error quaternion Δq between the aimed attitude quaternion q_{aimed} and the estimated attitude quaternion q_{estim} is computed. Δq is not determined as a simple difference between q_{aimed} and q_{estim} but as the quaternion product

$$\Delta q = q_{aimed}^{-1} \star q_{estim}. \tag{3.34}$$

Δq represents the transformation from $\mathcal{R}_{aimed}$ to $\mathcal{R}_{estim}$, the latter corresponding to the frame defined by the estimation of the attitude of $\mathcal{R}_g$. From these errors signals $\Delta\omega$ and Δq, the control torque is computed through weighting of each channel by the control gains D and K. The resulting control torque Γ_c reads as

$$\Gamma_c = -\underbrace{\begin{bmatrix} 0 & 2K_x & 0 & 0 \\ 0 & 0 & 2K_y & 0 \\ 0 & 0 & 0 & 2K_z \end{bmatrix}}_{K} \begin{bmatrix} \Delta q_0 \\ \Delta q_1 \\ \Delta q_2 \\ \Delta q_3 \end{bmatrix} - \underbrace{\begin{bmatrix} D_x & 0 & 0 \\ 0 & D_y & 0 \\ 0 & 0 & D_z \end{bmatrix}}_{D} \begin{bmatrix} \Delta\omega_x \\ \Delta\omega_y \\ \Delta\omega_z \end{bmatrix}. \tag{3.35}$$

The computation of Γ_c takes into account small angles approximation. That is the Euler angle error is assumed to be twice the vector components of the error quaternion as in equation (3.26) i.e.

$$\begin{bmatrix} \Delta\phi \\ \Delta\theta \\ \Delta\psi \end{bmatrix} \simeq 2 \begin{bmatrix} \Delta q_1 \\ \Delta q_2 \\ \Delta q_3 \end{bmatrix}, \text{ when } \Delta q_i \ll 1 \text{ and } i \in \{1, 2, 3\}. \tag{3.36}$$

Furthermore, we observe that all the components of the above vectors tend to zero when the aimed frame $\mathcal{R}_{aimed}$ and the geometrical frame $\mathcal{R}_g$ are superimposed. The structure of such controller is given in figure 3.18. This controller is nonlinear due to the error quaternion computation which can be written as a matrix product involving the aimed quaternion components. A simplified version of figure 3.18 is given in figure 3.19 in order to make easier the final system presentation figure 3.29.

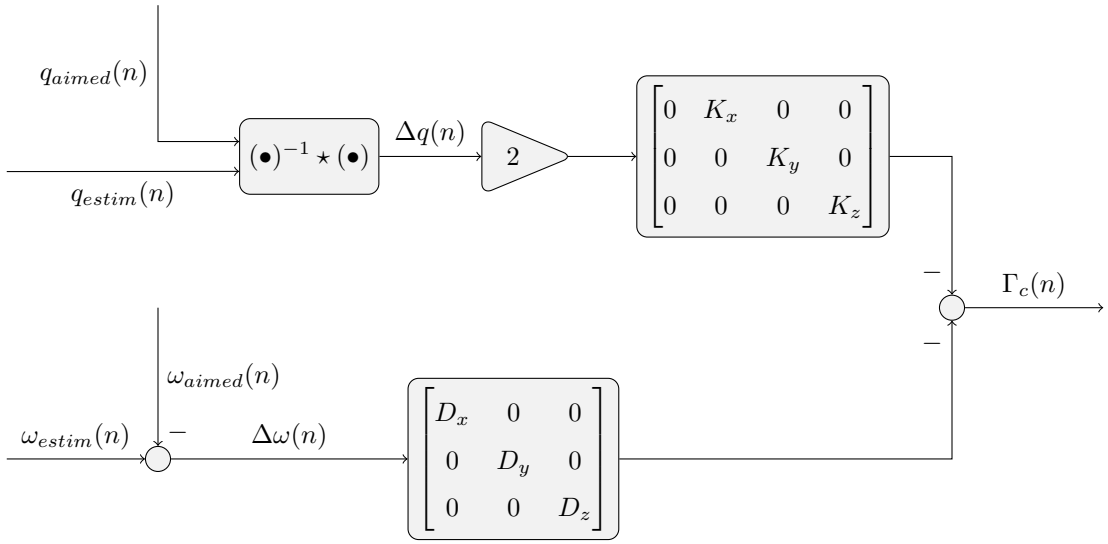

Figure 3.18: Block diagram of controller structure

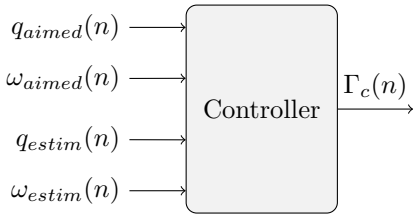

Figure 3.19: Shorten block diagram of the controller

3.7 Actuator, how to generate torque and initiate the motion?

The role of the actuator is to create the torque Γ_{ACS} corresponding to the control torque Γ_c commanded by the controller to ensure reference tracking. As the torque applied to the launcher is produced by thrusters which can only be set to ON or OFF, the ACS cannot produce a torque that corresponds exactly to $\Gamma_c(n)$ at every sampling instant. Indeed, there is no way to control the level of force produced by the thrusters since the valves that control propellant ejection can only be either fully open or completely closed. When a thruster is set to ON, it generates a certain amount of force which, when associated to the force produced by another opposite thruster, produces a torque. The force produced by the thrusters has a constant value and so Γ_{ACS} can only take a constant value too as the position of the thrusters is fixed in $\mathcal{R}_g$. Thus it cannot take the same values as Γ_c. We will see soon how this issue can be solved by adjusting the duration for which the thrusters are set to ON instead of the level of thrust they produce. Finally, independently from the propellant, the force created when a thruster is turned ON cannot be known exactly a priori due to the propellant physical state, the propellant quantity variations and the vehicle states. This will have to be taken into account during the analysis.
Figure 3.20 shows an example with six thrusters grouped in two clusters of three nozzles and labeled T_1 to T_6. The role of these thrusters is to generate a force by burning or ejecting some propellant which can be hot or cold gas. The torque results form the activation of two thrusters or more. Basically, torque is created about each axis via the activation of two designated thrusters, a negative torque can be created through the activation of a different pair of thrusters. For instance in the figure, thrusters T_3 and T_5 could be switched ON to produce a positive torque about X_g. For a negative torque we should switch ON T_6 and T_2. When two thrusters associated this way are set to ON, they produce a constant torque of value denoted by Γ_{av}. This strategy could be reproduced for three thrusters or more at the cost of more

propellant consumption.

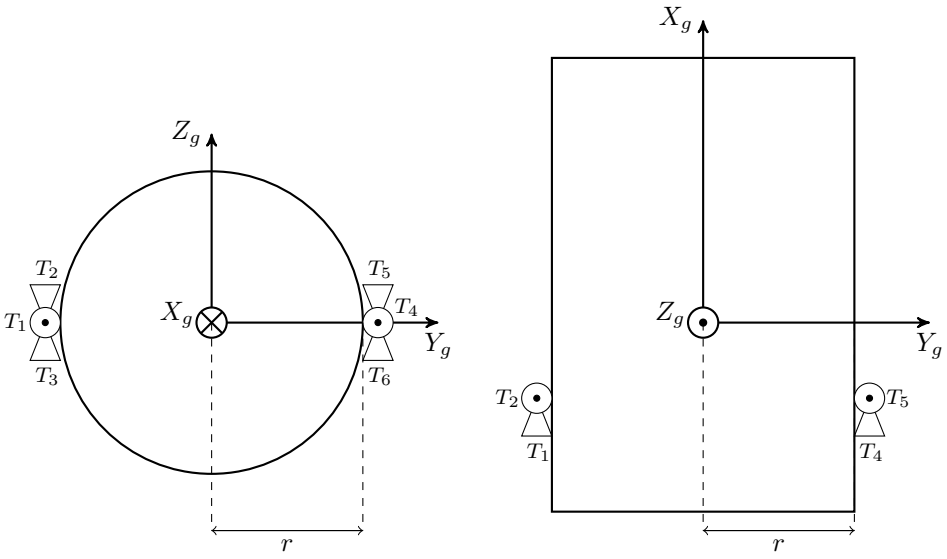

Figure 3.20: Example of thrusters positioning

The trouble making feature of the torque production process that is to be studied is the highly nonlinear ON/OFF behavior of the thrusters. To model this very complex system without loosing any key feature of torque generation, we consider that the torque about each one of the three axes is produced by a Pulse-Width Modulator (PWM) whose typical input and output signals are depicted in figure 3.21.

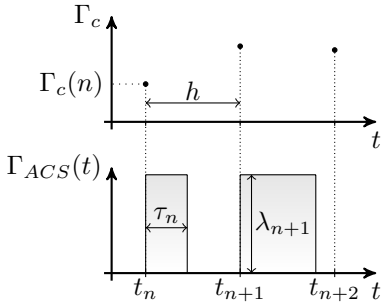

Figure 3.21: Input and output signals of a PWM

This figure shows that over every sampling interval $T_n = [t_n, t_{n+1})$ where $\forall n \in \mathbb{N}, t_n = nh$ and h is the sampling period, the PWM produces one pulse with a width denoted by τ_n depending on the sampled input $\Gamma_c(n)$ and a constant height λ_n. The height λ_n can vary during the flight due to the number of thrusters activations, the state of the vehicle, etc. However, since we will consider one maneuver at a time, the height of the pulses will not be considered to be time-varying but only uncertain. The nominal absolute value of the height is Γ_{av}, the nominal torque produced by the association of thrusters explained above. This value is determined for each axis using the available torque about this axis. For instance, from figure 3.20, we said that to produce a positive torque about the longitudinal axis X_g, we need to switch ON thrusters T_3 and T_5. We assumed that both of them produce a constant nominal force of F_{th}. The distance of the thrusters from the rotation axis (here X_g) is determined to be r and so the nominal available torque is $2F_{th}r = \Gamma_{av}$ in Nm. The same can be done for each axis to define a different available torque about each axis. Since the maneuvers about the longitudinal axis X_g are more demanding in terms of acceleration than for the transverse axes Y_g and Z_g, we usually observe a larger available torque

about X_g than about Y_g or Z_g. Furthermore, it is worth noticing that for the modeling of the ACS thrusters we considered the thrusters to be at equal distance from the axis of rotation, that the thrust produced was exactly equal and that there were no misalignment of the forces. Consequently, opening a pair of thrusters produces exclusively some torque about one axis and causes no force perturbations or torque perturbation about the other axes. Yet the modeling these effects could be done easily.

We mentioned previously that a PWM operator models torque creation about each axis. Hence from each one of the three components of the commanded torque Γ_c, the pulse width τ_n is determined by

$$\tau_n = \begin{cases} 0, & \text{if } |\Gamma_c(n)| < \Gamma_{min} \\ \frac{|\Gamma_c(n)|}{\Gamma_{av}} h, & \text{if } \Gamma_{min} \leq |\Gamma_c(n)| < \Gamma_{av} \\ h, & \text{if } |\Gamma_c(n)| \geq \Gamma_{av} \end{cases}, \tag{3.37}$$

where Γ_{av} is the nominal available torque about the axis and Γ_{min} the torque value corresponding to the minimum opening time of the thrusters. This constraint models the facts that the thrusters cannot be opened and closed for a too short duration. The nominal value of this duration is 50 ms and the corresponding torque Γ_{min} can be computed from (3.37). The value of Γ_{min} is obtained from the Minimum Impulse Bit (MIB). The nominal height of the pulses is given by

$$\lambda_n = \text{sign}(\Gamma_c(n))\Gamma_{av}, \tag{3.38}$$

and we will see later on how to take into account the fact that the torque produced by the thrusters is not known exactly. The representation and modeling of the thrusters producing the torque needed for control is now covered. As it is presented here, the actuator model captures the features that are essential for an accurate representation of the actual ACS.
Finally, the actuator can be sketched as in figure 3.22 where the PWM block must be seen as a three-inputs three-outputs PWM where each channel is independent from the other and the modulated components of the three dimensional output Γ_{ACS} are defined as in (3.37-3.38) and look like the signals of figure 3.21.

Figure 3.22: Block diagram of the model of the actuator

3.8 Simulations

In order to represent the behavior of the system we just described, we ran some simulations. For these, the inertia matrix is

$$I_g^{(2)} = \begin{bmatrix} 22500 & -50 & -1100 \\ -50 & 42000 & -250 \\ -1100 & -250 & 44000 \end{bmatrix}.$$

The vector of available torque is

$$\Gamma_{av} = \begin{bmatrix} 400 \\ 200 \\ 100 \end{bmatrix}$$

and the minimum opening time of the thrusters is 50 ms. In addition to that, we use the quaternion representation of the attitude. Figures 3.23, 3.24 and 3.25 represent the attitude, angular speed and delivered torque values during a slew maneuver. The initial Euler angles are $E^{(0)} = [0°, 0°, 0°]$ and the final aimed attitude is $E^{(aimed)} = [30°, 35°, 45°]$. We observe that the aimed attitude and angular speed (dotted lines) are always very well tracked by the actual velocity and attitude (solid lines). Figures 3.26, 3.27 and 3.28 represent the attitude, angular speed and delivered torque values during a spin maneuver. We see on these ones the effect of the gyroscopic couplings on the transverse axes.

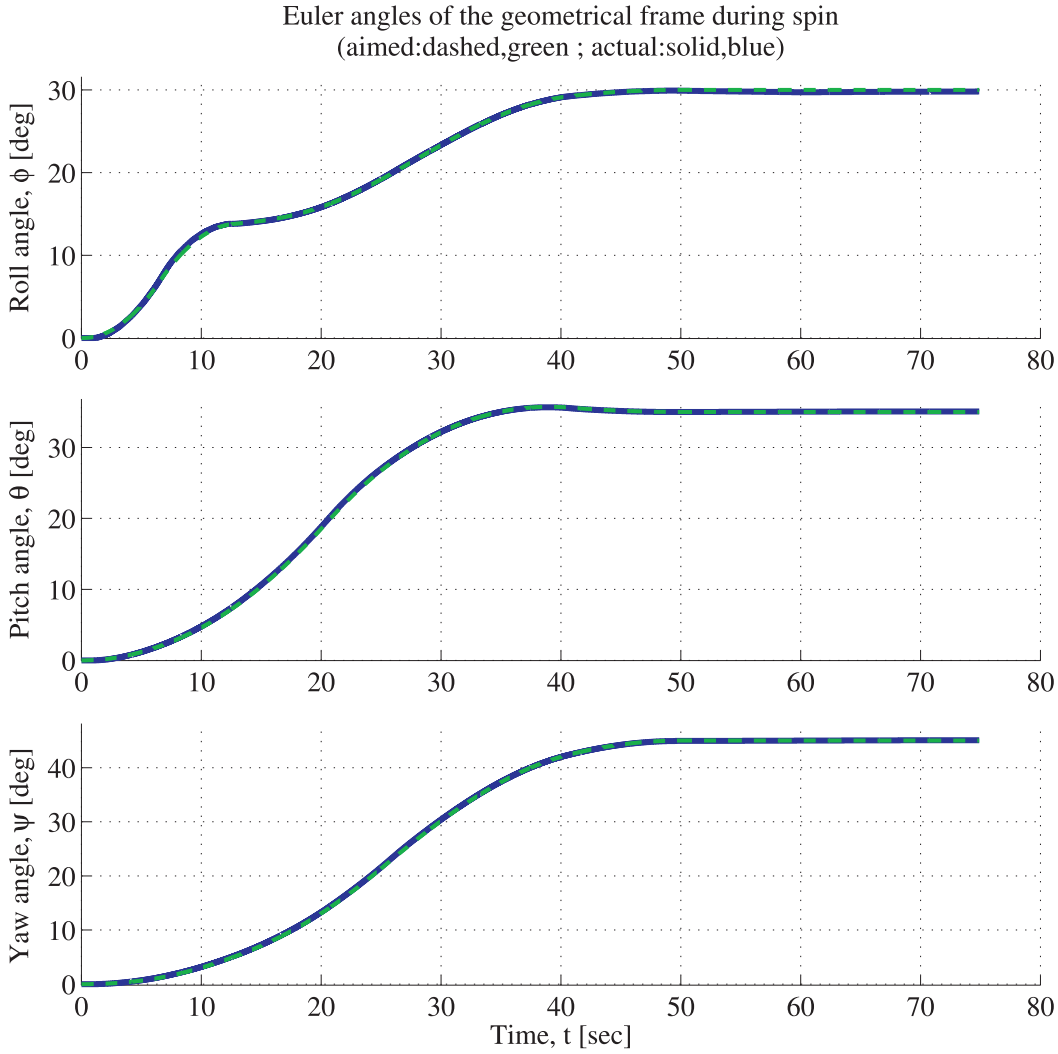

Figure 3.23: Evolution of the Euler angles of the launcher during slew maneuver.

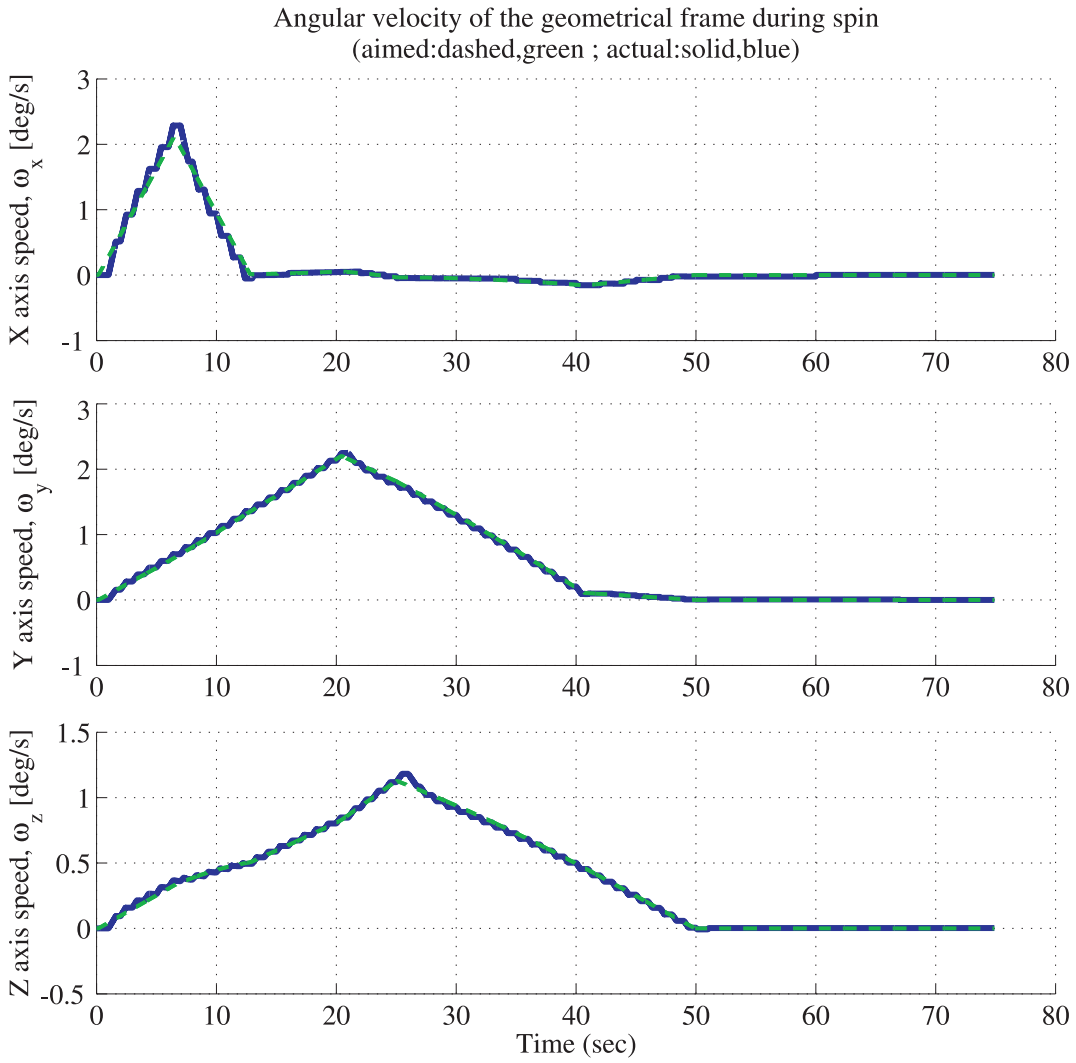

Figure 3.24: Evolution of the angular velocity components of the launcher during slew maneuver.

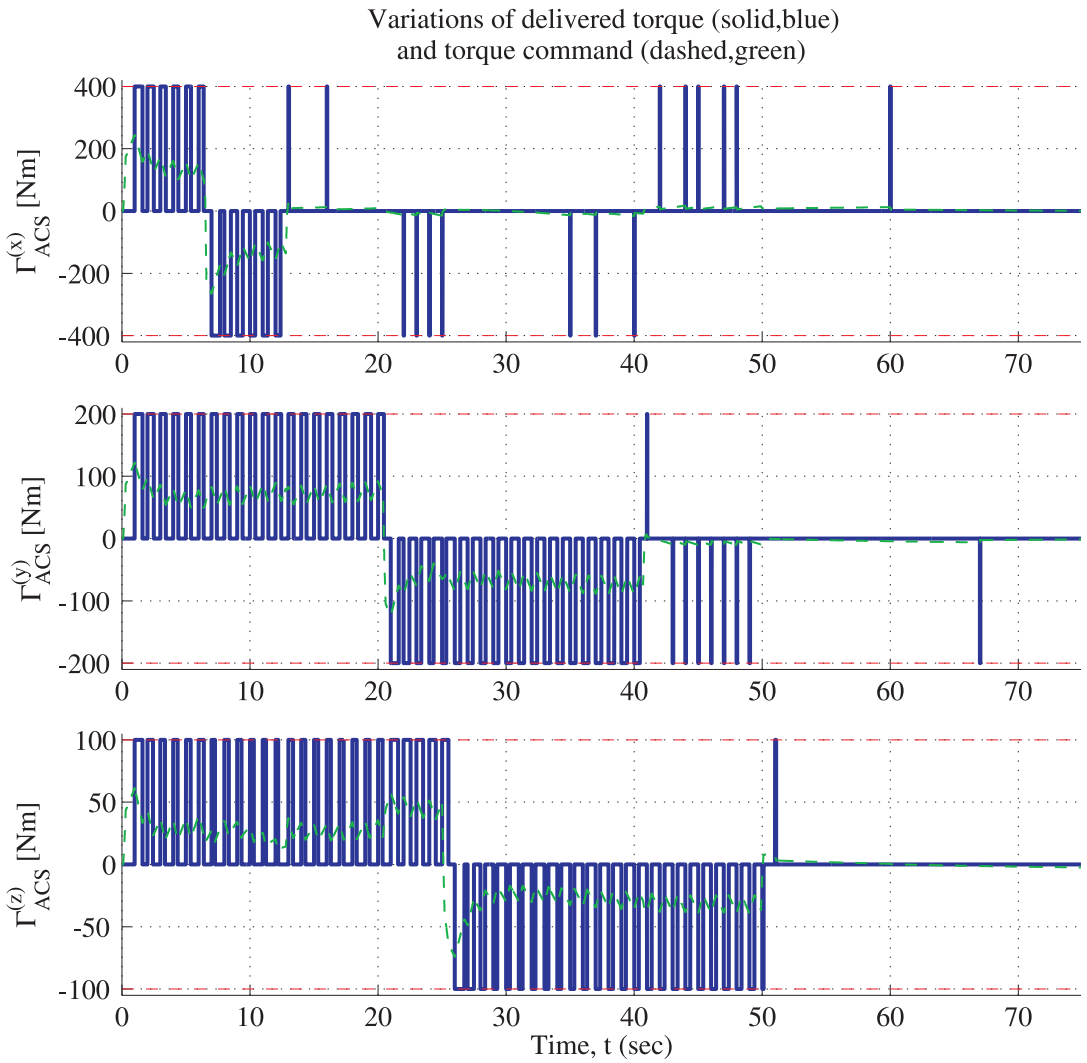

Figure 3.25: Evolution of the torque command and the torque delivered to the launcher by the ACS during slew maneuver.

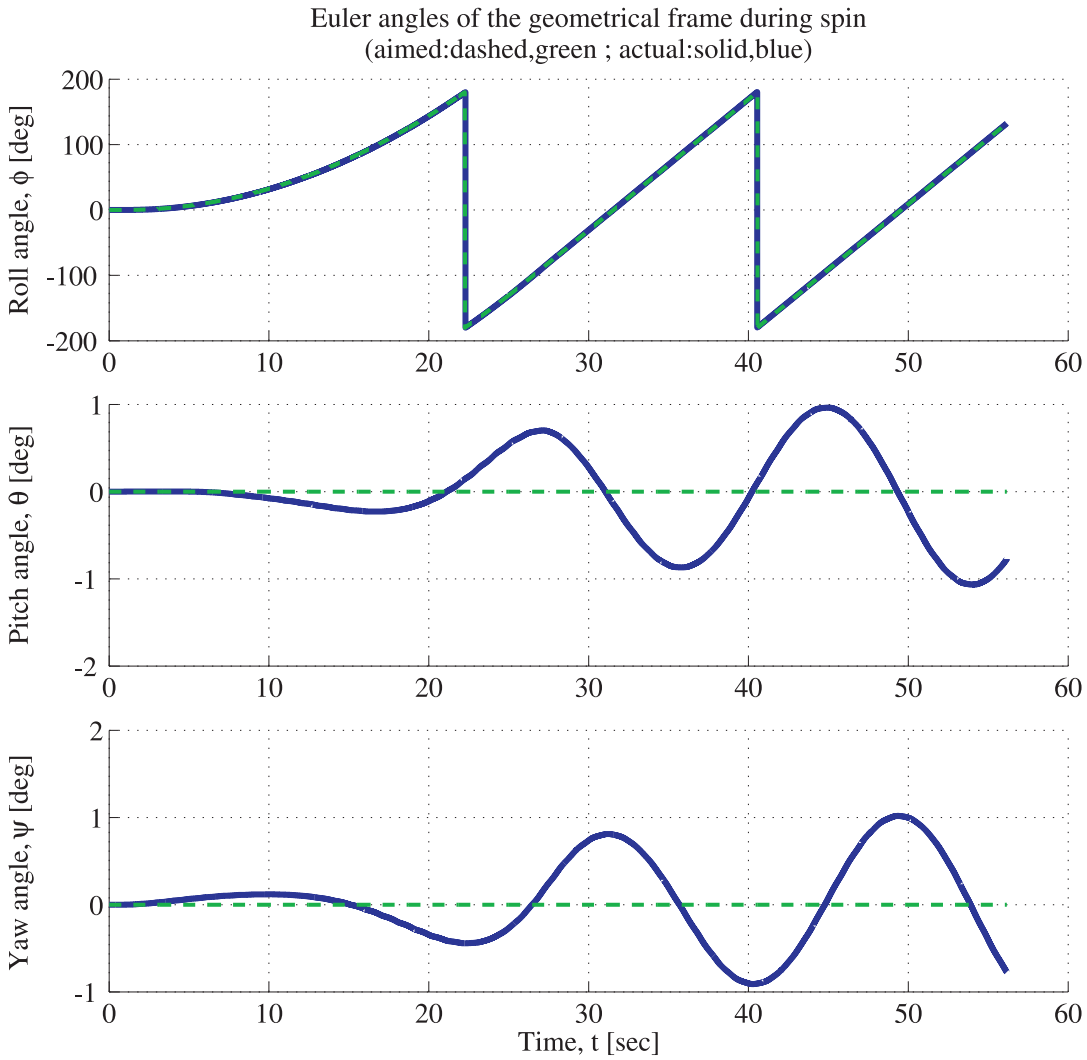

Figure 3.26: Evolution of the Euler angles of the launcher during spin maneuver.

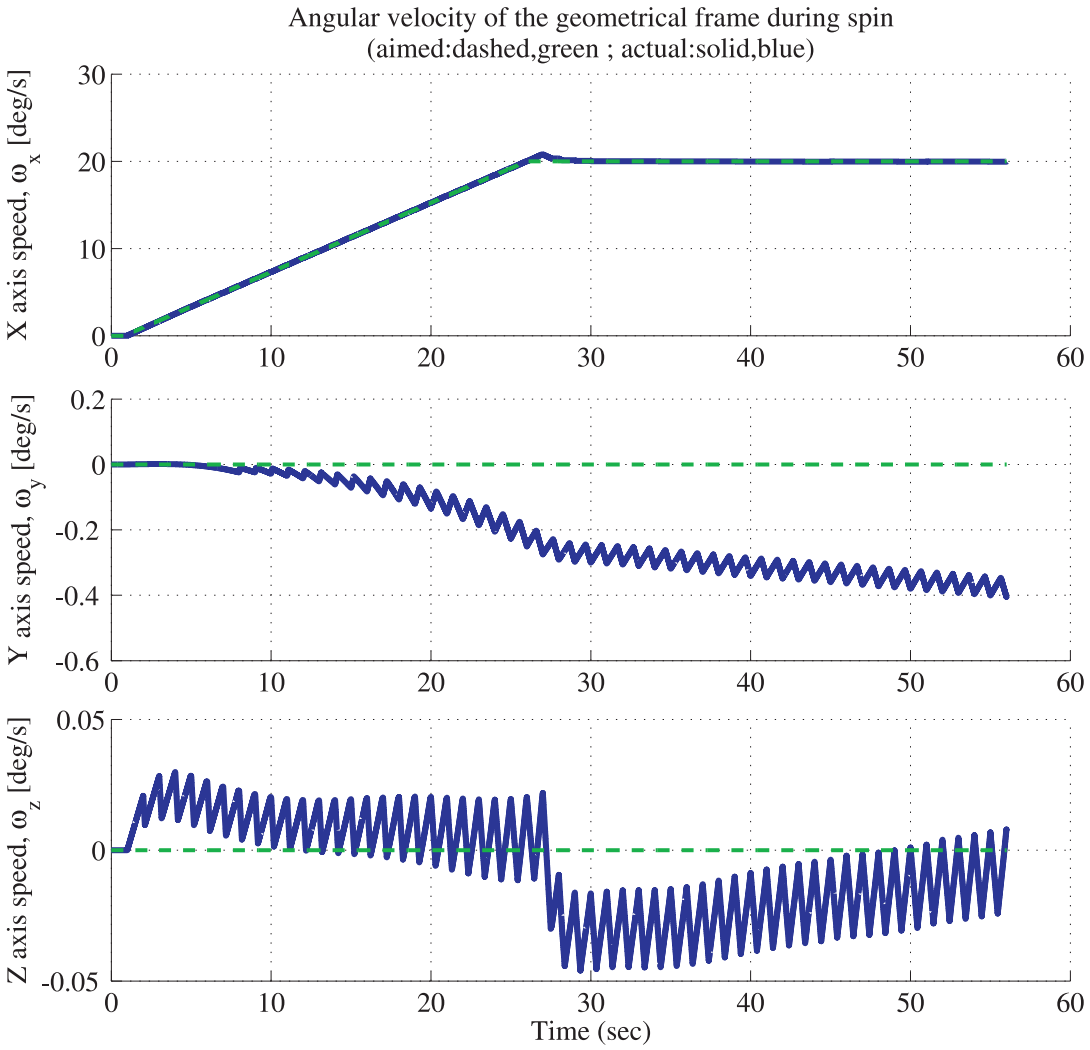

Figure 3.27: Evolution of the angular velocity components of the launcher during spin maneuver.

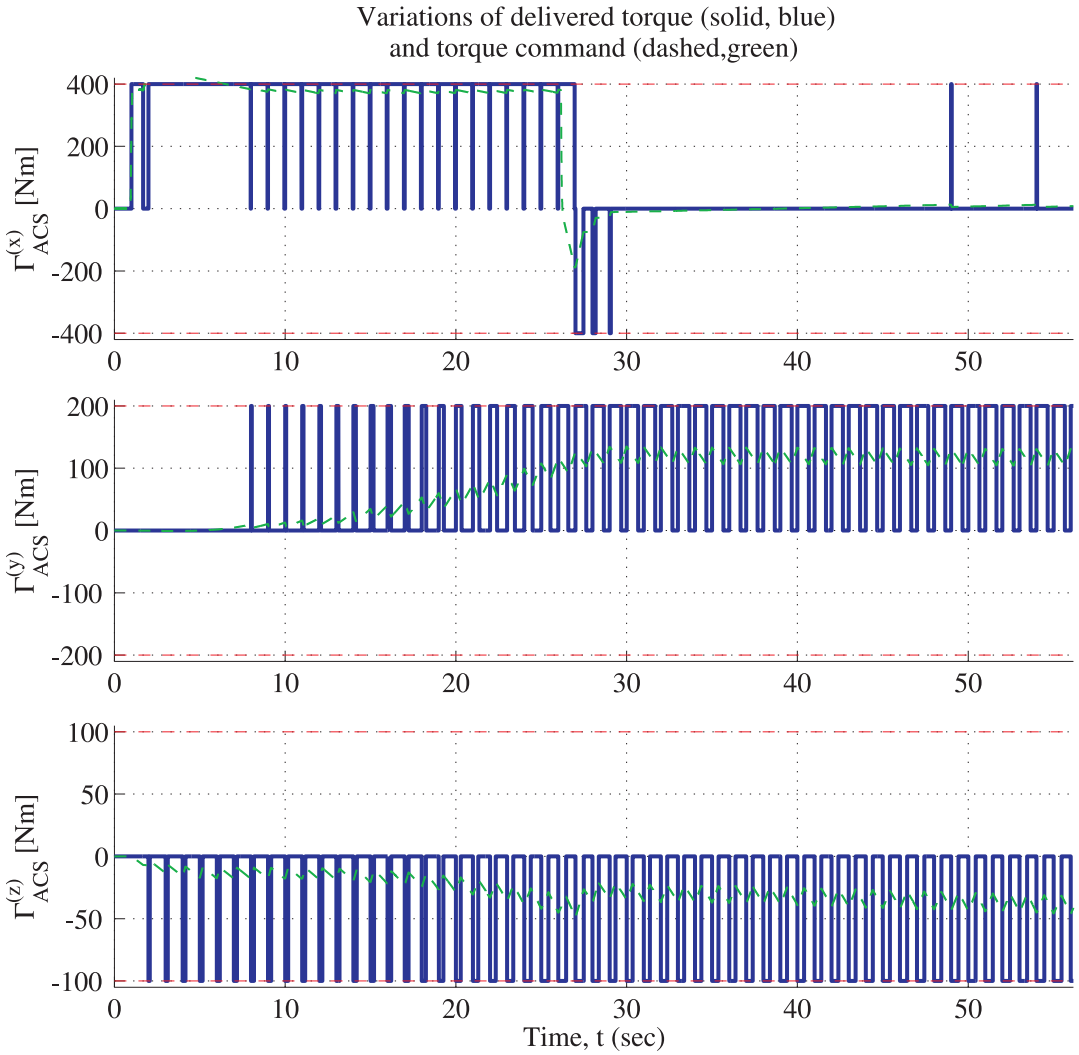

Figure 3.28: Evolution of the torque command and the torque delivered to the launcher by the ACS during spin maneuver.

3.9 Conclusions and closed-loop representation

This chapter aimed to present the system to be studied. The modeling done along the previous sections results in the closed-loop block diagram presented in figure 3.29.

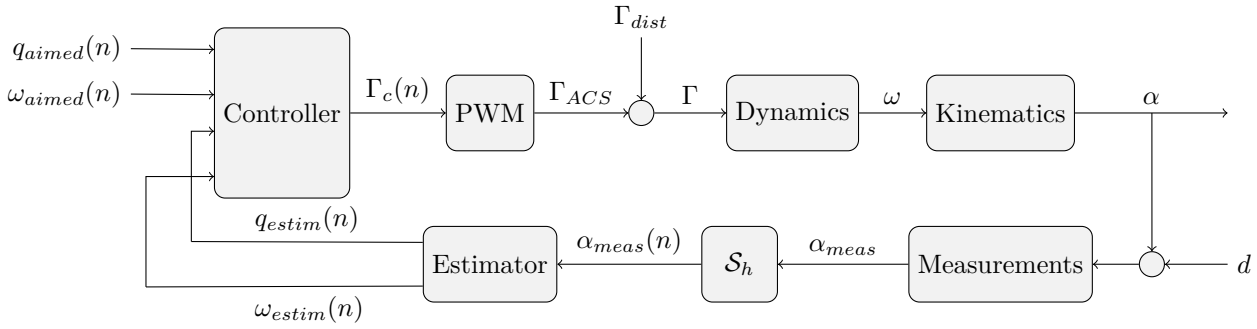

Figure 3.29: Full closed loop representation

Some simplifications have been done for the modeling but we kept as good representativeness as possible and the model has the trouble making characteristics of the launchers that Astrium ST and ESA engineers want to address during the project. The core of the system is the dynamic model. Its behavior is described by the equation of motion and the kinematic equation. The different ways to represent the attitude of the launcher have been presented. To measure the state of this physical model and allow reference tracking, the measurement and state reconstruction process as well as the controller have been defined. This part of the model will not be investigated thoroughly but further investigations on the subject should take care of it. Finally, the actuator of the Attitude Control System (ACS) have been modeled using a Pulse-Width Modulator (PWM) with saturation and threshold applied to the opening duration. This representation is very common in the field but lacks of dedicated investigations. As it is defined here, the model gathers the main subsystems that are known from engineering experience to be challenging for control law validation but also to be driving the behavior of the system. In particular, we mention the dynamic model and the actuator model. We will study them in details but separately later on in chapters 5 and 6.
The kinematic block remains problematic. The main question about it is whether it really affects the stability or not. From the experience gathered during this three year project, it seems that two points of view are opposed in the field. First, some people think that attitude representation is just a matter of finding a basis to express the position of the launcher. Assuming that, there should be no reason that the chosen representation e.g. Euler angles or quaternions, could influence the stability. On the other hand, the kinematic state equations we presented in section 3.3 are nonlinear in the states and result in signals with equilibrium states of infinite energy e.g. remember the norm of the identity quaternion. The latter characteristic could result in infeasible stability test as we will see later on. Even though some researches on the topic consider this issue [Wen and Kreutz-Delgado, 1991], [Ahmed et al., 1998], [Costic et al., 2001] and [Pereira and Vettori, 2006], addressing rigorously the stability of systems as ours remains very complex.

The system we are interested in has been defined, we are going to present some analytical tools for robustness analysis and especially Integral Quadratic Constraints (IQC).

Chapter 4

Robustness analysis with Integral Quadratic Constraints

4.1 Introduction

In system analysis, robustness assessment is crucial to ensure that the implementations of the designed system will behave as expected i.e. as the model which has been used for design. For obvious practical reasons, control laws are designed using models of the system to be controlled. The control laws development occurs long before the actual implementation on the real system. Prior to the V&V process, the control law is usually evaluated on a highly accurate simulation model before eventual hardware-in-the-loop laboratory testing. During these stages and even more during V&V, some unmodeled dynamics and also uncertain parameters cause the system to be controlled to be a disturbed version of the nominal model used for controller design. These dissimilarities may cause the real system to behave differently than expected and the overall system performance to degrade. In the worst cases, they may cause the system to go unstable in certain flight conditions. This is the reason why during the design and the analysis, it is necessary to consider how the system behavior will change with those perturbations and unmodeled phenomenon in order to establish how stability and performance margins will degrade. This is exactly the purpose of robustness analysis. This analysis takes place in a setup defined to allow introducing perturbations in a nominal system and assessing how the system will "react" to them.
This field has been developed since the 50's and has known tremendous advances in the 80's and early 90's. Three different theories allowing to study the robust stability and robust performance of systems are commonly described: absolute stability theory, input-output theory and robust control theory. Since all the methods rely on the same system representation, we will first introduce the Linear Fractional Representation (LFR). The purpose of the second section is to review the classical robustness analysis methods that emerged during the second half of the XXth century. The three techniques we present are based on the three different theories whose paradigm will be briefly discussed. After, we present the IQC framework for stability analysis, how an IQC describes an operator and finally we show some stability results using IQC description of operators. Finally, we will present the classical IQC multipliers in the aim to carry on the stability analysis of a space launcher.

Definitions We introduce the notations which will be used in the next chapters with $m, n \in \mathbb{N}_*$

Definition 1 $\mathbb{H}_\infty^{m\times n}$ *is the space of measurable functions bounded in the open right half plane.*

Definition 2 $\mathbb{RH}_\infty^{m\times n}$ *is the set of real rational transfer functions with no pole in the closed right half*

plane. This set contains the transfer functions that are said to be stable in the sense $Re(\lambda) < 0$ *or A Hurwitz, A being the state-matrix of the state-space equations.*

Definition 3 $\otimes$ *is the Kronecker product.*

4.2 Linear Fractional Representation

In this starting section, we aim to present the system representation all robustness analysis techniques rely on. Basically, it consists in a separation of the troublesome elements in the system from the others. The following paragraph aims to define this representation and shows how efficient and appropriate it is for robustness analysis.

Linear ordinary differential equations induced by laws of physics are usually used to model physical systems. Nevertheless, we want to deal with complex systems with nonlinear physics and involving numerous nonlinear devices and uncertain parameters. Indeed some parts of the system we study are unknown or uncertain e.g. mass repartitions; time-varying e.g. the force produced by the thrusters; nonlinear e.g. gyroscopic couplings; and so cannot be represented by linear ordinary differential equations. As a consequence, the resulting system model does not fit in the classical control theory framework and requires a particular attention. We are now going to see that all robustness analysis techniques (e.g. the small-gain theorem, the μ-analysis or IQC-based analysis) cope with these issues by the mean of a particular representation. This way of describing a complex system is called the Linear Fractional Representation (LFR). The LFR separates the system model into two subsystems. Generally speaking, one subsystem is an idealized system model which is split from a second subsystem, the so-called perturbation. The idealized system is usually ideal in the sense that it represents roughly the actual system while being "easy" to analyze. For instance, this is a system whose norm is easy to compute or whose asymptotic stability is easy to establish. On the contrary, the perturbation model gathers the elements which are not "ideal" from a control system engineer point of view but are needed to represent the original system accurately. Finally, since assessing the stability of the idealized part should not be difficult thanks to classical linear control theory, it is then possible to build on that and check whether ideal stable system affected by the possibly nonlinear, uncertain, time-varying perturbation block remains stable or not and if yes, up to which "size" of the perturbation. It is worth noticing that most of the time, the idealized subsystem will be a LTI system represented by its transfer function matrix.

Let us now give a more graphical representation of this. Considering a model S with input $u \in \mathcal{L}^{n_u}$ and output $y \in \mathcal{L}^{n_y}$ as the one figure 4.1. Such a mathematical model generally arises from the modeling of a real system.

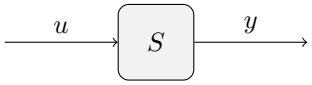

Figure 4.1: System S as initially modeled

As mentioned earlier, the equations describing S generally contains "troublesome" elements that are not entering in the classical linear control theory framework. These "trouble making" elements can be uncertainties, parameters varying with time, nonlinearities, etc. and prevent from using classical linear control theory for stability analysis. To face that issue, we split the system into two subsystems M and Δ. M will contain the dynamics of S which are known, time-invariant and linear for say "well-behaved" dynamics of the system while Δ will contain what is left i.e. the "troublesome" parts of the system. In other words, we can see M as an idealized version of S while Δ completes the system to make the interconnection of M and Δ representative of S. With such a construction the resulting representation (M, Δ) remains equivalent to S. This representation (M, Δ) is called a LFR of S and a general block diagram representation is given figure 4.2. We refer to input $z \in \mathcal{L}^{n_z}$ as the perturbation

input. Similarly, we call the output $w \in \mathcal{L}^{n_w}$ the perturbation output. We name them so as these channels link the perturbation operator Δ to the nominal system M. When we refer to "perturbations", we think about all what is out of the frame of classical linear control theory i.e. all the elements which are not LTI and known exactly. That means Δ gathers the uncertain parameters, the time-varying parameters, the nonlinear operators, etc. It is through these channels that Δ will affect the nominal behavior of S described by M. Notice that w and z do not necessarily have a physical meaning.
Let us discuss briefly the role of $d \in \mathcal{L}^{n_d}$ and $e \in \mathcal{L}^{n_e}$ in figure 4.2 even though they will not be our first center of interest. d is in general a perturbation signal like a measurement noise, an exogenous perturbation, etc. e is a signal that allows to measure the performance of the system. For instance, it can be the attitude error for the assessment of the tracking precision or the actuator output to measure the propellant consumption. Hence, it is interesting in system analysis to know how d influences e. For instance, we could investigate on how noisy measurements affects propellant consumption. Moreover, in robustness analysis it is also important to know how the influence of d on e will change with the introduction of a perturbation block Δ. Roughly, a perturbation signal d is usually well rejected by the nominal system. This is when there is no perturbation i.e. $\Delta = 0$. It is generally true since the controller has been designed such that the nominal transfer from d to e has low gain and satisfies the performance constraints. However, when Δ affects the nominal system the disturbance rejection can degrade resulting in values of e that are not acceptable performance-wise. This is why d and e are called the performance channels and the analysis of the Δ-dependent operator from d to e is called robust performance analysis.

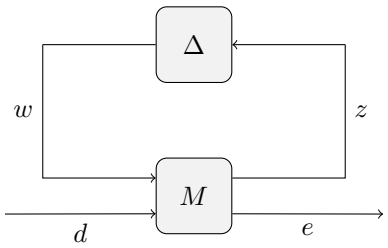

Figure 4.2: Linear fractional Representation of S

The interconnection of M and Δ in figure 4.2 can be referred to as upper LFR and denoted by $\mathcal{F}_u(M, \Delta)$. It means that the Δ block is above M and perturbation channels are the first inputs and outputs of M. In this case, the transfer function matrix of M can be partitioned into four blocks $M_{11} \in \mathbb{RH}_\infty^{n_z \times n_w}$, $M_{12} \in \mathbb{RH}_\infty^{n_z \times n_d}$, $M_{21} \in \mathbb{RH}_\infty^{n_e \times n_w}$ and $M_{22} \in \mathbb{RH}_\infty^{n_e \times n_d}$,

$$M := \begin{bmatrix} M_{11} & M_{12} \\ M_{21} & M_{22} \end{bmatrix}. \tag{4.1}$$

Hence we have the input-output relationship:

$$\begin{bmatrix} z \\ e \end{bmatrix} = \begin{bmatrix} M_{11} & M_{12} \\ M_{21} & M_{22} \end{bmatrix} \begin{bmatrix} w \\ d \end{bmatrix}. \tag{4.2}$$

Reversely, the LFR figure 4.3 is referred to as lower LFR and denoted $\mathcal{F}_l(M, \Delta)$. Generally, we will use upper LFR during this study.
$\mathcal{F}_u(M, \Delta)$ is the operator from input d to output e i.e. $e = \mathcal{F}_u(M, \Delta)(d)$. It is defined as a function of the nominal linear part M of the system and the perturbation Δ in the following manner:

$$\mathcal{F}_u(M, \Delta) = M_{22} + M_{21}\Delta \left(I - M_{11}\Delta\right)^{-1} M_{12}. \tag{4.3}$$

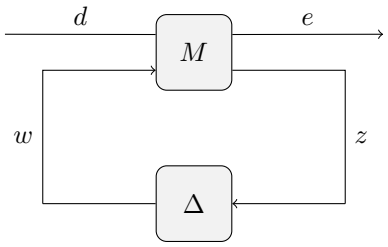

Figure 4.3: Lower Linear fractional Representation of S

$\mathcal{F}_u(M, \Delta)$ can be seen as a nominal mapping M_{22} perturbed by Δ while M_{11}, M_{12}, M_{21} reflect prior knowledge on how the perturbation affects the nominal map M_{22}. In the definition of $\mathcal{F}_u(M, \Delta)$, we observe two main things:

1. for $\Delta = 0$, the perturbation channels are void. In this case, the system is perfectly known, linear time-invariant as $\mathcal{F}_u(M, \Delta) = M_{22}$. Thus $\mathcal{F}_u(M, \Delta)$ will have its nominal behavior i.e. the behavior of the ideal system M_{22}. As soon as $\Delta \neq 0$, this ideal behavior will deteriorate due to the introduction of couplings between the perturbation input w and performance output e.

2. for $M_{11} = 0$, i.e. the case when the perturbation output do not influence the perturbation input, the transfer from performance input to performance output is still affected by the uncertainties through the perturbation term $M_{21}\Delta M_{12}$ determined from equation (4.3).

Likewise, the lower LFR operator $\mathcal{F}_l(M, \Delta)$ can be defined by permutation of the subscripts in eq. (4.3) and with the appropriate blocks definition:

$$\mathcal{F}_l(M, \Delta) = M_{11} + M_{12}\Delta \left(I - M_{22}\Delta\right)^{-1} M_{21}. \tag{4.4}$$

The previous definitions show how the system is split into a nominal system and a perturbation system to be studied. Our last remark will dwell on the fact that for any of the above LFR operators to be valid, the existence of an inverse for $I - M_{11}\Delta$ in (4.3) and $I - M_{22}\Delta$ in (4.4) is compulsory. Interconnections for which these terms have a causal inverse will be referred to as well-posed. Furthermore, the goal of robust stability is to ensure the boundedness of $I - M_{11}\Delta$ (resp. $I - M_{22}\Delta$) since under the assumption that $M \in \mathbb{RH}_\infty$, this will ensure the boundedness of $\mathcal{F}_u(M, \Delta)$ (resp. $\mathcal{F}_l(M, \Delta)$). The different methods we are going to describe will address different types of stability. Furthermore, depending on the system the perturbation block can have a different nature or structure. When talking about the nature of the operator Δ, we mean that the operators inside Δ can be different. As an example Δ can be a multiplication by an uncertain parameter, a multiplication by a time-varying gain, a nonlinear operator, etc. The robustness analysis techniques will deal with the nature of Δ differently leading to more or less conservative results. The structure of Δ describes both the couplings between its inputs and outputs and how the coupled inputs and outputs are linked. For instance, a structured Δ can have two inputs and two outputs, the firsts being the inputs and outputs of a saturation operator, the seconds being the inputs and outputs of a delay operator. Hence the first input does not influence the second output and the reverse holds. Here again, some techniques will allow taking into account the structure and/or the type of relationship between coupled inputs and outputs while others will not. This will cause the robustness results to be more or less conservative.
We are now going to describe the main techniques used for robustness analysis. All the methods have their characteristics and these must be well known and understood to choose the method in accordance to the characteristics of the system.

4.3 Classical methods for robust validation

4.3.1 Lyapunov based methods

At the end of the XIXth century, Alexandr Mihailovich Lyapunov started his PhD studies with the idea that if the total energy in a system is dissipated, then the system must be stable. He presented his works as well as the associated properties and theorems about stability of systems in 1892 in his PhD thesis [Lyapunov, 1892]. Despite these very early works, Lyapunov theory remained rarely used as it was resulting in hard calculations and equations which were not solvable at the time. In facts, from many results it is possible to derive Linear Matrix Inequalities (LMI) whose feasibility guarantees the stability. As a consequence, they were at the time applied only to systems with low dimensions (e.g. order < 4) when solutions were reachable by hand. The theory started to be fully exploited when the capabilities to solve LMI systems bettered in the second part of the XXth century. The research effort culminated with publications by Stephen Boyd [Boyd et al., 2004] and others as [Nesterov and Nemirovskii, 1994]. The book of Hassan Khalil [Khalil, 1996] presents the essentials of Lyapunov theory and more precisions about the results given in the present paragraph can be found in it.
Let us start by giving a definition of an autonomous system. Such a system is in some sense isolated as it has its initial state as only "input". It can be described by the state equation:

$$\dot{x} = f(x), \tag{4.5}$$

where $f : D \to \mathbb{R}^n$ is a locally Lipschitz map from a domain $D \subseteq \mathbb{R}^n$ into $\mathbb{R}^n$. We define an equilibrium point of the system $\bar{x} \in D$ to be a root of f, that is

$$f(\bar{x}) = 0. \tag{4.6}$$

From these definitions Lyapunov worked on characterizing the local and global stability of $\bar{x}$. That means he tried to answer the questions: *does the state vector of the system naturally moves toward $\bar{x}$? under which conditions? on the contrary, does it tend to move away from $\bar{x}$?* This resulted in the definitions of unstable, stable and asymptotically stable equilibrium points. See for instance page 96 of [Khalil, 1996]. We can now state the following stability theorem:

Theorem 1 (Lyapunov stability for nonlinear systems) *Let $\bar{x} = 0$ be an equilibrium point for (4.5). Let $V : S \to \mathbb{R}^n$ be a continuously differentiable function on a neighborhood S of $\bar{x} = 0$, such that*

$$V(0) = 0 \text{ and } V(x) > 0 \text{ over } S - \{0\},$$
$$\dot{V}(x) \leq 0 \text{ in } S.$$

Then the equilibrium point $\bar{x} = 0$ is stable.
Moreover, if

$$\dot{V}(x) < 0 \text{ in } S - \{0\},$$

then the equilibrium point $\bar{x} = 0$ is asymptotically stable.

If the hypotheses of theorem 1 are valid, and in addition to that, $\|x\| \to \infty$ implies $V(x) \to \infty$, then the equilibrium point is globally asymptotically stable. Theorem 1 and the so-called Lyapunov function V are the core of Lyapunov's theory. The main interest of this method is that it is possible to reach a stability proof without solving the nonlinear differential equations describing the system. This is of course an advantage when these differential equations are difficult to solve. However, the blind search of a suitable

V can be very laborious. For physical systems, energy-like functions are usually appropriate but if not there is no other way than trying and testing with Lyapunov function candidate of a given structure. It could be the main explanation of the fact that the theory has been used to prove the stability of many particular systems, leading to widely used results. A couple of basic examples are presented next.

Example 2 (Stability of linear autonomous systems) *To simplify the autonomous system from (4.5), consider that it is a linear system with state matrix $A \in \mathbb{R}^{n\times n}$. The state equation reads as:*

$$\dot{x} = Ax. \tag{4.7}$$

We can study the asymptotic stability of the system (4.7) by looking for a quadratic Lyapunov function candidate

$$V(x) = x^T P x \tag{4.8}$$

where P is a real symmetric positive definite matrix to make V positive definite. To guarantee $\dot{V}(x) < 0$, we determine the derivative of V with respect to time along the trajectories of (4.7) and obtain the equalities:

$$\begin{aligned} \dot{V}(x) &= x^T P \dot{x} + \dot{x}^T P x \\ &= x^T \left(A^T P + P A\right). \end{aligned} \tag{4.9}$$

From the definition of V and $\dot{V}$ in (4.8) and (4.9), respectively, we can ensure global asymptotic stability of the system with theorem 1 by making sure that $P \in \mathbb{R}^{n\times n}$, $P = P^T$ is a solution of the LMI constraints:

$$\begin{cases} P \succ 0, \\ A^T P + P A \prec 0. \end{cases} \tag{4.10}$$

Here, we can think about the numerous extensions that can be drawn from this result. For instance for more complex state equations or if we consider that the input comes from some particular actuator. A well known example for the use of the Lyapunov method for feedback systems is given below.

Example 3 (Lure's problem) *Lure's problem consists in the stability analysis of the interconnection of a linear time-invariant strictly proper system M_0 with a memoryless sector bounded nonlinearity ψ_0 as in figure 4.4. For convenience, we will only present the scalar case. The reader can fond the multi-input multi-output result in [Khalil, 1996].*

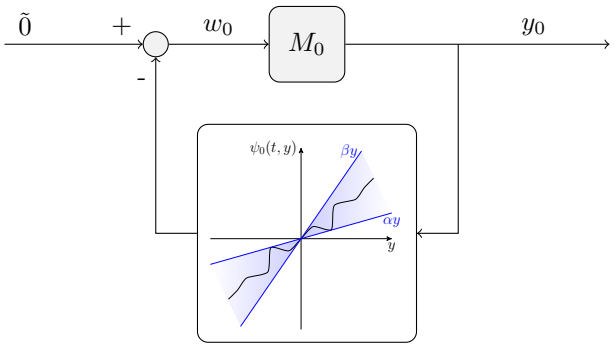

Figure 4.4: Setup of Lure's problem for ψ_0 in the sector (α, β)

The possibly time-varying nonlinearity ψ_0 satisfies the sector condition (α, β):

$$\forall y, \forall t \geq 0, \quad \alpha y^2 \leq y\psi_0(t,y) \leq \beta y^2. \tag{4.11}$$

We observe that these two inequalities can be equivalently reformulated as:

$$\forall y, \forall t \geq 0, \quad (\psi_0(t,y) - \alpha y)(\beta y - \psi_0(t,y)) \geq 0. \tag{4.12}$$

Since this expression is quadratic, we can recast it into a quadratic form such as:

$$\forall y, \forall t \geq 0, \quad \begin{bmatrix} y \\ \psi_0(t,y) \end{bmatrix}^T \begin{bmatrix} -\alpha\beta & \frac{\alpha+\beta}{2} \\ \frac{\alpha+\beta}{2} & -1 \end{bmatrix} \begin{bmatrix} y \\ \psi_0(t,y) \end{bmatrix} \geq 0. \tag{4.13}$$

This formulation will be useful later on.
The analysis of such a feedback system can be done through the analysis of another linear system interconnected with a nonlinearity ψ in the sector $(0,k), k > 0$ as in figure 4.5. The transformation consists in integrating the "minimum gain" of the nonlinearity ψ_0 i.e. the lower-limit α of the sector bound, in the system M_0 of figure 4.4. It results in the definition of the system M, the nonlinearity ψ and the interconnection sketch figure 4.5.

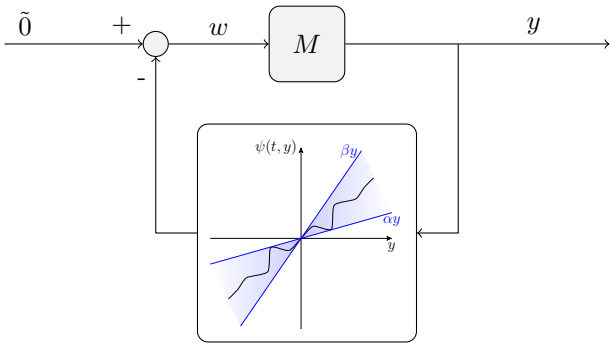

Figure 4.5: Setup of Lure's problem for ψ in the sector $(0,k)$

In this framework, the use of a so-called Lure-type Lyapunov function introducing $\eta > 0$ and $P = P^T > 0$ as below allows to determine a condition for absolute stability of the interconnection. The Lure type Lyapunov function reads as

$$V(x) = x^T P x + 2\eta \int_0^y \psi(y) d\sigma, \tag{4.14}$$

where a state-space realization of M is:

$$\begin{cases} \dot{x} = & Ax + Bw, \\ y = & Cx. \end{cases} \tag{4.15}$$

To find a stability condition, we use the fact that for $\alpha = 0$ and $\beta = k$, the sector condition (4.11) reads as:

$$\forall t \geq 0, \quad \begin{bmatrix} x(t) \\ w(t) \end{bmatrix}^T \begin{bmatrix} 0 & -kC^T \\ -kC & -2 \end{bmatrix} \begin{bmatrix} x(t) \\ w(t) \end{bmatrix} \geq 0. \tag{4.16}$$

This expression comes from (4.13) and

$$\begin{bmatrix} y \\ \psi_0(t,y) \end{bmatrix} = \begin{bmatrix} C & 0 \\ 0 & -I \end{bmatrix} \begin{bmatrix} x(t) \\ w(t) \end{bmatrix}.$$

Then let us determine the negativity condition for $\dot{V}(x)$. First, we calculate the derivative

$$\begin{aligned} \dot{V}(x) = & \; x^T(A^TP + PA)x + w^TB^TPx + x^TPBw - \eta(w^TCAx + x^TA^TC^Tw + w^T(CB + B^TC^T)w) \\ = & \begin{bmatrix} x(t) \\ w(t) \end{bmatrix}^T \begin{bmatrix} A^TP + PA & PB - \eta A^TC^T \\ B^TP - \eta CA & -\eta(CB + B^TC^T) \end{bmatrix} \begin{bmatrix} x(t) \\ w(t) \end{bmatrix}. \end{aligned} \tag{4.17}$$

Hence negative definiteness of $\dot{V}(x)$ is guaranteed by

$$\begin{bmatrix} A^TP + PA & PB - \eta A^TC^T \\ B^TP - \eta CA & -\eta(CB + B^TC^T) \end{bmatrix} \prec 0. \tag{4.18}$$

Finally, by the S-procedure from [Yakubovich, 1971], a sufficient condition for asymptotic stability of the system presented in figure 4.4 is the existence of $\eta > 0$ and $P = P^T > 0$ such that:

$$\begin{bmatrix} A^TP + PA & PB - kC^T - \eta A^TC^T \\ B^TP - kC - \eta CA & -2 - \eta(CB + B^TC^T) \end{bmatrix} \prec 0. \tag{4.19}$$

The feasibility of this LMI guarantees absolute stability of Lure's interconnection in figure 4.4. Even though it is now easy to solve with a computer, such problems have been unsolvable numerically for a long time after the theoretical results came up.

The literature about Lyapunov theory based results is abundant, especially since we are able to solve LMI problems with efficiency and good accuracy as presented in [Nesterov and Nemirovskii, 1994] and [Boyd et al., 2004]. These results from the field of numerics allow to solve large LMI systems and so to assess the stability of any nonlinear, time-varying system with Lyapunov theory without solving the corresponding differential equations. For instance, solving (4.10) was not possible for large problems before the advances in computing technologies and algorithms.
In the case when we want to address the stability of a nonlinear system and there is no available result in the literature, the stability analysis using Lyapunov theory follows the so-called Lyapunov direct method described hereunder:

1. study the system,
2. elaborate a Lyapunov function candidate,
3. verify whether stability conditions are satisfied.

This very basic process can lead to very difficult problems especially when looking for negative definiteness of $\dot{V}$ over the whole state space i.e. to look for global asymptotic stability. Hence, numerous works are dealing with local stability. However, such results can be seen as less attractive from an engineering point of view since they guarantee stability over a bounded set of initial conditions in the state space. The main drawback of the use of Lyapunov theory in stability analysis is also its main

advantage. The freedom of choosing any positive function of the states as a Lyapunov function candidate makes this choice very consequential and so very difficult. Indeed, as the set of positive functions of the state vector is very vast, in general we will choose the Lyapunov candidate functions within a predefined set to make the search for a Lyapunov function proving stability tractable e.g. the set of positive quadratic functions of the state vector. Consequently, not finding a Lyapunov function of this set that fulfills the stability conditions does not guarantee that the system is not stable. In other words, the choice of one type of Lyapunov function (e.g. quadratic or energy like, Lure-type,etc.) can cause the stability test to fail only because the choice is not appropriate. Another drawback is that for the analysis of a particular system, we have to build a dedicated Lyapunov function causing the use of such a method in the traditional design process quite difficult. Indeed, in the industry, the usual starting point of the analysis process is a very simple model. For this particular model we can eventually construct a Lyapunov function that proves global stability. Later the model complexity is increased to obtain more representative results and the new model may require a completely different Lyapunov function for its stability proof. Hence this tool is not as flexible as the methods we will present later on. A well described numerical solution for the search of structured quadratic Lyapunov functions is given in [Boyd and Yang, 1989]. Some examples of complex Lyapunov functions for particular systems can be found in [Tarbouriech and Gomes Da Silva Jr, 2000] and [Seuret and Gomes Da Silva Jr, 2011] for sampled-data systems with saturated inputs, in [Gahinet et al., 1996] for slowly time-varying scalar parameters, in [Fridman et al., 2005] for robust control of sampled-data systems, in [Liu et al., 2010] for stability analysis of systems with sawtooth delays.
For stability analysis with Lyapunov theory, the LFR do not need to be explicitly defined since the state-space equations do not need to have particular properties. Hence, Lyapunov theory based robustness analysis accounts for the nature and structure of the "trouble making" elements of the system without describing it as such but only because they appear in the state-space equations. Nevertheless, since each stability result derived from Lyapunov theory seems to be suitable only for very specific systems and lacks flexibility, we are now going to present a different method which deals with input-output characteristics of the signals in an interconnection and so which is much more general.

4.3.2 Small gain theorem

The most famous result on robust stability comes from George Zames [Zames, 1966] who derived in 1966 open-loop conditions for the stability of time-varying nonlinear feedback systems by evaluating their input to output gain. The result is based on a representation of the system as the interconnection between two subsystems considered as black boxes. What is taken care of is that when two operators with a given input-output characteristic are interconnected in a feedback structure as in figure 4.6, the resulting feedback system remains stable as long as d_1 and d_2 remain bounded.

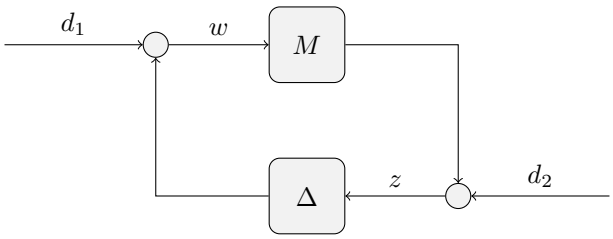

Figure 4.6: System interconnection for Small Gain Theorem

In figure 4.6, d_1 and d_2 can be seen as exogenous signals like references or perturbations. As long as these signals remain bounded according to some norm, the stability implies that all the signals in this interconnection will remain bounded. This is guaranteed by the boundedness of the systems in the

interconnection. For the statement of the small gain theorem, we introduce the system norm $\|\bullet\|$. It can be any operator norm induced by the norm of a Banach linear space of signals.

Theorem 2 (Small-gain theorem) *In figure 4.6, assuming that there exists a causal inverse of* $I - M\Delta$*, if* $\|M\|\|\Delta\| < 1$ *then the interconnection is stable.*

It is worth noticing that as long as we can characterize the operators in Δ by the chosen norm $\|\bullet\|$, we can use the small-gain theorem. The main drawback is that it considers the norm of Δ without taking care of its structure. The small-gain theorem gives conservative results in general. However, the introduction of multipliers or the use of loop transformations can result in conservatism reduction as mentioned in [Jönsson, 2001].

The small-gain theorem is a powerful result in the sense that it can be used for any type of system as long as we can characterize its norm. It means that Δ (but also M) can be anything from a LTI stable system to a nonlinear time-varying operator with uncertain parameters. In facts, this property is very useful for the analysis of complex systems such as space launchers as they involve various types of subsystems which can be discrete or continuous time, linear or nonlinear, time-varying or time-invariant, known or unknown. Any system resulting from the combination of all these types of subsystems can be analyzed using the small-gain theorem.
The main drawback in using small-gain theorem for robust stability and performance assessment is that it does not take into account the structure of the subsystems that form the system. More precisely, if the operator Δ is known to have inputs and outputs which are decoupled, we cannot account for this in the analysis with the small-gain theorem. This feature can be very detrimental to the conservatism of the technique since all systems present structure as we will see it later on when building simple system interconnections. A second drawback is that the small-gain theorem views Δ as a black box and considers only its input and output norms with no care for the nature of the sub-blocks defining Δ. In facts, the analyzes with the small-gain theorem of a system with Δ being a an unknown time-invariant parameter and with Δ being a time-varying nonlinearity are exactly the same although these two operators may not have the same consequences on the system stability. To apply the small-gain theorem, we will simply compute a norm of Δ and compare it to the norm of M.
The most well known technique dealing with structured Δ blocks is the μ-analysis.

4.3.3 μ-analysis

The μ-analysis was first presented by John Doyle in [Doyle, 1982] and [Doyle et al., 1982]. He proposed a systematic way to take the structure of the perturbation i.e. the structure in the Δ block, into account for robustness analysis of uncertain systems. The structure of an perturbation block Δ corresponds to the size and position of the sub-blocks defining it and whose inputs and outputs are decoupled. μ-analysis was a huge advance in control theory when it appeared. A few years later, structured singular value techniques have been complemented with synthesis techniques in [Doyle, 1985] and the potential of the method was exploited for the analysis of mixed uncertain operators as in [Fan et al., 1991]. Here the system standard interconnection for robust stability analysis from [Doyle, 1982] depicted in figure 4.7.
In the configuration figure 4.7, Δ is a structured stable LTI perturbation such that for all $\omega \in [0, \infty)$, $\Delta(j\omega)$ belongs to a set $\bar{\Delta}$ and M is the stable transfer function from perturbation output w to perturbation input z. We can now introduce the definition of the structured singular value.

Definition 4 (The structured singular value μ) *Let us define the set of structured uncertainty blocks* $\bar{\Delta}$*:*

$$\begin{aligned}\bar{\Delta} = \{&diag\left[\delta_1^r I_{t_1}, \ldots, \delta_V^r I_{t_V}\ ,\ \delta_1^c I_{r_1}, \ldots, \delta_S^c I_{r_S}\ ,\ \Delta_1, \ldots, \Delta_F\right], \\ &\delta_k^r \in \mathbb{R}, \delta_i^c \in \mathbb{C}, \Delta_j \in \mathbb{C}^{m_j \times n_j}\}.\end{aligned} \tag{4.20}$$

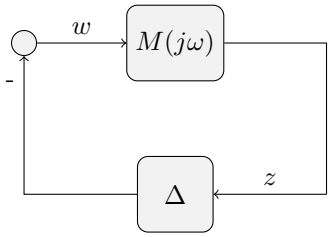

Figure 4.7: System interconnection for μ-analysis

Matrices from $\bar{\Delta}$ *are block diagonal with real scalar, complex scalar and complex matrices as diagonal blocks. Given the matrix* $M(j\omega) \in \mathbb{C}^{n\times m}$ *with* $\omega \in [0,\infty)$, $\mu_{\bar{\Delta}}(M(j\omega))$, *the structured singular value of* $M(j\omega)$ *with respect to* $\Delta(j\omega) \in \bar{\Delta}$ *is defined as:*

$$\mu_{\bar{\Delta}}(M) = \frac{1}{\min\{\bar{\sigma}(\Delta(j\omega)), \Delta(j\omega) \in \bar{\Delta}, det(I - M(j\omega)\Delta(j\omega)) = 0\}}, \tag{4.21}$$

unless no $\Delta(j\omega) \in \bar{\Delta}$ *makes* $(I - M(j\omega)\Delta(j\omega))$ *singular, then* $\mu_{\bar{\Delta}}(M(j\omega)) = 0$.

The definition presents $\mu_{\bar{\Delta}}(M(j\omega))$ as the inverse of the measure of the smallest structured $\Delta(j\omega)$, "small" in the sense of $\bar{\sigma}$, that causes instability of the interconnection figure 4.7 [Packard and Doyle, 1993]. One of the properties of $\mu_{\bar{\Delta}}(M(j\omega))$ is that it looks for $\Delta(j\omega)$ blocks causing singularity only among the operators of $\bar{\Delta}$ only.
From this, we can state the stability theorem for systems with structured LTI uncertainties.

Theorem 3 (μ-analysis) *Consider the interconnection figure 4.7 and a real number* $\gamma > 0$. M *is a given, stable, linear, time-invariant, finite-dimensional system. The interconnection is stable for all* Δ *such that for all* $\omega \in [0,\infty)$, $\Delta(j\omega) \in \bar{\Delta}$ *and* $\bar{\sigma}(\Delta(j\omega)) < \gamma$ *if and only if*

$$\sup_{\omega\in[0,\infty)} \mu_{\bar{\Delta}}(M(j\omega)) \leq \frac{1}{\gamma}. \tag{4.22}$$

In the assumptions of the stability theorem, we can find a key feature of μ-analysis. This technique allows to address the stability of interconnections of LTI operators. Although it is absolutely crucial, this assumption is often misunderstood by control system engineers. No time-varying systems can be analyzed with the above theorem. Nevertheless, when it comes to the analysis of time-invariant systems or systems that can be assumed as not varying with time, then the μ-analysis is perfectly suitable. Equation (4.22) is similar to the small-gain stability condition in paragraph 4.3.2. Indeed, the stability condition (4.22) involves a measure of M given by μ_Δ that has to be lower than $1/\gamma$ where γ is a measure of Δ (here the $\mathcal{H}_\infty$ norm). As a comparison, in paragraph 4.3.2 the stability condition could have been written as

$$\|M\| < \frac{1}{\|\Delta\|} \tag{4.23}$$

to be compared to (4.22). Here appears one crucial thing about the way of thinking in modern robustness analysis. The improvement brought by the measure by the structured singular value $\mu_{\bar{\Delta}}$ is that it "measures" M while taking into account which channels of M are affected by the outputs of Δ. The assessment of the robustness of systems is done by "measuring" the blocks in the system and check whether the open-loop has a gain less than one. The "measure" can be given with different methods e.g. singular value or structured singular value.
Today, the computation of the bounds of μ is accessible, efficient, and it can be very accurate (see e.g. [Packard and Doyle, 1993]). Thus we can appreciate fully the power of this method. Indeed, in a process

of verification and validation, one of the main points is to address the robustness of the system in the face of parametric uncertainties. This type of uncertainty appears almost everywhere from the dimensions (mass, size, inertia) to subsystem parameters (voltage, force, resistance) but also in the environment. In comparison with the small-gain theorem, μ does look into the "black box" to take advantage of what is known about the structure of the perturbation. It decouples the inputs and outputs of Δ which are known to be decoupled allowing to diminish the conservatism of the analysis with respect to the small-gain theorem as shown very early by [Doyle, 1982]. The main drawback is a counterpart of the fact that μ-based tools are dealing perfectly with parametric uncertainties. Time-variations or nonlinearities are not handled by the structured singular value as it has been defined in this paragraph. Some attempts to extend the framework to time-varying uncertainty as [Paganini, 1995] showed good result but that are not accessible from the theoretical point of view and so difficult to introduce as routine methods in the industry. It means we have no convenient way obtain stability or performance certificates for time-varying and/or nonlinear systems using the structured singular values. This pushes us toward more advanced analysis techniques that will enable us to assess the stability and performance of complex systems such as space launchers.

4.3.4 Conclusion

The previous paragraphs aimed to give a brief overview of the main tools available for robust validation. The main difference among them is a matter of philosophy. The three methods are dealing with the system to be assessed with different approaches.
First, absolute stability theory (Lyapunov's theory) does not take into account "uncertainties" or "parameters" or "nonlinearities" explicitly. It relies on a model which can be arbitrarily complex and is hoped to be representative of reality. Nothing else is considered but what is covered by the state-space equation of the model (4.5). As we analyze the nonlinear model, a proof of stability with Lyapunov direct method guarantees stability of the system that was defined and nothing else. No margins can be given, only a possibly conservative YES/NO answer to the question: *is the present system stable?*.
On the opposite side, the input-output theory (small-gain) splits the model between two or more sub-models generally separating the known and the unknown in the system to be studied. The analysis follows on by determining the input-output behavior of each block. The actual process and phenomenon occurring in the blocks are neglected. Finally, stability is assessed by ensuring the compatibility between each part. For instance, the small-gain theorem aims to make sure that the norm of the signals in the interconnection of the sub-models does not go to infinity. When the interconnection separates the known from the unknown (e.g. the nominal system from the perturbations affecting it), we can give a bound on the norm of the perturbation block which guarantees the stability. More generally, input-output theory allows to quantify the variations in the norms of the systems such that their interconnection remains stable in the sense of the chosen norm. Thus we can determine stability margins. The robust stability result is given as a tolerance of the nominal system to an unstructured perturbation up to a certain size determined by the chosen measure (e.g. singular value or structured singular value).
The μ-analysis framework pushes further the approach of input-output theory. Similarly to the framework of the small-gain theorem described above, two subsystems are considered: the "known" one and the "unknown" one. Then the idea is to find a measure of the known system that takes into account the structure of the unknown part when seeking for a condition of stability of the interconnection. This condition is a condition on a measure of the perturbation Δ allowing us to evaluate the stability margins. Currently, input-output methods are the most widely used in the industry because they are taught in universities and also because the tools needed to analyze systems quickly and efficiently are already available. Development of Semi-Definite Program (SDP) solvers such that SeDuMi [Sturm, 1999], SDPT3 [Toh et al., 1999] and LMILAB [Gahinet and Nemirovskii, 1993]; and the associated parsers: YALMIP [Löfberg, 2004] and TKLMITOOL [El Ghaoui et al., 1995] allowed efficient implementations of the vari-

ous results that can now be used easily. Concerning Lyapunov theory, it does not benefit from the same advantages as its competitors. Despite the great development of solvers, the theory remains too involved mathematically speaking even though its energy interpretation is very pragmatic and well understood by engineers. Another point to dwell on is that Lyapunov theory does not benefit from the same flexibility as the input-output robustness analysis methods.
Among these remarks, one last will give the motivation for further investigations toward more advanced analysis techniques. So far, the two methods we mentioned that can handle nonlinear time-varying systems are the small-gain theorem and the Lyapunov theory based analysis. In the previous section, these two were presented as too conservative and not flexible enough, respectively. This is why we need to investigate other techniques that will permit to perform robustness analysis in a less conservative and more efficient way.

4.4 Robust validation with IQC

The previous short review of available robustness analysis techniques showed the need for an analytical tool able to handle the variety of complex systems with flexibility (easy evolution of the analysis model), reduced conservatism (resulting stability domains are close to the actual stability domain of the system) and capacity to account for the structure of the perturbation (consider decoupled channels in Δ). Since the Integral Quadratic Constraint (IQC) theory seems to fulfill these needs, it is interesting for us to describe how the IQC framework is defined. In addition to that first remark, we also mention the fact that a previous ESA project resulted in the implementation of a upper level Matlab® toolbox allowing to perform IQC analyzes easily. We will refer to its user guide many times in this thesis as [Köroglu et al., 2008]. It contains a good description of the IQC-based analysis method and present a thorough review of IQC literature.
The IQC-based robustness analysis method has been presented in 1997 by Alexandre Megretski and Anders Rantzer in [Megretski and Rantzer, 1997] as a unifying approach between the main fields in control theory: absolute stability theory, input-output theory and robust control theory. The theory developed in their article builds upon works of many including mainly Yakubovich [Yakubovich, 1967], [Yakubovich, 1982], who explicitly made use of IQC during the 70's to deal with stability analysis of nonlinear systems. It also comes from works on input-output theory by Jan Willems [Willems, 1971] or George Zames in [Zames, 1966] and [Zames and Falb, 1968], and from studies of the robust control field by John Doyle [Doyle, 1982] and many others. In facts, these authors represent the three main fields the theory has its roots in. IQC theory merges these different robustness analysis methods in one framework. The following paragraphs aim to present IQC based stability analysis as well as the way IQC can be used to describe operators.

4.4.1 Signals and systems for IQC validation

Signals

For the study, we will focus on signals from the linear space of time-functions $\mathcal{L}^n$ defined on the positive time axis $[0;+\infty)$. The $\mathcal{L}_2$ norm of a size-n signal $x \in \mathcal{L}^n$ is defined as

$$\|x\|_{\mathcal{L}_2} = \left(\int_0^{+\infty} |x(t)|^2 \mathrm{dt} \right)^{1/2}, \tag{4.24}$$

where $|\bullet|$ is the Euclidean norm i.e. the 2-norm over $\mathbb{R}^n$, that is $|\bullet| = \sqrt{\langle \bullet, \bullet \rangle_{\mathbb{R}^n}}$. The signals for which the $\mathcal{L}_2$ norm exists and is finite are the ones we will consider. They belong to $\mathcal{L}_2^n$ defined as

$$\mathcal{L}_2^n := \{ x \in \mathcal{L}^n \mid \|x\|_{\mathcal{L}_2} < \infty \}. \tag{4.25}$$

The energy of signals in $\mathcal{L}_2$ is bounded since the energy is defined as the squared $\mathcal{L}_2$ norm. The energy of a signal $x \in \mathcal{L}^n$ will be denoted $\|x\|_E$ and so we will have the following property for all $x \in \mathcal{L}_2^n$

$$\|x\|_{\mathcal{L}_2}^2 = \|x\|_E < \infty. \tag{4.26}$$

The linear space $\mathcal{L}_2^n$ is a Hilbert space with inner product defined as the bilinear form $\langle \bullet, \bullet \rangle_{\mathcal{L}_2}$ from $\mathcal{L}_2^n \times \mathcal{L}_2^n$ to $\mathbb{R}$:

$$\langle x, y \rangle_{\mathcal{L}_2} = \int_0^{+\infty} x(t)^T y(t) \mathrm{dt}. \tag{4.27}$$

This inner-product induces a norm over $\mathcal{L}_2^n$ because $\|x\|_{\mathcal{L}_2}^2 = \langle x, x \rangle_{\mathcal{L}_2}$. Lastly, since any $x \in \mathcal{L}_2^n$ has a Fourier transform

$$\mathcal{F}\{x(t)\} = \hat{x}(j\omega) = \int_0^{+\infty} x(t) e^{-j\omega t} \mathrm{dt}$$

where ω is the frequency in rad.s^{-1}, Parseval's theorem states as:

$$\langle x, y \rangle_{\mathcal{L}_2} = \frac{1}{2\pi} \int_{-\infty}^{+\infty} \hat{x}(j\omega)^* \hat{y}(j\omega) \mathrm{d}\omega. \tag{4.28}$$

To conclude this paragraph, we put the emphasis on the useful fact that time-domain and frequency-domain expressions are perfectly equivalent thanks to the definition of the inner-product and Parseval's theorem. This mathematical property and its consequences will be useful later on:

$$\|x\|_{\mathcal{L}_2}^2 = \langle x, x \rangle_{\mathcal{L}_2} = \int_0^{+\infty} x(t)^T x(t) \mathrm{dt} = \frac{1}{2\pi} \int_{-\infty}^{+\infty} \hat{x}(j\omega)^* \hat{x}(j\omega) \mathrm{d}\omega = \|x\|_E < \infty. \tag{4.29}$$

$\mathcal{L}_{2e}$ space

$\mathcal{L}_2$ signals have been defined, we now define a slightly larger class of signals that is the extended $\mathcal{L}_2$ space denoted by $\mathcal{L}_{2e}$. These signals do not necessarily have a finite $\mathcal{L}_2$ norm but their truncation of any length has finite norm. For all signal $x \in \mathcal{L}_{2e}^n$, the following holds:

$$\forall T \geq 0, \quad \left(\int_0^T |x(t)|^2 \mathrm{dt} \right)^{\frac{1}{2}} < \infty. \tag{4.30}$$

To give the definition of $\mathcal{L}_{2e}^n$, let us consider $T \in \mathbb{R}_+$, the truncation operator is defined as:

$$\forall x \in \mathcal{L}^n, \quad P_T(x)(t) = \begin{cases} x(t) & \text{, if } t \leq T \\ 0 & \text{, if } t > T \end{cases}. \tag{4.31}$$

From the definition (4.31), we can recast (4.30) for all signal $x \in \mathcal{L}_{2e}^n$:

$$\forall T \geq 0, \quad \|P_T(x)\|_{\mathcal{L}_2} < \infty. \tag{4.32}$$

As a consequence, we obtain:

$$\mathcal{L}_{2e}^n := \{ x \in \mathcal{L}^n \mid \forall T \geq 0, P_T(x) \in \mathcal{L}_2^n \}. \tag{4.33}$$

Systems

After defining the signals that are considered for system analysis with IQC, the systems generating these signals are described hereunder. Generally speaking, the systems will be represented as mappings from $\mathcal{L}^{n_u}$ to $\mathcal{L}^{n_y}$. Indifferently, we will refer to systems as systems, operators, mappings or functions. The main characteristic that is going to be investigated is the induced $\mathcal{L}_2$ gain. The induced $\mathcal{L}_2$ gain of a system $G : \mathcal{L}^{n_u} \to \mathcal{L}^{n_y}$ is defined as

$$\|G\|_{\mathcal{L}_2 \to \mathcal{L}_2} = \max_{u \in \mathcal{L}_2^{n_u},\, u \neq 0} \frac{\|Gu\|_{\mathcal{L}_2}}{\|u\|_{\mathcal{L}_2}}. \tag{4.34}$$

The system G is said to be bounded if its induced $\mathcal{L}_2$ gain (4.34) is finite. Pragmatically, it means that when the input signal of G has finite energy, the resulting output has finite energy too. For convenience and clarity, we drop the subscript and for now on $\|G\|$ will denote the induced $\mathcal{L}_2$ gain of G if no other precision is given. During this study, $\mathcal{L}_2$ bounded systems will be referred to stable systems in the sense of the $\mathcal{L}_2$ norm. A well known example of system is given below.

Example 4 (Linear systems) *A Linear Time Invariant (LTI) system S is defined by its state-space representation*

$$\begin{cases} \dot{x} = & Ax + Bu \\ y = & Cx + Du \\ x_0 = & x(0), \end{cases} \tag{4.35}$$

with $A \in \mathbb{R}^{n \times n}$, $B \in \mathbb{R}^{n \times n_u}$, $C \in \mathbb{R}^{n_y \times n}$ and $D \in \mathbb{R}^{n_u \times n_y}$. S maps $u \in \mathcal{L}^{n_u}$ into $y \in \mathcal{L}^{n_y}$ whose expression is given for $t \geq 0$ by Cauchy's formula:

$$y(t) = Ce^{At}x_0 + \int_0^t Ce^{A(t-\tau)}Bu(\tau)d\tau + Du(t). \tag{4.36}$$

The system in the example above is also causal. Causality means that at any time instant, the output does not depend on the future values of the input signal. Mathematically speaking, we can define causality using the truncation operator P_T defined in (4.31). The system G is said to be causal if it satisfies

$$P_T(G(u)) = G(P_T(u)) \text{ for all } T > 0,\ u \in \mathcal{L}_{2e}^{n_u}. \tag{4.37}$$

We defined the signals and systems that we are going to consider for the robustness analysis of systems under LFR presented in section 4.2. We can now go ahead and present how to describe the perturbation operator Δ with an IQC.

4.4.2 Description of operators with IQC

Definitions

In this paragraph we present the most classical mathematical expressions of IQC.
For this, let us define H a symmetric matrix of $\mathbb{R}^{n_h \times n_h}$ and Φ a LTI system with $n_z + n_w$ inputs and n_h outputs with transfer function in $\mathbb{RH}_\infty$. In addition to that, we consider a causal $\mathcal{L}_2$ bounded operator Δ. With H and Φ, we can define an IQC as a sign constraint on the weighted norm of

$$P_T\left(\Phi\left(\begin{bmatrix} z \\ \Delta(z) \end{bmatrix}\right)\right).$$

This IQC aims to gather information about how Δ operates on its input z. This will become clearer shortly.

Definition 5 (Hard IQC) *The $\mathcal{L}_2$ bounded and causal operator Δ is said to satisfy the hard IQC defined by (Φ, H) if*

$$\int_0^T \left(\Phi \begin{bmatrix} z(t) \\ \Delta(z)(t) \end{bmatrix} \right)^T H \left(\Phi \begin{bmatrix} z(t) \\ \Delta(z)(t) \end{bmatrix} \right) dt \geq 0 \tag{4.38}$$

for all $T \geq 0$ and all signals $z \in \mathcal{L}_{2e}^{n_z}$.

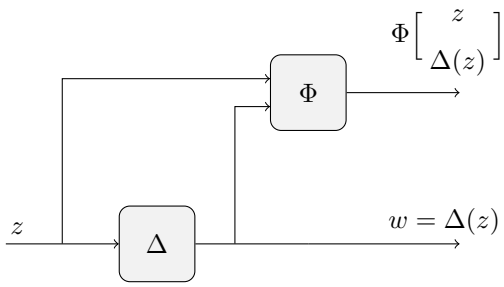

Figure 4.8: Sketch of the IQC constraint

Figure 4.8 is a schematic representation of the setup needed to obtain (4.38). As it has been said before, an IQC is used to describe the behavior of the operator Δ. In this framework, if for all input signal z from $\mathcal{L}_{2e}^{n_z}$ the weighted norm of the truncated output of Φ fulfills (4.38) then the resulting IQC will give some information about how Δ transforms z into $w = \Delta(z)$. Φ and H will be the operators defining the IQC and so they will be the ones carrying the information about our perturbation operator Δ.
According to definition (4.38), saying that Δ satisfies the hard IQC defined by (Φ, H) means that for any input signal of Δ from $\mathcal{L}_{2e}^{n_z}$, the constraint (4.38) holds. We can also say that (Φ, H) defines a valid IQC for Δ.
Now let us suppose that $z \in \mathcal{L}_2^{n_z}$. As Δ is $\mathcal{L}_2$ bounded and Φ is stable, we have

$$\Phi \left(\begin{bmatrix} z \\ \Delta(z) \end{bmatrix} \right) \in \mathcal{L}_2^{n_h}$$

which has a well-defined Fourier transform:

$$\mathcal{F} \left\{ \Phi \begin{bmatrix} z \\ \Delta(z) \end{bmatrix} \right\} = \Phi(j\omega) \begin{bmatrix} \hat{z}(\omega) \\ \widehat{\Delta(z)}(\omega) \end{bmatrix}.$$

From that, by setting $T \to \infty$ and using Parseval's identity, (4.38) can be used to define a so-called soft IQC:

$$\int_{-\infty}^{\infty} \begin{bmatrix} \widehat{z}(\omega) \\ \widehat{\Delta(z)}(\omega) \end{bmatrix}^* \Phi(j\omega)^* H \Phi(j\omega) \begin{bmatrix} \widehat{z}(\omega) \\ \widehat{\Delta(z)}(\omega) \end{bmatrix} d\omega \geq 0. \tag{4.39}$$

A more general definition follows.

Definition 6 (Soft IQC) *Let us consider the operator* $\Pi : j\mathbb{R} \to \mathbb{C}^{(n_z+n_w)\times(n_z+n_w)}$ *essentially bounded and Hermitian on the imaginary axis. The bounded operator* Δ *is said to satisfy the soft IQC defined by* Π *if for all signals* $z \in \mathcal{L}_2^{n_z}$ *the integral inequality*

$$\int_{-\infty}^{+\infty} \begin{bmatrix} \hat{z}(j\omega) \\ \widehat{\Delta(z)}(j\omega) \end{bmatrix}^* \Pi(j\omega) \begin{bmatrix} \hat{z}(j\omega) \\ \widehat{\Delta(z)}(j\omega) \end{bmatrix} d\omega \geq 0 \tag{4.40}$$

holds.

Hence if the bounded operator Δ satisfies a hard IQC it satisfies a soft IQC for any input of finite energy. The soft IQC defined above is more simply called IQC as it is the most general form encountered and also the one that is described and used in [Megretski and Rantzer, 1997]. The $\mathcal{L}_2$ framework authorizes different IQC expressions. For instance, (4.40) is the result of the application of Parseval's theorem on

$$\int_{0}^{+\infty} \begin{bmatrix} z(t) \\ \Delta(z)(t) \end{bmatrix}^T \Pi \left(\begin{bmatrix} z(t) \\ \Delta(z)(t) \end{bmatrix} \right) dt \geq 0 \tag{4.41}$$

where $\Pi(\bullet)$ is the time-domain characterization of Π from (4.40). Lastly, the previous expressions (4.40) and (4.41) can also be expressed as an inner-product of $\mathcal{L}_2$ as

$$\left\langle \begin{bmatrix} z \\ \Delta(z) \end{bmatrix}, \Pi \left(\begin{bmatrix} z \\ \Delta(z) \end{bmatrix} \right) \right\rangle \geq 0. \tag{4.42}$$

Thanks to these different expressions, an IQC can be defined in various ways and we are going to take advantage of that to account for the knowledge we have about the "troublesome" operator Δ and put this knowledge in Π. The knowledge can be about the time-domain or the frequency-domain representation of the inputs and outputs of Δ, the energy transfer, the correlation between z and $\Delta(z)$. A concrete approach to define a valid IQC for an operator Δ relies on energy transfers and is presented in the following paragraph.

Classical virtual experiment

To start with a pragmatic approach of IQC description of an operator, a simple virtual experiment based on the structure of figure 4.8 can be done. This experiment is presented in [Megretski and Rantzer, 1995]. Defined as in the previous paragraph, an IQC can be seen as an inequality describing the correlation between the input and output of a nonlinear block Δ. The virtual experiment consists in measuring the difference between the energy of weighted z and weighted $\Delta(z)$. The weighting is done by a continuous linear filter C. It allows defining an IQC that covers the bounded operator Δ. In this figure, the frequency-domain representation of C is the stable LTI transfer function matrix

$$C(j\omega) = \begin{bmatrix} C_{11}(j\omega) & C_{12}(j\omega) \\ C_{21}(j\omega) & C_{22}(j\omega) \end{bmatrix}, \tag{4.43}$$

with zero initial conditions.

In the test setup figure 4.9, we want to verify that the first output of C always has larger energy than the second. In that case, the setup can be used to derive an IQC satisfied by Δ and defined by the multiplier

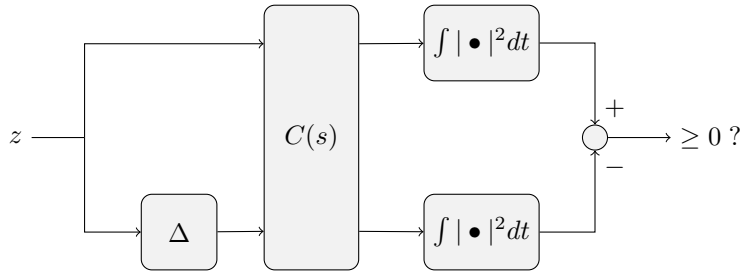

Figure 4.9: Virtual experiment for IQC construction

$$\Pi_C(j\omega) = C(j\omega)^* \begin{bmatrix} I & 0 \\ 0 & -I \end{bmatrix} C(j\omega). \tag{4.44}$$

In facts, when the test is valid, the following equivalences hold for all signal $z \in \mathcal{L}_2$. For convenience, we do not write the dependence of the terms in the frequency ω when the equations are too large.

$$\begin{aligned}
& \|C_{11}(j\omega)\hat{z}(j\omega) + C_{12}(j\omega)\widehat{\Delta z}(j\omega)\|^2_{\mathcal{L}_2} - \|C_{21}(j\omega)\hat{z}(j\omega) + C_{22}(j\omega)\widehat{\Delta z}(j\omega)\|^2_{\mathcal{L}_2} && \geq 0 \\
\Leftrightarrow \quad & \int_{-\infty}^{\infty} \left(C_{11}\hat{z} + C_{12}\widehat{\Delta z}\right)^* \left(C_{11}\hat{z} + C_{12}\widehat{\Delta z}\right) - \left(C_{21}\hat{z} + C_{22}\widehat{\Delta z}\right)^* \left(C_{21}\hat{z} + C_{22}\widehat{\Delta z}\right) d\omega && \geq 0 \\
\Leftrightarrow \quad & \int_{-\infty}^{\infty} \begin{bmatrix} \hat{z} \\ \widehat{\Delta z} \end{bmatrix}^* \begin{bmatrix} C_{11}^*C_{11} - C_{21}^*C_{21} & C_{11}^*C_{12} - C_{21}^*C_{22} \\ C_{12}^*C_{11} - C_{22}^*C_{21} & C_{12}^*C_{12} - C_{22}^*C_{22} \end{bmatrix} \begin{bmatrix} \hat{z} \\ \widehat{\Delta z} \end{bmatrix} d\omega && \geq 0 \\
\Leftrightarrow \quad & \int_{-\infty}^{\infty} \begin{bmatrix} \hat{z}(j\omega) \\ \widehat{\Delta z}(j\omega) \end{bmatrix}^* \Pi_C(j\omega) \begin{bmatrix} \hat{z}(j\omega) \\ \widehat{\Delta z}(j\omega) \end{bmatrix} d\omega && \geq 0,
\end{aligned}$$

with Π_C defined in (4.44). The classical example $C(s) = I$ gives the gain bound $\|\Delta\| \leq 1$.
To give a more practical aspect to the description of operators with IQC, the next paragraphs exhibit concrete examples where one property of an operator is translated into an IQC using one of the definitions of paragraph 4.4.2.

Energy gain bound

The example is about using the energy gain bound of Δ to build an IQC. We saw in paragraph 4.4.1 that the nonlinear operators to be considered are all supposed to have a finite $\mathcal{L}_2$ induced gain $\|\Delta\|_{\mathcal{L}_2 \to \mathcal{L}_2}$ i.e. a finite energy gain.
Let us define the $\mathcal{L}_2$ induced gain of $\Delta : \mathcal{L}_2^{n_z} \to \mathcal{L}_2^{n_w}$ to be equal to $\gamma > 0$. Using the definition (4.34), we have

$$\forall z \in \mathcal{L}_2^{n_z}, \quad \|\Delta(z)\|_{\mathcal{L}_2} \leq \gamma \|z\|_{\mathcal{L}_2} \tag{4.45}$$

which holds. Using the time-domain definition of the $\mathcal{L}_2$-norm (4.24) and squaring the terms in the above inequality, we obtain

$$\forall z \in \mathcal{L}_2^{n_z}, \quad \int_0^{+\infty} \left(\gamma^2 z(t)^T z(t) - (\Delta z)(t)^T (\Delta z)(t)\right) dt \geq 0.$$

The integrand can expressed as a quadratic form defined by the static multiplier Π_γ. The multiplier Π_γ

defines an IQC satisfied by the operator Δ with energy gain γ^2:

$$\forall z \in \mathcal{L}_2^{n_z}, \quad \int_0^{+\infty} \begin{bmatrix} z(t) \\ (\Delta z)(t) \end{bmatrix}^T \underbrace{\begin{bmatrix} \gamma^2 I & 0 \\ 0 & -I \end{bmatrix}}_{\Pi_\gamma} \begin{bmatrix} z(t) \\ (\Delta z)(t) \end{bmatrix} dt \geq 0. \tag{4.46}$$

We observe that the information we have about Δ (the value γ of its $\mathcal{L}_2$-norm) appears in Π_γ. Hence Π_γ carries the information we know about Δ.

Time-domain representations

We also said that an IQC could be defined from the knowledge of the time-domain representation of the input and output of operator Δ.
Let us now consider that the operator Δ is a memoryless time-varying sector-bounded nonlinearity. In such a context, Δ is defined as follows:

$$\Delta \; : \; \begin{cases} \mathbb{R}_+ \times \mathbb{R} & \rightarrow & \mathbb{R} \\ (t, z(t)) & \rightarrow & \Delta(t, z(t)). \end{cases} \tag{4.47}$$

Please notice that we present the scalar case knowing that a similar result can be obtained for multi-input multi-output nonlinearities. The sector condition with bounds the real parameters α and β such that $\alpha < \beta$ reads as:

$$\forall t \in \mathbb{R}_+, \forall z(t) \in \mathbb{R}, \quad \alpha z(t)^2 \leq \Delta(t, z(t)) z(t) \leq \beta z(t)^2. \tag{4.48}$$

The characteristic plot of such a nonlinearity could be sketched as in figure 4.10.

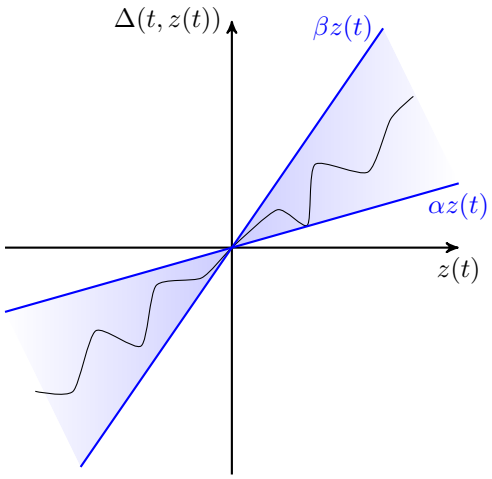

Figure 4.10: Characteristic plot of a sector bounded nonlinearity

Now to define an IQC that captures the sector bounded nonlinearity Δ defined by (4.47-4.48), we have to manipulate the time-domain expression of the sector condition (4.48). To make the equations easier

to read, $\Delta(t, z(t))$ will be replaced by $(\Delta z)(t)$. The following holds for all time $t \geq 0$ and all $z(t) \in \mathbb{R}$:

$$\begin{aligned}
& \beta z(t)^2 \geq \Delta(t, z(t))z(t) \geq \alpha z(t)^2, \\
\Leftrightarrow \quad & ((\Delta z)(t) - \alpha z(t))\,(\beta z(t) - (\Delta z)(t)) \geq 0 \\
\Leftrightarrow \quad & (\alpha+\beta) z(t)(\Delta z)(t) - \alpha\beta z(t)^2 - (\Delta z)(t)^2 \geq 0 \\
\Leftrightarrow \quad & \begin{bmatrix} z(t) \\ (\Delta z)(t) \end{bmatrix}^T \underbrace{\begin{bmatrix} -\alpha\beta & \frac{\alpha+\beta}{2} \\ \frac{\alpha+\beta}{2} & -1 \end{bmatrix}}_{\Pi_{\alpha,\beta}} \begin{bmatrix} z(t) \\ (\Delta z)(t) \end{bmatrix} \geq 0
\end{aligned}$$

The last line can be integrated over the positive time axis since $z \in \mathcal{L}_2$ to give an IQC defined by $\Pi_{\alpha,\beta}$ that describes Δ memoryless time-varying sector-bounded nonlinearity:

$$\forall z \in \mathcal{L}_2, \quad \int_0^{+\infty} \begin{bmatrix} z(t) \\ (\Delta z)(t) \end{bmatrix}^T \underbrace{\begin{bmatrix} -\alpha\beta & \frac{\alpha+\beta}{2} \\ \frac{\alpha+\beta}{2} & -1 \end{bmatrix}}_{\Pi_{\alpha,\beta}} \begin{bmatrix} z(t) \\ (\Delta z)(t) \end{bmatrix} dt \geq 0. \tag{4.49}$$

Again, we see here that the multiplier $\Pi_{\alpha,\beta}$ is parameterized by the characteristic values of the nonlinearity Δ which are the bounds α and β of the sector in which $\Delta(z)(t)$ lies. It shows how the multiplier carries the information we have about Δ. This short paragraph shows how time-domain representation of the input and output signals of a nonlinearity can be used to create an IQC describing it. The next paragraph introduces the use of frequency domain representations in the constructions of IQC.

Frequency-domain representations

To define an IQC using the frequency-domain representation of z and $\Delta(z)$, we look again at the gain bound presented in paragraph 4.4.2. Consider that during the analysis of the nonlinear device Δ, we performed an energy calculation of its input and output weighted by some transfer functions $F_{in} \in \mathbb{RH}_\infty^{n_z \times n_z}$ and $F_{out} \in \mathbb{RH}_\infty^{n_w \times n_w}$ respectively. Such a characterization can be defined by experiment in a setup such as the one presented figure 4.11.

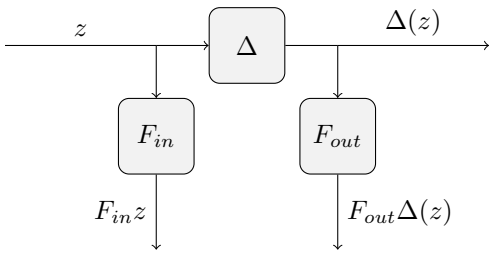

Figure 4.11: Experiment for definition of block diagonal frequency dependent multipliers

Differently from paragraph 4.4.2, we now have a bound on the energy of the weighted signals $F_{in}(z)$ and $F_{out}(\Delta(z))$. We can write this as follows:

$$\forall z \in \mathcal{L}_2^{n_z}, \quad \|F_{out}(\Delta z)\|_{\mathcal{L}_2} \leq \gamma \|F_{in}(z)\|_{\mathcal{L}_2}.$$

Using the frequency domain expression of the $\mathcal{L}_2$ norm and squaring it, the norm constraint reads as

$$\forall z \in \mathcal{L}_2^{n_z}, \quad \int_{-\infty}^{+\infty} \left(\gamma^2 \hat{z}(j\omega)^* F_{in}(j\omega)^* F_{in}(j\omega) \hat{z}(j\omega) - \widehat{\Delta(z)}(j\omega)^* F_{out}(j\omega)^* F_{out}(j\omega) \widehat{\Delta(z)}(j\omega) \right) \mathrm{d}\omega \geq 0. \tag{4.50}$$

From the above equation we write the integral quadratic constraint:

$$\forall z \in \mathcal{L}_2^{n_z}, \quad \int_{-\infty}^{+\infty} \begin{bmatrix} \hat{z}(j\omega) \\ \widehat{\Delta(z)}(j\omega) \end{bmatrix}^* \begin{bmatrix} \gamma^2 F_{in}(j\omega)^* F_{in}(j\omega) & 0 \\ 0 & -F_{out}(j\omega)^* F_{out}(j\omega) \end{bmatrix} \begin{bmatrix} \hat{z}(j\omega) \\ \widehat{\Delta(z)}(j\omega) \end{bmatrix} \mathrm{d}\omega \geq 0. \tag{4.51}$$

The above experiment is a simplification of the one from paragraph 4.4.2. It allows to take a very pragmatic approach to define IQC and helps to characterize Δ with notions that are very common in a engineering point of view. IQC in the frequency-domain can be used in order to characterize the spectrum of the output of the perturbation. For instance, since many of the operators or systems we consider are low-pass, we can also describe that with an IQC as presented in [Summers et al., 2013]. The interest in introducing the weighting transfer functions $F_{in} \in \mathbb{RH}_\infty^{n_z \times n_z}$ and $F_{out} \in \mathbb{RH}_\infty^{n_w \times n_w}$ will appear later on when we will start looking for stability tests.

Structured operators

Conical combination Previously, we saw how to describe a perturbation operator Δ by considering its input and output in order to build an IQC. Now let us discuss the case when the analysis of the operator results in different IQC containing information about different features of the operator. That is for instance the case when the operator has a particular output spectrum and fulfills a sector condition. In this case we can define a single IQC gathering all the data about Δ by conical combination of the multiplier describing the spectrum constraint and the multiplier describing the sector bound.
Let us consider the general case of N different IQC describing $\Delta : \mathcal{L}_2^{n_z} \to \mathcal{L}_2^{n_w}$. That is, for all $k \in \{1; \ldots; N\}, N \in \mathbb{N}$, the IQC defined by operator $\Pi_k : j\mathbb{R} \to \mathbb{C}^{(n_z+n_w)\times(n_z+n_w)}$ is satisfied by Δ. As a result, for all $z \in \mathcal{L}_2^{n_z}$ and for all $k \in \{1; \ldots; N\}$, we have

$$\int_{-\infty}^{+\infty} \begin{bmatrix} \hat{z}(j\omega) \\ \widehat{\Delta(z)}(j\omega) \end{bmatrix}^* \Pi_k(j\omega) \begin{bmatrix} \hat{z}(j\omega) \\ \widehat{\Delta(z)}(j\omega) \end{bmatrix} d\omega \geq 0$$

that holds. It means that during the study of the inputs and outputs of Δ, we found N IQC satisfied by Δ. Since each Π_k defines a positive integral, we can take any positive numbers τ_k and compute the operator $\Pi = \sum_{k=1}^{N} \tau_k \Pi_k$ to define an IQC which will be satisfied by Δ. This conic combination of the Π_k gives an operator Π defining an IQC that captures Δ. It allowed to convert a set of N valid IQC for Δ into an infinite number of valid IQC for Δ. Hence, we will see later on that performing this conical combination is a way to try to reduce the conservatism of the description and so of the stability test to come. Indeed, the variables $\tau_k, k \in \{1; \ldots; N\}$ can be considered as degrees of freedom of the stability test as we have to look for one combination that makes the stability test feasible. In facts, it allows describing Δ with an IQC defined by a multiplier belonging to a vaster set.
In addition to that, it is also worth mentioning that adding IQC this way can only reduce the conservatism since it adds new degrees of freedom to the LMI problem that will be solved in paragraph 4.4.3. That is the more multipliers are available the better is the chance to find a combination of them that is suitable to satisfy the stability criterion. We will see later on how looking for new IQC describing an operator and adding them up can improve the stability results.

Diagonal augmentation The second type of combination we are going to describe occurs when a structured operator needs to be described with an IQC. To do so, we present a simple example of structured operator Δ that we will describe with a structured multiplier Π.
Let us consider the perturbation operator Δ defined by:

$$\Delta = \begin{pmatrix} \Delta_1 & 0 \\ 0 & \Delta_2 \end{pmatrix}. \tag{4.52}$$

Δ has inputs in $\mathcal{L}_2^{n_{z_1}+n_{z_2}}$ and outputs in $\mathcal{L}_2^{n_{w_1}+n_{w_2}}$. The sizes of Δ_1 and Δ_2 are defined accordingly. To start, we can perform two completely independent studies aiming to define two IQC covering Δ_1 and Δ_2, respectively. After the analysis of the inputs and outputs of Δ_1 and Δ_2, we obtain the operators Π_1 and Π_2 that define the IQC satisfied by Δ_1 and Δ_2, respectively. We need to find an operator Π to define the IQC that will describe Δ from (4.52). To do so, we combine the two multipliers Π_1 and Π_2 by diagonal augmentation to obtain the following multiplier:

$$\Pi = \begin{bmatrix} \Pi_1^{(11)} & 0 & \Pi_1^{12} & 0 \\ 0 & \Pi_2^{11} & 0 & \Pi_2^{12} \\ \Pi_1^{21} & 0 & \Pi_1^{22} & 0 \\ 0 & \Pi_2^{21} & 0 & \Pi_2^{22} \end{bmatrix}. \tag{4.53}$$

Finally, for all $z_1 \in \mathcal{L}_{2e}^{n_{z_1}}$ and $z_2 \in \mathcal{L}_{2e}^{n_{z_2}}$ such that $z = \begin{bmatrix} z_1 & z_2 \end{bmatrix}^T$, the IQC defined by Π in (4.53) is valid. That is:

$$\int_{-\infty}^{+\infty} \begin{bmatrix} \hat{z}_1(j\omega) \\ \hat{z}_2(j\omega) \\ \widehat{\Delta(z_1)}(j\omega) \\ \widehat{\Delta(z_2)}(j\omega) \end{bmatrix}^* \Pi(j\omega) \begin{bmatrix} \hat{z}_1(j\omega) \\ \hat{z}_2(j\omega) \\ \widehat{\Delta(z_1)}(j\omega) \\ \widehat{\Delta(z_2)}(j\omega) \end{bmatrix} d\omega = \int_{-\infty}^{+\infty} \begin{bmatrix} \hat{z}(j\omega) \\ \widehat{\Delta(z)}(j\omega) \end{bmatrix}^* \Pi(j\omega) \begin{bmatrix} \hat{z}(j\omega) \\ \widehat{\Delta(z)}(j\omega) \end{bmatrix} d\omega \geq 0$$

The IQC above is simply the reformulation of the sum of the IQC defined by Π_1 and the IQC defined by Π_2. This can easily be extended to Δ operators with higher dimension (e.g. K sub-blocks Δ_k). It shows a crucial feature of IQC description of operators. Indeed, when constructing the LFR of the system, we always observe structured perturbation blocks. These blocks gather uncertain or/and time-varying parameters and different nonlinearities whose inputs and outputs are decoupled and which need to be described as precisely as possible to limit the conservatism. Here it is shown that we can define IQC for each one of the blocks of the structured operator Δ independently and then merge them to obtain an operator describing Δ whose sub-blocks have the same structure. This fact also shows that the IQC description of an operator can be used for the analysis of any system in which the same block appears.
As a consequence, when we use IQC in a V&V process, we can start with a very simple model with one perturbation described by a given IQC, and continue the analysis by adding new perturbation blocks. It is easy as we only need to find an IQC valid for the new perturbation blocks and augment the first IQC multiplier with the new ones.

4.4.3 Stability theorems

The framework is now defined and the previous examples were meant to present some of the many ways to cover operators with IQC. The next step aims to show how to use the IQC description of a perturbation operator Δ of the LFR to prove the stability of its interconnection with M.

General IQC theorem

For the statement of the main IQC stability theorem, we take into consideration the interconnection depicted figure 4.12. The theorem to be presented is the one introduced in [Megretski and Rantzer, 1997]. It covers the main cases of use of soft IQC in system analysis.

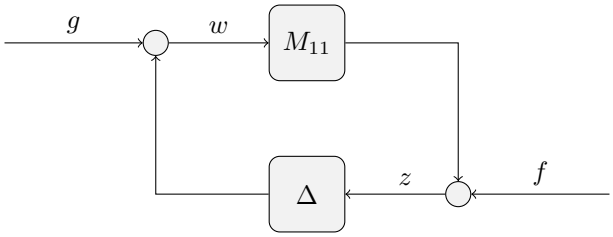

Figure 4.12: System interconnection for IQC stability theorem

The feedback configuration figure 4.12 is

$$\begin{cases} z = & M_{11}w + f \\ w = & \Delta(z) + g, \end{cases} \tag{4.54}$$

where $f \in \mathcal{L}_{2e}^{n_z}$, $g \in \mathcal{L}_{2e}^{n_w}$ are the exogenous signals of the interconnection (e.g. noises, perturbations, references), and $M_{11} : \mathcal{L}_{2e}^{n_w} \to \mathcal{L}_{2e}^{n_z}$ and $\Delta : \mathcal{L}_{2e}^{n_z} \to \mathcal{L}_{2e}^{n_w}$ are causal operators. In addition to that, M_{11} is assumed to be LTI and stable while Δ is bounded. Let us also suppose that we have a $\Pi : j\mathbb{R} \to \mathbb{C}^{(n_z+n_w)\times(n_z+n_w)}$ which is essentially bounded and takes Hermitian values on the imaginary axis. We can now state the main stability theorem which guarantees the $\mathcal{L}_2$ boundedness of $(I - M_1 1\Delta)^{-1}$ in $\mathcal{F}_u(M, \Delta)$ and so the $\mathcal{L}_2$ stability of the LFR figure 4.12.

Theorem 4 (Main theorem) *Assume that*

1. *for any $\tau \in [0; 1]$, $I - \tau M_{11}\Delta$ has a causal inverse;*
2. *for any $\tau \in [0; 1]$, the IQC defined by Π is satisfied by $\tau\Delta$, that is*

$$\int_{-\infty}^{+\infty} \begin{bmatrix} \hat{z}(j\omega) \\ \widehat{\tau\Delta(z)}(j\omega) \end{bmatrix}^* \Pi(j\omega) \begin{bmatrix} \hat{z}(j\omega) \\ \widehat{\tau\Delta(z)}(j\omega) \end{bmatrix} d\omega \geq 0$$

   holds;

3. *there exists $\varepsilon > 0$ such that*

$$\forall \omega \in \mathbb{R}, \begin{bmatrix} M_{11}(j\omega) \\ I \end{bmatrix}^* \Pi(j\omega) \begin{bmatrix} M_{11}(j\omega) \\ I \end{bmatrix} \preceq \varepsilon I_{n_w}. \tag{4.55}$$

Then the feedback system (4.54) is stable (i.e. $(I - M_{11}\Delta)^{-1}$ is bounded).

The following remarks are noteworthy:

- If

$$\Pi = \begin{bmatrix} \Pi_{11} & \Pi_{12} \\ \Pi_{12}^* & \Pi_{22} \end{bmatrix} \tag{4.56}$$

  has $\Pi_{11} \geq 0$ and $\Pi_{22} \leq 0$, then if Δ satisfies the IQC defined by Π then for all $\tau \in [0,1]$, $\tau\Delta$ satisfies the IQC defined by Π.

- Assumption 3 can be simplified to:

$$\forall \omega \in [0,\infty), \begin{bmatrix} M_{11}(j\omega) \\ I \end{bmatrix}^* \Pi(j\omega) \begin{bmatrix} M_{11}(j\omega) \\ I \end{bmatrix} \prec 0 \tag{4.57}$$

  in the case when M_{11} is a rational transfer function. It will be the case most of the time.

Analogously, the robust stability of $\mathcal{F}_l(M,\Delta)$ can be assessed by replacing M_{11} by M_{22}.

In the subsequent example, we show how this theorem as a very well known particular case...

Example 5 (Link with small-gain theorem) *Let us consider that in the interconnection figure 4.12, Δ is an uncertain LTI dynamic block with bounded $\mathcal{H}_\infty$ norm i.e.*

$$\|\Delta\|_\infty = \max_\omega \bar{\sigma}(\Delta(j\omega)) \leq \gamma;$$

and M_{11} is a rational LTI transfer function with all its poles in the left-hand plane.
We know from paragraph 4.4.2 that Δ satisfies the IQC defined by Π_γ (4.46). This multiplier reads as

$$\Pi_\gamma = \begin{bmatrix} \gamma^2 I & 0 \\ 0 & -I \end{bmatrix}.$$

Furthermore, let us assume that the interconnection of M_{11} and Δ is well-posed. From this simple setup, we fulfill the first two assumptions of theorem 4: our system is assumed to be well-posed and the type of perturbation operator we have satisfies the IQC defined by Π_γ. Consequently, to guarantee the stability we need to verify the Frequency Domain Inequality (FDI) of the third assumption (4.55) simplified into (4.57) by definition of M_{11}. Expanding (4.57) gives:

$$\begin{aligned}
& \forall \omega \in [0,\infty), \quad \begin{bmatrix} M_{11}(j\omega) \\ I \end{bmatrix}^* \Pi_\gamma \begin{bmatrix} M_{11}(j\omega) \\ I \end{bmatrix} \prec 0 \\
\Leftrightarrow \quad & \forall \omega \in [0,\infty), \quad \begin{bmatrix} M_{11}(j\omega) \\ I \end{bmatrix}^* \begin{bmatrix} \gamma^2 I & 0 \\ 0 & -I \end{bmatrix} \begin{bmatrix} M_{11}(j\omega) \\ I \end{bmatrix} \prec 0 \\
\Leftrightarrow \quad & \forall \omega \in [0,\infty), \quad \gamma^2 M_{11}(j\omega)^* M_{11}(j\omega) - I \prec 0 \\
\Leftrightarrow \quad & \forall \omega \in [0,\infty), \quad \bar{\sigma}(M_{11}(j\omega)) < 1/\gamma \\
\Leftrightarrow \quad & \forall \omega \in [0,\infty), \quad \|M_{11}\|_\infty < 1/\gamma.
\end{aligned}$$

We observe that the FDI from the main stability theorem for IQC analysis is equivalent to the small-gain theorem condition for stability given in paragraph 4.3.2 with the $\mathcal{H}_\infty$-norm.

The following paragraph briefly presents another stability result based on IQC description in order to show the variety of IQC that can be used to assess the stability of systems. Indeed, IQC must be seen as means to capture the behavior of Δ operators and can have different form depending on the system of interest. What we would like to emphasize is that no matter what is the form of the IQC, hard, soft, anything else such as for instance the IQC from chapter 6, there exists a theorem to prove the stability of the LFR associating Δ to another system.

Stability of pulse-modulated systems

This short paragraph is presented here in order to insist of the fact that first and foremost, IQC are means of describing operators. In the context of robust stability analysis, the operators that need to be described with IQC are the "trouble making" operators Δ of LFR and we saw before that IQC are a convenient way to cover complex operators. In this framework, the first thing to do when intending a robustness analysis with IQC is to capture the input-output behavior of Δ with an IQC. After this, depending on the type of IQC that is determined, different theorems leading to different conclusions about the stability can be used but this step is generally much easier than the previous one so it requires less work.
As an example, the following theorem aims to prove the stability of pulse-modulated systems. It has been proposed by Arkadij Gelig and Aleksandr Churilov who built on results from Russian mathematicians including Vladimir Yakubovich. An almost exhaustive survey of their works on pulse-modulated systems can be found in [Gelig and Churilov, 1998] and is completed by [Churilov and Gessen, 2003]. Other references about the works done in this research group will be given in the dedicated section of chapter 6. They focused on finding a proof of stability for systems including a pulse-modulator: highly nonlinear device with discrete-time behavior frequently encountered in power electronics and used for the modeling of attitude control system for space launchers. To do so, they intended to address the stability issues of a LFR such as the one figure 4.13 in which M_{11} is a LTI stable system and $\mathcal{Q}$ is a nonlinear block mimicking the pulse-modulator behavior

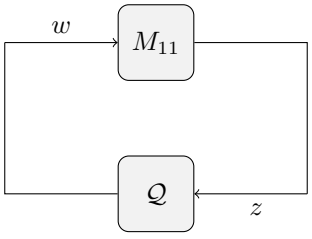

Figure 4.13: System interconnection for pulse-modulated systems stability theorem

This nonlinear block $\mathcal{Q}$ is described by the following IQC:

$$\int_0^{t_n} \begin{bmatrix} z(t) \\ w(t) \end{bmatrix}^T \begin{bmatrix} \Pi_{11}^{GC} & \Pi_{12}^{GC} \\ \Pi_{12}^{GC\,T} & \Pi_{22}^{GC} \end{bmatrix} \begin{bmatrix} z(t) \\ w(t) \end{bmatrix} \mathrm{dt} \geq 0, \tag{4.58}$$

where $w = \mathcal{Q}(z)$ and t_n is the n^{th} sampling instant and the subscript GC stands for Gelig and Churilov. Here Π^{GC} is a static multiplier carrying information about $\mathcal{Q}$. The main difference between the above IQC (4.58) and IQCs (4.38) and (4.40) is that the upper-bound of the integration domain of the IQC takes discrete values t_n for $n \in \mathbb{N}$. Nevertheless, the stability of interconnection figure 4.13 can be assessed as

the IQC contains some information about the pulse-modulator. Under the assumptions that the rational transfer function of M_{11} has all its poles in the open left half plane, that its relative degree is not less than 2 and that the IQC (4.58) holds, [Gelig and Churilov, 1998] page 63 formulates the following stability result:

Theorem 5 (Stability of pulse-modulated systems) *A sufficient condition for asymptotic stability of the interconnection figure 4.13 is the validity of the Frequency Domain Inequality (FDI) for all* $\omega \in [0;\infty]$*:*

$$\begin{bmatrix} M_{11}(j\omega) \\ I \end{bmatrix}^* \begin{bmatrix} \Pi_{11}^{GC} & \Pi_{12}^{GC} \\ \Pi_{12}^{GC\,T} & \Pi_{22}^{GC} \end{bmatrix} \begin{bmatrix} M_{11}(j\omega) \\ I \end{bmatrix} \prec 0. \tag{4.59}$$

For more precision about this result, we invite the reader to take a look at [Gelig and Churilov, 1998], [Gelig and Churilov, 1993], [Chaudenson et al., 2013b] and chapter 6 of this thesis in which way to use the result has been simplified and IQC description has been improved.
Our point here was to present another kind of stability result based on the representation of a perturbation operator by an IQC hence showing again that IQC are first of all a mean to describe nonlinear operators. We could observe that despite the fact that we described $\mathcal{Q}$ with a different kind of IQC, we were still able to address the stability of the LFR figure 4.13.

How to check stability?

The main stability theorem of IQC theory has been given in theorem 4. However, the third assumption of this theorem is a FDI (4.55) that must be verified for infinitely many frequency values ω. The validity of this FDI will determine whether the system is stable or not. Hence, it has to be easy to implement and the computations have to be efficient and reliable. Of course, a pragmatic approach would consist in griding the real axis of frequency, check whether the inequality (4.55) is satisfied at each point of the grid or not. Nevertheless, to make the use of IQC practical and the stability test rigorous, the FDI stability condition should be recast in a way such that they can be efficiently tested and the process implemented easily on a computer and also such that the test is done for the whole positive axis of frequencies. A well-known result by V.A. Yakubovich developed with the help of works by Popov and Kalman allows transforming the FDI in a finite set of LMI. This result described in [Rantzer, 1996] reads in our framework as

Theorem 6 (KYP lemma) *Given* $A \in \mathbb{R}^{n\times n}$ *a Hurwitz matrix,* $B \in \mathbb{R}^{n\times n_w}$ *such that* (A,B) *is controllable, and* $H = H^T$ *a real symmetric matrix from* $\mathbb{R}^{(n+n_w)\times(n+n_w)}$*, the following statements are equivalent:*

- *For all* $\omega \in \mathbb{R}_+$*,*

$$\begin{bmatrix} (j\omega I - A)^{-1}B \\ I \end{bmatrix}^* H \begin{bmatrix} (j\omega I - A)^{-1}B \\ I \end{bmatrix} \prec 0; \tag{4.60}$$

- *There exists a symmetric matrix* $X = X^T \in \mathbb{R}^{n\times n}$ *such that the LMI*

$$\begin{bmatrix} A & B \\ I & 0 \end{bmatrix}^T \begin{bmatrix} 0 & X \\ X & 0 \end{bmatrix} \begin{bmatrix} A & B \\ I & 0 \end{bmatrix} + H \prec 0, \tag{4.61}$$

  holds.

Notice that we give here the case where the third assumption of the IQC stability theorem 4 is a strict inequality. The KYP lemma allows recasting the frequency domain inequality (4.55) needed for stability into a LMI condition a the cost of mild equations manipulations. Indeed, in the general IQC stability theorem we need (4.57) to be valid:

$$\forall \omega \in \mathbb{R}, \quad \begin{bmatrix} M_{11}(j\omega) \\ I \end{bmatrix}^* \Pi(j\omega) \begin{bmatrix} M_{11}(j\omega) \\ I \end{bmatrix} \prec 0.$$

The KYP lemma can be applied to (4.57) above by considering that $\Pi(j\omega)$ is factorized into $\Pi(j\omega) = \Psi(j\omega)^* H \Psi(j\omega)$. In the FDI, it gives:

$$\forall \omega \in \mathbb{R}, \quad \left(\Psi(j\omega) \begin{bmatrix} M_{11}(j\omega) \\ I \end{bmatrix} \right)^* H \left(\Psi(j\omega) \begin{bmatrix} M_{11}(j\omega) \\ I \end{bmatrix} \right) \prec 0.$$

From the factorization, we then search for a state-space realization (A, B, C, D) of

$$\Omega(j\omega) = \Psi(j\omega) \begin{pmatrix} M_{11}(j\omega) \\ I \end{pmatrix} \tag{4.62}$$

such that the FDI looks like (4.60). To do so, we use the state-space representation

$$\Omega(j\omega) = C(j\omega I - A)^{-1} B + D = \begin{bmatrix} C & D \end{bmatrix} \begin{bmatrix} (j\omega I - A)^{-1} B \\ I \end{bmatrix}.$$

The above equation allows recasting the frequency dependent robust stability condition (4.57) into a computationally tractable rigorous test. The state-space realization of Ω as a function of those of M_{11} and Ψ is given in [Jönsson, 1996] and presented below.
Let us consider the state-space realizations

$$\begin{cases} \Psi(s) = & C_\Psi (sI - A_\Psi)^{-1} B_\Psi + D_\Psi, \\ M_{11}(s) = & C_M (sI - A_M)^{-1} B_M + D_M. \end{cases} \tag{4.63}$$

With the above notations we define

$$\hat{C} = \begin{bmatrix} C_M \\ 0 \end{bmatrix}, \text{ and } \hat{D} = \begin{bmatrix} D_M \\ I \end{bmatrix}. \tag{4.64}$$

Finally, the definitions in (4.63) and (4.64) allow expressing the state-space realization:

$$A = \begin{bmatrix} A_\Psi & B_\Psi \hat{C} \\ 0 & A_M \end{bmatrix}, \quad B = \begin{bmatrix} B_\Psi \hat{D} \\ B_M \end{bmatrix}, \tag{4.65}$$

$$C = \begin{bmatrix} C_\Psi & D_\Psi \hat{C} \end{bmatrix}, \quad D = \begin{bmatrix} D_\Psi \hat{D} \end{bmatrix}. \tag{4.66}$$

Conservatism reduction with conical combinations Briefly we are going to present how the introduction of the τ_k of paragraph 4.4.2 can help to reduce the conservatism. For this, let us consider that the multiplier Π above is defined by the conical combination of N multipliers Π_k defining valid IQC for the operator Δ:

$$\forall k \in \{1,\dots,N\}, \forall z \in \mathcal{L}_2, \quad \int_{-\infty}^{+\infty} \begin{bmatrix} \hat{z}(j\omega) \\ \widehat{\Delta(z)}(j\omega) \end{bmatrix}^* \Pi_k(j\omega) \begin{bmatrix} \hat{z}(j\omega) \\ \widehat{\Delta(z)}(j\omega) \end{bmatrix} d\omega \geq 0. \tag{4.67}$$

The conical combination is defined with a set of positive weightings $\{\tau_k\}_{k\in\{1,\dots,N\}}$ such that:

$$\Pi = \sum_{k=1}^{N} \tau_k \Pi_k. \tag{4.68}$$

In such conditions, the factorization of Π can be written without loss of generality as:

$$\forall \omega \in \mathbb{R}, \quad \Pi(j\omega) = \Psi'(j\omega)^* \left(\sum_{k=1}^{N} \tau_k H_k \right) \Psi'(j\omega) \prec 0. \tag{4.69}$$

As a consequence, introducing the state-space realization of Ω defined above (4.62), the LMI of the KYP lemma is given by:

$$\begin{bmatrix} A & B \\ I & 0 \end{bmatrix}^T \begin{bmatrix} 0 & X \\ X & 0 \end{bmatrix} \begin{bmatrix} A & B \\ I & 0 \end{bmatrix} + \sum_{k=1}^{N} \tau_k H_k \prec 0. \tag{4.70}$$

In the above LMI, the τ_k are decision variables. Consequently, the solver can look for a combination of positive τ_k that fulfills LMI (4.70) and so guarantee the FDI condition of stability of the IQC general stability theorem to be valid. Such conical combinations of multipliers allow to look for one valid IQC among the infinite number of feasible combinations of valid IQC such that the FDI is valid. This is where the possible conservatism reduction comes from as explained next. First, if we have just one valid IQC, we can still use a positive parameter τ to weight the multiplier and eventually make (4.70) feasible for some τ. Secondly, in the case when we have several IQC describing one operator, we can weight each multiplier with a positive τ_k and look for solutions of (4.70). Possibly, it will be easier to solve the LMI of the stability test.
To conclude, the conical combinations resulting from the association of several IQC describing one operator introduce new degrees of freedom in the stability test obtained by the KYP lemma and so could potentially reduce the conservatism of the test. We will see applications of this techniques in chapter 6.

4.5 Classic multipliers available for robustness analysis in the IQC framework

As mentioned previously, the framework for IQC analysis was first presented in the mid-90's in the article [Megretski and Rantzer, 1997]. In this context, the interest in defining IQC that describe the variety of operators that can be found in system analysis increased dramatically. Now, most of the common "troublesome" devices that can be encountered in the Δ block of a LFR have a dedicated multiplier that defines an IQC they satisfy. Building upon these theoretical results, the IQC-β toolbox presented in [Kao et al., 2004], [Megretski et al., 2000] was the first attempt to make the use of IQC easy and efficient through a Matlab® toolbox. Another Matlab® toolbox called LPVMAD [Köroglu et al., 2008]

was used during this thesis, the following section aims to show very briefly the key multipliers it is made of.

The multipliers presented hereunder are the main ones that can be found in the toolbox LPVMAD. The description is more involved on the theoretical point of view that the four examples given in paragraph 4.4.2. The multipliers define IQC that cover the following classical types of perturbations:

- linear time-invariant dynamic perturbations with norm bounds,
- linear time-invariant static perturbations with specified uncertainty regions,
- nonlinear, possibly time-varying, static uncertainties with sector bounds.

The description aims to give a general overview of the frame the multipliers are built in. Again, it is to illustrate how to define an IQC describing an operator Δ. For further information, the reader is invited to refer to [Köroglu et al., 2008] and the references therein as they contain thorough explanations, definitions and useful details resulting from the implementation. In appendix A the others multipliers of LPVMAD are defined.

4.5.1 LTI dynamic uncertainties

The first type of perturbation block that we are going to describe with an IQC is the dynamic LTI perturbation. It is commonly used to take into account system dynamics which are neglected in the analysis model. In this example, Δ is a linear time-invariant transfer function matrix with n_z inputs, n_w outputs and a finite $\mathcal{H}_\infty$-norm. We consider such uncertainties as belonging to the set $\mathcal{U}_1$ defined by

$$\mathcal{U}_1 = \left\{ \Delta \in \mathbb{H}_\infty^{n_w \times n_z} \middle| \|\Delta\|_\infty \leq \beta \right\} \tag{4.71}$$

where β is a positive number. In [Köroglu et al., 2008], a multiplier denoted by $\Pi_{ltid} \in \mathbb{RH}_\infty^{(n_z+n_w)\times(n_z+n_w)}$ where *ltid* stands for "linear time-invariant dynamics" is used to cover such $\Delta \in \mathcal{U}_1$ with an IQC. It is defined for all $\omega \in [0, \infty)$ by a matrix $Y \in \mathbb{R}^{d\times d}, Y \succ 0$ and $H \in \mathbb{RH}_\infty^{d\times 1}$ by

$$\Pi_{ltid}(j\omega) = \begin{pmatrix} H(j\omega) \otimes I_{n_z} & 0 \\ 0 & H(j\omega) \otimes I_{n_w} \end{pmatrix}^* \begin{pmatrix} \beta^2 Y \otimes I_{n_z} & 0 \\ 0 & -Y \otimes I_{n_w} \end{pmatrix} \begin{pmatrix} H(j\omega) \otimes I_{n_z} & 0 \\ 0 & H(j\omega) \otimes I_{n_w} \end{pmatrix}. \tag{4.72}$$

Since the mathematical expressions deriving from the definition of the multiplier are very large, we present only the key facts leading to the satisfaction of the IQC defined by Π_{ltid} by $\Delta \in \mathcal{U}_1$. Π_{ltid} is obtained using the norm bound on operators of $\mathcal{U}_1$. Let us consider $\Delta \in \mathcal{U}_1$, its norm bound leads to the valid sign constraint

$$\forall \omega \in [0, \infty), \quad \beta^2 I_{n_z} - \Delta(j\omega)^* \Delta(j\omega) \geq 0. \tag{4.73}$$

Furthermore, we have the identity

$$\forall \omega \in [0, \infty), \quad (H(j\omega) \otimes I_{n_w})\Delta(j\omega) = (I_d \otimes \Delta(j\omega))(H(j\omega) \otimes I_{n_z}). \tag{4.74}$$

As a consequence, if we write down the IQC defined by Π_{ltid} (4.72), we can immediately apply the above equality such that checking the non-negativeness of the integrand boils down to verifying that

$$\forall \omega \in [0, \infty), \quad \begin{pmatrix} I_{dn_z} \\ I_d \otimes \Delta(j\omega) \end{pmatrix}^* \begin{pmatrix} \beta^2 Y \otimes I_{n_z} & 0 \\ 0 & -Y \otimes I_{n_w} \end{pmatrix} \begin{pmatrix} I_{dn_z} \\ I_d \otimes \Delta(j\omega) \end{pmatrix} \geq 0. \tag{4.75}$$

Expanding the inequality using properties of the Kronecker product, we obtain that the above necessary condition for the validity of the IQC defined by Π_{ltid} can be recast in

$$\forall \omega \in [0, \infty), \quad Y \otimes [\beta^2 I_{n_z} - \Delta(j\omega)^* \Delta(j\omega)] \geq 0. \tag{4.76}$$

The above inequality is always true since $\Delta \in \mathcal{U}_1$ and $Y \succ 0$. This multiplier has the role of the frequency dependent D-scales introduced in [Packard and Doyle, 1993] to compute the structured singular value. It allows us to hint how μ-analysis can be seen as a particular case of IQC-based robustness analysis.
A key fact here is that the multiplier Π_{ltid} is parameterized by H and Y. Y is defined as a positive definite matrix and H belongs to the set of real rational norm-bounded transfer function matrix of size $d \times 1$. These two terms allow to introduce "degrees of freedom" in the definition of the multiplier used to capture $\Delta \in \mathcal{U}_1$. Indeed, Y and H allow defining different multipliers from the only assumption $\|\Delta\|_\infty \leq \beta$ and these multipliers may cover the perturbation operator Δ from $\mathcal{U}_1$ in (4.71) differently. To make the multiplier definition workable, it is common practice to define H as being generated from a basis transfer function. This basis can be parameterized as the one used to generate the multipliers from LPVMAD. An instance of a typical H used in LPVMAD is

$$H(s) = \begin{pmatrix} 1 \\ \frac{1}{s-\varphi} \\ \vdots \\ \frac{1}{(s-\varphi)^{d-1}} \end{pmatrix}, \tag{4.77}$$

where $\varphi < 0$. $d-1$ is the degree of the transfer function H. Different combinations of φ and d can lead to different results for the stability test as we will see it in chapter 5. In addition to that, other basis transfer function can be used, see e.g. [Megretski et al., 2000].

4.5.2 LTI parametric uncertainties

The next uncertain block to be described with an IQC is the static LTI perturbation. In engineering terms, these perturbations are very well-known as uncertain parameters. Thus it is now assumed that Δ has an uncertain parameter $\delta \in \mathcal{D} = [\underline{\delta}, \bar{\delta}] \subset \mathbb{R}$ with $\underline{\delta} < \bar{\delta}$. Assuming that the parameter is repeated, we consider the perturbation Δ as belonging to $\mathcal{U}_{ltis}$ defined as

$$\mathcal{U}_2 = \left\{ \Delta(\delta) = \delta I_r \in \mathbb{R}^{r \times r} \middle| \delta \in [\underline{\delta}, \bar{\delta}] \right\}. \tag{4.78}$$

To determine the multiplier Π_{ltis} which defines an IQC satisfied by such a $\delta \in \mathcal{U}_2$ we consider an "inflated" perturbation operator $\Theta(\delta) = \delta I_{dr}$ derived from $\Delta(\delta)$. Here, $d-1$ is the degree of the transfer function H defined in the LPVMAD toolbox in the manner of (4.77) but for repeated uncertainties as

$$H(s) = \begin{pmatrix} 1 \\ \frac{1}{s-\varphi} \\ \vdots \\ \frac{1}{(s-\varphi)^{d-1}} \end{pmatrix} \otimes I_r \in \mathbb{RH}_\infty^{dr \times r}. \tag{4.79}$$

From these definitions, we observe the commutation identity involving H, $\Delta(\delta)$ and $\Theta(\delta)$:

$$\forall \omega \in [0, \infty), \forall \delta \in \mathcal{D}, \quad H(j\omega)\Delta(\delta) = \Theta(\delta) H(j\omega). \tag{4.80}$$

This identity can be used if we are able to determine matrices S such that for all $\delta \in \mathcal{D}$, the inequality

$$\begin{pmatrix} I_{dr} \\ \Theta(\delta) \end{pmatrix}^T S \begin{pmatrix} I_{dr} \\ \Theta(\delta) \end{pmatrix} \geq 0 \tag{4.81}$$

holds. Indeed, with such an S and thanks to the commutation identity, left and right multiplication of (4.81) by H^* and H, respectively guarantees the validity of

$$\forall \omega \in [0, \infty), \quad \begin{pmatrix} I_r \\ \Delta(\delta) \end{pmatrix}^* \begin{pmatrix} H(j\omega) & 0 \\ 0 & H(j\omega) \end{pmatrix}^* S \begin{pmatrix} H(j\omega) & 0 \\ 0 & H(j\omega) \end{pmatrix} \begin{pmatrix} I_r \\ \Delta(\delta) \end{pmatrix} \geq 0 \tag{4.82}$$

for all $\delta \in \mathcal{D}$ and with H from (4.79). Of course, this relationship can be integrated over the frequencies to give a valid IQC satisfied by $\Delta \in \mathcal{D}$. Of course, based on the assumptions available on the range of variation of δ, we can make the definition tractable by defining a "structure" for the matrix S. For instance, in our case where $\mathcal{D} = [\underline{\delta}, \bar{\delta}]$, we can set S to be

$$S := \begin{pmatrix} -\underline{\delta}\bar{\delta}X & \frac{\underline{\delta}+\bar{\delta}}{2}X \\ \frac{\underline{\delta}+\bar{\delta}}{2}X & -X \end{pmatrix} \tag{4.83}$$

with $X \in \mathbb{R}^{dr \times dr}, X \succ 0$ to make sure that the quadratic constraint (4.81) holds for all $\delta \in \mathcal{D}$. This is done thanks to a sector condition on $\delta \in [\underline{\delta}, \bar{\delta}]$. As a consequence, the multiplier we use to define an IQC satisfied by a repeated static parameter in $[\underline{\delta}, \bar{\delta}]$ is

$$\Pi_{ltis}(j\omega) = \begin{pmatrix} H(j\omega) & 0 \\ 0 & H(j\omega) \end{pmatrix}^* \begin{pmatrix} -\underline{\delta}\bar{\delta}X & \frac{\underline{\delta}+\bar{\delta}}{2}X \\ \frac{\underline{\delta}+\bar{\delta}}{2}X & -X \end{pmatrix} \begin{pmatrix} H(j\omega) & 0 \\ 0 & H(j\omega) \end{pmatrix} \tag{4.84}$$

where $ltis$ stands for "linear time-invariant static". Once more, we observe that the information about δ that are the bounds on its feasible values $\underline{\delta}$ and $\bar{\delta}$ can be found in the definition of Π_{ltis}. Again, X and H will play the role of relaxation variables.

4.5.3 Sector bounded perturbations

To finish this brief review of the main multipliers in LPVMAD, we consider a sector bounded nonlinearity Δ as the one seen in paragraph 4.4.2. In this example, Δ is a one-input one-output operator belonging to $\mathcal{U}_3$ defined below:

$$\Delta \in \mathcal{U}_3 = \left\{ \Delta, \forall t \geq 0, \forall v(t) \in \mathbb{R}, \begin{bmatrix} z(t) \\ (\Delta z)(t) \end{bmatrix}^T \begin{bmatrix} -\alpha\beta & \frac{\alpha+\beta}{2} \\ \frac{\alpha+\beta}{2} & -1 \end{bmatrix} \begin{bmatrix} z(t) \\ (\Delta z)(t) \end{bmatrix} \geq 0 \right\}. \tag{4.85}$$

To build the multiplier that will define an IQC satisfied by such a Δ we introduce, as for the description of linear time-invariant dynamic perturbations with norm bounds, the constant scaling $x > 0$ and define Π_{nlsb} as:

$$\Pi_{nlsb} = \begin{bmatrix} -x\alpha\beta & x\frac{\alpha+\beta}{2} \\ x\frac{\alpha+\beta}{2} & -x \end{bmatrix}. \tag{4.86}$$

$nlsb$ stands for "nonlinear sector bounded" and Π_{nlsb} defines an IQC which is satisfied by any nonlinearity from $\mathcal{U}_3$.

4.6 Conclusion

The present chapter aimed to define the IQC framework. The setup for IQC analysis relies on the well-known LFR of systems. From this representation, stability can be obtained following a few simple steps. First, it is needed to ensure that the LFR is well-posed. This is the case of most physical systems. Secondly, we have to define a valid IQC for the perturbation operator Δ of the LFR. To do so, we can (and we have to) use the information that is available about Δ. Information about the sub-blocks of Δ can be used thanks to the nice feature of IQC that allows merging multipliers characterizing different operators when they are involved in the same perturbation Δ by diagonal augmentation. The information that is contained in an IQC can be an energy bound, a sector condition, a passivity condition, a frequency-domain characteristic, etc. This is another force of the method as many operator properties can be expressed by an IQC, especially those which are commonly referred to in systems engineering. Moreover, the combination of IQC describing one operator is easy and is done by conical combination. This can reduce the conservatism as verified in chapter 6. Once the IQC satisfied by Δ is described, we need to make sure that the operator Δ, represented by its IQC multiplier Π, and the nominal part M of the LFR are compatible. This is done by the verification of a FDI transformed into a finite number of LMI thanks to the KYP lemma. In this context, conical combinations allow to look for solution of the LMI test guaranteeing stability into a larger domain of decision variables and so can allow to reduce the conservatism of the stability test. Other properties of the multipliers can be used to reduce the conservatism of the stability test. For instance, different settings for the poles and degrees of the transfer function H (4.77) can help to reduce the conservatism as seen in chapter 5.
Finally, as presented here, the IQC based stability analysis seems to have all the properties needed for the analysis of complex and large systems as space launchers. Indeed, it accounts for the uncertainty structure, it is flexible and it has various parameters that can be used to reduce the conservatism of the stability test. We will observe in the analyzes that the main drawback of IQC analysis is the numerical conditioning of the LMI stability tests resulting from the application of the KYP lemma to the FDI guaranteeing the $\mathcal{L}_2$ stability of the LFR.
To summarize the chapter, table 4.1 shows, for each methods previously described, the type of uncertainty it can handle and if it accounts for the structure. This will be helpful when looking for the appropriate analytical tool to perform robust V&V of a space launcher.

Table 4.1: Analytical tools for robust V&V

	Δ_{ltis}	Δ_{ltid}	Δ_{ltv}	Δ_{nl}
Small-gain	✓	✓	✓	✓
μ-analysis	✓	✓	✗	✗
Lyapunov	✓	✓	✓	✓
IQC	✓	✓	✓	✓

Chapter 5

Influence of nonlinear uncertain dynamics and robustness analysis

5.1 Introduction

The application presented in this chapter originates from the paper [Chaudenson et al., 2013a]. The works are described with more precisions and more explanations than in the paper. Some of the ideas and results were not published, they complete the paper and will hopefully improve the understanding of our findings.
The study consists in the search of a LFR that is representative of the nonlinear uncertain equation of motion of a space launcher. Through some simple observations and the analysis of Newton's equation for a rotating rigid body, we defined factorizations of the matrices appearing in this three degree-of-freedom equation. It allowed us to perform robustness analysis in the IQC framework and with a Lyapunov theory based tool. As expected, after the robust stability analysis some time-domain simulations pushed us toward robust performance analysis due to the violation of several performance criteria during the simulations. Consequently, we intended to setup the framework of a robust performance analysis as a robust stability analysis. A few leads and results are given.

5.2 Model setup

To start, we setup the analysis model from the pre-analysis model defined in chapter 3.

5.2.1 Dynamic model

The equation of motion of a rotating rigid body has been presented in chapter 3 along paragraph 3.2.3. I_g denotes the inertia matrix in the geometrical frame $\mathcal{R}_g$. The state variable of the dynamic model is the angular speed $\omega \in \mathbb{R}^3$ expressed in $\mathcal{R}_g$. The differential equation describing the motion of a rotating rigid body with matrix expression of the cross-product has been given in (3.8). It is given below for convenience (5.1) together with the definition of matrices (5.2).

$$\dot{\omega} = I_g^{-1} \left(\Gamma - P(\omega) I_g \omega \right) \tag{5.1}$$

$$I_g = \begin{bmatrix} I_x & -I_{xy} & -I_{xz} \\ -I_{xy} & I_y & -I_{yz} \\ -I_{xz} & -I_{yz} & I_z \end{bmatrix}, I_x, I_y, I_z > 0 \ , \ I_{xy}, I_{xz}, I_{yz} \geq 0 \text{ and } P(\omega) = \begin{bmatrix} 0 & -\omega_z & \omega_y \\ \omega_z & 0 & -\omega_x \\ -\omega_y & \omega_x & 0 \end{bmatrix} . \quad (5.2)$$

The two matrices in (5.1) are trouble making for control law validation i.e. for robustness analysis, with analytical methods. The reason why is investigated in the following paragraphs.

Inertia matrix The inertia matrix I_g is not known precisely. Here "not precisely" means that we know the values of the inertia terms with a certain degree of uncertainty. The uncertainties in the inertia are caused by an approximative knowledge of the mass repartitions of the upper-stage and the payload. Indeed, measuring the inertia of a body is a complex process, especially when it is as big as the upper-stage of a space launcher with its payload. It results in approximate estimations of the terms in the inertia matrix. Of course, the uncertainties on such crucial parameters of the motion need to be taken into account during the control law validation process and so we will introduce the inertia uncertainties in the analysis model. The nominal values of the diagonal terms of the inertia matrix (I_x, I_y and I_z) are in general two orders of magnitude larger than the off-diagonal terms (I_{xy}, I_{xz} and I_{yz}) as the launcher tends to be axis symmetric. Moreover, uncertainties in center of gravity position can also be seen as uncertainties on the inertia thanks to Huygens theorem stated for the frames $\mathcal{R}_g$ and $\mathcal{R}_{g'} = (G', X_g, Y_g, Z_g)$ with

$$G' = \begin{bmatrix} x \\ y \\ z \end{bmatrix}_{\mathcal{R}_g} , \quad (5.3)$$

as

$$I_{g'} = I_g + m \begin{bmatrix} y^2 + z^2 & -xy & -xz \\ -xy & x^2 + z^2 & -yz \\ -xz & -yz & x^2 + y^2 \end{bmatrix} , \quad (5.4)$$

where m is the body mass. Notice that the mass of the vehicle is much easier to measure than the inertia. In the context of our works, m can be significantly larger than 10 tons.
Since customers are more and more demanding in terms of payload asymmetry and center of gravity displacement, the off-diagonal inertia terms deserve to be investigated too. As mentioned earlier, their nominal value is smaller than the diagonal terms one. Consequently, we consider large variations from nominal by affecting them with an uncertain multiplying factor ranging from 0 to 10. As for the off-diagonal terms, the uncertainty affecting the diagonal terms will be chosen to be multiplicative as this will be defined in section 5.3. Current engineering practices generally consider an uncertainty of $\pm 10\%$ for I_x, I_y and I_z. Considering the usual values of the diagonal inertia terms on the examples we study (from $20,000$ kg.m^2 to $50,000$ kg.m^2), this level of uncertainty can represent variations of the inertia parameters up to $\pm 5,000$ kg.m^2.
The purpose of this study is to assess the robust stability of the launcher with respect to the uncertain inertia matrix. To get an idea of the effect of uncertain inertia terms on the behavior of the launcher, we

can consider the one-dimensional approximation of equation (5.1) that is

$$I\dot{\omega} = \gamma, \tag{5.5}$$

where $I \in \mathbb{R}_+$ is the inertia around the axis of rotation, ω the angular rate around this axis and γ the torque applied about this axis. Now if $I = I_0(1+\delta)$ with $\delta \in [-0.1, 0.1]$ i.e. 10% uncertainty on the inertia. It is equivalent to approximately 10% of uncertainty on γ. This simple approximation allow us to have an idea about the influence of the inertia unertainty on the motion of the launcher. Indeed, for the three dimensional case, the uncertainty "caused" on the torque by the uncertain inertia is approximately equal. From this simple pragmatic argument, we see that the uncertainty on the inertia matrix has direct consequence on the control capabilities of the ACS.
Therefore, guaranteeing stability and performance for a large inertia uncertainty domain would allow to relax the technical specifications on the mass repartitions, on the position of the center of gravity of the payload. That means enforcing less constraints to the customers and so being more attractive to them. Moreover, it also allows to design an ACS such that it provides enough acceleration to the launcher to meet the technical specifications and performance criteria. These are the reasons why investigating robustness with respect to inertia uncertainties is crucial to guarantee the launcher competitiveness and also the fulfillment of the performance and precision requirements.

Coupling matrix The second issue in the equation of motion, from a control system engineer point of view, is the cross-product expressing the gyroscopic couplings. In paragraph 3.2.4, it has been expressed under the form of a matrix product. This matrix product involves the coupling matrix $P(\omega)$ defined in (5.2). $P(\omega)$ is a skew-symmetric matrix defined with the three components of the angular velocity vector ω. Again, $P(\omega)$ varies with time during the flight as the angular speed components ω_x, ω_y and ω_z do. We know two things about the variations of the ω_i that will be useful in the analysis. First, there are angular speeds at which the launcher is considered to be lost and the mission failed. They define a flight envelope within which the three components can vary. Basically, if the launcher reaches such angular rates, it cannot physically recover and so the mission is aborted. Secondly, the rate of variation of the angular speed components can also be approximated. While modeling the launcher in chapter 3, we described the three sources of torque in the equations of motion that are the ACS, the external disturbances and the gyroscopic couplings. The amplitude of all these torques can be determined a priori. For the ACS torque, we know approximatively the available torque and the inertia so using the one degree-of-freedom equation (5.5), we can evaluate the values that can be taken by the acceleration generated by the ACS torque. For the perturbations, they are sometimes predicted in real-time and if not they can be estimated a priori. Concerning the gyroscopic couplings, we performed their computation in section 3.2.6 and the same can be done over the whole flight envelope. From this information, we can establish an estimation of the angular acceleration $\dot{\omega}$ that completes the information we have about the flight envelope. The knowledge about the angular velocities in $P(\omega)$ will guide us for the linear fractional transformation that we aim to perform before the robustness analysis.
The goal of the application to follow is to determine how the aforementioned features of the nonlinear uncertain equations of motion will affect the stability of the space launcher. Before that, we need to define the other subsystems in the closed-loop.

5.2.2 Approximation of the kinematic equation

The second crucial issue for the stability analysis of the closed-loop system of figure 3.29 is the kinematic subsystem. Since section 3.3, we know that there exist two main ways to represent the attitude of the launcher: the Euler angles and the quaternions. Both representations rely on equations which are neither linear nor time-invariant. On the first hand, the Euler angles equations presented in (3.18) allow

computing the derivatives of the angles using nonlinear relations involving the current values of the angles and the angular speed. In the other hand, the quaternion based kinematic equation (3.25) is a matrix product with a matrix made of time-varying terms. We mentioned in section 3.9 that the issue about the consequences of the type of representation on the stability and performance of the vehicle is still an open question. Indeed, the two opposing points of view concerning the influence of the kinematic equation on stability can be summarized as follow:

1. One way to consider the kinematic variables consists in seeing them as coordinates of the vehicle position expressed in a particular basis. In this case, obtaining the attitude variables E or q from $\int \omega \text{ dt}$ is assumed to correspond to a change of basis. Hence we can assume that the expression of the attitude and the attitude error with $\int \omega \text{ dt}$ or E or q does not influence the stability of the system. This assumption about the attitude variables can be supported by the fact that the "small-angle" approximation shows that for small displacements from the reference frame, the attitude variables $\int \omega \text{ dt}$ and E and $2q$ can be considered as equal. However, the "small-angle" approximation is almost never valid during the flight so a stronger argument should be given to validate this assumption.

2. The other way to analyze the kinematic equation is simply to consider that it represents another nonlinear subsystem of the model and so to perform its analysis as the other blocks representing physical devices in the model as in [Pereira and Vettori, 2006].

For this application, we will assume that the first point of view is true or at least representative of the actual launcher stability and performance characteristics. It means that we will consider the kinematic block as an identity operator associated with an integrator as in figure 5.1:

$$\alpha = \int \omega \, dt. \tag{5.6}$$

For further studies, we could imagine completing the analysis with a proper model of the kinematic equations. Indeed, even though the assumption which is taken about the kinematics may not be valid, the factorization of the equations of motion which is presented in the following sections can be used for an analysis on a more accurate model.

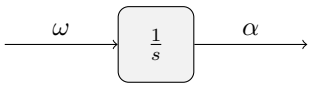

Figure 5.1: Block diagram of the simplified kinematic block for analysis

5.2.3 Modeling of the feedback path

As it was already mentioned, the main drawbacks of analytical tool for robustness analysis is that they rely on simpler models than simulators used for Monte-Carlo validations [Hanson and Beard, 2010]. This is due to the fact that the systems we need to study are extremely complex and some approximations have to be done to fit in the theoretical framework of the analytical tool. For instance, stability of a rocket, of an airplane or of an energy grid is influenced by so many subsystems and parameters that the current stability tests are too demanding in terms of computational capacity even tough they are totally feasible theoretically. Consequently, we need the knowledge of engineers to make the right hypotheses and approximations without compromising the representativeness of the model and so of the stability result.
Since the feedback path presented in section 3.5 is very complex and involves a sampler and an estimation model, we consider the continuous measurement of the current attitude α to be the only one available.

Thus the closed-loop we aim to analyze has continuous-time signals only. Moreover, for the robust stability analysis, no external perturbations should be considered so the signal α' defined in (3.30) is equal to $\alpha_{meas} = \alpha$ since $\alpha_{dist} = 0$. It means that no noise is considered. The representation of the trivial measurement step model for analysis is given in figure 5.2.

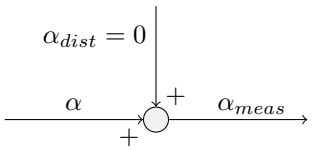

Figure 5.2: Block diagram of the measurement step for analysis

Concerning the state reconstruction stage, it is simplified too and the measurement block now produces a continuous-time signal. To get a prediction of the angular speed ω, we derivate the measured attitude $\alpha_{meas} = \alpha$ through a high-pass derivative filter $\mathcal{F}$ with bounded gain defined by

$$\mathcal{F}(s) = \frac{\omega_f s}{s + \omega_f}, \tag{5.7}$$

where ω_f is such that the frequency domain representation of the derivation is representative over the bandwidth of the closed-loop system. Hence the estimation process can be represented as in figure 5.3.

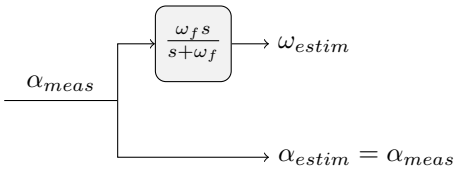

Figure 5.3: Block diagram of the estimation step

The considered feedback path is very different from the one presented in chapter 3. This compromise had to be done since the analysis of the dynamic model was our main goal in this study. As it is computationally demanding, it was necessary to simplify the rest of the closed-loop and in particular the feedback path. The leads for a better representation of the feedback path are twofold:

1. The measurement process modeling can be improved by adding a time-delay to the path. Regarding the current devices used for measurements, this time-delay would be uncertain time-invariant and ranging in a bounded set of values. Concerning the noises resulting from the measurement step, they can be taken into account for a robust performance analysis using the very same model as for this application. This is going to be done later on in section 5.6. Furthermore, an obvious improvement would be to take the sampling into account and consider the hybrid closed-loop.

2. The estimation process relies on a prediction model which is commonly defined as a quasi Linear Parameter Varying (quasi-LPV) system. Of course, simpler models can be implemented. For instance, in the continuous-time framework we set up for our application, the result of an implementation of a LTI prediction model would just increase the size of the nominal part of the LFR to be defined. Concerning the case when the prediction model is a LPV model, it can also be handled by the IQC methods.

5.2.4 Controller

The controller model accounts for the attitude variables which are used for this application. Indeed, since from paragraph 5.2.2 we have the simple relationship $\alpha = \int \omega \, \mathrm{dt}$, we consider that the attitude error can

be computed using the relationship $\Delta\alpha = \alpha_{estim} - \alpha_{aimed}$. The resulting error calculation and torque command calculation steps are depicted figure 5.4.

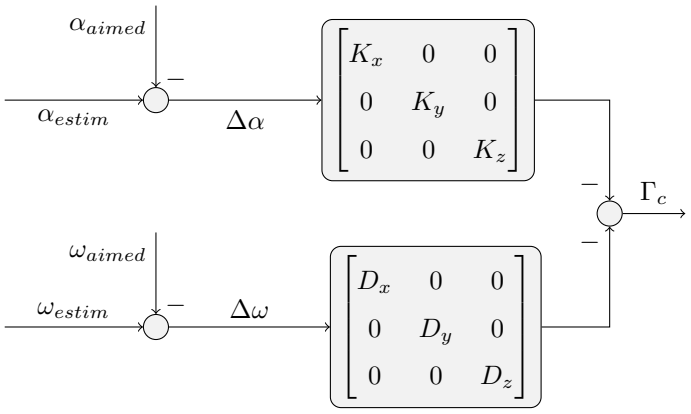

Figure 5.4: Block diagram of controller structure for analysis

The controller structure of figure 5.4 associated to the feedback path we use gives the classical control configuration pictured figure 5.5. This representation merges the derivative filter which is used for the estimation of the angular speed ω in paragraph 5.2.3 with the gains introduced in (3.35). The whole forms classical Proportional-Derivative (PD) filters defined by for the axis β by

$$C_\beta^{(\mathrm{PD})}(s) = K_\beta + D_\beta \frac{\omega_f s}{s + \omega_f} \text{ with } \beta \in \{x, y, z\}. \tag{5.8}$$

The $C_\beta^{(\mathrm{PD})}(s)$ are gathered into a single controller $C(s)$ with three inputs and three decoupled outputs

$$\mathcal{C}(s) = \begin{bmatrix} C_x^{(\mathrm{PD})}(s) & 0 & 0 \\ 0 & C_y^{(\mathrm{PD})}(s) & 0 \\ 0 & 0 & C_z^{(\mathrm{PD})}(s) \end{bmatrix}. \tag{5.9}$$

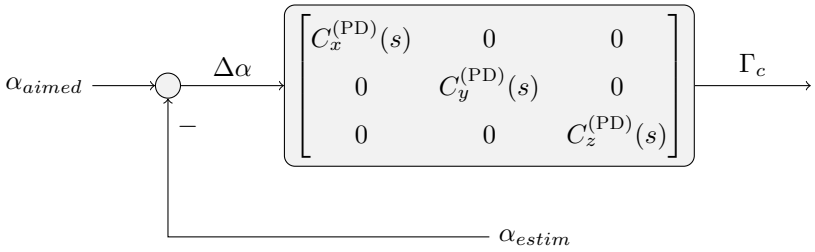

Figure 5.5: Compact block diagram of controller structure for analysis

5.2.5 Actuator

The last subsystem to be defined for this application is the actuator. Since we focus on the equation of motion and not the actuator, the later is modeled in a simple fashion for computational purposes. However, this approximation is proved to be relevant in chapter 6 and it is also widely used in the industry. We chose to model the PWM actuator as a saturation. The saturation is a widely used nonlinearity so its analysis with IQC can be done easily. Moreover, the chosen setting of the saturation

allows to generate a signal Γ_{ACS} whose effect on the dynamic model is similar to the modulated signal of a PWM. Indeed, we will see later on in chapter 6 that low-frequency components of Γ_{ACS} are driving the motion of the vehicle more than the high-frequency harmonics. When appropriately defined, the saturation $\phi_{ACS} = \phi_{\Gamma_{av}}$ generates a satisfying approximation of the low-frequency harmonics from Γ_{ACS}. We define the saturation used to represent the PWM by

$$\phi_{ACS} : \begin{cases} \mathcal{L}^3 & \rightarrow & \mathcal{L}^3 \\ \Gamma_c & \rightarrow & \Gamma_{ACS} \end{cases}, \tag{5.10}$$

$$\forall \Gamma_c \in \mathcal{L}^3, \quad \phi_{ACS}(\Gamma_c) = \begin{bmatrix} \phi^{(x)}_{\Gamma_{av}}(\Gamma^{(x)}_c) \\ \phi^{(y)}_{\Gamma_{av}}(\Gamma^{(y)}_c) \\ \phi^{(z)}_{\Gamma_{av}}(\Gamma^{(z)}_c) \end{bmatrix}$$

$$\text{with } \phi^{(\beta)}_{ACS}(\Gamma^{(\beta)}_c) = \begin{cases} \Gamma^{(\beta)}_c & \text{if } |\Gamma^{(\beta)}_c| < \Gamma^{(\beta)}_{av} \\ \text{sign}(\Gamma^{(\beta)}_c)\Gamma^{(\beta)}_{av} & \text{if } |\Gamma^{(\beta)}_c| \geq \Gamma^{(\beta)}_{av} \end{cases} \text{ and } \beta \in \{x, y, z\}, \tag{5.11}$$

where $\Gamma_{av} \in \mathbb{R}^3$ represents the vector of torques available for control defined in section 3.7. In the definition of the saturation ϕ_{ACS} given in (5.10-5.11), we observe that we have in fact three independent saturations $\phi^{(\beta)}_{\Gamma_{av}}(\bullet)$, $\beta \in \{x, y, z\}$, each one affecting a dedicated channel with a given saturation level $\Gamma^{(\beta)}_{av}$.

5.2.6 Closed-loop overview

The previous paragraphs aimed to define the launch with IQC. The block diagram figure 5.6 summarizes the above paragraphs and gives an overview of the analysis model. We notice that with the three degree-of-freedom equation of motion (5.1), we represent the dynamics with accuracy. Indeed, we still have a nonlinear uncertain closed-loop and it remains challenging to analyze despite the simplifications of the kinematics and the feedback path. As the LFR introduced in section 4.2 seems suitable to represent our system, we are going to reformulate it and fit it into the robustness analysis framework.

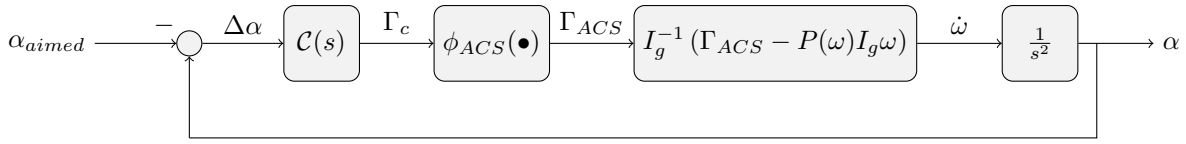

Figure 5.6: Analysis of the equation of motion, closed-loop of the analysis model

5.3 LFR of the nonlinear uncertain model

In this section we transform the closed-loop analysis model of figure 5.6 into a LFR.

5.3.1 Dynamic model transformation

Finding a LFR of the space launcher model figure 5.6 will allow us to assess its robustness to uncertain inertia. It has to be done in a cost effective fashion and with a representative model. By "cost effective", we

mean that we aim to define a perturbation block Δ with reduced size such that the stability test remains computationally tractable despite the number of uncertain parameters. Even if we have the tractability of the stability test as a constraint, we want to find a LFR that covers all the feasible trajectories of the nonlinear uncertain analysis model. This will be our main concern during the construction of the LFR.

Factorization of the inertia matrix and the coupling matrix

To define the LFR of the analysis model, we define a factorization of the equation of motion (5.1) modeling the uncertain launcher flying within its flight envelope described in section 5.2. The block diagram of the equation of motion has been given figure 3.4. After the definition, we spotted two trouble making elements in the equation: the uncertain time-invariant inertia matrix I_g and the time-varying coupling matrix $P(\omega)$. Indeed, $P(\omega)$ has the components of the angular speed vector ω as off-diagonal terms and so it varies with time. To cope with the latter issue, we consider the terms in $P(\omega)$ as uncertain time-varying parameters representing the angular speed of the launcher. Hence, we change the notation to

$$P(\hat{\omega}(t)) = \begin{bmatrix} 0 & -\hat{\omega}_z(t) & \hat{\omega}_y(t) \\ \hat{\omega}_z(t) & 0 & -\hat{\omega}_x(t) \\ -\hat{\omega}_y(t) & \hat{\omega}_x(t) & 0 \end{bmatrix}. \tag{5.12}$$

The parameters $\hat{\omega}_\beta,\ \beta \in \{x, y, z\}$ are the time-varying uncertain parameters that represent the components of the angular speed vector $\omega_\beta,\ \beta \in \{x, y, z\}$. With the "hat" notation, they are distinguished from the components $\omega_\beta,\ \beta \in \{x, y, z\}$ of the actual angular speed vector. This is a conservative representation but an appropriate choice of the ranges of variations will allow to cover all the feasible trajectories of the system. The $\hat{\omega}_\beta$ will have the same range of variation as the real angular speed components $\omega_\beta,\ \beta \in \{x, y, z\}$.
The assumption on the coupling matrix P makes it an uncertain matrix. Hence I_g and $P(\hat{\omega})$ are now uncertain matrices. In order to obtain a quasi-LPV representation of the system, we define a factorization of matrices I_g and $P(\hat{\omega})$. This motivates the following definitions and transformations.
Let us introduce two diagonal matrices $I_d \in \mathbb{R}^{9\times 9}$ with the uncertain time-invariant terms of I_g and $P_d(t) \in \mathbb{R}^{6\times 6}$ with the uncertain time-varying angular speed parameters of $P(\hat{\omega})$. In each matrix, the uncertain terms appear as many times as they do in the original matrix:

$$I_d = \begin{bmatrix} I_x & 0 & 0 & 0 & 0 & 0 & 0 & 0 & 0 \\ 0 & I_y & 0 & 0 & 0 & 0 & 0 & 0 & 0 \\ 0 & 0 & I_z & 0 & 0 & 0 & 0 & 0 & 0 \\ 0 & 0 & 0 & I_{xy} & 0 & 0 & 0 & 0 & 0 \\ 0 & 0 & 0 & 0 & I_{xy} & 0 & 0 & 0 & 0 \\ 0 & 0 & 0 & 0 & 0 & I_{xz} & 0 & 0 & 0 \\ 0 & 0 & 0 & 0 & 0 & 0 & I_{xz} & 0 & 0 \\ 0 & 0 & 0 & 0 & 0 & 0 & 0 & I_{yz} & 0 \\ 0 & 0 & 0 & 0 & 0 & 0 & 0 & 0 & I_{yz} \end{bmatrix} \in \mathbb{R}^{9\times 9}, \tag{5.13}$$

$$\forall t \geq 0, \quad P_d(t) = \begin{bmatrix} \hat{\omega}_z(t) & 0 & 0 & 0 & 0 & 0 \\ 0 & \hat{\omega}_z(t) & 0 & 0 & 0 & 0 \\ 0 & 0 & \hat{\omega}_y(t) & 0 & 0 & 0 \\ 0 & 0 & 0 & \hat{\omega}_y(t) & 0 & 0 \\ 0 & 0 & 0 & 0 & \hat{\omega}_x(t) & 0 \\ 0 & 0 & 0 & 0 & 0 & \hat{\omega}_x(t) \end{bmatrix} \in \mathbb{R}^{6\times 6}. \tag{5.14}$$

The reason why we define such matrices will become clear shortly. For I_d and $P_d(t)$ to make sense, we associate them to so-called placement matrices. These placement matrices aim to put each one of the terms of the diagonal of I_d and $P_d(t)$ in a 3×3 matrix in order to reconstruct the matrices I_g and $P(\hat{\omega})$ from I_d and P_d through the computation of matrix products.
We start by defining the placement matrices for the factorization of I_g. There exist $M_1 \in \mathbb{R}^{3\times 9}$ and $M_2 \in \mathbb{R}^{9\times 3}$ such that

$$I_g = M_1 I_d M_2. \tag{5.15}$$

The placement matrices are defined as

$$M_1 = \begin{bmatrix} 1 & 0 & 0 & 1 & 0 & 1 & 0 & 0 & 0 \\ 0 & 1 & 0 & 0 & 1 & 0 & 0 & 1 & 0 \\ 0 & 0 & 1 & 0 & 0 & 0 & 1 & 0 & 1 \end{bmatrix} \tag{5.16}$$

and

$$M_2 = \begin{bmatrix} 1 & 0 & 0 & 0 & -1 & 0 & -1 & 0 & 0 \\ 0 & 1 & 0 & -1 & 0 & 0 & 0 & 0 & -1 \\ 0 & 0 & 1 & 0 & 0 & -1 & 0 & -1 & 0 \end{bmatrix}^T. \tag{5.17}$$

Secondly, we define the placement matrices for the factorization of $P(\hat{\omega})$. There exist $T_1 \in \mathbb{R}^{3\times 6}$ and $T_2 \in \mathbb{R}^{6\times 3}$ such that

$$P(\hat{\omega}) = T_1 P_d(t) T_2 \tag{5.18}$$

with

$$T_1 = \begin{bmatrix} 1 & 0 & 1 & 0 & 0 & 0 \\ 0 & 1 & 0 & 0 & 1 & 0 \\ 0 & 0 & 0 & 1 & 0 & 1 \end{bmatrix} \tag{5.19}$$

and

$$T_2 = \begin{bmatrix} 0 & 1 & 0 & -1 & 0 & 0 \\ -1 & 0 & 0 & 0 & 0 & 1 \\ 0 & 0 & 1 & 0 & -1 & 0 \end{bmatrix}^T . \tag{5.20}$$

The goal will be to introduce these factorizations into the model depicted figure 5.6 in order to separate the known terms i.e. the nominal values of the uncertain terms, from the unknown terms i.e. the uncertainties affecting the inertia terms and the angular speed parameters.

Introduction of the perturbations

Thanks to the factorizations (5.15) and (5.18), we put all the uncertain terms of the matrices of the equation of motion (5.1) on the diagonal of the newly defined matrices I_d and $P_d(t)$. The goal of this transformation was to isolate them. Indeed, we can now easily access to the uncertain terms of I_g and $P(\hat{\omega})$ placed in I_d and $P_d(t)$, respectively, to affect them with an uncertain parameter.

Uncertain inertia matrix We mentioned during the analysis model definition that the inertia terms are affected by multiplicative uncertainty. Thank to the definition of I_d, this feature can easily be written in an equation. To do so, we introduce the perturbation matrix

$$\Delta_I = \begin{bmatrix} \delta_x & 0 & 0 & 0 & 0 & 0 & 0 & 0 & 0 \\ 0 & \delta_y & 0 & 0 & 0 & 0 & 0 & 0 & 0 \\ 0 & 0 & \delta_z & 0 & 0 & 0 & 0 & 0 & 0 \\ 0 & 0 & 0 & \delta_{xy} & 0 & 0 & 0 & 0 & 0 \\ 0 & 0 & 0 & 0 & \delta_{xy} & 0 & 0 & 0 & 0 \\ 0 & 0 & 0 & 0 & 0 & \delta_{xz} & 0 & 0 & 0 \\ 0 & 0 & 0 & 0 & 0 & 0 & \delta_{xz} & 0 & 0 \\ 0 & 0 & 0 & 0 & 0 & 0 & 0 & \delta_{yz} & 0 \\ 0 & 0 & 0 & 0 & 0 & 0 & 0 & 0 & \delta_{yz} \end{bmatrix} \in \mathbb{R}^{9\times 9}. \tag{5.21}$$

This uncertainty matrix has the same size as I_d (5.13) and exactly the same structure. We observe that I_d contains as many terms as I_g. It means that we may have reached the smallest Δ_I for this kind of factorization and so we cannot hope for further reduction of the size of Δ_I using this method. In Δ_I the δ_β terms, with $\beta \in \{x, y, z, xy, xz, yz\}$, are the relative uncertainty of their associated inertia term. For instance, if I_y has a nominal value $I_y^{(0)}$ affected by an uncertainty of $\pm n\%$, then its actual value is given by $I_y = I_y^{(0)}(1 + \delta_y)$ with $\delta_y \in [-n/100, n/100]$. To apply this simple calculation to all the inertia terms in I_d, we gather their nominal values in $I_d^{(0)}$ and define

$$I_d = I_d^{(0)}(I_9 + \Delta_I). \tag{5.22}$$

The calculation in (5.22) allows applying one specific uncertainty to each one of the six inertia terms. Hence we now have all the inertia terms affected by their "own" uncertainty. To express the uncertain

inertia matrix I_g we can use (5.15) with (5.22) and obtain

$$I_g = M_1 I_d^{(0)} (I_9 + \Delta_I) M_2. \tag{5.23}$$

We remark that the nominal value $I_g^{(0)}$ of the inertia matrix I_g can be expressed as

$$I_g^{(0)} = M_1 I_d^{(0)} M_2. \tag{5.24}$$

Uncertain coupling matrix To find a factorization of $P(\hat{\omega})$ we can proceed the same way as for the inertia matrix I_g. Earlier on in (5.14), we defined a diagonal matrix $P_d(t)$ containing the uncertain time-varying parameters of $P(\hat{\omega}(t))$ and a factorization of it with the matrices T_1 and T_2 from (5.19) and (5.20), respectively.
In accordance to the structure of $P_d(t)$, we define the uncertain time-varying matrix $\Delta_\omega(t)$. This matrix contains the time-varying uncertainties affecting each one of the angular speed parameters $\hat{\omega}_\beta,\ \beta \in \{x, y, z\}$. The nominal values of the speed parameters are gathered in

$$\forall t \geq 0, \quad P_d^{(0)} = \begin{bmatrix} \hat{\omega}_z^{(0)} & 0 & 0 & 0 & 0 & 0 \\ 0 & \hat{\omega}_z^{(0)} & 0 & 0 & 0 & 0 \\ 0 & 0 & \hat{\omega}_y^{(0)} & 0 & 0 & 0 \\ 0 & 0 & 0 & \hat{\omega}_y^{(0)} & 0 & 0 \\ 0 & 0 & 0 & 0 & \hat{\omega}_x^{(0)} & 0 \\ 0 & 0 & 0 & 0 & 0 & \hat{\omega}_x^{(0)} \end{bmatrix} \in \mathbb{R}^{6\times 6} \tag{5.25}$$

while the perturbation on the nominal values of $P_d^{(0)}$ are

$$\forall t \geq 0, \quad \Delta_\omega(t) = \begin{bmatrix} \delta\omega_z(t) & 0 & 0 & 0 & 0 & 0 \\ 0 & \delta\omega_z(t) & 0 & 0 & 0 & 0 \\ 0 & 0 & \delta\omega_y(t) & 0 & 0 & 0 \\ 0 & 0 & 0 & \delta\omega_y(t) & 0 & 0 \\ 0 & 0 & 0 & 0 & \delta\omega_x(t) & 0 \\ 0 & 0 & 0 & 0 & 0 & \delta\omega_x(t) \end{bmatrix}. \tag{5.26}$$

We consider the angular speed parameters $\hat{\omega}_\beta$ to be affected by additive uncertainties. With the definitions (5.25) and (5.26), we can define the diagonal matrix $P_d(t)$ as the sum of its nominal value and its uncertain part:

$$\forall t \geq 0, \quad P_d(t) = P_d^{(0)} + \Delta_\omega(t). \tag{5.27}$$

Now if we want to get back the coupling matrix $P(\hat{\omega})$ and its cross-product matrix structure (5.2), we have to use the placement matrices T_1 and T_2 with the factorized expression of $P(\hat{\omega})$ derived in (5.18) to derive

$$\forall t \geq 0, \quad P(\hat{\omega}(t)) = P(t) = T_1 P_d(t) T_2 = T_1 (P_d^{(0)} + \Delta_\omega(t)) T_2. \tag{5.28}$$

We see that from (5.28) we can recover $P(\hat{\omega}^{(0)})$ defined as

$$\forall t \geq 0, \quad P(\hat{\omega}^{(0)}) = P^{(0)} = T_1 P_d^{(0)} T_2. \tag{5.29}$$

LFR of the equation of motion

Definitions (5.23) and (5.28) can be used to find a LFR of the equation of motion (5.1). Indeed, they can be recast such that the nominal matrices $I_g^{(0)}$ from (5.24) and $P(\hat{\omega}^{(0)})$ from (5.29) are introduced

$$I_g = \underbrace{M_1 I_d^{(0)} M_2}_{I_g^{(0)}} + M_1 I_d^{(0)} \Delta_I M_2, \tag{5.30}$$

and

$$\forall t \geq 0, \quad P(\hat{\omega}) = \underbrace{T_1 P_d^{(0)} T_2}_{P(\hat{\omega}^{(0)})} + T_1 \Delta_\omega(t) T_2. \tag{5.31}$$

By simple manipulations, the inverse of I_g can also be expressed

$$I_g = I_g^{(0)} + M_1 I_d^{(0)} \Delta_I M_2 \tag{5.32}$$

$$= I_g^{(0)} \left(I_3 + {I_g^{(0)}}^{-1} M_1 I_d^{(0)} \Delta_I M_2 \right), \tag{5.33}$$

gives

$$I_g^{-1} = (I_g^{(0)} + M_1 I_d^{(0)} \Delta_I M_2)^{-1} \tag{5.34}$$

$$= \left(I_3 + {I_g^{(0)}}^{-1} M_1 I_d^{(0)} \Delta_I M_2 \right)^{-1} {I_g^{(0)}}^{-1}. \tag{5.35}$$

To visualize these factorizations and see how the uncertainties affect the motion of the launcher, we introduce them in the block diagram of the equation of motion in figure 3.4. This is done in figure 5.7.

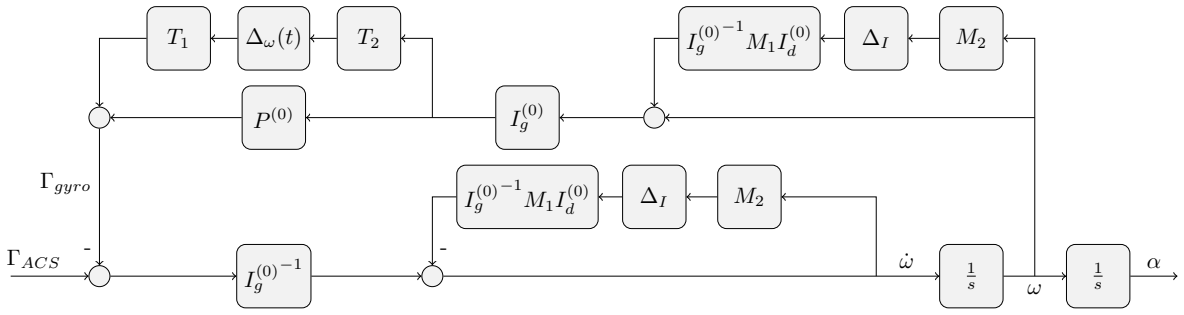

Figure 5.7: Block diagram for the factorized equation of rotational motion

The resulting representation of the dynamic block separates the known nominal parameters of the equation of motion from their unknown perturbations Δ_I and $\Delta_\omega(t)$. Hence we will obtain the LFR from this representation.

5.3.2 Linear fractional transformation of the actuator

For robustness analysis, a common way to describe the saturation operator ϕ_{ACS} chosen as an actuator model uses a unit gain and a dead-zone operator ψ_{ACS}. The dead-zone nonlinearity $\psi_{ACS} = \psi_{\Gamma_{av}}$ with

output channels defined by the saturation vector Γ_{av} identical to the one in (5.11) is defined by

$$\psi_{ACS} : \left\{ \begin{array}{ccc} \mathcal{L}^3 & \rightarrow & \mathcal{L}^3 \\ \Gamma_c & \rightarrow & \psi_{ACS}(\Gamma_c) \end{array} \right. , \tag{5.36}$$

and

$$\forall \Gamma_c \in \mathcal{L}^3,\ \psi_{ACS}(\Gamma_c) = \begin{bmatrix} \psi^{(x)}_{\Gamma_{av}}(\Gamma^{(x)}_c) \\ \psi^{(y)}_{\Gamma_{av}}(\Gamma^{(y)}_c) \\ \psi^{(z)}_{\Gamma_{av}}(\Gamma^{(z)}_c) \end{bmatrix}$$

$$\text{with } \psi^{(\beta)}_{\Gamma_{av}}(\Gamma^{(\beta)}_c) = \left\{ \begin{array}{ll} 0 & \text{if } |\Gamma^{(\beta)}_c| < \Gamma^{(\beta)}_{av} \\ \Gamma^{(\beta)}_c - \text{sign}(\Gamma^{(\beta)}_c)\Gamma^{(\beta)}_{av} & \text{if } |\Gamma^{(\beta)}_c| \geq \Gamma^{(\beta)}_{av} \end{array} \right. \text{ and } \beta \in \{x, y, z\}, \tag{5.37}$$

One of the main feature of the saturation nonlinearity ϕ_{ACS} from (5.10-5.11) is that it can be defined using the dead-zone nonlinearity ψ_{ACS} from (5.36-5.37). Indeed, we have the relationship

$$\phi_{\Gamma_{av}} = Id - \psi_{\Gamma_{av}}, \tag{5.38}$$

where the operator Id is the identity operator. This setup is the one represented in figure 5.8. The point in using this transformation of the saturation ϕ_{ACS} into (5.38) is twofold. First, this representation is adapted for LFR. Indeed, this representation splits the saturation operator into two blocks, one is the nominal i.e. the direct gain 1, and the other is the trouble making part perturbing the nominal behavior through the dead-zone output. This representation is appropriate to build a LFR and so to use IQC based analysis results. Secondly, the so-called modified sector condition fulfilled by the dead-zone operator ψ_{ACS} can be used to ensure the stability of the system by the application of the theorem presented in the next section. The modified sector condition captures completely the input-output characteristic of ψ_{ACS} and it is one of its main advantages. As a drawback, we will see that it gives local stability certificates only.

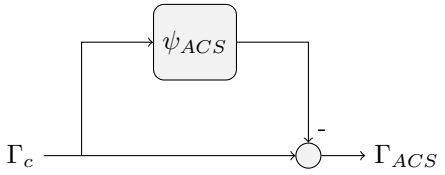

Figure 5.8: Block diagram of LFR of the saturation operator $\phi_{\Gamma_{av}}$

There is a drawback which is assumed to have no consequence on the results validity based on engineering considerations but needs to be mentioned. The IQC tool models the dead-zone operator as a memoryless nonlinear operator in a sector using the multiplier Π_{nlom} defined in appendix A equation (9.11). Since the dead-zone nonlinearity ψ_{ACS} belongs to the sector $(0, 1)$, it causes the analysis model to be singular along the upper limit of the sector. Basically, what happens here is that the multiplier covers the dead-zone nonlinearity ψ_{ACS} exactly the same way as it would cover the saturation operator ϕ_{ACS}. In other words, its "sees" ψ_{ACS} exactly as ϕ_{ACS}. In the linear part of the saturation, ϕ_{ACS} behaves as a gain of 1. If we introduce this gain in the representation figure 5.8 instead of ψ_{ACS}, then the gain from Γ_c to Γ_{ACS} is zero and the closed-loop is fictively open. Consequently, if the open-loop transfer function of the nominal system in not in $\mathbb{RH}_\infty$ we have a singularity and the IQC stability theorem cannot be used. As we have

a double integrator in the nominal path of the analysis model, the singularity occurs.
In our analysis, this issue is avoided by setting the sector to be $(0, 1-\varepsilon)$ with ε being a small positive real number. The shortcoming of this assumption is that the sector $(0, 1-\varepsilon)$ does not represent fully the dead-zone nonlinearity. Indeed, as emphasized in figure 5.9, the characteristic plot of ψ_{ACS} intersects the upper-limit of the sector (the line with slope $\beta = 1-\varepsilon$) and gets off it. Hence the whole characteristic plot of ψ_{ACS} does not lie between the limits of the sector. It means that with a sector $(0, 1-\varepsilon)$, all the feasible trajectories of the system with the dead-zone are not covered. Nevertheless, the sector $(0, 1-\varepsilon)$ is considered as a relevant approximation for values of the input signal Γ_c that has each one of its component satisfying

$$\forall \beta \in \{x, y, z\}, |\Gamma_c^{(\beta)}| \leq \frac{\Gamma_{av}^{(\beta)}}{\varepsilon}. \tag{5.39}$$

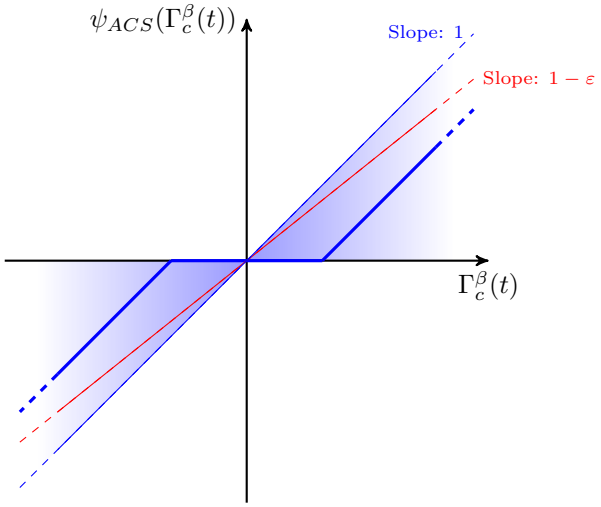

Figure 5.9: Sector conditions $(0, 1)$ and $(0, 1-\varepsilon)$ with dead-zone ψ_{ACS}, ε has been deliberately taken large enough to see that the sector limit and the dead-zone characteristic will intersect for some value of $\Gamma_c^\beta(t)$.

The value $\Gamma_{av}^{(\beta)}/\varepsilon$ is the value of $\Gamma_c^{(\beta)}(t)$ above which the output of the dead-zone is out of the sector limits. Regarding the values we will give to ε, this intersection occurs for very large inputs $\Gamma_c^{(\beta)}(t)$. Such input cannot be generated in the real system due to other physical limitations. From an engineering point of view, the singularity is not a problem. From a mathematically rigorous point of view, the analysis of such case where a nonlinearity is represented by a sector causing a singularity gives local stability results as in [Peaucelle et al., 2012] and [Gomes da Silva Jr. and Tarbouriech, 2005]. To strengthen this assumption, we will also verify during the simulations that the limit (5.39) is not exceeded.
To dispense with the aforementioned drawback, we can restrict the sector to $(0, 1-\varepsilon)$ or use one of the two methods given below.

1. A pragmatic approach would be to reconsider the definition of the integrators in the dynamic and kinematic blocks of figure 5.6. Indeed, as we need a strictly stable open-loop for the nominal part to be strictly stable i.e. transfer function in $\mathbb{RH}_\infty$, we could imagine to replace the integrators by low-pass filters with finite low-frequency gain. It would cause the poles of the open-loop transfer function to have negative real part while physically, it would not change anything to the representativeness of the analysis model thanks to a suitable tuning of the cut-off frequency and the static gain. Moreover, this is common engineering practice to take this assumption.

2. The technique presented in [Gomes da Silva Jr. and Tarbouriech, 2005] and [Biannic et al., 2006] that relies on the so-called modified sector condition can efficiently tackle the singularity issue. This method will be presented in section 5.4 and used during the analysis section 5.5 to draw local stability results.

To conclude, the saturation operator ϕ_{ACS} has been put in a LFR involving a dead-zone operator ψ_{ACS}. A singularity has been bypassed by a reduction of the size of the sector covering ψ_{ACS}. As we are going to see it in the next section, this approximation will not be needed to implement the Lyapunov theory based tool to be used for the stability assessment. Before that, the LFR representation of ϕ_{ACS} is going to enable us to define the LFR of the closed-loop required to perform the robust stability analysis.

5.3.3 LFR of the space launcher

We defined separately the LFR of the uncertain nonlinear equation of motion and the LFR of the actuator. To perform the robustness analysis, we now need to represent the whole closed-loop under LFR. First of all and to give an overview of it, we modified the closed-loop from figure 5.6 by introducing the new representations we obtained of the equation of motion figure 5.7 and of the actuator figure 5.8. The resulting block diagram is given figure 5.10. This block diagram can be recast into a more classic LFR

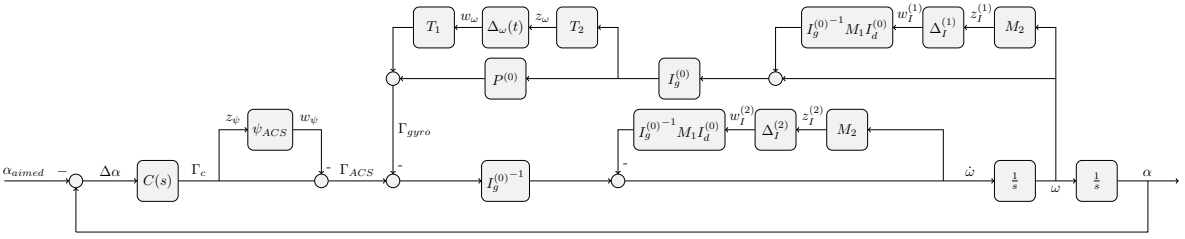

Figure 5.10: Block diagram for closed-loop LFR

by the definition of a nominal LTI block M_{dyn} and a block diagonal perturbation operator Δ_{dyn} as in figure 5.11. The subscript *dyn* is used to remember that this application is dedicated to the analysis of the dynamic model of the space launcher. As we are not into a robust performance analysis yet, the M_{dyn} block we define corresponds to the M_{11} block from figure 4.12 as we only consider the perturbation inputs and outputs. Consequently, only the z_i and w_i are kept in the LFR. In this interconnection, the

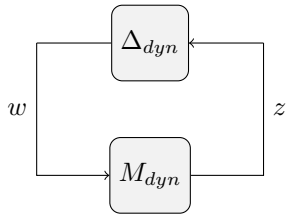

Figure 5.11: Linear fractional Representation of the closed-loop analysis model

trouble making nonlinear time-varying block Δ_{dyn} is defined by

$$\Delta_{dyn} = \begin{bmatrix} \Delta_I^{(1)} & 0_{9\times9} & 0_{9\times6} & 0_{9\times3} \\ 0_{9\times9} & \Delta_I^{(2)} & 0_{9\times6} & 0_{9\times3} \\ 0_{6\times9} & 0_{6\times9} & \Delta_\omega(t) & 0_{6\times3} \\ 0_{3\times9} & 0_{3\times9} & 0_{3\times6} & \psi_{ACS} \end{bmatrix}. \tag{5.40}$$

We use superscript labels (1) and (2) to distinguish the two occurrences of Δ_I in the block diagram figure 5.10. We see that the size of the overall perturbation block Δ_{dyn} is depending on the size of the matrices I_d and P_d defined for the factorization of the inertia matrix I_g and the coupling matrix $P(\hat{\omega}(t))$. Hence, a way to reduce the size of Δ_{dyn} is to find smaller factorization matrices. We can associate to Δ_{dyn} the perturbation signals:

$$z = \begin{bmatrix} z_I^{(1)} \\ z_I^{(2)} \\ z_\omega \\ z_\psi \end{bmatrix} \in \mathcal{L}^{27} \text{ and } w = \Delta_{dyn}(z) = \begin{bmatrix} w_I^{(1)} \\ w_I^{(2)} \\ w_\omega \\ w_\psi \end{bmatrix} = \begin{bmatrix} \Delta_I^{(1)} z_I^{(1)} \\ \Delta_I^{(2)} z_I^{(2)} \\ \Delta_\omega(t) z_\omega \\ \psi_{ACS}(z_\psi) \end{bmatrix} \in \mathcal{L}^{27}. \tag{5.41}$$

We defined the perturbation block of the LFR Δ_{dyn}, we can now define a state-space realization of the LTI nominal part M_{dyn}. To do so, we define (A_c, B_c, C_c, D_c) as a state-space realization of the controller $\mathcal{C}$ from (5.9) and define the state-space equations of the operator M_{dyn} from w to z:

$$\begin{cases} \dot{x} &= Ax + Bw \\ z &= Cx + Dw \end{cases} \tag{5.42}$$

where the state vector $x \in \mathbb{R}^9$ is

$$x = \begin{bmatrix} \omega \\ \alpha \\ x_c \end{bmatrix}, \tag{5.43}$$

and the matrices (A, B, C, D) are

$$A = \begin{bmatrix} -{I_g^{(0)}}^{-1} P^{(0)} I_g^{(0)} & -{I_g^{(0)}}^{-1} D_c & {I_g^{(0)}}^{-1} C_c \\ I_3 & 0_{3\times3} & 0_{3\times3} \\ 0_{3\times3} & -B_c & A_c \end{bmatrix}, \tag{5.44}$$

$$B = \begin{bmatrix} B_u & B_{nl} \end{bmatrix} \text{ with} \tag{5.45}$$

$$B_u = \begin{bmatrix} -{I_g^{(0)}}^{-1} P^{(0)} M_1 I_d^{(0)} & -{I_g^{(0)}}^{-1} M_1 I_d^{(0)} & -{I_g^{(0)}}^{-1} T_1 \\ 0_{3\times9} & 0_{3\times9} & 0_{3\times6} \\ 0_{3\times9} & 0_{3\times9} & 0_{3\times6} \end{bmatrix} \text{ and } B_{nl} = \begin{bmatrix} -{I_g^{(0)}}^{-1} \\ 0_{3\times3} \\ 0_{3\times3} \end{bmatrix},$$

$$C = \begin{bmatrix} C_u \\ C_{nl} \end{bmatrix} \text{ with} \tag{5.46}$$

$$C_u = \begin{bmatrix} M_2 & 0_{9\times3} & 0_{9\times3} \\ -M_2 {I_g^{(0)}}^{-1} P^{(0)} I_g^{(0)} & -M_2 {I_g^{(0)}}^{-1} D_c & M_2 {I_g^{(0)}}^{-1} C_c \\ T_2 I_g^{(0)} & 0_{6\times3} & 0_{6\times3} \end{bmatrix} \text{ and } C_{nl} = \begin{bmatrix} 0_{3\times3} & -D_c & C_c \end{bmatrix},$$

$$D = \begin{bmatrix} D_{u,u} & D_{u,nl} \\ 0_{3\times24} & 0_{3\times3} \end{bmatrix} \text{ with} \tag{5.47}$$

$$D_{u,u} = \begin{bmatrix} 0_{9\times9} & 0_{9\times9} & 0_{9\times6} \\ -M_2 {I_g^{(0)}}^{-1} P^{(0)} M_1 I_d^{(0)} & -M_2 {I_g^{(0)}}^{-1} M_1 I_d^{(0)} & -M_2 {I_g^{(0)}}^{-1} T_1 \\ T_2 M_1 I_d^{(0)} & 0_{6\times9} & 0_{6\times6} \end{bmatrix} \text{ and } D_{u,nl} = \begin{bmatrix} 0_{9\times3} \\ -M_2 {I_g^{(0)}}^{-1} \\ 0_{6\times3} \end{bmatrix}.$$

In the above definitions, the perturbation signals z and w were split into two components corresponding to the uncertain perturbation channels (subscript u) and the perturbation channels coming from the nonlinearity (subscript nl)

$$z_u = \begin{bmatrix} z_I^{(1)} \\ z_I^{(2)} \\ z_\omega \end{bmatrix} \in \mathcal{L}^{24}, \quad z_{nl} = \begin{bmatrix} z_\psi \end{bmatrix} \in \mathcal{L}^3 \text{ and } w_u = \begin{bmatrix} w_I^{(1)} \\ w_I^{(2)} \\ w_\omega \end{bmatrix} \in \mathcal{L}^{24}, \quad w_{nl} = \begin{bmatrix} w_\psi \end{bmatrix} \in \mathcal{L}^3. \tag{5.48}$$

As we can see in (5.45), (5.46) and (5.47), the matrices are split accordingly.

The setup is now adapted to the analytical tools we want to use to perform to the stability analysis. We turned the closed-loop system described in section 5.2 and depicted in figure 5.6 into a LFR (M_{dyn}, Δ_{dyn}) explicitly defined by (5.40) and (5.42).

5.4 A Lyapunov-based tool for robust stability analysis

This section aims to present the other robustness analysis tool which will be used to perform the robust stability analysis of the space launcher LFR in figure 5.11. It relies on Lyapunov theory and will give us another stability result.

5.4.1 Model representation

To assess the robust stability of the analysis model defined in section 5.2 and transformed into a LFR in section 5.3, we want to use a Lyapunov-based method which addresses efficiently the stability of constrained input systems. By constrained inputs we mean inputs limited in amplitude by a saturation operator as ϕ_{ACS}. This method is based on the modified sector condition used in [Biannic et al., 2006]. It allows assessing the stability of our launcher model by solving LMI using the saturation description with a dead-zone operator defined in (5.36-5.37). In order to have an overview of these LMI, we give the stability theorem and extend it to systems with uncertain time-invariant and/or time-varying parameters. We will put the emphasis on the difficulty caused by the uncertainties we have in our model.
Initially, the result is about linear saturated systems described by the Lure like state-space equation

(5.49). Hence our analysis model adapted to this framework should be defined as:

$$\begin{cases} \dot{x} = & Ax + B\psi_{ACS}(z) \\ z = & Cx \end{cases} \tag{5.49}$$

where $A \in \mathbb{R}^{n\times n}$, $B \in \mathbb{R}^{n\times 3}$ and $C \in \mathbb{R}^{3\times n}$ are the state-space matrices and $\psi_{ACS}(\bullet)$ is the dead-zone operator. Here the size if the dead-zone operator and the input and output matrices is fit to the sizes encountered in our space launcher model. The system LFR with a dead-zone operator ψ_{ACS} obtained after the modeling phase in the previous section is perfectly suitable to this framework. As a consequence, under some restrictions, we can use the results in the next paragraph to assess the stability of our space vehicle. For this we will extend the original result to uncertain state-space representations.

5.4.2 Robust stability analysis

Considering that from the nominal part M_{dyn} of our LFR depicted figure 5.11 we can define the matrices (A, B, C) to obtain a state-space representation of the system as (5.49), the following theorem allows to ensure asymptotic stability of the system without uncertainties inside an ellipsoid of initial conditions.

Theorem 7 (Constrained inputs [Gomes da Silva Jr. and Tarbouriech, 2005]) *If there exist matrices $W \in \mathbb{R}^{n\times n}$ symmetric positive definite, $S \in \mathbb{R}^{3\times 3}$ diagonal positive definite and $Y \in \mathbb{R}^{3\times n}$ such that the LMI conditions*

$$\begin{cases} \begin{bmatrix} WA^T + AW & BS + Y^T \\ S^T B^T + Y & -2S \end{bmatrix} & < 0 \quad , \\ \begin{bmatrix} W & WC_i^T - Y_i^T \\ C_i W - Y_i & \Gamma_{av_i}^2 \end{bmatrix} & \geq 0 \quad i \in \{1, 2, 3\}, \end{cases} \tag{5.50}$$

are verified then the ellipsoid $\Sigma(P)$ in (5.51) with $P = W^{-1}$ is a domain of asymptotic stability for system (5.49):

$$\Sigma(P) = \left\{ x \in \mathbb{R}^n \;\middle|\; x^T P x \leq 1 \right\}. \tag{5.51}$$

It means that for any initial condition vector $x_0 \in \Sigma(P)$, the state vector x converges asymptotically toward the equilibrium point of the autonomous system. Notice that C_i denotes the i^{th} row of C and Y_i denotes the i^{th} row of Y.

In the case where A and B in (5.49) linear rational dependence on the components of the parameter vector $\theta \in \mathbb{R}^p$ and that the uncertain parameters are not repeated, an extension of theorem 7 can be given. Here without loss of generality we assume that θ belongs to a subset of $\mathbb{R}^p$ defined as the convex hull of a set of points $\mathcal{V}$. $\mathcal{V}$ defines the set of N vertices of the polytope of feasible parameter combinations and $\mathrm{Co}(\bullet)$ the convex hull of a set of points. The extension of the theorem aims to guarantee the stability of the uncertain Lure-like system inside the convex hull of the set of matrices

$$\mathcal{P}_{\mathcal{V}} := \{(A(\theta), B(\theta), C(\theta) \mid \theta \in \mathcal{V}\} \subset \mathbb{R}^{n\times n} \times \mathbb{R}^{n\times 3} \times \mathbb{R}^{3\times n} \tag{5.52}$$

denoted by $\mathrm{Co}(\mathcal{P}_{\mathcal{V}})$ i.e. the convex envelope of the N realizations of $(A(\theta), B(\theta), C(\theta))$ for $\theta \in \mathcal{V}$. If we can check simultaneously the constraints (5.50) for the N state-space realizations $(A(\theta), B(\theta), C(\theta)) \in \mathcal{P}_{\mathcal{V}}$, we can ensure robust local asymptotic stability of the well-posed parameter dependent system as

in [Boyd and Yang, 1989] for systems with unrepeated parameters. These considerations lead to an extension of the theorem in [Gomes da Silva Jr. and Tarbouriech, 2005] to uncertain systems with non repeated uncertainties. In this case, to prepare the analysis of our space-launcher model we only consider A and B to be parameter dependent as we will see it in paragraph 5.5.3:

$$\left\{\begin{array}{rcll} \dot{x} & = & A(\theta)x + B(\theta)\psi_{ACS}(z) & \\ z & = & Cx & . \\ \theta & \in & \mathrm{Co}(\mathcal{V}) \subset \mathbb{R}^p & \end{array}\right. \tag{5.53}$$

Theorem 8 (Uncertain systems with constrained inputs (unrepeated uncertainties)) *If there exist matrices $W \in \mathbb{R}^{n\times n}$ symmetric positive definite, $S \in \mathbb{R}^{3\times 3}$ diagonal positive definite and $Y \in \mathbb{R}^{3\times n}$ such that the LMI conditions*

$$\left\{\begin{array}{ll} \begin{bmatrix} WA_k^T + A_kW & B_kS + Y^T \\ S^TB_k^T + Y & -2S \end{bmatrix} & < 0, \quad k \in \{1,\ldots,N\}, \\ \begin{bmatrix} W & WC_i^T - Y_i^T \\ C_iW - Y_i & \Gamma_{av_i}^2 \end{bmatrix} & \geq 0, \quad i \in \{1,2,3\}. \end{array}\right. \tag{5.54}$$

are verified then the ellipsoid $\Sigma(P)$ in (5.51) with $P = W^{-1}$ is a domain of asymptotic stability for system (5.53):

$$\Sigma(P) = \left\{x \in \mathbb{R}^n \middle| x^TPx \leq 1\right\}. \tag{5.55}$$

Here, the state-space realization of the uncertain parameter-dependent system at the k^{th} vertex of $Co(\mathcal{V})$ is given by (A_k, B_k, C).

Notice that the uncertain parameter vector $\theta \in \mathbb{R}^p$ can contain parametric time-invariant uncertainties and parametric time-varying uncertainties. Furthermore, we put the emphasis on the fact that this result holds only for non repeated uncertain parameters. For instance, it means that if in a LFR of a system, the Δ block contain several times the same parameter, theorem 8 does not hold and takes the form of property 1. To understand better the difference between the non repeated and the repeated case, let us define the set of realizations $(A(\theta), B(\theta), C(\theta))$ for $\theta \in \mathrm{Co}(\mathcal{V})$:

$$\mathcal{S}_{\mathrm{Co}(\mathcal{V})} := \{(A(\theta), B(\theta), C(\theta)) \mid \theta \in \mathrm{Co}(\mathcal{V})\}. \tag{5.56}$$

This is the set of realizations of (5.53) for which we would like to prove stability. When the uncertainties of the system are not repeated e.g. they appear only once in the perturbation block of the LFR, the set $\mathcal{S}_{\mathrm{Co}(\mathcal{V})}$ is a subset of $\mathrm{Co}(\mathcal{P}_\mathcal{V})$. That is

$$\mathcal{S}_{\mathrm{Co}(\mathcal{V})} \subseteq \mathrm{Co}(\mathcal{P}_\mathcal{V}). \tag{5.57}$$

As a consequence, any state-space representation in $\mathcal{S}_{\mathrm{Co}(\mathcal{V})}$ can be expressed as a convex combination of the state-space realizations in $\mathrm{Co}(\mathcal{P}_\mathcal{V})$. Since in theorem 7, the A, B (and C) matrices enter the LMI linearly (5.50), any convex combination of matrices for which the stability is proved simultaneously i.e. for the same W, S, Y, results in a locally stable system with the region of attraction defined by $\Sigma(P)$ (5.55). However, if one (or more) of the uncertain parameters appears more than once, the set containment relationship (5.57) does not hold. In [Boyd and Yang, 1989], repeated uncertainties make impossible the proof of negative definiteness of the Lyapunov function derivative. In facts, for systems with repeated

uncertainties the theorem can only be recast into the following non-informative property.

Property 1 (Uncertain systems with constrained inputs (repeated uncertainties)) *If there exist three matrices $W \in \mathbb{R}^{n\times n}$ symmetric positive definite, $S \in \mathbb{R}^{3\times 3}$ diagonal positive definite and $Y \in \mathbb{R}^{3\times n}$ such that the LMI conditions*

$$\begin{cases} \begin{bmatrix} WA_k^T + A_kW & B_kS + Y^T \\ S^TB_k^T + Y & -2S \end{bmatrix} < 0, \quad k \in \{1,\dots,M\}, \\ \begin{bmatrix} W & WC_i^T - Y_i^T \\ C_iW - Y_i & \Gamma_{av_i}^2 \end{bmatrix} \geq 0, \quad i \in \{1,2,3\}. \end{cases} \tag{5.58}$$

are verified then the ellipsoid $\Sigma(P)$ in (5.51) with $P = W^{-1}$ is a domain of asymptotic stability for the realizations of system (5.53) such that $(A(\theta), B(\theta), C) \in \mathcal{S}_{Co(\mathcal{V})} \cap Co(\mathcal{P}_\mathcal{V})$.

This property is not useful alone since there exists no way to determine whether $\mathrm{Co}(\mathcal{P}_\mathcal{V})$ covers $\mathcal{S}_{\mathrm{Co}(\mathcal{V})}$ well or not i.e. to find how "large" the intersection is.

Regarding the definition of Δ_{dyn} (5.40), we are allowed to perform an analysis of our system represented by the LFR figure 5.11 only for for simplified cases presenting only uncertainties with non-repeated parameters or to guarantee the stability over a set of realizations of the system which cannot be characterized. Nevertheless, the constraints (5.50) and (5.54) can be easily implemented and solved with Matlab®. Even though the result presented above is not strictly comparable to the IQC stability test from chapter 4, it will allow us to have another "point of view" on the robust stability of our system.
Concerning the relevance of this result in the context of a space launcher flight, we point out that during a mission, a controller switch generally occurs at the beginning of each maneuver. As a result, we may be in the situation where the launcher has to recover from non zero initial conditions. The results of the previous paragraph will allow us to certify the asymptotic recovery from the set of initial condition $\Sigma(P)$.

We can now go further and perform the robust stability analysis of the system.

5.5 Robust stability analysis

5.5.1 Introduction

The system resulting from the transformations of section 5.3 and depicted in figure 5.10 was designed for robust stability analysis with the IQC toolbox described in [Köroglu et al., 2008]. Indeed, the LFR with perturbation block Δ_{dyn} contains operators and uncertainties that are satisfying IQC defined by the multipliers of LPVMAD given in appendix A. Concerning the analysis with the Lyapunov-based method described in section 5.4, we will have to restrict the model to simple cases for the results to have an easy interpretation. Again, the LFR of the closed-loop will be of great help in paragraph 5.5.3.
We have three different types of perturbation sub-blocks in Δ_{dyn} from (5.40). They are described in the following short paragraphs. The levels of uncertainty given below are "nominal" levels of uncertainty. The analyzes will account for different uncertainty sets depending on the results obtained for the nominal uncertainties.

1. The Δ_I are time-invariant parametric uncertainties affecting the terms of the inertia matrix I_x, I_y, I_z, I_{xy}, I_{xz} and I_{yz}. Each one of the two Δ_I perturbation blocks needed to model the uncertain equation of motion contains the same set of six different uncertainties. Δ_I appears twice to model I_g and I_g^{-1}. The time-invariance assumption holds since variations in mass repartitions e.g. propellant

consumption, remain very small during a maneuver. Consequently, uncertainties about the inertia are mostly due to approximative initial inertia measurements. The level of uncertainty for which we need to prove the stability of the system is $\pm 10\%$ for the diagonal terms I_x, I_y and I_z while the off-diagonal terms I_{xy}, I_{xz} and I_{yz} can range from -100% to $+900\%$ off their nominal value. The uncertainties on off-diagonal terms are large since their measure is more difficult than the measure of the diagonal terms.

2. Δ_ω contains time-varying parametric uncertainties representing the angular speeds. Since the angular speeds are always changing with time during a maneuver, the time-variations need to be taken into account. There are three different parameters, each one corresponding to the angular speed about one of the three axes of $\mathcal{R}_g$. We decided to describe them as affected by additive uncertainty because their nominal value is generally set to zero. The amplitude of the uncertainty is defined from the flight envelope of the launcher. We remember that with this flight envelope we wanted to cover all the "flyable" state vectors. Hence, we consider that the nominal angular velocity vector is

$$\hat{\omega}^{(0)} = \begin{bmatrix} \hat{\omega}_x^{(0)} \\ \hat{\omega}_y^{(0)} \\ \hat{\omega}_z^{(0)} \end{bmatrix} = \begin{bmatrix} 0 \\ 0 \\ 0 \end{bmatrix}, \tag{5.59}$$

and we assume the parameters associated to the angular speeds are such that for all $t \geq 0$,

$$\hat{\omega}_x(t) \in [-100 \text{ deg.s}^{-1}, +100 \text{ deg.s}^{-1}],$$
$$\hat{\omega}_y(t), \hat{\omega}_z(t) \in [-50 \text{ deg.s}^{-1}, +50 \text{ deg.s}^{-1}].$$

The nominal angular velocity vector is set to zero for the study. Of course, it could have been defined differently. To provide a more accurate description of the angular speed variations, we can use the arguments from paragraph 3.2.6 to evaluate the bounds on the time-variations of the angular speeds i.e. the angular accelerations. We consider that $|\dot{\hat{\omega}}_\beta| < 1 \text{ deg.s}^{-2}, \beta \in \{x, y, z\}$.

3. The dead-zone nonlinearity $\psi_{ACS} = \psi_{\Gamma_{av}}$ is a sector bounded operator. When needed, the sector will be $(0, 1-\varepsilon)$ with $\varepsilon = 10^{-3}$. Since it also has a bounded incremental gain, see e.g. figure 5.9, we determine it to be 1. Roughly, the incremental gain corresponds to the slope of the dead-zone characteristic in figure 5.9. Three other features of ψ_{ACS} are interesting for IQC-based stability analysis. First, according to the general definition of ψ_{ACS} in (5.36) and (5.37) and as we can see it on figure 5.9, the characteristic of the dead-zone nonlinearity is odd i.e. it is symmetric with respect to the point $(0, 0)$ in the input/output plane. Secondly, the characteristic is monotone. In particular it is monotonically nondecreasing. Finally, the dead-zone operator is memoryless thus its output at the time-instant $t = t'$ depends only on its input at time t'.

The characteristics of the operators in the block diagonal perturbation operator Δ_{dyn} are going to be useful for the preparation of the stability tests in the coming paragraphs. Before continuing, we dwell on the fact that our IQC based tool is the only one that is able to take into account the time-invariance or time-variations of the uncertain parameters.

5.5.2 Robust stability analysis with the IQC-based method

The robustness of the launcher is going to be evaluated with the IQC tool LPVMAD available at ESA and presented in [Köroglu et al., 2008]. The three types of perturbations described in the above introduction all have their dedicated multiplier already implemented. By "dedicated" we mean that since

these types of perturbation have been thoroughly studied in the literature, there exist multipliers that define IQC which capture the perturbation and describe them well enough for the stability test to have reduced conservatism. This is the main reason why we are going to use them. In some sense, the fact that such multipliers are available drove our search toward a factorized version of the equation of motion (5.1) involving parametric time-invariant and time-varying uncertainties. Concerning the nonlinear sector bounded odd monotone dead-zone operator used for ACS modeling, we knew it was appropriately captured by a multiplier in LPVMAD so we used it in the perturbation block.
To be more general, there are two different ways to prepare an IQC analysis. The first one corresponds to the one used here where we look for a representation of the system involving operators that are well described by already existing IQC multipliers. Consequently, the representation of a perturbation operator Δ with such multipliers is more likely to result in a reduce conservatism stability test. For instance, the multiplier used to describe Δ_I derives from the well-known works in [Packard and Doyle, 1993] that are currently the bests to describe LTI static uncertainties. This so-called "multiplier driven" approach based on modeling more than on the search for an IQC multiplier describing a trouble making operator. The second method to prepare an IQC-based robustness analysis is the one we will use in the application of chapter 6 where the goal is to build new multipliers for operators that are not encountered very often in the literature. In this case the modeling of the system into a LFR is less complex than the one done here but we have to work on the definition of valid IQC.
In general, when performing IQC-based stability analysis, we can either do some loop transformations to fit the model of interest in an existing framework with known multipliers or take the system model as it is and characterize the trouble making operators with new IQC. Nevertheless, we will see in chapter 6 that it can be helpful to perform loop transformations when looking for IQC describing complex operators.
The goal of the next paragraph is to give the definition of the frequency dependent part of the multipliers that define IQC satisfied by Δ_{dyn}. A more precise definition can be found in appendix A.

Multipliers and basis transfer function

The multipliers to be used for the analysis of the LFR in figure 5.10 are the dynamic multipliers from LPVMAD. There description can be found in section 4.5 or in the second appendix. The multiplier Π_{ltis} we use to describe the time-invariant parametric uncertainties of Δ_I is described in paragraph 4.5.2 and reads as

$$\Pi_{ltis}(j\omega) = \begin{pmatrix} H(j\omega) & 0 \\ 0 & H(j\omega) \end{pmatrix}^* \begin{pmatrix} -x\underline{\delta}\bar{\delta}I_d & x\frac{\underline{\delta}+\bar{\delta}}{2}I_d \\ x\frac{\underline{\delta}+\bar{\delta}}{2}I_d & -xI_d \end{pmatrix} \begin{pmatrix} H(j\omega) & 0 \\ 0 & H(j\omega) \end{pmatrix} \in \mathbb{RH}_\infty^{2r\times 2r}. \tag{5.60}$$

for a scalar uncertainty repeated r times and with $H \in \mathbb{RH}_\infty$. Its version for one scalar uncertainty has been introduced in paragraph 4.5.2. We will use Π_{ltvs} to define an IQC that captures the time-varying parameters in Δ_ω. Its description is done in paragraph 9.1 and it is defined as:

$$\Pi_{ltvs}(j\omega) = \begin{pmatrix} H_{er}(j\omega) & 0 \\ 0 & H_{el}(j\omega) \end{pmatrix}^* S \begin{pmatrix} H_{er}(j\omega) & 0 \\ 0 & H_{el}(j\omega) \end{pmatrix}. \tag{5.61}$$

Defined as such, the multiplier requires the definition of the block-symmetric matrix S and the operators

H_{er} and H_{el}, extensions of a transfer function $H \in \mathbb{RH}_\infty$ for which the swapping lemma reads as

$$H_{el}\begin{bmatrix}\delta I_r \\ \dot{\delta} I_{n_H} H_B\end{bmatrix} = \underbrace{\begin{bmatrix}\delta I_q & 0 \\ 0 & \dot{\delta} I_{n_H}\end{bmatrix}}_{\Delta_{el}} H_{er}, \tag{5.62}$$

where n_H is the number of state variables of H. The exact definition of H_{er} and H_{el} can be found in (9.3) as a function of a state-space realization of H. Finally, to derive an IQC which is satisfied by ψ_{ACS} we will use the Zames-Falb criterion based multiplier Π_{nlom} from paragraph 9.2. The way to determine the multiplier is complex and of no interest here. It is defined by

$$\Pi_{nlom}(j\omega) = \begin{bmatrix}0 & x + g_0 - G(j\omega) \\ x + g_0 - G(-j\omega) & -\frac{2}{\beta}x - \frac{1}{\mu}(2g_0 - G(j\omega) - G(-j\omega))\end{bmatrix}, \tag{5.63}$$

in which x, g_0 and G are defined from a transfer function $H \in \mathbb{RH}_\infty$ and fulfill some constraints showed in paragraph 9.2.
The three multipliers have a common property: they can be frequency dependent. We saw that a transfer function denoted by $H \in \mathbb{RH}_\infty$ was needed to define them; (4.84), (9.9) and (9.11), respectively. As we need a way to span $\mathbb{RH}_\infty$ efficiently, it is common practice to use basis transfer functions to parameterize H. In the tool, the transfer function $H \in \mathbb{RH}_\infty$ is built as follow:

$$H(s) = \begin{bmatrix} I_r \\ \frac{1}{s-\varphi} I_r \\ \frac{1}{(s-\varphi)^2} I_r \\ \vdots \\ \frac{1}{(s-\varphi)^{(d-1)}} I_r \end{bmatrix} \in \mathbb{RH}_\infty^{(dr \times r)}. \tag{5.64}$$

where r is the number of repetition of the uncertain parameter (time-invariant or time-varying) or $r = 1$ for the odd monotone nonlinearity, $d \in \{1, 2, 3, \ldots\}$ and $\varphi < 0$. This transfer function was used to generate multipliers in LPVMAD e.g. see [Köroglu and Scherer, 2007], but others can be used e.g. see [Kao et al., 2004]. Regarding the definition we will use here (5.64), we have two free parameters to determine the transfer function H. We can set its pole φ which of course has to be strictly stable. That is because we must have $H \in \mathbb{RH}_\infty$. Moreover we can choose the order $d-1$ of the transfer function. These "degrees of freedom" will be useful for the stability test as different values of the parameters can lead to stability test with different levels of conservatism. In the tool LPVMAD, the parameters can be chosen independently for each perturbation. Hence we can chose a H as in (5.64) with different parameters φ, d for each perturbations e.g. the perturbation on I_x can have a different transfer function from I_{xy}, $\hat{\omega}_x(t)$ and the first channel of the dead-zone. The result of the stability test can be strongly influenced by the multiplier setup. For this reason, we will give the stability results with the poles and the size of the bases transfer function of the frequency dependent multipliers. The interest in using different poles and degrees appear in the KYP lemma (lemma 6) formulation of the FDI stability condition (4.55) of the general IQC stability theorem. Indeed, changing the pole φ and degree $d-1$ of H change the state-space realization of the factorization Ω defined in (4.62). Hence as the LMI to be solved are different, we can expect different stability result. In particular, we can hope for conservatism reduction.
The dynamic multipliers are crucial for reducing the conservatism of robustness analyzes of complex

systems. One question comes up now: how to determine the best basis transfer function? and then, how to select the parameters giving less conservative stability tests? So far, no proper "method" has been given in the literature for the choice of the bests pole and size. Only tests can tell whether a setting is good or not. Nevertheless, from our extensive use of the tool, the following hints can be given:

1. Increasing the order of H i.e. increasing d usually diminishes the conservatism of the stability test. It appears very obviously when changing d form 1 to 2 since for $d = 1$, H is the identity and we have only static weighting in our multipliers. The main drawback is the dramatic increase in computational time for values of d larger or equal to 4 when the system is as large as ours. To give an hint about the computation time required for our stability tests, we will give the computation duration for the results to be presented.

2. During our works, it appeared that the choice of φ was very influential in some cases. Hence we chose to perform the stability test over a grid of values of φ in order to find the best values. Of course, this method is time consuming and it is hard to perform such a local optimization for stability test with several frequency dependent multipliers due to the computational effort required.

Robustness analysis

To represent the uncertainty set over which we are able to prove the stability, we defined the (δ_d, δ_{od}) plane. δ_d represents the maximum percentage of uncertainty on the diagonal terms of the inertia matrix (subscript d) while δ_{od} represents the maximum uncertain multiplying factor that can affect the off-diagonal terms in the inertia matrix I_g. This multiplying factor is more convenient to represent the large uncertainties affecting the off-diagonal terms. Of course, the uncertainty is still a percentage of uncertainty but we use a different scale to represent it. We also dwell on the fact that the uncertainties affecting the inertia terms remain independent. With δ_d and δ_{od} we just set the maximum uncertainty on the terms. For instance, $\delta_{od} = 17$ corresponds to an uncertainty of 1600%. Hence we have the following:

$$\begin{aligned} &\delta_x, \delta_y, \delta_z \in [-\delta_d, +\delta_d]\%, \\ &\delta_{xy}, \delta_{xz}, \delta_{yz} \in [-100, +100(\delta_{od} - 1)]\,\%,\ \delta_{od} \geq 1. \end{aligned} \tag{5.65}$$

The other operators in the perturbation matrix Δ_{dyn} are the uncertain time-varying speed parameters ranging within the nominal flight envelope and the actuator modeled by ψ_{ACS} is characterized by Γ_{av} are as described in the setup. Notice that the multiplier Π_{nlom} used to describe ψ_{ACS} is not taking into account the level of saturation Γ_{av}. It accounts only for the facts that ψ_{ACS} is an odd monotone sector bounded nonlinearity with bounded incremental gain. Consequently, the stability results that we are going to obtain with IQC are not depending on the torque available for control.
In this setup, what we aimed to do during the stability analysis was to maximize δ_{od} for a given δ_d. The algorithm implemented was very simple. It relied on the dichotomy method to find a lower-bound of the maximum δ_{od} for which the stability can be proved for a given δ_d.

The multiplier Π_{dyn} that defines an IQC satisfied by Δ_{dyn} as in (4.40) can be defined as

$$\Pi_{dyn}(\varphi,d,j\omega)=\begin{bmatrix}\Pi^{(11)}_{ltis,d} & 0 & 0 & 0 & \Pi^{(12)}_{ltis,d} & 0 & 0 & 0\\ 0 & \Pi^{(11)}_{ltis,od} & 0 & 0 & 0 & \Pi^{(12)}_{ltis,od} & 0 & 0\\ 0 & 0 & \Pi^{(11)}_{ltvs,\omega} & 0 & 0 & 0 & \Pi^{(12)}_{ltvs,\omega} & 0\\ 0 & 0 & 0 & \Pi^{(11)}_{nlom,\psi} & 0 & 0 & 0 & \Pi^{(12)}_{nlom,\psi}\\ \Pi^{(21)}_{ltis,d} & 0 & 0 & 0 & \Pi^{(22)}_{ltis,d} & 0 & 0 & 0\\ 0 & \Pi^{(21)}_{ltis,od} & 0 & 0 & 0 & \Pi^{(22)}_{ltis,od} & 0 & 0\\ 0 & 0 & \Pi^{(21)}_{ltvs,\omega} & 0 & 0 & 0 & \Pi^{(22)}_{ltvs,\omega} & 0\\ 0 & 0 & 0 & \Pi^{(21)}_{nlom,\psi} & 0 & 0 & 0 & \Pi^{(22)}_{nlom,\psi}\end{bmatrix} \tag{5.66}$$

$$\Pi^{(ij)}_{ltis,d}=\begin{bmatrix}\Pi^{(ij)}_{ltis,I_x} & 0 & 0\\ 0 & \Pi^{(ij)}_{ltis,I_y} & 0\\ 0 & 0 & \Pi^{(ij)}_{ltis,I_z}\end{bmatrix}\in\mathbb{RH}^{6\times6}_\infty,\ \Pi^{(ij)}_{ltis,od}=\begin{bmatrix}\Pi^{(ij)}_{ltis,I_{xy}} & 0 & 0\\ 0 & \Pi^{(ij)}_{ltis,I_{xz}} & 0\\ 0 & 0 & \Pi^{(ij)}_{ltis,I_{yz}}\end{bmatrix}\in\mathbb{RH}^{12\times12}_\infty,$$

$$\begin{aligned}\Pi^{(ij)}_{ltvs,\omega}&=\begin{bmatrix}\Pi^{(ij)}_{ltvs,\omega_x} & 0 & 0\\ 0 & \Pi^{(ij)}_{ltvs,\omega_y} & 0\\ 0 & 0 & \Pi^{(ij)}_{ltvs,\omega_z}\end{bmatrix}\in\mathbb{RH}^{6\times6}_\infty \quad\text{and}\\ \Pi^{(ij)}_{nlom,\psi}&=\begin{bmatrix}\Pi^{(ij)}_{nlom,\psi_x} & 0 & 0\\ 0 & \Pi^{(ij)}_{nlom,\psi_y} & 0\\ 0 & 0 & \Pi^{(ij)}_{nlom,\psi_z}\end{bmatrix}\in\mathbb{RH}^{3\times3}_\infty.\end{aligned} \tag{5.67}$$

where the dependence of the sub-blocks of the multiplier in the parameters and the frequency is not written for simplicity and $i,j\in\{1,2\}$. Using this multiplier in (4.40) gives the valid IQC

$$\forall\hat{z}\in\mathcal{L}_2^{27},\quad \int_{-\infty}^{\infty}\begin{bmatrix}\widehat{z}(j\omega)\\ \widehat{\Delta_{dyn}(z)}(j\omega)\end{bmatrix}^*\Pi_{dyn}(\varphi,d,j\omega)\begin{bmatrix}\widehat{z}(j\omega)\\ \widehat{\Delta_{dyn}(z)}(j\omega)\end{bmatrix}d\omega\geq0 \tag{5.68}$$

that fulfills the second assumption of theorem 4. As we have 27 uncertainty channels, $\Pi_{dyn}(\varphi,d)$ is in $\mathbb{RH}^{54\times54}_\infty$. This multiplier is obtained by simple diagonal augmentation with multipliers defining each one of the perturbation operators in Δ_{dyn}. It is important to notice that the multiplier Π_{dyn} from (5.66) does not correspond exactly to the structure of Δ_{dyn} from (5.40) but to a recast version of Δ_{dyn} in which the channels affected by the same uncertainty are grouped. Indeed, in (5.40), the sub-blocks $\Delta_I^{(1)}$ and $\Delta_I^{(2)}$ contain the same terms and for simplicity of the implementation, we re-ordered Δ_{dyn} and the associated inputs and outputs in M_{dyn} from (5.42).
The setup of the IQC tool is summed up in table 5.1.
The multipliers for the uncertain inertia terms $\Pi_{ltis,d}$ and $\Pi_{ltis,od}$ are static during our analysis. Indeed, with the setup of table 5.1, we are already at the limit of what can be solved on a desktop PC. Even

Table 5.1: IQC tool setup for analysis robustness with respect to uncertain nonlinear equation of motion

Diagonal inertia		Off-diagonal inertia		Speed parameters		Saturation	
$\Pi_{ltis,I_x}, \Pi_{ltis,I_y}, \Pi_{ltis,I_z}$		$\Pi_{ltis,I_{xy}}, \Pi_{ltis,I_{xz}}, \Pi_{ltis,I_{yz}}$		$\Pi_{ltvs,\omega_x}, \Pi_{ltvs,\omega_y}, \Pi_{ltvs,\omega_z}$		$\Pi_{nlom,\psi_x}, \Pi_{nlom,\psi_y}, \Pi_{nlom,\psi_z}$	
d_d	φ_d	d_{od}	φ_{od}	d_ω	φ_ω	d_ψ	φ_ψ
1	–	1	–	3	-0.96	2	-1

for a degree 1 multiplier i.e. d_d or d_{od} equal to 2, the size of the problem and so the computational time would have skyrocketed. In this framework, the computation of the stability region in the (δ_d, δ_{od}) plane on figure 5.12 takes about 9 hours on a 64 bits desktop PC with Intel® Core i7 processor at 2.80 GHz and Matlab® Parallel Toolbox to compute the boundary of the feasibility region for 30 different relative uncertainty on diagonal terms.

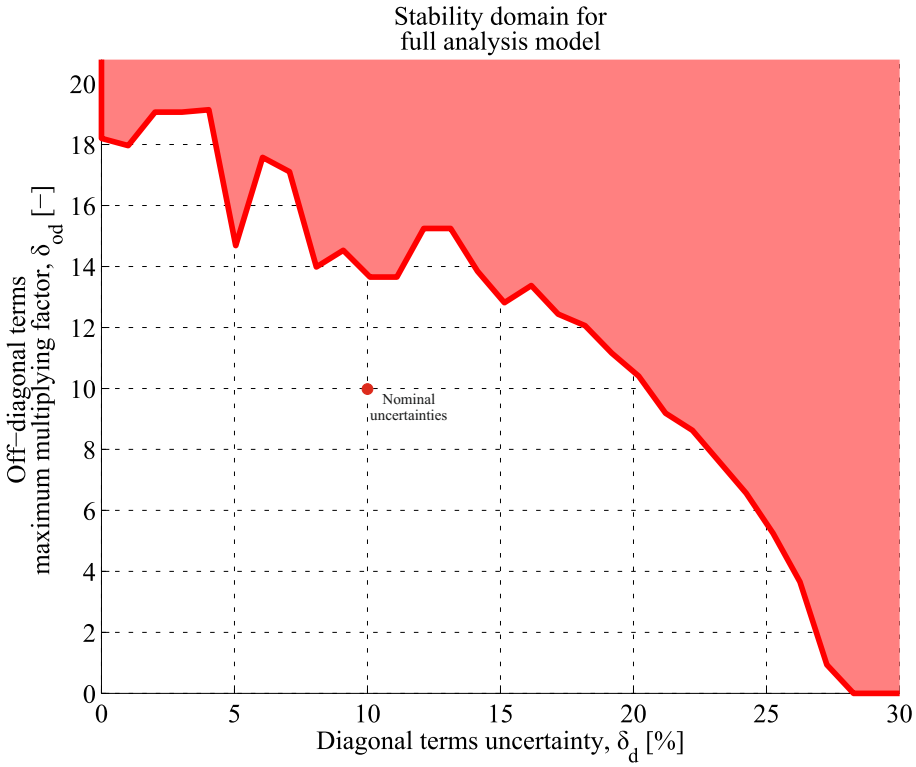

Figure 5.12: Stability region found in the setup of table 5.1

Beside its size which is large, the main characteristic of this stability region is its non-smooth upper-boundary. Indeed, we observe for $\delta_d \in [0, 20]\%$ that the maximum value of δ_{od} for which the stability can be proved is not varying smoothly with δ_d. This shape can be explained by the size of the problem we are trying to solve for which numerical issues may arise. In addition to that, the point $(10\%, 10)$ representing the "nominal" inertia uncertainties is belonging to the feasibility region. It means that for the "nominal uncertainties", the stability is proved with the IQC method.

Conclusion on IQC robust stability analysis

The IQC-based robust stability analysis of the LFR model figure 5.10 was performed in this section. As the main goal was to address the stability of the system with a full model of the uncertain nonlinear equation of motion, we essentially focused on this part of the model from chapter 3. The LFR obtained

after the analysis model transformation was a very large 27×27 perturbation block Δ_{dyn} (5.40). However, the size can hardly be reduced a priori except if a smaller factorization of I_g and $P(\hat{\omega})$ can be found. Despite this fact, with the LPVMAD tool we managed to show the feasibility of the stability test with the IQC defined by Π_{dyn} resulting in the region of stability map pictured in figure 5.12. The first thing is that the "$(10\%, 10)$" objective fixed by the industrial partners was achieved. Indeed, when beginning the study we wanted to prove the stability of the closed-loop model for 10% relative uncertainty on the diagonal terms of I_g and an uncertain multiplying factor up to 10 for the off-diagonal terms. Figure 5.12 shows that $(10\%, 10)$ belongs to the stability domain. To proceed to this particular test presented in [Chaudenson et al., 2013a], we had to make some trade-off on the conservatism. Indeed, even though the multipliers used for IQC analysis of parametric uncertainties with LPVMAD are known to be non-conservative in certain cases e.g. see [Packard and Doyle, 1993], we had to limit them to constant scalings inducing some conservatism. This had to be done because of the computational burden that would have been added by dynamic multipliers weighting the 18 channels of inertia uncertainties. A priori, being able to proceed to the test with dynamic multipliers could reduce the conservatism.
Secondly, the numerical troubles that seem to appear for low uncertainty level on δ_d could have two principal reasons. First, for this range of uncertainties on the diagonal terms, it seems that the margins on the uncertainties of the off-diagonal terms cannot be larger. For instance, if we apply a $\pm 15\%$ uncertainty to I_x whose nominal value is $22,500$ kg.m^2 and in the mean time the off-diagonal term I_{xz} with nominal value $1,100$ kg.m^2 is affected by a multiplying factor between 0 and 18, then the actual values of I_x and I_{xz} range within $[18,450; 25,875]$ and $[0; 19,800]$, respectively. In such cases, I_{xz} can get larger than I_x and this is impossible by definition of the terms in the inertia matrix (3.3). This case at the edge of the feasible values of the inertia terms obviously results in numerical instability. An extension of these works could be to enforce this constraint and see wheter it is possible or not to prove the stability for all physically possible inertia products I_{xy}, I_{xz}, I_{yz}.
In order to have another result about the stability of our analysis model, we are now going to perform the robust stability analysis with the method from paragraph 5.5.3.

5.5.3 Robust stability analysis with the Lyapunov-based method

We observed while setting up the framework of Lyapunov-based robust stability analysis of constrained systems that the use of theorem 8 was not straightforward for our system since it does not allow analyzing systems with repeated uncertainties conveniently. Nevertheless, we are going to evaluate the region of attraction $\Sigma(P)$ guaranteed by this method. To do so, we have to simplify our analysis model. This is a significant drawback since we worked on a representative description of the uncertain equations of motion to have meaningful robust stability results. We will first perform the analysis of the system without uncertainties. This analysis model will not describe gyroscopic coupling and inertia unknown parameters. Secondly, we will analyze the system without gyroscopic couplings but with uncertain diagonal inertia matrix terms and finally the case of a diagonal known inertia matrix will be analyzed.
To start the analysis with the Lyapunov theory based method from section 5.4, we introduce the generalized form of the uncertain state-space representation of our system. From this representation, we will derive the study cases to be addressed.

Realizations of the system over the parameter set

In the state-space representation of the nominal part the LFR figure 5.11 (5.42-5.47) and the perturbation operator description (5.40), we can separate the inputs and outputs related to uncertainty channels (subscript u) to those linked to nonlinearities channels (subscript nl) as it was done when we defined the LFR. We split z and w from (5.41) into: z_u, z_{nl} and w_u, w_{nl} as in (5.48). The state-space matrices are split accordingly in the LFR nominal part definition (5.44-5.47) and the state-space equations below

(5.69) written with the definitions in (5.44-5.47):

$$\begin{cases} \dot{x} = & Ax + B_u w_u + B_{nl} w_{nl} \\ z_u = & C_u x + D_{u,u} w_u + D_{u,nl} w_{nl} \\ z_{nl} = & C_{nl} x \end{cases} \quad \text{and} \quad \begin{cases} w_u = & \Delta_u z_u \\ w_{nl} = & \psi_{ACS}(z_{nl}) \end{cases} . \tag{5.69}$$

In the LFR, we assumed that the perturbation Δ_{dyn} had a block structure such as

$$\Delta_{dyn} = \begin{bmatrix} \Delta_u & 0_{24\times 3} \\ 0_{3\times 24} & \Delta_{nl} \end{bmatrix} \text{ with } \Delta_u = \begin{bmatrix} \Delta_I^{(1)} & 0_{9\times 9} & 0_{9\times 6} \\ 0_{9\times 9} & \Delta_I^{(2)} & 0_{9\times 6} \\ 0_{6\times 9} & 0_{6\times 9} & \Delta_\omega(t) \end{bmatrix} \text{ and } \Delta_{nl} = \psi_{ACS}(\bullet). \tag{5.70}$$

where Δ_u gathers the parametric uncertainties and Δ_{nl} is the nonlinear operator ψ_{ACS}. The parametric uncertainties in Δ_u are causing troubles when we intend to use theorem 8 since they contain repeated parameters.

Using these preliminary definitions, we can determine a parameter-dependent state-space representation of our space launcher model that fits into the framework described in section 5.4. To do so, we use the definition of the LFR figure 5.11. We recast the state-space form (5.69) by introducing $w_u = \Delta_u z_u$ in the left-hand equations of (5.69). This way we find the matrices $\mathcal{A}(\Delta_u)$ and $\mathcal{B}(\Delta_u)$ of the state-space representation in (5.71). They depend rationally on the parameters of Δ_u;

$$\begin{cases} \dot{x} = & \mathcal{A}(\Delta_u)x + \mathcal{B}(\Delta_u)w_{nl}, \\ z_{nl} = & C_{nl}x, \end{cases} \quad \text{and } w_{nl} = \Delta_{nl}(z_{nl}) = \psi_{ACS}(z_{nl}). \tag{5.71}$$

From (5.69), we determine

$$\begin{cases} \mathcal{A}(\Delta_u) = & A + B_u\Delta_u(I_{24} - D_{u,u}\Delta_u)^{-1}C_u, \\ \mathcal{B}(\Delta_u) = & B_{nl} + B_u\Delta_u(I_{24} - D_{u,u}\Delta_u)^{-1}D_{u,nl}. \end{cases} \tag{5.72}$$

(5.71) corresponds to a LFR defined by $(M_{nl}(\Delta_u), \psi_{ACS})$ where $(\mathcal{A}(\Delta_u), \mathcal{B}(\Delta_u), C_{nl})$ s a state-space realization of $M_{nl}(\Delta_u)$. The parameter-dependent matrices from (5.72). Such a LFR is depicted figure 5.13.

The LFR $\mathcal{F}_u(M_{dyn}, \Delta_u)$ is well-posed i.e. $I_{24} - D_{u,u}\Delta_u$ is causally invertible. This is true because it is defined only with static gains and by the use of the small-gain theorem. According to the definitions of Δ_I in (5.21) and Δ_ω in (5.26), the parametric perturbation block Δ_u has $p = 9$ uncertain parameters assumed to range in a plane parallel box. Six are used to represent the uncertain inertia, three for the uncertain time-varying speed parameters.

We already mentioned the crucial issue coming from the repetition of all the uncertain parameters of our model several times in the Δ_u block from (5.70). Consequently, the stability analysis of the full model of figure 5.13 with theorem 8 is compromised. Indeed, due to the repetition of the uncertain parameters in Δ_u, the robust stability analysis can only be done using property 1. This property gives much less information about the stability of the system than theorem 8. To perform the stability analysis we are going to analyze particular instances of the analysis model to obtain more meaningful stability results applying theorem 8. During these study cases, Δ_u will be simplified such that it does not have repeated parameters. This will dramatically decrease the representativeness of the analysis model but it is the

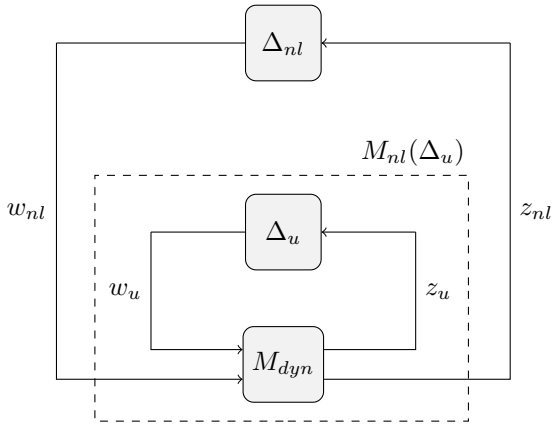

Figure 5.13: Linear fractional Representation of the closed-loop system for LPV characterization

only way to use theorem 8 in a straightforward manner.
The following study cases are derived from the full analysis model (5.71) in which some channel are considered to be void. Consequently, when building them we will just mention the outputs of the original system that are considered and the resulting parametric uncertainty block.

Analysis model parameters For the study cases, the nominal angular speed is set to zero (5.59). That is $P^{(0)} = 0_{3\times 3}$. Moreover, the nominal inertia matrix is set to

$$I_g^{(0)} = \begin{bmatrix} 22500 & -50 & -1100 \\ -50 & 42000 & -250 \\ -1100 & -250 & 44000 \end{bmatrix}.$$

Finally, the nominal flight envelope and the nominal perturbations on the inertia terms are those specified in the introduction of the robustness analysis paragraph 5.5.1.

System without uncertainties

As a first test of the Lyapunov based technique of section 5.4, we intend to perform the stability analysis of the constrained input system without uncertainties. In the LFR of the full model defined in section 5.3, it means that $\Delta_I = \Delta_\omega = 0$. That is

$$\Delta_u = 0_{24\times 24} \tag{5.73}$$

in (5.70). Consequently, the state-space realization of the nominal part of the LFR only has three inputs and three outputs which are corresponding to the nl channels of the full model section 5.3. These are input-output 25 to 27.
In this framework, theorem 7 applies since no uncertainties are considered. As mentioned when we described the theory in section 5.4. Solving this problem leads to an ellipsoidal region of attraction $\Sigma(P)$. Therefore, in the implementation of the stability test we add a LMI constraint aiming to maximize the volume of the ellipsoid of asymptotically stable initial conditions. Since maximizing the volume of $\Sigma(P)$ corresponds to maximizing the trace of W (see e.g. [Vandenberghe et al., 1998]), to find the largest region

of attraction we solve the convex optimization problem that reads as:

$$\text{Minimize } \rho \text{ subject to } \begin{cases} \begin{bmatrix} WA^T + AW & BS + Y^T \\ S^T B^T + Y & -2S \end{bmatrix} < 0, \\ \begin{bmatrix} W & WC_i^T - Y_i^T \\ C_i W - Y_i & \Gamma_{av_i}^2 \end{bmatrix} \geq 0, \quad i \in \{1,2,3\}, \\ \begin{bmatrix} W & I_n \\ I_n & \rho I_n \end{bmatrix} \geq 0. \end{cases} \tag{5.74}$$

for W symmetric positive and S diagonal positive. In (5.74), we have two LMI that ensure stability and one aiming to maximize the volume of the 9-dimensional ellipsoid $\Sigma(P) \subset \mathbb{R}^9$. To have a more concrete view on its meaning on the "size" of the stable initial conditions, we can try to fit a sphere centered at the origin in it. We do it for the initial angular speed $\omega_0 \in \mathbb{R}^3$, for the initial attitude $\alpha_0 \in \mathbb{R}^3$ and for the controller state $x_{c0} \in \mathbb{R}^3$. Table 5.2 gathers the radii of the largest sphere that fits in $\Sigma(P)$.

Model	$\lvert\omega_0\rvert < r_\omega$	$\lvert\alpha_0\rvert < r_\alpha$	$\lvert x_{c0}\rvert < r_{x_c}$
No uncertainty	2.95 deg.s^{-1}	1.58 deg	46.2 Nm.deg^{-1}

Table 5.2: Radii of the largest sphere for each component (case 1)

We observe that the region of attraction of the stable equilibrium point $\bar{x} = 0$ are already very small when compared to the initial conditions that can be encountered during a regular mission. This is when considering no uncertainties on the inertia and no gyroscopic couplings except the nominal ones which are zero in the conditions of the stability test ($P^{(0)} = 0_{3\times3}$). Thus we can expect more reduction of the certified region of attraction when introducing uncertainties in the model.

System with static couplings and uncertain diagonal inertia terms

The second study case consists in analyzing the system without gyroscoping couplings. To visualize such a configuration, we can say that it is the system in which the feedback path of figure 3.4 is removed. Physically, it means that the only couplings we consider are static coupling induced by the asymmetry of the launcher i.e. the off-diagonal terms of the inertia matrix I_g. The static couplings cause each component of the torque Γ_{ACS} to be split over the three axes of the launcher and so to induce a disturbing acceleration on the other axes. In the configuration depicted figure 5.7, we keep only the first three components of $\Delta_I^{(2)}$. Indeed, despite the removal of the coupling path, we also need to assume that the off-diagonal terms are fixed to have a system with unrepeated parameters and allow using theorem 8.
To obtain the state-space representation of the model to be analyzed, we just need to select the appropriate inputs and outputs of the system described by the matrices in (5.44-5.47). More precisely, we need to account for inputs 10 to 12 (parameters for diagonal inertia in $\Delta_I^{(2)}$) and 25 to 27 (inputs and outputs of ψ_{ACS}) of our original LFR nominal model section 5.3. Furthermore, the first three outputs of the reduced system are linked to the reduced perturbation matrix

$$\Delta_1 = \begin{bmatrix} \delta_x & 0 & 0 \\ 0 & \delta_y & 0 \\ 0 & 0 & \delta_z \end{bmatrix}. \tag{5.75}$$

As mentioned before, we consider the diagonal terms to be uncertain to $\pm 10\%$. Since after normalization the three parameters in Δ_1 vary in $[-1;1]$, we can determine the 2^3 realizations $(A_k, B_k),\ k \in \{1,\dots,2^3\}$ of the system at the corners of the parameter box with the relationships in (5.72) and use theorem 8. As in the nominal study case, the parameter ρ is used to maximize the volume of the region of attraction ellipsoid $\Sigma(P)$. Then we can use the realizations (A_k, B_k) and solve

$$\text{Minimize } \rho \text{ subject to }, \begin{cases} \begin{bmatrix} WA_k^T + A_k W & B_k S + Y^T \\ S^T B_k^T + Y & -2S \end{bmatrix} < 0, \quad k \in \{1,\dots,2^3\}, \\ \begin{bmatrix} W & WC_i^T - Y_i^T \\ C_i W - Y_i & \Gamma_{av_i}^2 \end{bmatrix} \geq 0, \quad i \in \{1,2,3\}, \\ \begin{bmatrix} W & I_n \\ I_n & \rho I_n \end{bmatrix} \geq 0. \end{cases} \tag{5.76}$$

for W symmetric positive and S diagonal positive. Again, the radius of the largest sphere which can be fit in the ellipsoid of stable initial conditions $\Sigma(P)$ is evaluated. The results are gathered in the second line of table 5.3 to be compared to the previous ones.

Model	$\lvert\omega_0\rvert < r_\omega$	$\lvert\alpha_0\rvert < r_\alpha$	$\lvert x_{c0}\rvert < r_{x_c}$
No uncertainty	2.95 deg.s^{-1}	1.58 deg	46.2 Nm.deg^{-1}
Uncertain I_x, I_y, I_z and no gyroscopic couplings	1.96 deg.s^{-1}	1.25 deg	37.5 Nm.deg^{-1}

Table 5.3: Radii of the largest sphere for each component (case 2)

As expected, the introduction of a $\pm 10\%$ uncertainty on the diagonal terms of the inertia matrix reduced the size of the region of attraction.
This study case does not give any information about the robustness of the system to uncertainties on the off-diagonal terms of the inertia matrix. In facts, we cannot use the Lyapunov based method of theorem 8 with repeated uncertainties and modeling uncertain off-diagonal terms in I_g with our factorizations implies the use of perturbation operators with repeated uncertainties. To bypass this issue, we performed the optimization routine of (5.76) over a fine mesh of the set of possible value of the uncertain off-diagonal terms in I_g. For each fixed values of I_{xy}, I_{xz} and I_{yz}, we determined the largest sphere fitting in the region of attraction. By taking the smallest among all the spheres obtained over the mesh, we could determine a region of attraction valid for any uncertain inertia with the parameters

$$\begin{aligned} &\delta_x, \delta_y, \delta_z \in [-10, +10]\%, \\ &\delta_{xy}, \delta_{xz}, \delta_{yz} \in [-100, +900]\,\%. \end{aligned} \tag{5.77}$$

The results are gathered in table 5.4.
This last study allows us to hint how the uncertainties on off-diagonal terms of the inertia influence the size of the region of attraction. As expected, the spheres contained in $\Sigma(P)$ have their size reduced when we vary the off-diagonal inertia terms within their nominal uncertainty set ($[-100\%; +900\%]$). Concerning the state of the controller, it is almost decreased to 0. Since a controller switching occurs at the beginning of the maneuver, we can expect the controller to have zero initial condition so it is not too problematic. However, the stability is now proved only for initial angular speed vector with size less than 1 deg.s^{-1} and this is below what is encountered in flight.

Model	$\|\omega_0\| < r_\omega$	$\|\alpha_0\| < r_\alpha$	$\|x_{c0}\| < r_{x_c}$
Uncertain I_x, I_y, I_z and no gyroscopic couplings	1.96 deg.s^{-1}	1.25 deg	37.5 Nm.deg^{-1}
Uncertain I_x, I_y, I_z, no gyroscopic couplings and mesh of uncertain I_{xy}, I_{xz}, I_{yz} values	0.91 deg.s^{-1}	1.25 deg	0.02 Nm.deg^{-1}

Table 5.4: Radii of the largest sphere for each component with off-diagonal uncertainties

System with gyroscopic couplings and diagonal inertia matrix

The last study case aims to assess the stability of a launcher model with gyroscopic couplings. To do so while fitting in the framework of theorem 8, we have to consider the inertia matrix to be known and diagonal. In this specific case, the dynamic equations boil down to the classical Euler equations for a rotating rigid body case which is of course covered by our system representation (see e.g. [Sidi, 1997] or [Hughes, 1986]).
To obtain the state-space representation of the model to be analyzed, we just need to select the appropriate inputs and outputs of the system described by the matrices in (5.44-5.47). More precisely, we need to account for inputs 19, 22 and 23 (angular speed parameters), and 25 to 27 (channels of ψ_{ACS}) of our original LFR nominal model. The perturbation block we use is

$$\Delta_2 = \begin{bmatrix} \delta\omega_z(t) & 0 & 0 \\ 0 & \delta\omega_y(t) & 0 \\ 0 & 0 & \delta\omega_x(t) \end{bmatrix}. \tag{5.78}$$

We consider the angular speed parameters to belong to the nominal flight envelope

$$\delta\omega_x(t) \in [-100 \text{ deg.s}^{-1}, +100 \text{ deg.s}^{-1}],$$

$$\delta\omega_y(t), \delta\omega_z(t) \in [-50 \text{ deg.s}^{-1}, +50 \text{ deg.s}^{-1}].$$

Since after normalization the three parameters in Δ_2 vary in $[-1; 1]$, we can determine the 2^3 realizations $(A_k, B_k),\ k \in \{1, \ldots, 2^3\}$ of the system at the corners of the parameter box with the relationships in (5.72) and use theorem 8 for non repeated uncertainties. Again, the parameter ρ is used to maximize the volume of the region of attraction ellipsoid $\Sigma(P)$. Together with the realizations of the system at the corners of the parameter box, it gives the convex optimization problem

$$\text{Minimize } \rho \text{ subject to }, \begin{cases} \begin{bmatrix} WA_k^T + A_kW & B_kS + Y^T \\ S^TB_k^T + Y & -2S \end{bmatrix} < 0 \quad , k \in \{1, \ldots, 2^3\} \\ \begin{bmatrix} W & WC_i^T - Y_i^T \\ C_iW - Y_i & \Gamma_{av_i}^2 \end{bmatrix} \geq 0 \quad , i \in \{1, 2, 3\}, \\ \begin{bmatrix} W & I_n \\ I_n & \rho I_n \end{bmatrix} \geq 0 \quad . \end{cases} \tag{5.79}$$

Even if the problem is stated identically in (5.76) and (5.79), the problems are different due to the different state-space realizations (A_k, B_k). In this case, the relationship between A, B and the angular

speed is taken into account. Again, the radius of the largest sphere which can be fit in the ellipsoid of stable initial conditions $\Sigma(P)$ is evaluated. The results are gathered in the last two lines of table 5.5.

Model	$\lvert\omega_0\rvert < r_\omega$	$\lvert\alpha_0\rvert < r_\alpha$	$\lvert x_{c0}\rvert < r_{x_c}$
No uncertainty	1.57 deg.s^{-1}	3.43 deg	46.2 Nm.deg^{-1}
Uncertain I_x, I_y, I_z and no couplings	1.25 deg.s^{-1}	2.71 deg	37.5 Nm.deg^{-1}
Fixed diagonal inertia matrix and nominal flight envelope	–	–	–
Fixed diagonal inertia matrix and reduced flight envelope (20% of original size)	0.62 deg.s^{-1}	0.62 deg	11.2 Nm.deg^{-1}

Table 5.5: Radii of the largest sphere for each component (case 3)

The modeling of the gyroscopic couplings in the Lyapunov-based analysis framework results in an unfeasible stability test. Even if the analysis model is far less representative than the original analysis model i.e. less complex and *a priori* "more" stable, the stability cannot be proved using this method.

Conclusion on Lyapunov-based analysis

The Lyapunov-based robust stability analysis of the LFR model from figure 5.10 was performed in this section. The theoretical result we intended to use was not the most appropriate for the analysis of the LFR model obtained from the equations of motion factorization in section 5.3. Indeed, since it was not able to cope with perturbation blocks with repeated uncertainties, we had to drastically simplify our model to fit in the framework.
However, the simple study cases we did gave small regions of attraction with respect to the initial conditions that may be encountered during the flight of our spacecraft. The conservatism of the result extended to uncertain systems made the "nominal" stability test infeasible for the study case aiming to represent the gyroscopic couplings while severely reducing the size of the region of attraction for the case with static coupling only. Indeed, as the modified sector condition used to model the dead-zone nonlinearity was proven to be rather efficient for reduced conservatism representation of the dead-zone nonlinearity, we guess that the conservatism is essentially due to the polytopic representation of the uncertain and time-varying system. By covering the set of feasible values of the parametric system with $\mathrm{Co}(\mathcal{P}_\mathcal{V})$ and by looking for a single non-parametric Lyapunov matrix P, we covered a very large set of uncertain time-varying systems causing the test to be too conservative.
Concerning the use of this formal tool on the full model, even if we considered several techniques, the results on simple cases prevented us to go ahead due to the conservatism. Obviously, other results should be applied to address the robust stability of this nonlinear uncertain model. However, one lead that could be fruitful and result in a moderate computational burden would be to determine a reasonably large set of points in $\mathrm{Co}(\mathcal{P}_\mathcal{V})$ whose convex hull matches with $\mathrm{Co}(\mathcal{P}_\mathcal{V})$ as precisely as possible and apply property 1 with a guarantee that $\mathcal{S}_{\mathrm{Co}(\mathcal{V})} \cap \mathrm{Co}(\mathcal{P}_\mathcal{V})$ is "close to" $\mathcal{S}_{\mathrm{Co}(\mathcal{V})}$. Of course, the way to obtain this guarantee is not straightforward.

5.5.4 Simulations

The subsequent paragraphs aim to show how the launcher behaves within its flight envelope when affected by inertia uncertainties. Two sets of simulations with parameters within the range of stable uncertainties

are done to present the uncertainties effect.

Despin simulation

To have a better idea about the behavior of the launcher within its flight envelope and stability region, we performed a batch of simulations of a de-spin maneuver consisting in reducing the angular speed about the roll axis i.e. the longitudinal axis X_g. We computed 500 trajectories. The first $2^6 = 64$ were done for inertia values at the vertices of the feasible inertia box and the remaining ones where picked randomly over the inertia box with a uniform distribution. The resulting speed trajectories are presented in figure 5.14.

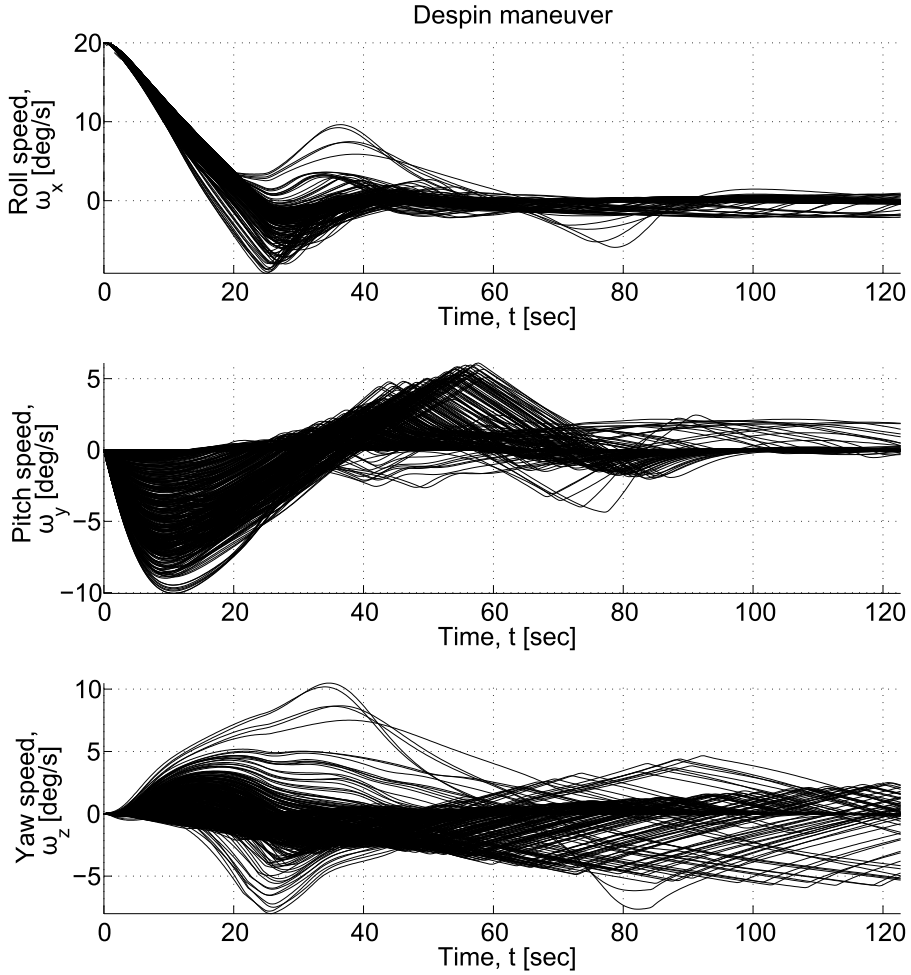

Figure 5.14: Angular speed trajectories for de-spin maneuver from 20 deg.s^{-1}

These trajectories have very long transient response and large error with respect to the aimed trajectory. Indeed, even though the speed seems to converge asymptotically to zero, the duration of the recovery is very long. We observe here how gyroscopic couplings can influence dramatically the motion when the rotational speed about one of the axes is large. We see their effect on the transverse axes Y_g and Z_g where the speeds are reaching values up to 10 deg.s^{-1} while the aimed speed is 0 deg.s^{-1}.
To offset these facts, one other factor may play an important role in the poor behavior exhibited in the simulation. The fact that we did not consider any kinematic equation but the simple identity $\omega = \dot{\alpha}$ may also be the cause of the slow recovery to zero angular speed. Indeed, we saw that this assumption was

valid for "small angles" approximation and in this situation, we are far from the domain of validity of this approximation. This indicates us that we should maybe put the emphasis on the attitude representation of this block during the analyzes to come.

"Small angles" simulation

To observe the behavior of the system when its trajectories are falling into the "small-angle" approximation, we prepared a setup for performance analysis by simulation. The setup is depicted in figure 5.15. Within this framework, we ran 200,000 simulations with random inertia parameters from the nominal uncertain parameter set to measure two things:

1. The ratio of $\|e\|_{\mathcal{L}_2}$ to $\|d\|_{\mathcal{L}_2}$,
2. The maximum attitude error i.e. $\max|e|$.

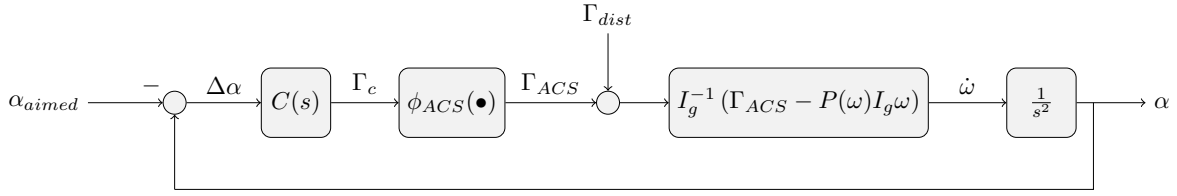

Figure 5.15: Closed-loop for performance analysis

To do so, we introduced a pulse of torque perturbation Γ_{dist} in figure 5.15 and observed the recovery of the system for different inertia matrices picked in the flight envelope. The pulse has a duration 1 ms and has energy of 1 Nm^2.s. For this batch of simulations, the uncertainty on the inertia parameters is increased to $\pm 20\%$ since the stability analysis allows it. The results are gathered in table 5.6 where ΔI represents the variations of the inertia terms with respect to their nominal value

$$I_g^{(0)} = \begin{bmatrix} 22,500 & -50 & -1,100 \\ -50 & 40,000 & -220 \\ -1,100 & -220 & 42,000 \end{bmatrix}.$$

The simulations corresponding to the two worst cases are presented in figure 5.16. To complement the data, the speed plots are also given in figure 5.17.

Conclusion about the simulations

The two batches of simulations we did showed different characteristics of the effect of uncertainties on the time-domain behavior of the analysis model. First, we ran simulations with a large amplitude maneuver. Since we were not within the framework of the "small-angles" approximation, the effect of the approximation of the kinematic equation is added to the effect of the uncertainties on the inertia parameters. As soon as the inertia parameters are different from nominal, the behavior deteriorates and the performance do not complies with the technical specifications of the de-spin maneuver. The second batch of simulations was done within the frame of the "small-angles" approximation. The perturbation of the inertia terms by uncertainties is obviously less influential. For the type of perturbation we used, the $\mathcal{L}_2$-norm of the error signal is almost unchanged over the uncertainty set we chose. Concerning the maximum error, we observe that the tracking accuracy is reduced for inertias picked within the uncertainty set but the relative change from nominal in the maximum error is only of 7%. If this

Table 5.6: Simulation results for the error response to an impulsive torque disturbance

Worst error		Worst $\mathcal{L}_2$-norm	
Nominal: 2.19×10^{-6}		Nominal: 5.42×10^{-6}	
$\max \lvert e \rvert$	2.36×10^{-6}	$\max \lVert e \rVert_{\mathcal{L}_2}$	$\simeq 5.42 \times 10^{-6}$
$I_{\lvert e \rvert}$	$\begin{bmatrix} 18,412 & -407 & -10,826 \\ -407 & 32,835 & -1,408 \\ -10,826 & -1,408 & 34,015 \end{bmatrix}$	$I_{\lVert e \rVert_{\mathcal{L}_2}}$	$\begin{bmatrix} 18,071 & -474 & -8,474 \\ -474 & 34,772 & -1,391 \\ -8,474 & -1,391 & 50,164 \end{bmatrix}$
ΔI	$\begin{bmatrix} -18 & +714 & +884 \\ +714 & -17 & +540 \\ +884 & +540 & -19 \end{bmatrix}$ %	ΔI	$\begin{bmatrix} -20 & +848 & +670 \\ +848 & -13 & +532 \\ +670 & +532 & +19 \end{bmatrix}$ %

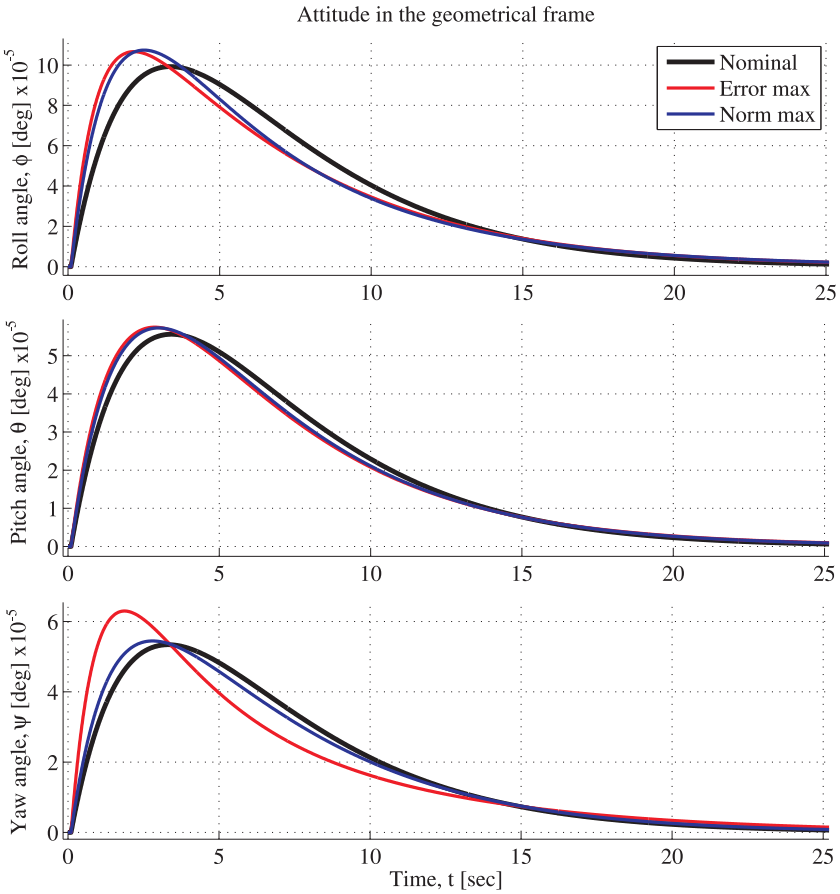

Figure 5.16: Attitude plots for simulations of the worst cases found by simulation

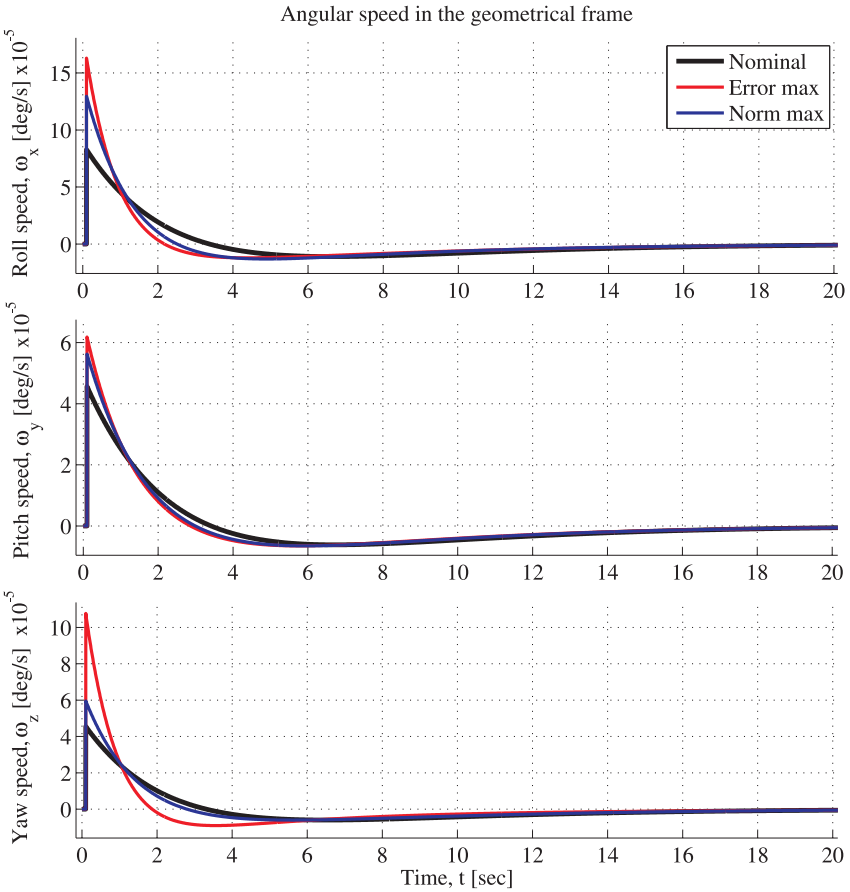

Figure 5.17: Speed plots for simulations of the worst cases found by simulation

value could be confirmed by more accurate simulations, the system would be considered as robust in performance when affected by inertia uncertainties. A lead to perform these simulations would be to "scale" the saturation level of ϕ_{ACS}. Indeed, for the "small-angles" approximation, the saturation is not active since the torque command Γ_c has very small amplitude. Hence, the performance degradation caused by actuator saturation does not occur as in the more representative de-spin simulations. Finding a way to activate the saturation under "small-angles" approximation could improve our understanding of performance degradation. One interesting study could also consist in running simulations of the pre-analysis model with the worst-case matrices and eventually confirm our conclusions.
Another aspect to look at is the type of inertia matrices for which we found the worst cases. They are given in table 5.6. Globally, the worst cases are achieved for very large off-diagonal terms with increases from nominal values from +500% up to +900% while for the diagonal terms, extreme values of the uncertainty set are founds with variations from nominal of ±20%. These results could be expected since large off-diagonal terms imply large gyroscopic couplings but also greater influence on the couplings on the dynamics of the principal axes of $\mathcal{R}_g$. Indeed, since the relative values of the off-diagonal terms with respect to the diagonal terms increases, the controller design we did for decoupled launcher is less relevant than for small off-diagonal terms.

5.6 Leads for robust performance analysis

The simulation results are pushing us to continue the robustness analysis and assess the robust performance of the nonlinear uncertain launcher model in the face of inertia uncertainties and gyroscopic couplings. To do so we are going to build upon the stability analysis framework to address the performance issues.

5.6.1 A criterion for robust performance

We already saw how the LFR of a system allows to assess its robust stability. In this paragraph, we use this representation to study the transfer from d to e in figure 4.2 given again below in figure 5.18. We are going to look for a characterization of the transfer between the so-called performance channels d and e. For a basic performance analysis of linear systems, we usually rely on the $\mathcal{H}_\infty$-norm to establish a simple relationship between d and e. However, since $\mathcal{F}_u(M,\Delta)$ is nonlinear as Δ_{dyn} in (5.40) is, we will use the $\mathcal{L}_2$ induced norm defined in (4.34). As a reminder, we give the expression of the transfer function from d to e:

$$\mathcal{F}_u(M,\Delta) = M_{22} + M_{21}\Delta\left(I - M_{11}\Delta\right)^{-1} M_{12}. \tag{5.80}$$

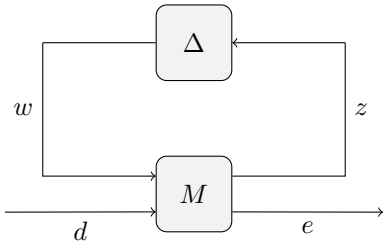

Figure 5.18: Linear fractional Representation of a system

In this framework, we would like to determine the $\mathcal{L}_2$-induced norm of $\mathcal{F}_u(M,\Delta)$ through the search of the smallest $\gamma_p \in \mathbb{R}_+$ such that the relation between d and e

$$\forall d \in \mathcal{L}_2^n, \quad \|e\|_{\mathcal{L}_2} \leq \gamma_p \|d\|_{\mathcal{L}_2} \tag{5.81}$$

holds. To determine an upper-bound of the value of γ_p in (5.81), we are going to set the robust performance problem as a robust stability problem.

5.6.2 Robust performance analysis as robust stability analysis

Thanks to the small-gain theorem presented in paragraph 4.3.2, we know the following result for the interconnection of two systems depicted in figure 5.19 described by a given norm $\|\bullet\|$.

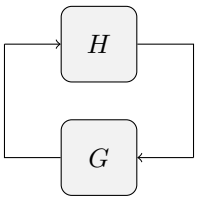

Figure 5.19: Basic system interconnection

Proposition 1 *The interconnection figure 5.19 is stable for all* $\|G\| < \gamma$ *if and only if* $\|H\| \leq 1/\gamma$

Knowing this, let us consider that G is an uncertain LTI block denoted by Δ_P such that $\|\Delta_P\|_\infty < 1/\gamma_p$ and H is $\mathcal{F}_u(M, \Delta)$. Since Δ_P is LTI, we have

$$\|\Delta_P\|_\infty = \|\Delta_P\|_{\mathcal{L}_2 \to \mathcal{L}_2}. \tag{5.82}$$

If we depict this configuration inspired by figure 5.19, we get the block diagram of figure 5.20.

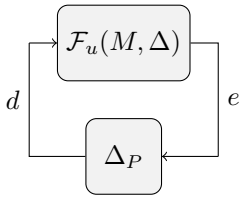

Figure 5.20: System interconnection for robust performance as robust stability

Then we can recast proposition 1 above into:

Proposition 2 *The interconnection of* Δ_P *and* $\mathcal{F}_u(M, \Delta)$ *in figure 5.20 is stable for all* $\|\Delta_P\|_\infty < \hat{\gamma}$ *if and only if* $\|\mathcal{F}_u(M, \Delta)\|_{\mathcal{L}_2 \to \mathcal{L}_2} < 1/\hat{\gamma}$.

5.6.3 Robust performance analysis

To prove the stability, and a certain level of performance, of the interconnection using the above proposition, we will use the IQC tool. Since we have the robust stability of the interconnection presented in figure 4.2, we know that the property 1 holds for $\Delta_P = 0$. Then we can increase the $\mathcal{H}_\infty$-norm of Δ_P i.e. $\|\Delta_P\|_\infty$, until the stability of the LFR figure 5.21 cannot be proved anymore. In such case we define the value of $\hat{\gamma}$ in the proposition as the maximum norm of Δ_P for which stability could be proved. Finally, $1/\hat{\gamma}$ gives an upper-bound of the $\mathcal{L}_2$ induced gain γ_p of the upper-LFR $\mathcal{F}_u(M, \Delta)$ i.e. an upper-bound of $\|\mathcal{F}_u(M, \Delta)\|_{\mathcal{L}_2 \to \mathcal{L}_2}$. Indeed, as usual in stability analysis, not being able to solve the stability test of the interconnection figure 5.20 for a given norm of Δ_P does not necessarily mean that the system is unstable due to the conservatism of the IQC description of the perturbation block Δ_{dyn} (5.40) and the performance block Δ_P.

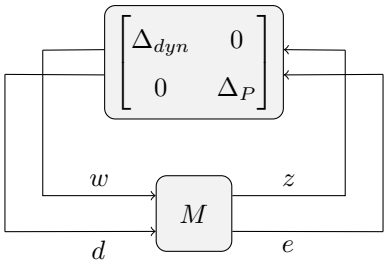

Figure 5.21: Structured LFR for robust performance analysis

The following figure 5.22 shows a map of the (δ_d, δ_{od}) plane. We defined δ_d as the maximum relative uncertainty on the diagonal terms of the inertia matrix. δ_{od} is the maximum multiplying factor for the off-diagonal terms of the inertia matrix as for the robust stability analysis. Considering this parameterization, we can represent the stability region we found during the robust stability analysis section 5.5.2 and, for instance, the iso-performance curves. The transfer that is investigated links a disturbing torque added to Γ_{ACS} to the attitude error $\Delta\alpha$. Along these curves, we have the same degradation of the estimation

$\hat{\gamma}$ of the nominal performance level. It shows how the performance degrades when the nonlinear system is affected by parametric uncertainties. Due to the computational burden, the saturation modeling the actuator is removed from the model. As a result, $\Gamma_c = \Gamma_{ACS}$.
For this analysis, the degree of the multiplier Π_{ltid} used to define an IQC satisfied by Δ_P defined in paragraph 4.5.1 is set to 2 i.e. $d = 3$. φ is set to its default value $\varphi = -1$. Otherwise, the parameters of the multipliers are kept the same as for the stability analysis.

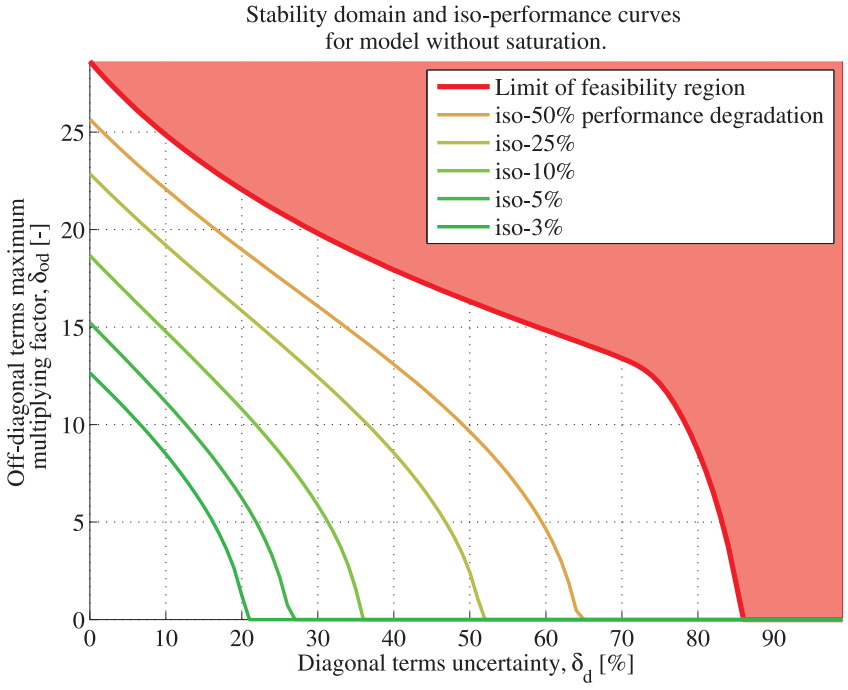

Figure 5.22: Feasibility region and iso-performance degradation curves for analysis model without saturation

5.6.4 Conclusion about robust performance

In the frame of aerospace applications, being able to perform robust performance analysis is absolutely compulsory. Indeed, even though guaranteeing stability of the launcher is crucial, we also need to guarantee very high performance levels in all "flyable" circumstances. For this, it is needed to start with reduced conservatism robust stability analysis of an accurate and representative model of the system. We intended to do so by defining the factorization of the equations of motion from which the LFR section 5.3 is derived. Afterwards, the setup for IQC stability analysis is re-used to perform the robust performance analysis. In figure 5.22, we plotted the results of the computation of the iso-performance curves of the LFR figure 5.20. Due to computing power limitations, we had to reduce the size of the perturbation block Δ_{dyn} from (5.40) and consider $\psi_{ACS} := 0$. This is the reason why we observe a large expansion of the feasibility domain with respect to the one depicted in figure 5.12. Regarding the iso-performance curves, it seems that the performance degradation remains very reasonable in terms of degradation of the peak gain of the transfer from d to e for $\delta_d \leq 20\%$ and $\delta_{od} \leq 10$. Then the performance degradation increases faster up to the limits of the feasibility domain, at which the performance degradation is "infinite". A conclusion that can be built upon the first batch of simuations (the de-spin maneuver) and this robust performance analysis is that the saturation plays an important role in the degradation of the performance level. Indeed, we first observed in the simulation plot velocity profiles indicating actuator saturation e.g. time ranges over which the speed varies linearly. Secondly, removing the saturation from

the robust performance analysis setup dramatically increased the size of the feasibility domain. These two facts showed the crucial impact of actuator saturation on robust performance.

Another point is worth to be mentioned. We performed the robust performance analysis with the full perturbation operator Δ_{dyn} from (5.40). However, the numerical issues already observed during the stability analysis (see non smooth boundary of the feasibility domain in figure 5.12) were much worse for the extended problem of robust performance analysis. The robust performance test appeared to be feasible for some uncertainty values but it occurred very sparsely over the region of the (δ_d, δ_{od}) plane we investigated. Thus it was not possible to present the results. It is expected that more computing power should partially solve this issue and allow mapping the stability domain with iso-performance curves.

5.7 Conclusion

This chapter aimed to present the work we did on validation of control laws for space launchers with an analysis model including full nonlinear dynamics and uncertain inertia matrix. Analytical robustness analysis and control law validation for the nonlinear uncertain equation of motion had never been done before by our industrial partners. To do so, a factorization of the uncertain inertia matrix I_g and the coupling matrix $P(\hat{\omega})$ has been found allowing the construction of a LFR of the 3D equation of rotating motion with reduced size with respect to the number of uncertain parameters. These parameters are considered scalar time-invariant for the inertia terms and scalar time-varying for the angular speeds. The representation we obtained through the parameterization was a LPV representation. The counterpart of this accurate modeling of the dynamics was the use of the simplest kinematic model.
The resulting analysis model covers all the "flyable" trajectories of the space launcher. It allowed to guarantee robust stability of the system when affected by the inertia uncertainty over a vast flight envelope. The "nominal" uncertainties which have been considered were given and were set to $\pm 10\%$ relative uncertainy on the diagonal terms and a multiplication of the off-diagonal terms by an uncertain factor between 0 and 10 i.e. off-diagonal terms of the inertia matrix can vary from -100% to $+900\%$ off their nominal value. The stability has been guaranteed with the IQC tool LPVMAD for a wider range of uncertainties as depicted in figure 5.12.
The simulations done after the analytical analysis showed unacceptable performance for a simple despin maneuver with random inertia parameters chosen over the given uncertainty domain. These results encouraged the preparation of a robust performance analysis aiming to investigate the performance degradation caused by inertia uncertainties, gyroscopic couplings and actuator saturation.
To assess how the inertia uncertainties, gyroscopic coupling and actuator saturation affect the transfer from torque disturbances to attitude error, a short robust performance analysis was performed. Robust performance analysis was done here as a robust stability analysis. Hence we added a new fictitious perturbation block to the LFR used for the stability analysis to evaluate the peak gain of the transfer from d to e. Involving new uncertainties increased the size of the LMI problem to be solved for the stability test. It caused the numerics to be inaccurate for the full problem as the multiplier used to define an IQC satisfied by extended perturbation block was in $\mathbb{RH}_\infty^{60\times 60}$. The computational burden and resulting numerical inaccuracies prevented us from going deeply into this analysis and from searching for less conservative results through high order multipliers describing the full problem. Consequently, a trade-off had to be made to make the computations feasible in a reasonable duration so we removed ψ_{ACS} from the analysis model and reused the static multipliers for the uncertain inertia parameters. Nevertheless, the IQC analysis tool allowed us to characterize the transfer from a torque disturbance input Γ_{dist} to the attitude error $\Delta\alpha$ of a simplified analysis model without saturation. We depicted iso-performance maps (see figure 5.22) within the stability domain of the simplified model. The iso-performance plots are readable and convenient to represent the performance characteristics over the stability region. Despite

the simplified approach, the similarity between the conclusions drawn from the simulation results and from the robust performance analysis confirmed the influence of the saturation on the stability and performance of our space launcher model. Indeed, the obvious rate saturations on the velocity plots of figure 5.17 have been linked to the large increase of the size of the feasibility domain obtained after removing ϕ_{ACS} from Δ_{dyn}.

As a more general conclusion, we indicate that the factorization of the equation of motion proposed for this application and published in [Chaudenson et al., 2013a] can be reused as it is rather compact. Nevertheless, it could be interesting to look for smaller factorizations as it would allow to make the computations quicker or to add new perturbation blocks to increase the representativeness of the analysis model. Another lead would be to find IQC that are satisfied by the operator which produces the gyroscopic torques Γ_{gyro} from $I_g\omega$. Since it is a 3-inputs 3-outputs operator, it would certainly allow reducing the size of Δ_{dyn} as well.

The drawback of the modeling is the way we represented the kinematic equations. Even if the "small-angles" approximation is accurate for small amplitude motion, it is not relevant over most of the flight envelope we considered and does not tell anything about the position of $\mathcal{R}_g$ with respect to $\mathcal{R}_{ref}$. Hence one capital improvement would be to find an appropriate representation for quaternion kinematic equation that fits with the robustness analysis framework of chapter 4.

The application to come focuses on the second part of the system which got all our interest during this study and which is the analysis of the effect of the PWM actuator on stability.

Chapter 6

Robust stability analysis of systems with pulse-width modulator

6.1 Introduction

The second issue we wanted to address during the project was the analysis of the influence of the PWM used for ACS modeling on the robust stability of a space launcher. The PWM, introduced as a model of the ACS thrusters during model description in section 3.7 has a nonlinear behavior. In the setup we consider here, it takes into account the sampled value of its input but it outputs a continuous time signal. The latter can only take a finite number of values and some of its characteristics are uncertain. Thus it is a device which is not easy to analyze with classical tools for stability analysis. Since they already encountered these issues, the industrial partners are impatient to get analytical characterization of the stability of systems including PWM. In order to try to provide a solution to that problem and to propose methods for robustness analysis of systems with PWM, we considered three different techniques. Two of them rely on IQC description of operators and stability analysis. At first, we take the "multiplier driven" approach previously used in chapter 5. In this study, we aim to model the PWM with perturbation operators that are described with multipliers defined in the literature and already implemented in LPVMAD [Köroglu et al., 2008]. The works were based on a very pragmatic approach aiming to define analytically the effect of the PWM on the angular speed of a simplified space launcher model. It results in the definition of a LFR involving classical operators that cover rigorously the set of feasible trajectories of the analysis model. This study was presented in the paper [Chaudenson et al., 2012]. Secondly, we used the hard IQC approach of [Gelig and Churilov, 1998]. In this framework, the transformation of the LFR with the PWM is conducted such that the resulting interconnection can be described with multipliers derived from the circle criterion and Popov criterion for sector bounded nonlinearities. We observed that the resulting system was comparable to the one obtained after the transformation of [Chaudenson et al., 2012]. In facts, a more rigorous mathematical approach allowed us to confirm that the modeling done before was relevant. We then brought two improvements to the results of [Gelig and Churilov, 1998]. We modified the conditions of application of their stability theorem to gain efficiency in the computations and we looked for new multipliers defining IQC capturing the behavior of the transformed perturbation operator. The ameliorations allowed to reduce the conservatism of the stability test and improve the computation efficiency. They were presented in [Chaudenson et al., 2013b]. To have different results on the problem, we used a third method based on Lyapunov theory. It was used with the aim to evaluate a recent validation method for sampled-data systems with constrained inputs and compare the results with the IQC results when possible. Even though the stability results are not directly comparable, it permitted us to evaluate the robustness of the launcher differently. The result we used is an extension of the theorem

presented in [Seuret and Gomes Da Silva Jr, 2011].

The system of interest for this application is made of a one dimensional model of the rigid launcher in exo-atmospheric flight with its ACS. The elements about this description are gathered in chapter 3. Figure 6.1 represents an overview of the simplified closed-loop block diagram we are going to analyze. The attitude error is the input to controller $\mathcal{C}$ and is denoted by $\Delta\alpha$. α_{aimed} and α are the attitude reference and the actual attitude, respectively. Notice that we do not consider any sampling and so we only have continuous time signals. The other signals of the closed-loop are the torque command Γ_c generated by the controller $\mathcal{C}$ and the torque Γ_{ACS} delivered by the PWM actuator. The pulse-modulated signal Γ_{ACS} directly inputs the space launcher physical model denoted by $\mathcal{D}$.

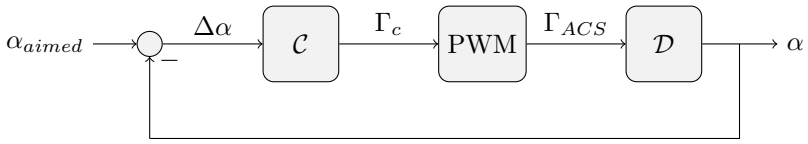

Figure 6.1: Closed-loop model for analysis as a pulse-modulated system

6.2 Analysis model

To assess the robustness of the launcher with PWM actuator, we have to transform and simplify the model for the analysis. The simplifications have been driven by the fact that we would like to evaluate the influence of the PWM actuator on the overall behavior. Thus the PWM model is more accurate than the model of the other subsystems. This is due to the usual modeling trade-off between representativeness and model complexity. This section aims to define the blocks of the closed-loop model pictured above in figure 6.1.

6.2.1 Dynamics and kinematics

The dynamic model we consider is one dimensional. It is the classical approximation for a rotating rigid body and we use it to model the angular motion of the launcher. The transfer function of the ideal dynamic model Dyn is defined by

$$Dyn(s) = \frac{\omega(s)}{\Gamma_{ACS}(s)} = \frac{1}{Js}, \tag{6.1}$$

where s is the Laplace variable, J is the inertia about the axis of rotation. It is the transfer function from the torque applied to the launcher by the thruster Γ_{ACS} to angular speed ω. To compute the attitude α of the launcher from ω, we also have a very simple kinematic model transfer function model Kin consisting in an integrator:

$$Kin(s) = \frac{\alpha(s)}{\omega(s)} = \frac{1}{s}. \tag{6.2}$$

Consequently, the overall transfer function of the space vehicle model is given by the transfer function

$$\mathcal{D}_{ideal}(s) = Kin(s)Dyn(s) = \frac{\alpha(s)}{\Gamma_{ACS}(s)} = \frac{1}{Js^2}. \tag{6.3}$$

This classical representation can be approximated in order to facilitate the analysis without loss of representativeness of the model.

Integrator approximation

We will see later on that the zero poles of the ideal transfer function of a space vehicle dynamic and kinematic model $\mathcal{D}_{ideal}$ may cause some troubles when applying certain analytical methods that require strictly stable nominal plants in the LFR. To overcome this issue and without loss of representativeness of the analysis model, we can assume that the pole is not zero but that there is a very small cut-off frequency ω_d such that the approximated integrator transfer function has a large but finite static gain. To represent an integrator, we consider the transfer function:

$$\mathcal{I}(s) = \frac{g_d}{s + \omega_d}. \tag{6.4}$$

Immediately, we find the transfer function of a perfect integrator by setting $g_d = 1$ and $\omega_d = 0$ in the definition of $\mathcal{I}(s)$. To have a frequency response of the approximated integrators that is representative a perfect integrator, we determine the appropriate gain g_d. g_d is defined as a function of the frequency at which we would like the gains of the ideal integrator and the approximated integrator $\mathcal{I}(s)$ to be equal. This frequency will be defined later on as the natural frequency of our system and for now it is denoted by $\omega_0 > 0$. Thus it gives

$$g_d = \sqrt{1 + \frac{\omega_d^2}{\omega_0^2}}. \tag{6.5}$$

Regarding the notations in (6.4), we have the relationship

$$\mathcal{D}(s) = \frac{1}{J}(\mathcal{I}(s))^2, \tag{6.6}$$

where we removed the subscript "ideal" because of the introduction of the generalized integrator $\mathcal{I}(s)$. This approximation was validated by the industrial partners. To keep a representative frequency-domain behavior over the frequency range of interest $[\omega_d, \omega_0]$, we select $\omega_d = 10^{-4}$ rad.s^{-1}. More generally, we consider that the approximated integrator cut-off frequency ω_d should be at least two orders of magnitude below the desired closed-loop natural frequency ω_0 to be defined below in paragraph 6.2.2. In addition to the helpful fact that $\mathcal{I}(s)$ has a pole with strictly negative real part, this approximation also avoids a singularity induced by the combination of the zero poles of the ideal space launcher dynamic and kinematic model $\mathcal{D}_{ideal}$ with a sector bounded nonlinear actuator as described in paragraph 5.3.2.

6.2.2 Attitude control

Now that motion of the space launcher has been modeled, we have to define the controller that will compute the torque command Γ_c needed for reference tracking. In the manner of the previous chapter in paragraphs 5.2.4 and 5.2.3, we introduce a derivative filter to model the estimation of the angular speed from measurements of the current attitude α. Inserting that filter in the general setup of the controller, we can reformulate it as a continuous proportional-derivative controller $\mathcal{C}$ with filtered derivative. Thus, the controller transfer function is defined by

$$\mathcal{C}(s) = K_p + K_d \frac{s\omega_f}{s + \omega_f}. \tag{6.7}$$

The control gains K_p and K_d are the proportional gain (subscript p) and the derivative gain (subscript d), respectively. They operate on the attitude error $\Delta\alpha$ and the estimated angular speed error $\mathcal{F}(s)\Delta\alpha$, respectively. Here $\mathcal{F}$ is the derivative filter introduced in the definition of $\mathcal{C}$. The pole of the derivative filter introduced to compute the estimated angular speed is denoted by ω_f. This filtering parameter is chosen to be at least one order of magnitude larger than the desired closed-loop natural frequency ω_0.

Hence the frequency response of the derivative filter is very similar to the one of a pure derivative filter over the bandwidth of interest approximated to $[\omega_d, \omega_0]$. Consequently, the basic tuning routine presented below applies.

Basic tuning for the controller

We now briefly present a launcher model which is useful for the tuning of the control gains. It helps defining K_p and K_d in a very simple manner. Indeed, in the closed-loop figure 6.1, if we consider no actuator, ideal derivation with $\omega_f = \infty$ in $\mathcal{F}$, and generalized integrators from paragraph 6.2.1 with $\omega_d = 0$ in $\mathcal{D}$ from (6.6), the closed-loop transfer function reads as

$$G(s) = \frac{\alpha(s)}{\alpha_{aimed}(s)} = \frac{1}{J} \frac{K_d s + K_p}{s^2 + \frac{K_d}{J} s + \frac{K_p}{J}}. \tag{6.8}$$

It is a relevant approximation of the transfer function from α_{aimed} to α over the frequency range of interest. The second order denominator allows to determine the control gains K_p and K_d such that the ideal closed-loop has a second order behavior with natural frequency ω_0 and damping ξ. This is given by the definitions of K_p and K_d:

$$\begin{cases} K_p = & \omega_0^2 J, \\ K_d = & 2\xi\omega_0 J. \end{cases} \tag{6.9}$$

Given ξ and ω_0, the relationships in (6.9) are used to determine rapidly values of K_p and K_d given the desired ω_0 and ξ. This gain tuning method was already the one used for the application in chapter 5. Even though it does not rely on the most accurate representation of the dynamics of a launcher since it represents a decoupled launcher, it will give to the closed-loop analysis model reasonable stability and performance margins to allow us to perform robustness analysis. Of course, better tunings can be found but we focus on analysis methods so this tuning is enough.
The controller model has now been set up. The goal of the coming paragraph is to present the actuator we investigate in the application.

6.2.3 Actuator model

The core of this application is the study of the effect of the ACS thrusters on the stability of the closed-loop system. In chapter 3, we modeled the thrusters as a PWM. For convenience, the PWM will be denoted by $\mathcal{P}$. Its input is Γ_c and its output is Γ_{ACS}. The main characteristic of a PWM is its sampling period $h > 0$. We will consider h to be known, constant, and non zero.
For all nonnegative integer n, the sampling period h defines sampling intervals T_n as:

$$\forall n \in \mathbb{N}, \quad T_n := [t_n, t_{n+1}). \tag{6.10}$$

In (6.10), t_n is referred to as the nth sampling instant. Since the sampling period is constant, we have

$$\forall n \in \mathbb{N}, \quad t_n = nh. \tag{6.11}$$

Considering these definitions, we give the general input/output law of the PWM as in chapter 3 but for the one-dimensional case:

$$\forall \Gamma_c \in \mathcal{L}^1, \quad \mathcal{P}(\Gamma_c)(t) = \Gamma_{ACS}(t) = \begin{cases} \lambda_n, & t \in [t_n, t_n + \tau_n), \\ 0, & t \in [t_n + \tau_n, t_{n+1}). \end{cases} \tag{6.12}$$

The shapes of Γ_c and Γ_{ACS} are sketched on figure 6.2. The definition of $\mathcal{P}$ introduces the same parameters τ_n and λ_n as in section 3.7. The pulse width τ_n is defined as a function of the sampled value of Γ_c denoted by $\Gamma_c(t_n)$ and is proportional to h. During the nth sampling period T_n, τ_n corresponds to the duration for which the thrusters are set to ON. The pulse height λ_n corresponds to the level of torque produced by the thrust generated when the thrusters are set to ON. λ_n is considered to have a constant absolute value equal to $\Gamma_{av} > 0$ while its sign is given by the sign of $\Gamma_c(t_n)$. The analytical definitions of λ_n and τ_n are:

$$\lambda_n = \quad sign\left(\Gamma_c(t_n)\right)\Gamma_{av},$$

$$\tau_n = \begin{cases} 0, & \text{if } |\Gamma_c(t_n)| < \Gamma_{min} \\ \frac{|\Gamma_c(t_n)|}{\Gamma_{av}} h, & \text{if } \Gamma_{min} \leq |\Gamma_c(t_n)| < \Gamma_{av} \\ h, & \text{if } |\Gamma_c(t_n)| \geq \Gamma_{av} \end{cases} . \tag{6.13}$$

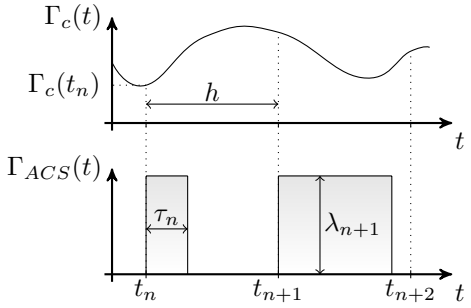

Figure 6.2: Sketch of the PWM input and output

The definitions above introduce two parameters of the system: $\Gamma_{min} \geq 0$ and $\Gamma_{av} > \Gamma_{min}$. Firstly, Γ_{min} is the value of the torque command Γ_c below which no pulse is produced. Indeed, we see in (6.13) that the pulse width τ_n depends proportionally on the sampled value of the torque command Γ_c if $\Gamma_{min} \leq |\Gamma_c(t_n)| < \Gamma_{av}$. However, the technical limitations of the thrusters hinder from producing torque for a too short duration i.e. thrusters cannot be set to ON for a too short duration. Hence Γ_{min} corresponds to this minimum pulse duration t_{min}. The definition of Γ_{min} is simple and comes from (6.13). It is the value of $\Gamma_c(t_n)$ for which we would have $\tau_n = t_{min}$, that is Γ_{min} is such that $\Gamma_{min}h = \Gamma_{av}t_{min}$. Secondly, Γ_{av} is the torque available for attitude control. It is a characteristic of the ACS thrusters since it represents the torque generated by the application of the nominal thrust to the launcher. It was already used in the application of chapter 5. According to the definition in (6.13), for torque commands Γ_c larger than Γ_{av} the opening duration is set to its maximum value h. From (6.13), we observe that the definition of τ_n depends on the value of the input Γ_c at sample time t_n. Consequently, τ_n looks like the result of the application of a saturation at h, and of a threshold at t_{min} to $|\Gamma_c(t_n)|$ weighted by h/Γ_{av}. It is now time to verify whether the IQC analysis of the stability of the closed-loop with PWM can be done or not.

Unbounded energy gain of the PWM

As a first verification, we need to check if the PWM defined by (6.12-6.13) has bounded $\mathcal{L}_2$-induced gain. To do so, we express the $\mathcal{L}_2$-norm of Γ_{ACS} under the assumption that Γ_c has bounded $\mathcal{L}_2$-norm i.e.

$\Gamma_c \in \mathcal{L}_2$. It reads as

$$\begin{aligned} \|\Gamma_{ACS}\|_{\mathcal{L}_2}^2 &= \int_0^{+\infty} |\Gamma_{ACS}(t)|^2 dt, \\ &= \sum_{n=0}^{n=+\infty} \int_{t_n}^{t_{n+1}} |\Gamma_{ACS}(t)|^2 dt, \\ &= \sum_{n=0}^{n=+\infty} \int_{t_n}^{t_n+\tau_n} |\lambda_n|^2 dt, \\ &= \sum_{n=0}^{n=+\infty} \Gamma_{av}^2 \tau_n, \\ &= \Gamma_{av}^2 \sum_{n=0}^{n=+\infty} \tau_n. \end{aligned} \tag{6.14}$$

(6.14) shows that to guarantee the finiteness of $\|\Gamma_{ACS}\|_{\mathcal{L}_2}$, we need to make sure that the series with general term τ_n converges toward a finite value. Hence we cannot draw any conclusion on the finiteness of $\|\Gamma_{ACS}\|_{\mathcal{L}_2}$ for now. According to (6.13), the last equality in (6.14) can be bounded as follow

$$\Gamma_{av}^2 \sum_{n=0}^{n=+\infty} \tau_n \leq h\Gamma_{av} \sum_{n=0}^{n=+\infty} |\Gamma_c(t_n)|. \tag{6.15}$$

Finally, another way to guarantee the finiteness of $\|\Gamma_{ACS}\|_{\mathcal{L}_2}$ is to make sure that the series with general term $|\Gamma_c(t_n)|$ converges toward a finite value. Unfortunately, in classical IQC analysis framework, we only assume that $\|\Gamma_c\|_{\mathcal{L}_2} < \infty$ and it does not help to prove the $\mathcal{L}_2$ boundedness of $\mathcal{P}$.
This simple fact shows that the preliminary works of any IQC-based robustness analysis of space launcher as a pulse-modulated system will be to recast the system with PWM in another equivalent system for which IQC-based stability analysis is possible. To make the analysis workable, we have to introduce operators with bounded $\mathcal{L}_2$-induced gain that represent $\mathcal{P}$.
We investigated IQC-based stability analysis of pulse-modulated systems in [Chaudenson et al., 2012] and [Chaudenson et al., 2013b]. Both papers rely on preparatory transformations bypassing the unboundedness issue.

6.2.4 Closed-loop model for analysis

This section aimed to describe the analysis model we built for this application. It is derived from the complete model described in chapter 3. Figure 6.3 shows the setup that we would like to analyze where $\mathcal{P}$ is the PWM operator defined in (6.12-6.13). We see here how we focus on the pulse-modulator as all other trouble making parts introduced in chapter 3 have been removed.

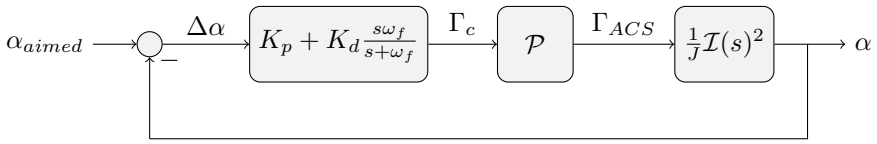

Figure 6.3: Closed-loop of analysis model for the second application

6.3 "Multiplier driven" LFR setup

In this section we aim to transform the model depicted figure 6.3 into one that can be analyzed with IQC. Doing this analysis is not straightforward since we saw in paragraph 6.2.3 that the PWM operator $\mathcal{L}_2$-induced gain cannot be bounded easily so the operator cannot be directly described with IQC. The loop transformation which we are going to present has been driven by two facts. First, we want to use

operators that can already be described with IQC of LPVMAD. Second, the observation of the closed-loop behavior suggests it. Indeed, we looked at the effect of the PWM output signal Γ_{ACS} on the state variables of the model figure 6.3. Particularly we were interested in determining the effect of the PWM on the angular speed of the launcher. The goal was to come up with a representation of the PWM including a nonlinear nominal operator and a perturbation operator.
The result of this modeling part will be twofold. Firstly, the definition of an equivalent closed-loop with $\mathcal{L}_2$ bounded perturbation operators will allow to perform soft IQC-based robust stability analysis with the LPVMAD toolbox. This will be done by representing the new operators by IQC defined by multipliers that are frequently encountered in the literature. Secondly, this representation will also allow to address the robustness issue with a Lyapunov theory based method which will be presented in section 6.5.

6.3.1 PWM modeling

The modeling of the PWM exposed here results from the observation of the time-domain representation of the angular velocity $\dot{\alpha}$ in the model figure 6.3. This angular velocity is denoted by ω_{pwm} where the subscript "*pwm*" means that this is the angular speed in the model with the PWM as an actuator. In facts, since ω_{pwm} results from the integration of the piecewise constant PWM output Γ_{ACS} weighted by the inertia, it has a piecewise affine profile. This profile leads us to consider the PWM angular velocity ω_{pwm} as the sum of the angular speed generated by a so-called nominal actuator and a perturbation signal from a nonlinear operator $\Delta_{PWM}(\bullet)$. The nominal operator is made of the saturation at Γ_{av} of gain 1 denoted by ϕ_{ACS} and defined in the previous chapter in (5.10-5.11), and a sample-and-hold operator $\mathcal{SH}_h$ with sampling and hold synchronized at h. The definition of the piecewise constant signal Γ_{sh} which outputs the nominal actuator $\mathcal{SH}_h(\phi_{ACS}(\bullet))$ with input Γ_c is given below (6.16). The subscript "*sh*" stands for "sample-and-hold" but the reader should not omit that the nominal torque Γ_{sh} also went through the saturation ϕ_{ACS}. The plot of ϕ_{ACS} is given in figure 6.4. Notice that the two operators $\mathcal{SH}_h$ and ϕ_{ACS} commute since ϕ_{ACS} is memoryless:

$$\forall n \in \mathbb{N}, \forall t \in T_n, \quad \Gamma_{sh}(t) = \mathcal{SH}_h(\phi_{ACS}(\Gamma_c(t))) = \phi_{ACS}(\Gamma_c(t_n)) \in [-\Gamma_{av}, +\Gamma_{av}]. \tag{6.16}$$

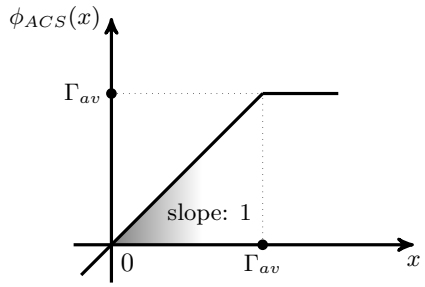

Figure 6.4: Characteristic plot of the nonlinearity ϕ_{ACS}

We will refer to Γ_{sh} as the nominal torque. We also introduce the acceleration produced by the nominal actuator. Γ_{sh} produces an angular acceleration $\dot{\omega}_{sh} = \Gamma_{sh}/J$ which has constant value over each sampling interval T_n like Γ_{sh}. The nominal actuator is depicted in figure 6.5.

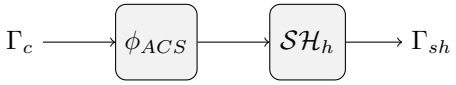

Figure 6.5: Actuator model for analysis

From these first statements, we depict the analysis model of figure 6.3 in figure 6.6 using the definition

of $\mathcal{D}$ from (6.6). To introduce the new operator Δ_{PWM}, the space launcher transfer function $\mathcal{D}$ has been split into a gain and two generalized integrators.

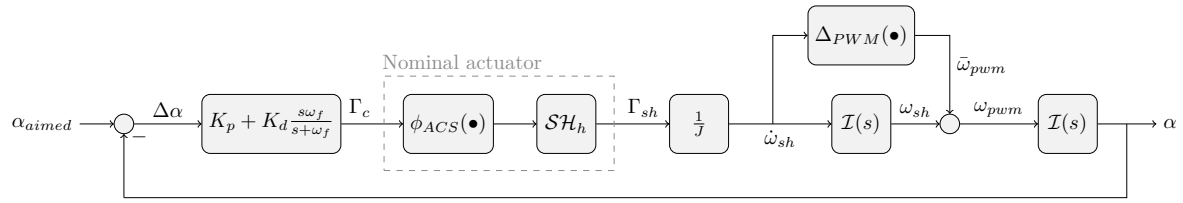

Figure 6.6: Transformed closed-loop model for analysis

This representation shows how the output of

$$\Delta_{PWM} : \begin{cases} \mathcal{L}^1 & \rightarrow & \mathcal{L}^1 \\ \dot{\omega}_{sh} & \rightarrow & \bar{\omega}_{pwm} \end{cases} \tag{6.17}$$

affects the angular speed ω_{sh} generated by the nominal actuator as a perturbation. We denote the output of Δ_{PWM} by $\bar{\omega}_{pwm}$. In this framework, we would like to define $\Delta_{PWM}(\dot{\omega}_{sh}) = \bar{\omega}_{pwm}$ such that

$$\forall t \geq 0, \quad \omega_{pwm}(t) = \omega_{sh}(t) + \bar{\omega}_{pwm}(t). \tag{6.18}$$

To determine the input-output relationship of the new operator Δ_{PWM}, the angular speed ω_{pwm} generated by the PWM output Γ_{ACS} is compared to the angular speed ω_{sh} obtained by integration of the nominal acceleration $\dot{\omega}_{sh}$. To find the definition of Δ_{PWM}, we consider that in the generalized integrators $\mathcal{I}(s)$ (6.4) of figure 6.6 are defined with $\omega_d = 0$ rad.s^{-1} and so $g_d = 1$. Hence for this analysis model we have "true" integrators.

Definition of Δ_{PWM} We can start the investigations leading to the definition of $\bar{\omega}_{pwm}$, the output of Δ_{PWM}. The input of Δ_{PWM} is the nominal acceleration $\dot{\omega}_{sh}$. As set as a goal in (6.18), we would like the sum of ω_{sh} and $\bar{\omega}_{pwm}$ to be equal to the angular speed ω_{pwm} that the launcher has when it is actuated with a PWM. To do so, we are going to define the signals ω_{pwm} and ω_{sh} where ω_{sh} is the speed generated by the nominal actuator (see figure 6.6).

First of all, we can use the definition of the PWM output signal Γ_{ACS} in (6.12-6.13) to determine an analytical expression of the angular speed ω_{pwm}. As ω_{pwm} is the result of the integration of the piecewise constant signal Γ_{ACS}/J, it is piecewise affine. This analytical definition is determined under the assumption that the torque produced by the thrusters is known and constant with value Γ_{av}. In the definition of the pulse height in (6.12), it means that $\forall n \in \mathbb{N}$, $|\lambda_n| = \Gamma_{av}$. Later on, we will reconsider this assumption to take into account the uncertainty affecting the torque produced by the thrusters.

To simplify the expression of the angular speed ω_{pwm}, we introduce some definitions and notations:

$$\forall t \geq 0, \exists n \in \mathbb{N}, t \in T_n, \quad \left\{ \begin{array}{rcll} \dot{\omega}_{av} & = & \frac{\Gamma_{av}}{J}, & \text{constant} \\ s(t) & = & \text{sign}(\Gamma_{sh}(t)), & \text{constant over } T_n \\ \dot{\omega}_c(t) & = & \frac{\Gamma_c(t)}{J}, & \text{time-varying} \\ \dot{\omega}_{sh}(t) & = & \frac{\Gamma_{sh}(t)}{J}, & \text{constant over } T_n \\ & = & \frac{\phi_{ACS}(\Gamma_c(t_n))}{J}, & \\ & = & \left\{ \begin{array}{ll} \dot{\omega}_c(t_n), & \text{if } |\Gamma_c(t_n)| < \Gamma_{av}, \\ s(t)\dot{\omega}_{av}, & \text{if } |\Gamma_c(t_n)| \geq \Gamma_{av}. \end{array} \right. & \end{array} \right. \tag{6.19}$$

We see in the last equality how the saturation ϕ_{ACS} is bounding the range of variation of $\dot{\omega}_{sh}$. Analogously to $\dot{\omega}_{sh}$, the "available acceleration" is denoted by $\dot{\omega}_{av}$. It is the acceleration produced by the application of Γ_{av} to the launcher modeled by the inertia J. Notice that $\dot{\omega}_{av}$ as a constant value. $\dot{\omega}_c = \Gamma_c/J$ represents the "acceleration command". We remark that according to (6.19),

$$\forall t > 0, t \in T_n, \quad s(t) = \text{sign}(\Gamma_{sh}(t)) = \text{sign}(\Gamma_{sh}(t_n)) = \text{sign}(\Gamma_c(t_n)). \tag{6.20}$$

The framework is now set up, we can now define ω_{pwm}. For this we consider that the speed at any instant $t \in T_n$ is the sum of the speed at t_n and the speed increment produced by the torque Γ_{ACS} from t_n to t:

$$\forall n \in \mathbb{N}, \forall t \in T_n, \quad \omega_{pwm}(t) = \omega_{pwm}(t_n) + \int_{t_n}^{t} \frac{\Gamma_{ACS}(\sigma)}{J} d\sigma. \tag{6.21}$$

Taking into account the definition of the PWM output Γ_{ACS} from (6.12), ω_{pwm} reads as:

$$\begin{array}{l} \forall t \in T_n, \quad \text{if } |\Gamma_c(t_n)| < \Gamma_{min}, \\ \qquad \omega_{pwm}(t) = \omega_{pwm}(t_n), \quad \forall t \in T_n, \\ \qquad \text{if } |\Gamma_c(t_n)| \geq \Gamma_{min}, \\ \qquad \omega_{pwm}(t) = \left\{ \begin{array}{ll} \omega_{pwm}(t_n) + s(t)\dot{\omega}_{av}(t - t_n) & , \forall t \in [t_n, t_n + \tau_n), \\ \omega_{pwm}(t_n) + s(t)\dot{\omega}_{av}\tau_n & , \forall t \in [t_n + \tau_n, t_{n+1}). \end{array} \right. \end{array} \tag{6.22}$$

From the definition of the piecewise constant saturated signal $\dot{\omega}_{sh}$ in (6.19), the signal ω_{sh} can also be defined by integration over time. As for the definition of ω_{pwm}, we consider the speed increment caused by the acceleration generated by the nominal actuator over a sampling period T_n:

$$\begin{array}{rcl} \forall t \in T_n, \quad \omega_{sh}(t) = & \omega_{sh}(t_n) + \int_{t_n}^{t} \dot{\omega}_{sh}(\sigma) d\sigma, \\ = & \omega_{sh}(t_n) + \dot{\omega}_{sh}(t)(t - t_n); \end{array} \tag{6.23}$$

where $\dot{\omega}_{sh}(t)$ is constant over T_n like Γ_{sh}. Now there is one important remark before defining $\bar{\omega}_{pwm}$. Since we considered the delivered torque $|\lambda_n|$ to be known and equal to Γ_{av} at all time, we can write for

any integer n that

$$\begin{aligned}\omega_{sh}(t_{n+1}) &= \omega_{sh}(t_n) + \dot{\omega}_{sh}(t)(t_{n+1} - t_n) \\ &= \omega_{sh}(t_n) + \dot{\omega}_{sh}(t)h \\ &= \omega_{sh}(t_n) + \frac{\phi_{ACS}(\Gamma_c(t_n))}{J}h \\ &= \omega_{pwm}(t_{n+1}) \text{ for all } n \text{ such that } |\Gamma_c(t_n)| \geq \Gamma_{min} \text{ and } \omega_{pwm}(t_n) = \omega_{sh}(t_n).\end{aligned} \tag{6.24}$$

The sequence of equalities allows to show by mathematical induction that the speed increment over a sampling period is equal for the nominal actuator and the PWM actuator as long as

$$\forall n \in \mathbb{N}, \quad |\Gamma_c(t_n)| \geq \Gamma_{min}. \tag{6.25}$$

At the cost of a loss of representativeness of the model, we can enforce this condition by setting Γ_{min} to zero. This assumption is the price to pay to have an operator Δ_{PWM} which as a bounded continuous output in the framework we designed. For the future developments of this section, we set

$$\Gamma_{min} = 0. \tag{6.26}$$

The assumption leads to the simplification of the definition of the pulse width below:

$$\forall n \in \mathbb{N}, \quad \tau_n = \begin{cases} \frac{|\Gamma_c(t_n)|}{\Gamma_{av}}h, & \text{if } |\Gamma_c(t_n)| < \Gamma_{av} \\ h, & \text{if } |\Gamma_c(t_n)| \geq \Gamma_{av} \end{cases}, \tag{6.27}$$

Under assumption (6.26), at each sampling time t_n we have ω_{sh} and ω_{pwm} which are equal if they are equal at $t = 0$. Hence the value of $\bar{\omega}_{pwm}$ will be zero for all $t = t_n, n \in \mathbb{N}$. We have analytical expressions for ω_{pwm} and ω_{sh}, let us now determine the difference between ω_{pwm} and ω_{sh} in order to define the output $\bar{\omega}_{pwm} = \omega_{pwm} - \omega_{sh}$ of the nonlinear perturbation operator Δ_{PWM}:

$\forall t \in \mathbb{R}_+, \exists n \in \mathbb{N}, t \in T_n,$

$$\bar{\omega}_{pwm}(t) = \begin{cases} s(t)\dot{\omega}_{av}(1 - \frac{|\dot{\omega}_{sh}(t)|}{\dot{\omega}_{av}})(t - t_n) & ,\forall t \in [t_n, t_n + \tau_n) \\ \dot{\omega}_{sh}(t)(t_{n+1} - t) & ,\forall t \in [t_n + \tau_n, t_{n+1}) \end{cases} \tag{6.28}$$

Notice that we used the fact that $\Gamma_{min} = 0$. In (6.28), we see again that the value of the angular speed ω_{sh} of the fictitious system with the nominal actuator from figure 6.5 and the angular speed ω_{pwm} generated by the PWM are equal at each sampling instant t_n as

$$\forall n \in \mathbb{N}, \quad \bar{\omega}_{pwm}(t_n) = 0. \tag{6.29}$$

The output signal of Δ_{PWM} is continuous at the sampling instants and so continuous for all $t \geq 0$. To get a better representation of the signals ω_{pwm} and ω_{sh}, figure 6.7 sketches them over a few sampling periods.

The output of Δ_{PWM} has been defined for any time instant $t \geq 0$. We achieved a transformation of the closed-loop system described in section 6.2 that takes the form of figure 6.6 and that is equivalent to it under the assumption $\Gamma_{min} = 0$.

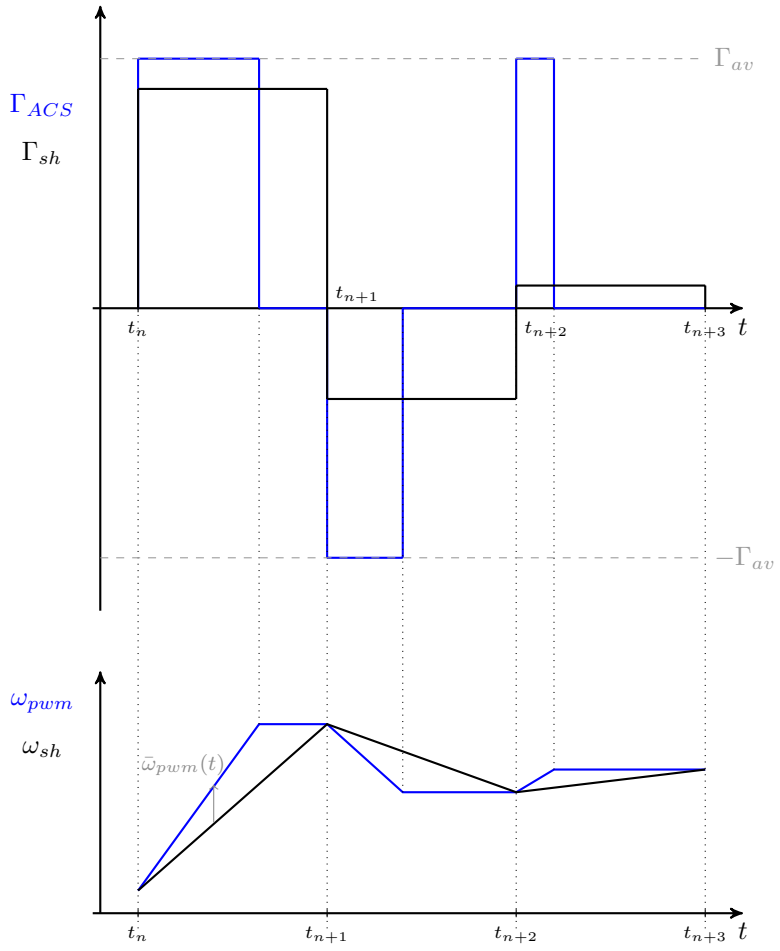

Figure 6.7: Torque and speed comparison, $\omega = \int \Gamma / J dt$

6.3.2 Torque uncertainties

One more step is needed before starting the analysis. To determine the analytical expression of $\bar{\omega}_{pwm}$, we assumed that the height of the pulses at the output of the PWM was known and constant at Γ_{av}. It causes the association of the nominal actuator with the operator Δ_{PWM} to represent an "ideal" PWM. As this assumption is not representative according to the model we defined in chapter 3 section 3.7, we have to define the pulse height as

$$\forall n \in \mathbb{N}, \forall t \in T_n, \quad \lambda_n = s(t)\Gamma_{av}(1 + \delta_\Gamma). \tag{6.30}$$

This expression accounts for a multiplicative parametric time-invariant uncertainty δ_Γ affecting the pulse height Γ_{av}. δ_Γ expresses the relative uncertainty on Γ_{av}. As $\dot{\omega}_{av} = \Gamma_{av}/J$, the nominal acceleration $\dot{\omega}_{av}$ is affected by the same uncertainty as Γ_{av}. δ_Γ is a static time-invariant parameter since we consider that during a maneuver the available torque is not changing. For the one-dimensional model we consider here, it is very simple to introduce this uncertainty into the model. To do so, let us express the angular speed $\omega_{pwm}^{(\delta_\Gamma)}$ generated by the PWM actuator under the assumption that $\Gamma_{min} = 0$ and the pulse height λ_n is

uncertain:

$$\forall n \in \mathbb{N}, \forall t \in T_n, \quad \omega_{pwm}^{(\delta_\Gamma)}(t) = \omega_{pwm}^{(\delta_\Gamma)}(t_n) + \begin{cases} s(t)\dot{\omega}_{av}(1+\delta_\Gamma)(t-t_n) & ,\forall t \in [t_n, t_n+\tau_n), \\ s(t)\dot{\omega}_{av}(1+\delta_\Gamma)\tau_n & ,\forall t \in [t_n+\tau_n, t_{n+1}). \end{cases} \tag{6.31}$$

To express the angular speed at time $t = t_n$, we can write:

$$\forall n \in \mathbb{N}, \quad \omega_{pwm}(t_n) = \omega(0) + \int_0^{t_n} \frac{\Gamma_{ACS}(\sigma)}{J} d\sigma, \tag{6.32}$$

where $\omega(0)$ is the initial angular speed and $\omega_{pwm}(0) = \omega_{sh}(0) = \omega(0)$. Thus we can use the definition of Γ_{ACS} (6.12) to find

$$\begin{aligned} \forall n \in \mathbb{N}, \quad \omega_{pwm}(t_n) = & \quad \omega(0) + \textstyle\sum_{k=0}^{n-1} \int_{t_k}^{t_{k+1}} \frac{\Gamma_{ACS}(\sigma)}{J} d\sigma, \\ = & \quad \omega(0) + \textstyle\sum_{k=0}^{n-1} \frac{\lambda_k \tau_k}{J}, \\ = & \quad \omega(0) + \textstyle\sum_{k=0}^{n-1} s(t_k)\dot{\omega}_{av}(1+\delta_\Gamma)\tau_k; \end{aligned} \tag{6.33}$$

where we use the definition of the uncertain λ_n from (6.30) and of τ_n from (6.13). Finally, with the definition of λ_n in (6.30), we observe that ω_{pwm} can be written as

$$\forall t \geq 0, \quad \omega_{pwm}(t) = \omega(0) + (1+\delta_\Gamma) \left(\sum_{k=0}^{n-1} \frac{s(t_k)\Gamma_{av}\tau_k}{J} + \begin{cases} s(t)\dot{\omega}_{av}(t-t_n) & ,t \in [t_n, t_n+\tau_n) \\ s(t)\dot{\omega}_{av}\tau_n & ,t \in [t_n+\tau_n, t_{n+1}) \end{cases} \right). \tag{6.34}$$

Between the parentheses we have the expression of the speed for a PWM with pulses of known height Γ_{av}. Notice that the value Γ_{av} used for the computation of τ_n is given and fixed. Hence under the assumption $\omega(0) = 0$, the angular speed generated by a PWM with unknown pulse height $\omega_{pwm}^{(\delta_\Gamma)}$ can be expressed as a function of ω_{pwm} by:

$$\omega_{pwm}^{(\delta_\Gamma)} = \dot{\alpha} = (1+\delta_\Gamma)\omega_{pwm}. \tag{6.35}$$

This last transformation leads to the closed-loop system in figure 6.8. We introduced δ_Γ, real time-invariant uncertainty on the delivered torque Γ_{ACS}. The transformations of the loop are now finished and figure 6.8 represents the initial closed-loop figure 6.3 but with a structure that allows performing IQC-based stability analysis with the toolbox LPVMAD.

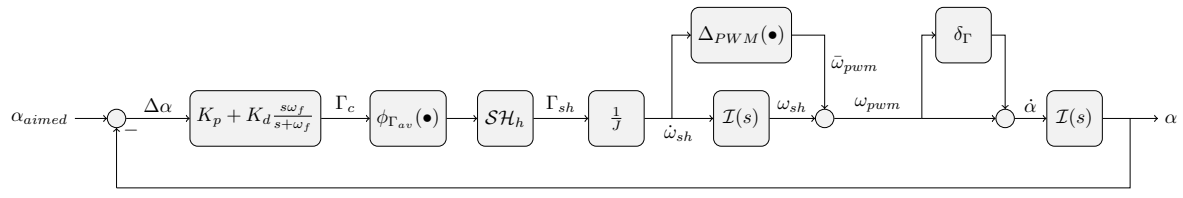

Figure 6.8: Closed-loop representation for analysis of the space launcher model as a sampled-data system

6.3.3 Transformed analysis model

The transformations we made to the original closed-loop analysis model led to the representation figure 6.8. In this figure, the PWM has been split into different blocks which are known to satisfy certain soft

IQC from the literature and readily implemented in LPVMAD. In figure 6.3, there was only one trouble making operator which was $\mathcal{P}$, the PWM. In figure 6.8, the PWM has been separated into four different blocks, we describe them in the following list.

- A saturation operator is used at the input of the nominal actuator. It is denoted by $\phi_{ACS}(\bullet)$ and defined as in (5.10-5.11). We will see later on that this nonlinearity alone is well suited to approximate the PWM.

- A sample-and-hold operator $\mathcal{SH}_h$ follows the saturation. It introduces the sampling effect observed in the definition of the PWM (6.12-6.13). Even if it is not a very "common" device in system analysis, $\mathcal{SH}_h$ can be modeled as a time-varying delay and this kind of operator can be described with IQC from the literature. See e.g. [Kao and Lincoln, 2004], [Kao and Rantzer, 2007]. In particular, systems with time-varying delays can be analyzed with the IQC toolbox LPVMAD.

- A nonlinear operator $\Delta_{PWM}(\bullet)$ is also introduced. Since its output $\bar{\omega}_{pwm}$ can be precisely defined in the time-domain, we can use the appropriate multiplier to capture its behavior and limit the conservatism of the stability test. Later on we will see that the construction of this operator also has a more mathematical explanation.

- Finally, an uncertain parameter δ_Γ is added to the closed-loop in order to model the unknown thrust, and so the unknown torque, produced by the thrusters. Since we consider that this force does not vary during a maneuver, this real parameter is considered to be time-invariant.

6.4 Stability analysis with soft IQC and LPVMAD

The model in the above paragraph is well suited for stability analysis with the IQC tool LPVMAD. Before analyzing the stability we are going to do the last transformations allowing the model to fit exactly in the IQC framework.

6.4.1 Model setup

The analysis model needs a few more transformations to fit in the IQC framework of LPVMAD.

Saturation First we modify the saturation $\phi_{ACS}(\bullet)$ as we already did for the first application in chapter 5 such that it is defined with the dead-zone operator $\psi_{ACS}(\bullet)$ defined in (5.36-5.37). This representation decomposes the system into a nominal path with unit gain and a perturbation path with the dead-zone $\psi_{ACS}(\bullet)$. For convenience, this setup is depicted again in figure 6.9. This configuration still exhibits the singularity we alluded to in paragraph 5.3.2. Basically, the problem is that the sector $(0, 1)$ that is generally used to represent the saturation nonlinearity also represents nonlinearities that can open the loop, resulting in a singularity if our open-loop system is not strictly stable. Here it is bypassed by the use an approximated sector bound $(0, 1 - \varepsilon)$ with $\varepsilon = 10^{-5}$.

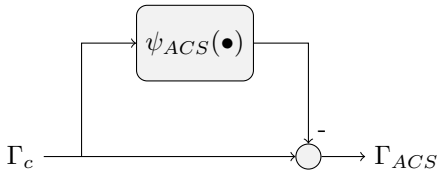

Figure 6.9: Block diagram of LFR of the saturation operator $\phi_{ACS}(\Gamma_c)$

Sample-and-hold Secondly, the closed-loop analysis model figure 6.8 contains a sample-and-hold operator $\mathcal{SH}_h$. It is used in the nominal actuator to model the sampling effect induced by the PWM. As mentioned before, such a device can be represented by a time-varying delay $D_{\tau(t)}$ where $\tau(t),\ t \geq 0$ is the value of the time-delay defined over each sampling period by

$$\forall n \in \mathbb{N}, \forall t \in T_n, \quad \tau(t) = t - t_n. \tag{6.36}$$

Once this time-varying time-delay $D_{\tau(t)} = \mathcal{SH}_h$ defined, the classical transformation to do is similar to the one done to the saturation operator. It is represented as in the setup of figure 6.10.

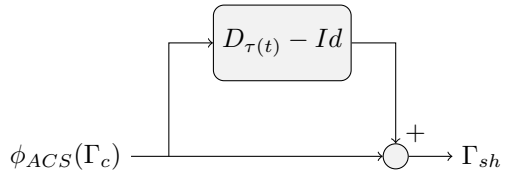

Figure 6.10: Block diagram of sample-and-hold $\mathcal{SH}_h$ in LFR

We see on the figure that the transformation separates a nominal path with gain 1 from the perturbation path with the operator $D_{\tau(t)} - Id$ where Id is the identity operator. The problem with $D_{\tau(t)} - Id$ is that it is not $\mathcal{L}_2$-gain bounded (see e.g. [Kao and Lincoln, 2004]). To subsume the operator $D_{\tau(t)} - Id$ to the IQC framework, we need to add an integrator at the input in order to define the operator

$$\Delta_\tau = (D_{\tau(t)} - Id) \circ \frac{1}{s} \tag{6.37}$$

with induced $\mathcal{L}_2$ gain bounded by the maximum value of τ over time as showed in [Kao and Lincoln, 2004]. According to its definition (6.36), the maximum value of the time-varying delay τ is h. As the introduction of this integrator on the input of $D_{\tau(t)} - Id$ modifies the operator, to represent $\mathcal{SH}_h$ with Δ_τ, we need to introduce a derivative filter in the system such that the effect of the integrator in Δ_τ is canceled out. In this setup, we can represent the time-varying delay as in figure 6.11. In this figure, we have ideal derivation so the block diagram is equivalent to figure 6.10.

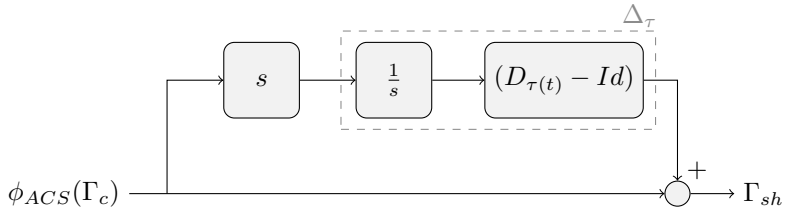

Figure 6.11: Block diagram of Δ_τ under LFR with ideal derivation

Thanks to the definition of the time-varying delay τ, the position of the filter at the input or at the output of Δ_τ does not matter. To recover the derivative of the output of Δ_τ, we use the derivative filter of the controller (6.7), the derivative filter $\mathcal{F}$ has the transfer function:

$$\mathcal{F}(s) = \frac{s\omega_f}{s + \omega_f}. \tag{6.38}$$

The block structure we take for the construction of the LFR and the analysis is depicted in figure 6.12. The representation of $D_{\tau(t)} - Id$ as $\mathcal{F}(s)\left[(D_{\tau(t)} - Id) \circ (1/s)\right]$ is an approximation but the appropriate choice of the filtering factor ω_f leads to a good representation of the effect of the delay over the closed-loop bandwidth thanks to the low-pass properties of the overall system.

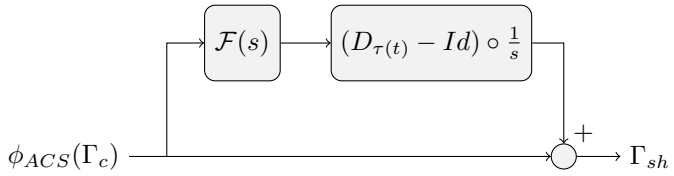

Figure 6.12: Block diagram of Δ_τ under LFR

Perturbation operator The third "trouble making" block in the closed-loop model is the operator Δ_{PWM} which was defined earlier to generate a "complement" $\bar{\omega}_{pwm}$ on the angular speed ω_{sh} to recover ω_{pwm}. We can define it as sector bounded nonlinearity. For that we need to find the appropriate α and β such that the nonlinearity Δ_{PWM} satisfies

$$\forall x \neq 0, \quad \alpha \leq \frac{\Delta_{PWM}(x)}{x} \leq \beta \text{ and } \Delta_{PWM}(0) = 0. \tag{6.39}$$

The definition of the sector bounds α and β can be obtained through the definition of the bounds of the ratio of $\bar{\omega}_{pwm}$ to $\dot{\omega}_{sh}$. From (6.28), we have for all $t \geq 0$ a $n \in \mathbb{N}$ for which $t \in T_n$ and the relationship

$$\frac{\bar{\omega}_{pwm}(t)}{\dot{\omega}_{sh}(t)} = \begin{cases} (\frac{\Gamma_{av}}{|\Gamma_c(t_n)|} - 1)(t - t_n) & ,\forall t \in [t_n, t_n + \tau_n), \\ (t_{n+1} - t) & ,\forall t \in [t_n + \tau_n, t_{n+1}). \end{cases} \tag{6.40}$$

holds when $|\Gamma_c(t_n)| \leq \Gamma_{av}$. In the case when $|\Gamma_c(t_n)| \geq \Gamma_{av}$, the ratio is equal to zero over T_n. From the definition of $\bar{\omega}_{pwm}/\dot{\omega}_{sh}$, we can establish the range of variations of the ratio. Notice that this ratio can be seen as the gain of the operator Δ_{PWM} since it is the ratio from output to input at all time instants. The ratio varies according to the continuous piecewise affine function of time defined in (6.40). As $|\Gamma_c(t_n)| < \Gamma_{av}$, the ratio increases with time over $[t_n, t_n + \tau_n)$ and decreases over $[t_n + \tau_n, t_{n+1})$. Hence it reaches a maximum

$$h - \tau_n$$

over each sampling period at $t = t_n + \tau_n$. The minimum absolute value is reached at the sampling instant $t = t_n$ or $t = t_{n+1}$ and is zero. Looking for the maximum and minimum of τ_n over $\mathbb{N}$ leads to the range of variation of the ratio:

$$\forall t \in \mathbb{R}_+, \exists n \in \mathbb{N}, t \in T_n, \quad \frac{\bar{\omega}_{pwm}(t)}{\dot{\omega}_{sh}(t)} \in [0, h]. \tag{6.41}$$

Consequently, in (6.39) we can set $\alpha = 0$ and $\beta = h$. When a nonlinearity satisfies a sector condition, we know it satisfies the IQC defined by the multiplier Π_{nlsb} defined in paragraph 4.5.3. Π_{nlsb} can be recovered very easily from (6.39) and reads as

$$\Pi_{nlsb} = \begin{bmatrix} -x\alpha\beta & x\frac{\alpha+\beta}{2} \\ x\frac{\alpha+\beta}{2} & -x \end{bmatrix} \tag{6.42}$$

where $x \geq 0$. The stability analysis of the system including Δ_{PWM} with IQC is feasible.

Uncertain torque Finally, the uncertainty δ_Γ we added to model the uncertainty that affects the torque generated by the thrusters is modeled as multiplicative relative time-invariant uncertainty and the setup figure 6.13 is suitable to find the LFR.

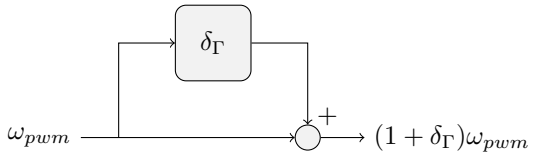

Figure 6.13: Introduction of the uncertainty δ_Γ

LFR representation of the system To have an overview of the model we will use for IQC analysis, we give in figure 6.14 a block diagram of closed-loop set up for robustness assessment with soft IQC and LPVMAD.

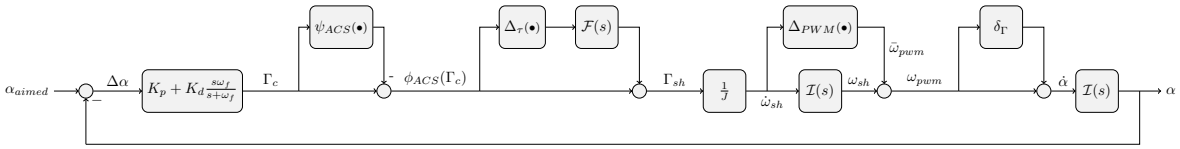

Figure 6.14: Transformed closed-loop model for IQC analysis

From this representation, it is easy to recast the system interconnection into the LFR with structured perturbation block $\Delta_{iqc,s}$ represented in figure 6.15. It is defined by:

$$\Delta_{iqc,s} = \begin{bmatrix} \psi_{ACS} & 0 & 0 & 0 \\ 0 & \Delta_\tau & 0 & 0 \\ 0 & 0 & \Delta_{PWM} & 0 \\ 0 & 0 & 0 & \delta_\Gamma \end{bmatrix}, \tag{6.43}$$

where the subscript iqc, s refers to "soft IQC". The nominal part of the LFR is denoted by $M_{iqc,s}$. Let us assume that (A_c, B_c, C_c, D_c) and (A_f, B_f, C_f, D_f) are state-space realizations of the controller and the derivative filter $\mathcal{F}$, respectively. To represent the integrators $\mathcal{I}(s)$, let us take the generalized form given in paragraph 6.2.1. A state-space realization of the linear transfer function $M_{iqc,s}$ in figure 6.15 is given by the equations

$$M_{iqc,s} : \begin{cases} \dot{x} = & Ax + Bw, \\ z = & Cx + Dw. \end{cases} \tag{6.44}$$

The state vector is given by

$$x = \begin{bmatrix} x_1 \\ x_2 \\ x_c \\ x_f \end{bmatrix} \tag{6.45}$$

where x_1 and x_2 are the states of the first and second integrator respectively, x_c is the state of the controller and x_f is the derivative filter state. The input and output vectors of $M_{iqc,s}$ have the same

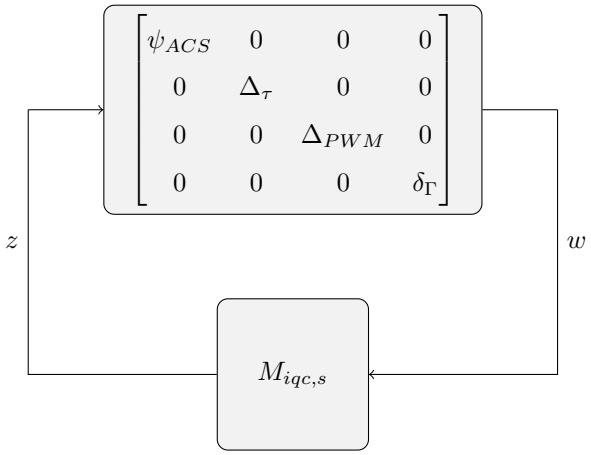

Figure 6.15: Structured LFR of analysis model for IQC analysis

structure as $\Delta_{iqc,s}$ and read as

$$z = \begin{bmatrix} z_\psi \\ z_\tau \\ z_{pwm} \\ z_\Gamma \end{bmatrix} \text{ and } w = \begin{bmatrix} w_\psi \\ w_\tau \\ w_{pwm} \\ w_\Gamma \end{bmatrix}, \tag{6.46}$$

so we have $w = \Delta_{iqc,s}(z)$. Finally, the matrices A, B, C and D defined as:

$$A = \begin{bmatrix} -\omega_d & -g_d\frac{D_c}{J} & g_d\frac{C_c}{J} & g_d\frac{C_f}{J} \\ g_d & -\omega_d & 0 & 0 \\ 0 & -B_c & A_c & 0 \\ 0 & -B_f D_c & B_f C_c & A_f \end{bmatrix}, \; B = \begin{bmatrix} -\frac{g_d}{J} & g_d\frac{D_f}{J} & 0 & 0 \\ 0 & 0 & g_d & g_d \\ 0 & 0 & 0 & 0 \\ -B_f & 0 & 0 & 0 \end{bmatrix},$$

$$C = \begin{bmatrix} 0 & -D_c & C_c & 0 \\ 0 & -D_f D_c & D_f C_c & C_f \\ 0 & -\frac{D_c}{J} & \frac{C_c}{J} & \frac{C_f}{J} \\ 1 & 0 & 0 & 0 \end{bmatrix} \text{ and } D = \begin{bmatrix} 0 & 0 & 0 & 0 \\ -D_f & 0 & 0 & 0 \\ -\frac{1}{J} & \frac{1}{J} & 0 & 0 \\ 0 & 0 & 1 & 0 \end{bmatrix}. \tag{6.47}$$

Notice that in the case where $\omega_d = 0$, we have $g_d = 1$, $x_1 = \omega_{sh}$ and $x_2 = \alpha$. If we do not have an ideal integral action i.e. $\omega_d > 0$, we consider that the states of the generalized integrators x_1 and x_2 are relevant approximations of the actual angular speed and attitude, respectively. Nevertheless, the subsequent analysis will be done for $\omega_d = 0$ since we used an approximated sector condition for ϕ_{ACS} as mentioned in the beginning of next paragraph.

The LFR is now set up. The last step before IQC analysis is to define properly the characteristics of the $\Delta_{iqc,s}$ block such that we can put them in LPVMAD.

6.4.2 Perturbations setup

The perturbation block $\Delta_{iqc,s}$ in (6.43) is made of four different operators whose key parameters are given below.

1. ψ_{ACS} is the dead-zone operator of (5.36-5.37). As before it is a memoryless nonlinearity in the sector $(0, 1)$ with odd and monotone characteristic, see e.g. figure 5.9. For the same reason as in section 5.3.2, we may have a singularity if the nominal part of the LFR, $M_{iqc,s}$, does not have all its poles with negative real part. As this is the case when $(g_d, \omega_d) = (1, 0)$, we will consider that ψ_{ACS} is in the sector $(0, 1 - \varepsilon)$ with $\varepsilon = 10^{-5} \ll 1$ as in section 5.3.2 at the price of an approximation of the dead-zone characteristic. The last feature of ψ_{ACS} that is relevant to the IQC tool is that it has finite incremental gain. In other words, it means that the characteristic of ψ_{ACS} depicted before in figure 5.9 has a finite maximum slope. For the dead-zone operator ψ_{ACS}, the maximum incremental gain is 1.

2. Δ_τ has bounded $\mathcal{L}_2$ induced gain thanks to the integrator in its definition (6.37) as showed by [Kao and Lincoln, 2004]. This gain is bounded by the maximum value of the time-delay τ from (6.36). Hence it has $\mathcal{L}_2$ gain h, the sampling period of the PWM operator. In reality, the sampling period h of the PWM is equal to 1 second so we aim to prove that the system is stable for this value.

3. Δ_{PWM}, is also considered as a memoryless sector bounded nonlinearity. We defined it to be belonging to the sector $(0, h)$.

4. δ_Γ is the uncertainty that affects the torque generated by the thrusters of the ACS Γ_{ACS}. For the study, it is considered that the torque value do not vary with time but is not exactly known. Hence it is determined from a nominal value set to $\Gamma_{av} = 380$ Nm affected by $\pm 30\%$ uncertainty. As a consequence, δ_Γ is considered to be in $[-0.3, +0.3]$.

All the parameters of the perturbation block have been given. The other parameters are gathered in table 6.1.

Table 6.1: System parameters

Inertia, J	22,500	kg.m^2
Natural frequency, ω_0	0.3	s^{-1}
Damping, ξ	1.0	-
Proportional Gain, K_p	$\omega_0^2 J$	kg.m^2.s^{-2}
Derivative Gain, K_d	$2\xi\omega_0 J$	kg.m^2.s^{-1}
Minimum pulse duration, τ_{min}	0	ms
Cut-off frequency of integrator, ω_d	0	s^{-1}
Pole of derivative filter, ω_f	2π	s^{-1}
Sector upper-bound approximation, ε	10^{-5}	-

One last remark can be done. It is about the saturation level of ϕ_{ACS} which is not taken as a parameter of the problem by the IQC tool. By definition, the saturation level of ϕ_{ACS} (5.10-5.11) is the nominal value of the available torque Γ_{av}, this parameter is also the upper and lower limit of the dead-zone ψ_{ACS} (5.36-5.37). However, it does not enter as a parameter of the multiplier Π_{nlom} of paragraph 9.2 that we use to describe ψ_{ACS} with LPVMAD. It means that the value of Γ_{av} is not an information about ψ_{ACS}

contained by Π_{nlom}. Hence the stability result which is given with this method is valid for any saturation level.
We can now perform the robustness analysis with the IQC tool LPVMAD.

6.4.3 Robust stability analysis with soft IQC

To represent the results of the stability analysis, we define a "feasibility region" of the IQC stability test in the (δ_Γ, h) plane. This region represents a set of relative uncertainty on the available torque δ_Γ and sampling period h within which we are able to prove the stability of the LFR $(M_{iqc,s}, \Delta_{iqc,s})$ with LPVMAD. To guarantee the stability of the system with its "nominal" uncertain parameters, we would like be able to prove the stability for the case:

$$\begin{cases} \delta_\Gamma \in [-30, +30]\%, \\ h = 1 \text{ s}. \end{cases} \tag{6.48}$$

In other words, we would like the stability test resulting from the application of the IQC stability theorem 4 to be feasible for the perturbation parameters in (6.48). It is important to keep in mind that if the stability test is feasible, then the system is guaranteed to be stable. Reversely, if the stability test is unfeasible, it does not say anything about the stability for the studied setup. This is why we speak about "feasibility region" and not "stability region". The feasibility region is a pessimistic estimate of the "stability region". It is due to the conservatism induced by the multipliers which are used to define IQC describing the perturbation block of the LFR.
We can now define the IQC which is satisfied by $\Delta_{iqc,s}$. In our application, the multiplier $\Pi_{iqc,s}$ defines an IQC satisfied by $\Delta_{iqc,s}$ that is

$$\forall \hat{v} \in \mathcal{L}_2, \quad \int_{-\infty}^{+\infty} \begin{bmatrix} \hat{z}(j\omega) \\ \widehat{\Delta_{iqc,s}(z)}(j\omega) \end{bmatrix}^* \Pi_{iqc,s}(\varphi, d, j\omega) \begin{bmatrix} \hat{z}(j\omega) \\ \widehat{\Delta_{iqc,s}(z)}(j\omega) \end{bmatrix} d\omega \geq 0, \tag{6.49}$$

where the IQC multiplier $\Pi_{iqc,s}$ is defined as

$$\Pi_{iqc,s}(\varphi, d, j\omega) = \left[\begin{array}{cccc|cccc} \Pi^{(11)}_{nlom} & 0 & 0 & 0 & \Pi^{(12)}_{nlom} & 0 & 0 & 0 \\ 0 & \Pi^{(11)}_{dmii} & 0 & 0 & 0 & \Pi^{(12)}_{dmii} & 0 & 0 \\ 0 & 0 & \Pi^{(11)}_{nlsb} & 0 & 0 & 0 & \Pi^{(12)}_{nlsb} & 0 \\ 0 & 0 & 0 & \Pi^{(11)}_{ltis} & 0 & 0 & 0 & \Pi^{(12)}_{ltis} \\ \hline \Pi^{(21)}_{nlom} & 0 & 0 & 0 & \Pi^{(22)}_{nlom} & 0 & 0 & 0 \\ 0 & \Pi^{(21)}_{dmii} & 0 & 0 & 0 & \Pi^{(22)}_{dmii} & 0 & 0 \\ 0 & 0 & \Pi^{(21)}_{nlsb} & 0 & 0 & 0 & \Pi^{(22)}_{nlsb} & 0 \\ 0 & 0 & 0 & \Pi^{(21)}_{ltis} & 0 & 0 & 0 & \Pi^{(22)}_{ltis} \end{array}\right] \in \mathbb{RH}_\infty^{8\times 8}, \tag{6.50}$$

and z is

$$z = \begin{bmatrix} z_\psi \\ z_\tau \\ z_{pwm} \\ z_\Gamma \end{bmatrix} \in \mathbb{R}^4. \tag{6.51}$$

Since $\Delta_{iqc,s}$ has 4 uncertainty channels, $\Pi_{iqc,s}(\varphi, d)$ is in $\mathbb{RH}_\infty^{8\times 8}$. This multiplier is obtained by diagonal augmentation (see paragraph 4.4.2) of the multipliers defining IQC for each ones of the operators in $\Delta_{iqc,s}$:

- Π_{nlom} (5.63) defines an IQC satisfied by ψ_{ACS},
- Π_{dmii} (9.13) defines an IQC satisfied by Δ_τ,
- Π_{nlsb} (4.86) defines an IQC satisfied by Δ_{PWM},
- Π_{ltis} (5.60) defines an IQC satisfied by δ_Γ.

In (6.50), the dependence of the sub-blocks of the multiplier in the parameters and the frequency is not mentioned for simplicity. Their definition can be found in chapters 4 or 9 and in [Köroglu et al., 2008]. We consider two dynamic multipliers Π_{nlom} and Π_{ltis}. φ denotes the poles of these multipliers and d contains the order of the transfer function H defined in paragraph 5.5.2 and involved in the definition of Π_{nlom} and Π_{ltis}. The poles and degrees used during the analysis are given in table 6.2. They can be defined independently from one uncertainty to another. The setup of the IQC tool is summed up in table 6.2. For precisions about the dynamic multipliers construction, the reader is invited to look at the IQC section of chapter 5.

Table 6.2: IQC tool setup for stability analysis of space launcher model with PWM actuator and torque uncertainties

Dead-zone		Uncertain torque	
Π_{nlom}		Π_{ltis}	
d_ψ	φ_ψ	d_Γ	φ_Γ
2 and 3	-1	2 and 3	-1

Since the problem has reduced size, we can set the multipliers used to describe the dead-zone nonlinearity (Π_{nlom}) and the uncertain torque (Π_{ltis}) to be dynamic. According to the definition of H (5.64), it means that $d \geq 2$. Indeed, we have this degree of freedom given by the definition of Π_{nlom} and Π_{ltis} in appendix A and it can help us to reduce the conservatism of the feasibility test. During the analysis and as presented in table 6.2, we considered that the d parameter of the transfer function basis from paragraph 5.5.2 was the same for both multipliers i.e. $d_\psi = d_\Gamma = d$ and compared the results obtained with $d = 2$ and $d = 3$. In this framework, the computation of the feasibility region in the (δ_Γ, h) plane on figures 6.16 takes less than 5 minutes in total. It is done on a 64 bits desktop PC with Intel® Core i7 processor at 2.80 GHz for $d = 2$ and $d = 3$ and 100 different values of δ_Γ. Thus we could have computed results for multipliers with greater orders but it seemed that it did not help to reduce the conservatism further. We represent two feasibility regions in the (δ_Γ, h) plane, the first one on figure 6.16 shows the stability region obtained for $d = 2$. Under the dashed curve, the $\mathcal{L}_2$ stability is guaranteed. The second feasibility region was computed for $d = 3$ and is depicted with the solid line. We observe that changing the order

of the dynamic multipliers from 2 to 3 allowed to enlarge the domain of the (δ_Γ, h) plane for which the stability can proved i.e. it reduces the conservatism.
Concerning the poles of the basis transfer functions, we intended to "optimize" their values and determine whether some combinations different from their default values $(\varphi_\psi, \varphi_\Gamma) = (-1, -1)$ give less conservative results or not. Through a grid search we observed no change in the feasibility regions resulting from the LMI tests when changing the poles φ_ψ and φ_Γ. Consequently, we kept the default values of φ_ψ and φ_Γ during the analysis.

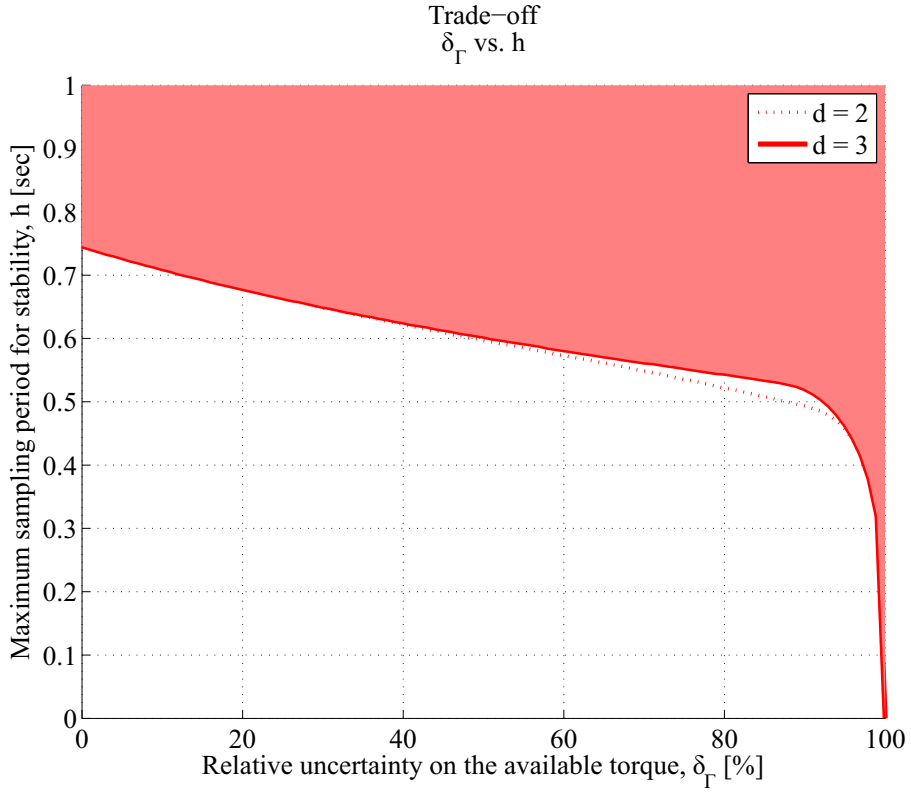

Figure 6.16: Feasibility region found in the setup of table 6.2

The feasibility domain depicted in the figure does not include the point for which we wanted to guarantee the stability of the system i.e. $(\delta_\Gamma, h) = (30\%, 1\text{s})$. Of course it does not mean that this point is unstable but only that we cannot prove the stability with $M_{iqc,s}$, $\Delta_{iqc,s}$, $\Pi_{iqc,s}$ and the IQC stability theorem. The conservatism of the stability test may come from the rough modeling of Δ_{PWM} as a nonlinearity in a sector. Indeed, we performed analytical definition of the input-output relationship of Δ_{PWM} but only described it as being bounded by a sector. This choice is motivated by the fact that using a bound, rather than an approximation, gives conservative but rigorous conditions. However, it does not take into account the very precise definition of Δ_{PWM} we had. Thus the IQC defined by Π_{nlsb} from paragraph 4.5.3 do not capture some of the features of Δ_{PWM} we had in the definition. This drawback could be avoided by the use of other multipliers describing Δ_{PWM} which we could conically combine with Π_{nlsb}. Another drawback of the method used in this section is that we had to remove the threshold from the definition of the PWM to be able to define rigorously Δ_{PWM}. It resulted in an easier analysis while causing a loss of representativeness of the analysis model.
Nevertheless, stability can be proved for values of both h and δ_Γ which are already rather large. Indeed, we know that the actual stability bound for the relative uncertainty on the torque denoted is $\pm 100\%$ since $\delta_\Gamma < -1$ changes the sign of the feedback and such case results in an unstable closed-loop. Hence

proving stability of the system for relatively large values of h (e.g. $>$ 600ms like here) for δ_Γ close to 1 shows that the perturbation sub-block that affects more the stability may not be Δ_{PWM}.
However, we can still expect a reduction of the conservatism by improving the multiplier defining the IQC that captures the operator Δ_{PWM}. A technique for the analysis of the pulse-modulated system with hard IQC will be investigated. Indeed, we will see in section 6.6 that the above closed-loop model is very similar to a more formally defined one that will be considered for an analysis with hard IQC. It confirms the assumption hinted in the present section. Low-pass systems with pulse-modulated actuation signals are not driven by the high harmonics of the pulse-modulated signals but essentially by their low-frequency components. Hence we are encouraged to keep on considering this representation of the PWM with two separated operators. Here we had the nominal actuator $\mathcal{SH}_h(\phi_{ACS}(\bullet))$ and Δ_{PWM}, later on we will define Δ_{PWM} with different notations but with a completely similar physical meaning.
In the following section, we analyze the setup of figure 6.8 with a method based on absolute stability theory.

6.5 Stability analysis as a sampled-data system

The analysis method of this section is presented in [Seuret and Gomes Da Silva Jr, 2011]. We aim to use it to perform a stability analysis of the model with PWM presented in figure 6.3 that was used in the previous section for soft-IQC based stability analysis. It will allow us to obtain another stability result about the closed-loop system with PWM actuator. The paper provides a sufficient asymptotic stability condition for sampled-data system with saturated input. We limit the stability theorem to the case of constant sampling periods but we will use an extension of it for uncertain systems. For the analysis of such sampled-data systems, works such as those of [Fridman et al., 2005], [Mirkin, 2007] and [Naghshtabrizi et al., 2008] could also be used.

6.5.1 Stability analysis of sampled-data systems with constrained inputs

Below is a summed up formulation of the problem addressed in [Seuret and Gomes Da Silva Jr, 2011]. Originally, it aims to synthesize a controller for a sampled-data system with saturated input that is robust to sampling period uncertainties. Generally, a sampled-data system is a system that uses samples of its continuous input to compute its continuous output. For our study, the result is simplified due to the assumption that the sampling period remains constant equal to h as mentioned earlier on in paragraph 6.2.3.
Let us consider the LTI system M_{sd} with state x and constrained sampled-data input depicted in figure 6.17, where the subscript "sd" stands for "sampled-data". This LFR-like representation involves the sample-and-hold operator $\mathcal{SH}_h : \mathcal{L}^n \to \mathcal{L}^n$, a gain $K \in \mathbb{R}^{m\times n}$ for static state-feedback and the saturation operator $\phi_{ACS} : \mathcal{L}^m \to \mathcal{L}^m$ already defined in (5.10-5.11). Considering the notations given in section 6.2 where t_k is a sampling instant and T_k is the sampling period $[t_k, t_{k+1})$, the input-output relationship of the sample-and-hold operator $\mathcal{SH}_h$ with sampling period h can be defined in the general multi-input multi-output case as

$$\forall x \in \mathcal{L}^m, \forall k \in \mathbb{N}, \forall t \in T_k, \quad \mathcal{SH}_h(x(t)) = x(t_k) = x_k. \tag{6.52}$$

From figure 6.17, we observe that the LTI system output is the continuous-time state vector in the context of the paper. Hence, we can define the state-space equations of M_{sd} to be

$$\begin{cases} \dot{x}(t) = & Ax(t) + Bu(t), \\ y(t) = & x(t), \end{cases} \tag{6.53}$$

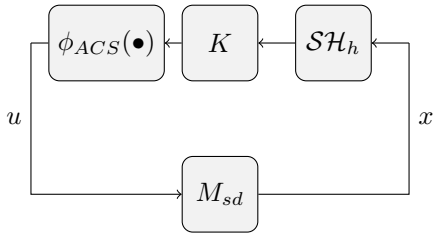

Figure 6.17: Model setup for analysis as a sampled-data system

where we have $A \in \mathbb{R}^{n\times n}$ and $B \in \mathbb{R}^{n\times m}$. The state-space equations (6.53) are associated to the definition of the constrained piecewise constant signal u given by

$$\forall k \in \mathbb{N}, \forall t \in T_k, \quad u(t) = \phi_{ACS}(K\mathcal{SH}_h(x)(t)) = \phi_{ACS}(Kx(t_k)). \tag{6.54}$$

The definition of u above allows recasting the state-space equation (6.53) into

$$\forall k \in \mathbb{N}, \forall t \in T_k, \quad \dot{x}(t) = Ax(t) + B\phi_{ACS}(Kx(t_k)). \tag{6.55}$$

As before in paragraph 6.4.1, the piecewise constant signal which outputs $\mathcal{SH}_h$ in (6.55) can be expressed as the output of a time-varying delay $D_{\tau(t)}$ with the delay τ defined by

$$\forall k \in \mathbb{N}, \forall t \in T_k, \quad \tau(t) = t - t_k. \tag{6.56}$$

Indeed, we have the relation

$$\forall k \in \mathbb{N}, \forall t \in T_k, \quad x(t_k) = x(t - \tau(t)). \tag{6.57}$$

that holds for τ from (6.56).

In such a context, theorem 2 from [Seuret and Gomes Da Silva Jr, 2011] defines an ellipsoid $\epsilon(P)$ (6.58) within which any initial state vector $x_0 \in \epsilon(P)$ will induce a trajectory of the system converging asymptotically to the origin:

$$\epsilon(P) = \left\{ x \in \mathbb{R}^n \middle| x^T P x \leq 1 \right\}, \tag{6.58}$$

where $P \in \mathbb{R}^{n\times n}$ and $P > 0$.

Theorem 9 ([Seuret and Gomes Da Silva Jr, 2011]) *For a given $h > 0$, assume that there exist, $\tilde{P} \in \mathbb{R}^{n\times n}$ with $\tilde{P} > 0$, $R \in \mathbb{R}^{n\times n}$ with $R > 0$, $S_1 \in \mathbb{R}^{n\times n}$ symmetric, $X \in \mathbb{R}^{n\times n}$ symmetric, $U \in \mathbb{R}^{m\times m}$ with $U > 0$ and diagonal, $G \in \mathbb{R}^{m\times n}$, $Y \in \mathbb{R}^{n\times n}$, $S_2 \in \mathbb{R}^{n\times n}$ and $N \in \mathbb{R}^{(3m+n)\times n}$ split into four matrices such that*

$$N = \begin{bmatrix} N_1^T & N_2^T & N_3^T & N_4^T \end{bmatrix}^T, N_{1,2,3} \in \mathbb{R}^{m\times n} \text{ and } N_4 \in \mathbb{R}^{n\times n}$$

satisfying

$$\begin{cases} \Psi^{(1)} = & \Pi_1 + h(\Pi_2 + \Pi_3) < 0 \\ \Psi^{(2)} = & \begin{bmatrix} \Pi_1 - h\Pi_3 & hN \\ hN^T & -hR \end{bmatrix} < 0 \\ \Psi^{(3)}(\Gamma_{av}^{(j)}) = & \begin{bmatrix} \tilde{P} & ((KY)_j - G_j)^T \\ (KY)_j - G_j & (\Gamma_{av}^{(j)})^2 \end{bmatrix} \geq 0, \forall j \in \{1, \ldots, m\} \end{cases} \tag{6.59}$$

with $(KY)_j$ *and* G_j *the* j^{th} *rows of* KY *and* G*, respectively. (6.59) takes into account the definitions:*

$$\Pi_1 = He\left(\begin{bmatrix} \eta AY - N_1 & \eta BKY + N_1\tilde{P} & -\eta Y & -\eta BU \\ -N_2 - S_2^T & N_2 + S_2^T & 0 & 0 \\ AY - N_3 & BKY + N_3 & -Y & -BU \\ -N_4 & G + N_4 & 0 & 0 \end{bmatrix}\right) + \begin{bmatrix} -S_1 & S_1 & 0 & 0 \\ S_1 & -S_1 & 0 & 0 \\ 0 & 0 & 0 & 0 \\ 0 & 0 & 0 & -2U \end{bmatrix}, \text{ with } \eta > 0,$$

$$\Pi_2 = He\left(\begin{bmatrix} 0 & 0 & 0 & 0 \\ 0 & 0 & 0 & 0 \\ S_1 & S_2 - S_1 & 0 & 0 \\ 0 & 0 & 0 & 0 \end{bmatrix}\right) + \begin{bmatrix} 0 & 0 & 0 & 0 \\ 0 & 0 & 0 & 0 \\ 0 & 0 & R & 0 \\ 0 & 0 & 0 & 0 \end{bmatrix},$$

$$\Pi_3 = \begin{bmatrix} 0 & 0 & 0 & 0 \\ 0 & X & 0 & 0 \\ 0 & 0 & 0 & 0 \\ 0 & 0 & 0 & 0 \end{bmatrix} \text{ where } He(X) = X + X^T.$$

(6.60)

Then for all initial conditions x_0 *belonging to the ellipsoidal set* $\epsilon(P)$ *from (6.58) defined by* $P = (Y^T)^{-1}\tilde{P}Y^{-1}$*, the corresponding trajectories of the system (6.55) converge asymptotically to the origin for the sampling* $h > 0$*.*

6.5.2 Stability analysis of uncertain sampled-data systems with constrained inputs

We observe that the constraints in (6.59) are bilinear matrix inequalities due to the parameter η in the definition of Π_1. If η is fixed, the constraints become LMI and so accessible to the usual numerical solvers. In particular, (6.59) are linear in the A and B matrices of (6.55) the LMI. Hence we can ensure stability of the system with uncertain non-repeated parameters with the same argument as for theorem 8 that uses [Boyd and Yang, 1989]. As long as we have a linear rational dependence of the state matrices on the uncertain non repeated parameters, we can look for $\tilde{P}$, R, S_1, S_2, G, N, X, Y, U that satisfy the constraints (6.59) at all the vertices of the parameter box.

To express this extended result, let us consider the vector $\theta \in \text{Co}(\mathcal{V}_\theta) \subset \mathbb{R}^p$ in which we gather the p uncertain parameters of the system. Assuming that the parameters in θ vary in a box, the set $\mathcal{V}_\theta$ collects the 2^p vertices of the set of feasible values of θ and Co denotes the convex hull. The state-space equation

derived from (6.55) is

$$\forall k \in \mathbb{N}, \forall t \in T_k, \quad \dot{x}(t) = A(\theta)x(t) + B(\theta)\phi_{ACS}(Kx(t_k)), \theta \in \mathrm{Co}(\mathcal{V}_\theta). \tag{6.61}$$

In the manner of paragraph 5.5.3, we can evaluate $A(\theta)$ and $B(\theta)$ at each one of the 2^p vertices $\mathcal{V}_\theta$ to define the system vertices $(A_l, B_l), l \in \{1, \ldots, 2^p\}$. Then if we can find one combination of matrices $\tilde{P}$, R, S_1, S_2, G, N, X, Y, U that satisfy the LMI for all the $(A_l, B_l), l \in \{1, \ldots, 2^p\}$, then the stability of the sampled-data system with constrained inputs and uncertain parameters in $\mathrm{Co}(\mathcal{V}_\theta)$ is proved over the region of attraction $\epsilon(P)$ (6.58). The theorem extension reads as follow.

Theorem 10 (Extension to uncertain systems) *For a given $h > 0$, assume that there exist, $\tilde{P} \in \mathbb{R}^{n\times n}, \tilde{P} > 0$, $R \in \mathbb{R}^{n\times n}, R > 0$, $S_1 \in \mathbb{R}^{n\times n}$ symmetric, $X \in \mathbb{R}^{n\times n}$ symmetric, $U \in \mathbb{R}^{m\times m}, U > 0$ diagonal, $G \in \mathbb{R}^{m\times n}$, $Y \in \mathbb{R}^{n\times n}$, $S_2 \in \mathbb{R}^{n\times n}$ and $N \in \mathbb{R}^{(3m+n)\times n}$ split into four matrices such that*

$$N = \begin{bmatrix} N_1^T & N_2^T & N_3^T & N_4^T \end{bmatrix}^T, N_{1,2,3} \in \mathbb{R}^{m\times n} \text{ and } N_4 \in \mathbb{R}^{n\times n}$$

satisfying

$$\forall l \in \{1, \ldots, 2^p\}, \begin{cases} \Psi_l^{(1)} = & \Pi_1^{(l)} + h(\Pi_2^{(l)} + \Pi_3^{(l)}) < 0 \\ \Psi_l^{(2)} = & \begin{bmatrix} \Pi_1^{(l)} - h\Pi_3^{(l)} & hN \\ hN^T & -hR \end{bmatrix} < 0 \\ \Psi_l^{(3)}(\Gamma_{av}^{(j)}) = & \begin{bmatrix} \tilde{P} & ((KY)_j - G_j)^T \\ (KY)_j - G_j & (\Gamma_{av}^{(j)})^2 \end{bmatrix} \geq 0, \forall j \in \{1, \ldots, m\} \end{cases} \tag{6.62}$$

with $(KY)_j$ and G_j the j^{th} rows of KY and G, respectively. (6.59) takes into account the definitions:

$$\begin{aligned} \Pi_1^{(l)} = & \; He\left(\begin{bmatrix} \eta A_l Y - N_1 & \eta B_l KY + N_1 P & -\eta Y & -\eta B_l U \\ -N_2 - S_2^T & N_2 + S_2^T & 0 & 0 \\ A_l Y - N_3 & B_l KY + N_3 & -Y & -B_l U \\ -N_4 & G + N_4 & 0 & 0 \end{bmatrix}\right) + \begin{bmatrix} -S_1 & S_1 & 0 & 0 \\ S_1 & -S_1 & 0 & 0 \\ 0 & 0 & 0 & 0 \\ 0 & 0 & 0 & -2U \end{bmatrix}, \text{ with } \eta > 0, \\ \Pi_2^{(l)} = & \; He\left(\begin{bmatrix} 0 & 0 & 0 & 0 \\ 0 & 0 & 0 & 0 \\ S_1 & S_2 - S_1 & 0 & 0 \\ 0 & 0 & 0 & 0 \end{bmatrix}\right) + \begin{bmatrix} 0 & 0 & 0 & 0 \\ 0 & 0 & 0 & 0 \\ 0 & 0 & R & 0 \\ 0 & 0 & 0 & 0 \end{bmatrix}, \\ \Pi_3^{(l)} = & \begin{bmatrix} 0 & 0 & 0 & 0 \\ 0 & X & 0 & 0 \\ 0 & 0 & 0 & 0 \\ 0 & 0 & 0 & 0 \end{bmatrix} \text{ where } He(X) = X + X^T. \end{aligned} \tag{6.63}$$

Then for all initial conditions x_0 belonging to the ellipsoidal set $\epsilon(P)$ from (6.58) defined by $P =$

$(Y^T)^{-1}\tilde{P}Y^{-1}$, *the corresponding trajectories of the system (6.61) converge asymptotically to the origin for the given sampling period* $h > 0$.

6.5.3 Closed-loop transformation

The system obtained after the transformation of the PWM into the combination of a nominal actuator and a perturbation operator Δ_{PWM} is depicted in figure 6.8. We observe that the loop setup is very similar to the setup of theorem 10 pictured figure 6.17. Indeed, $\mathcal{SH}_h$ and ϕ_{ACS} are used in our representation. Hence it should be possible to fall into the scope of theorem 10 with few transformations and so to perform the analysis of the model as an uncertain sampled-data system with constrained inputs.

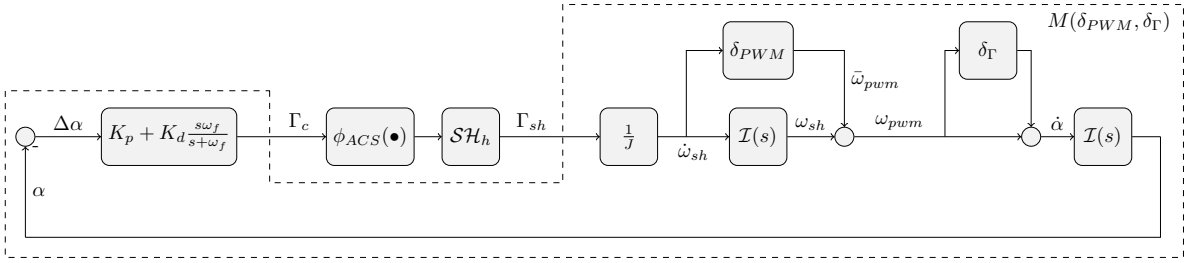

Figure 6.18: Separation of the nominal part of the closed-loop

To get the expression of the K matrix of the LFR setup figure 6.17, we express the state-space matrices of $M(\delta_{PWM}, \delta_\Gamma)$ represented figure 6.18. For this we consider that the perturbation blocks Δ_{PWM} and δ_Γ are uncertain parameters. Immediately, as δ_Γ is defined as an uncertain time-invariant parameter it fits into the representation we want to obtain. Secondly, to cover all the feasible trajectories of the output of Δ_{PWM}, we consider it as a time-varying parameter denoted by $\delta_{PWM}(t)$. The characterization of δ_{PWM} can be obtained by evaluating the ratio of the output of Δ_{PWM} to its input $\dot{\omega}_{sh}$. It has already been done in paragraph 6.4.2 (6.41) when we defined the sector bounds of Δ_{PWM}. The ranges of variations of the parameters δ_{PWM} and δ_Γ will be given later on. For now, we have to express the state matrices of the operator from Γ_{sh} to Γ_c to determine the parameter dependent state-space equations of $M(\delta_{PWM}, \delta_\Gamma)$ on figure 6.18. For the stability analysis, the performance input α_{aimed} and output α are void. We consider the generalized integrator $\mathcal{I}(s)$ defined in paragraph 6.2.1 instead of the ideal integrators as in figure 6.18. For convenience, we give the transfer function of the generalized integrator:

$$\mathcal{I}(s) = \frac{g_d}{s + \omega_d}. \tag{6.64}$$

To advance gradually, the first relationships we look for are the state-space equations of the operator from Γ_{sh} to α as it contains the trouble making parameters δ_{PWM} and δ_Γ. This transfer function is referred to as the dynamic model (even though it contains a representation of the kinematics too) and we denote it by the subscript "d". x_1 and x_2 are the state variables of the first and second integrator $\mathcal{I}(s)$, respectively. We can define $(A_d(\delta), B_d(\delta), C_d, 0)$ a state-space realization of the dynamic model as

$$A_d(\delta) = \begin{bmatrix} -\omega_d & 0 \\ g_d(1+\delta_\Gamma) & -\omega_d \end{bmatrix}, \quad B_d(\delta) = \frac{g_d}{J} \begin{bmatrix} 1 \\ \delta_{PWM}(1+\delta_\Gamma) \end{bmatrix}, \quad C_d = \begin{bmatrix} 0 & 1 \end{bmatrix}; \tag{6.65}$$

The state matrices of the dynamic model depend on the parameters δ_{PWM} and δ_Γ gathered in

$$\delta = \begin{bmatrix} \delta_{PWM} \\ \delta_\Gamma \end{bmatrix} \in \mathcal{U} \subset \mathbb{R}^2, \tag{6.66}$$

where $\mathcal{U}$ is a rectangle of $\mathbb{R}^2$ and we omit deliberately the dependence of δ_{PWM} in t. We can give the state-space equations

$$\begin{cases} \dot{x}_d = & A_d(\delta)x_d + B_d(\delta)\Gamma_{sh} \\ \alpha = & C_d x_d, \end{cases} \tag{6.67}$$

and the definition of state vector

$$x_d = \begin{bmatrix} x_1 \\ x_2 \end{bmatrix} \in \mathbb{R}^2. \tag{6.68}$$

We can now express the state-space matrices of the operator $M(\delta_{PWM}, \delta_\Gamma)$ from Γ_{sh} to Γ_c. Let us assume that (A_c, B_c, C_c, D_c) is the state-space realization of the controller and x_c is its state variable, we have

$$A(\delta) = \begin{bmatrix} A_d(\delta) & 0 \\ -B_c C_d & A_c \end{bmatrix}, \quad B(\delta) = \begin{bmatrix} B_d(\delta) \\ 0 \end{bmatrix}, \quad C = \begin{bmatrix} -D_c C_d & C_c \end{bmatrix}, \tag{6.69}$$

the matrices in

$$M(\delta_{PWM}, \delta_\Gamma) : \begin{cases} \dot{x} = & A(\delta)x + B(\delta)\Gamma_{sh} \\ \Gamma_c = & Cx, \end{cases} \tag{6.70}$$

where the state vector x is

$$x = \begin{bmatrix} x_1 \\ x_2 \\ x_c \end{bmatrix} = \begin{bmatrix} x_d \\ x_c \end{bmatrix} \in \mathbb{R}^3. \tag{6.71}$$

Notice that since the result in [Seuret and Gomes Da Silva Jr, 2011] takes into account the presence of the time-varying delay $\mathcal{SH}_h$, the derivative filter from figure 6.12 is not needed here. From the matrices in (6.69) and the state-space equations in (6.70), we can fit our closed-loop model in the framework of figure 6.17. This is done by setting $K = C$ with C from (6.69) and defining the output of $M(\delta_{PWM}, \delta_\Gamma)$ from (6.70) to be x instead of Γ_c. This is possible because the sampling can be done on the state vector or on the output as the matrix C of (6.69) does not vary with time i.e.

$$\mathcal{SH}_h(Cx) = C\mathcal{SH}_h(x). \tag{6.72}$$

Setting $K = C$ ensures the feedback of the attitude α and the angular speed ω. In addition to that, we also have $\mathcal{SH}_h(\phi_{ACS}) = \phi_{ACS}(\mathcal{SH}_h)$. Finally, in the setup of figure 6.17, the system can be represented by figure 6.19. The system derived from $M(\delta)$ with the state vector as output is denoted by $M_{sd}(\delta)$. The system is now ready to be analyzed.

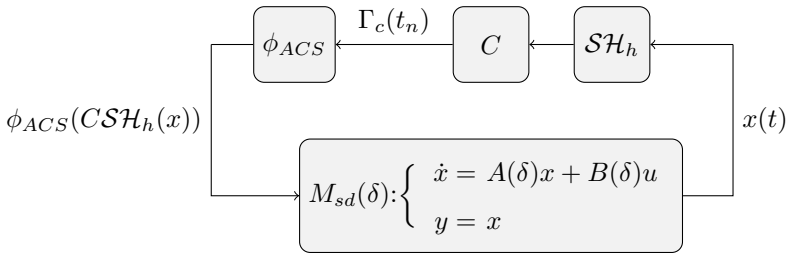

Figure 6.19: Model setup for analysis of the uncertain sampled-data system

6.5.4 Vertices computation for the parameter dependent "open-loop"

To apply theorem 10, we need to compute the system vertices of the open-loop operator $M_{sd}(\delta)$ of figure 6.19. $M_{sd}(\delta)$ is a parameter dependent system defined with the same A and B matrices as $M(\delta)$ from (6.70) but with output the state vector in place of the torque command Γ_c. The $A(\delta)$ and $B(\delta)$ matrices of $M(\delta)$, and so of $M_{sd}(\delta)$, depend on the two parameters of δ, δ_{PWM} and δ_Γ. For this analysis model, the dependence of the state-space matrices in the parameters is multi-affine so the set containment relationship (5.57) is valid. The vertices of the parameter box are gathered in $\mathcal{V}_\delta$. We can evaluate the matrices $A(\delta)$ and $B(\delta)$ for the parameter combinations in $\mathcal{V}_\delta$ (6.73) to determine four vertex systems $\mathcal{V}_{M_{sd}(\delta)}$ (6.74). As the problem has small dimension, we can give the expressions of the parameter vectors in $\mathcal{V}_\delta$

$$\mathcal{V}_\delta = \left\{ \underbrace{\begin{bmatrix} \delta_{PWM}^{(min)} \\ \delta_\Gamma^{(min)} \end{bmatrix}}_{\delta_1}, \underbrace{\begin{bmatrix} \delta_{PWM}^{(min)} \\ \delta_\Gamma^{(max)} \end{bmatrix}}_{\delta_2}, \underbrace{\begin{bmatrix} \delta_{PWM}^{(max)} \\ \delta_\Gamma^{(min)} \end{bmatrix}}_{\delta_3}, \underbrace{\begin{bmatrix} \delta_{PWM}^{(max)} \\ \delta_\Gamma^{(max)} \end{bmatrix}}_{\delta_4} \right\}; \tag{6.73}$$

and of the systems in $\mathcal{V}_{M_{sd}(\delta)}$

$$\mathcal{V}_{M_{sd}(\delta)} = \left\{ \underbrace{(A(\delta_1), B(\delta_1))}_{(A_1,B_1)}, \underbrace{(A(\delta_2), B(\delta_2))}_{(A_2,B_2)}, \underbrace{(A(\delta_3), B(\delta_3))}_{(A_3,B_3)}, \underbrace{(A(\delta_4), B(\delta_4))}_{(A_4,B_4)} \right\}; \tag{6.74}$$

We have $2^2 = 4$ vertices for our polytope of models. The (A_l, B_l), $l \in \{1, \ldots, 2^2\}$ matrices defined in (6.74) are the ones required to use theorem 10. To perform the feasibility test of the LMI set, we need to determine the range of variations of the parameters. This is determining $\delta_{PWM}^{(min)}$, $\delta_{PWM}^{(max)}$, $\delta_\Gamma^{(min)}$ and $\delta_\Gamma^{(max)}$ such that

$$\begin{cases} \forall t, \delta_{PWM}(t) \in & [\delta_{PWM}^{(min)}, \delta_{PWM}^{(max)}], \\ \delta_\Gamma \in & [\delta_\Gamma^{(min)}, \delta_\Gamma^{(max)}]. \end{cases} \tag{6.75}$$

This step is very quick since the range of variations of δ_{PWM} has already been investigated in paragraph 6.4.1. For simplicity, the range is given again:

$$\forall t \in \mathbb{R}_+, \exists n \in \mathbb{N}, t \in T_n, \quad \delta_{PWM}(t) = \frac{\bar{\omega}_{pwm}(t)}{\dot{\omega}_{sh}(t)} \in [0, h].$$

Furthermore, the range of variation of the relative uncertainty on the delivered torque δ_Γ is given. The

"nominal" uncertainty level is ±30%. Nevertheless, during the analysis we will study how the feasibility region of the stability test is in the (δ_Γ, h) plane. Hence, we will consider no fixed level of uncertainty.

6.5.5 Robust stability analysis

We can now perform the robustness analysis with theorem 10. Its application results in the definition of an ellipsoid of stable initial conditions $\epsilon(P)$ (6.58). Notice that since between each maneuver, the controller switches from one setup to another, having non-zero initial conditions during the flight is possible. Consequently, we add to the LMI stability conditions another constraint aiming to verify that a predefined ellipsoid $\epsilon(P_0)$ is a subset of $\epsilon(P)$. We set the length of the semi-axes of the ellipsoid $\epsilon(P_0)$ such that it covers initial conditions we expect to find. We chose an initial attitude of $\pm\theta(0)$ deg and an initial angular rate of $\pm\omega(0)$ deg.s^{-1}. We will then assess the stability for different sizes of $\epsilon(P_0)$. Concerning the state of the controller x_c we give it a very small value and hope for it not to limit the feasibility test. This assumption is due to the usual zero initial conditions in the controller. The corresponding LMI can be found in [Seuret and Gomes Da Silva Jr, 2011] and reads as

$$\begin{bmatrix} -P_0 & I \\ I & -(Y+Y^T)+P \end{bmatrix} \prec 0, \quad Y \text{ being the one in the stability theorem.} \tag{6.76}$$

Added to the LMI ensuring stability within the ellipsoid defined by P, the above LMI ensures that $\epsilon(P_0) \subset \epsilon(P)$ and so the launcher is stable for the predefined initial conditions.
Another parameter is of interest here, it is the saturation level Γ_{av} i.e. the available torque for control about the axis of rotation. This parameter was not considered in the IQC section while it defines the modified sector condition LMI found in the stability conditions (6.62) of the theorem we intend to use now. We set its value to $\Gamma_{av} = 380$ Nm.

In the set of constraints whose feasibility guarantees the stability of the initial conditions in $\epsilon(P)$ in theorem 10, there is a free parameter $\eta > 0$. As mentioned earlier on, this free parameter causes the constraints to be bilinear matrix inequalities (BMI). To overcome this issue, η can be considered as a fixed parameter in the LMI constraints of the stability test. In the implementation, we searched for feasibility of (6.62) and (6.76) for values of η chosen over a grid. Depending on the value η the stability test can be feasible or infeasible so it is worth it to investigate a wide range of values for η. In some sense, η allows reducing the conservatism of the stability test as depending on its value the result of the test can change. Once the LMI implemented, to get a first view on the regions of attraction we are going to encounter, we started by considering that there where no uncertainty in the system, that is

$$\begin{cases} \delta_{PWM}(t) &= 0, \ \forall t \\ \delta_\Gamma &= 0. \end{cases} \tag{6.77}$$

With the above assumptions, the system is the closed-loop with the nominal actuator as actuator model. Hence there is no PWM and no uncertain torque. The study consists in the search for the largest sampling period h for a given value $(\theta(0), \omega(0))$ of the semi-axes of $\epsilon(P_0)$. That corresponds to answering the question: "Up to which value of h am I sure that $\epsilon(P_0)$ defined by $(\theta(0), \omega(0))$ is a region of attraction for the zero equilibrium point?". The results are gathered in table 6.3.
These first results show that initial attitude $\alpha(0)$ has much more influence on the feasibility of the test than initial angular speed $\omega(0)$. This is a counterintuitive result since we know that for a space launcher, the recovery from large initial angular velocity values is more difficult than recovery from large initial attitude. Moreover, even for the smallest ellipsoid of stable initial conditions we consider, the maximum

Table 6.3: Maximum sampling period h for a given ellipsoid of stable initial condition with $\eta = 2.0457$

$\theta(0)$ \ $\omega(0)$	1 deg.s^{-1}	2 deg.s^{-1}	3 deg.s^{-1}	4 deg.s^{-1}
1 deg	971 ms	909 ms	865 ms	799 ms
2 deg	505 ms	496 ms	479 ms	452 ms
3 deg	245 ms	238 ms	228 ms	211 ms
4 deg	58 ms	54 ms	46 ms	32 ms

sampling period h for which we can prove stability is only 971 ms. It is still less than the sampling period currently in use on Astrium ST launchers that is $1,000$ ms. In this setup, one feasibility test lasts about 7 minutes on a 64 bits desktop PC with Intel® Core i7 processor at 2.80 GHz. It allowed us to search for a "better" value of η i.e. one that reduces the conservatism of the test and gives a larger maximum value of h. We proceeded to this search with the ellipsoid of "stable" initial conditions $(\alpha(0), \omega(0))$ defined by $(2 \text{ deg}, 2 \text{ deg.s}^{-1})$. The result for this ellipsoid from table 6.3 is a maximum sampling period of 496 ms for $\eta = 2.0457$. By searching to improve the maximum from this value of η, we managed to prove the stability for a sampling period up to 512 ms by taking $\eta = 2.1501$. The improvement is small with respect to the duration it took to search for this new η. Nevertheless, we will use this new value for the following investigations.

After this first step, we introduced the operator Δ_{PWM} by taking into account the parameter δ_{PWM}. As indicated by the definition of Δ_{PWM}, there is no threshold in the definition of the pulse width τ_n from (6.27). From this, we know that the range of variations of $\delta_{PWM}(t)$ is given by (6.41) and remembered below:

$$\forall t \in \mathbb{R}_+, \quad \frac{\bar{\omega}_{pwm}(t)}{\dot{\omega}_{sh}(t)} \in [0, h].$$

To observe what are the consequences of the introduction of the PWM on stability, we search for the maximum sampling period h for which the stability can be proved for a given ellipsoid of stable conditions $\epsilon(P_0)$ defined by $(\theta(0), \omega(0))$. The results are gathered in table 6.4.

Table 6.4: Maximum sampling period h for a given ellipsoid of stable initial condition with $\eta = 2.1501$

$\theta(0)$ \ $\omega(0)$	1 deg.s^{-1}	2 deg.s^{-1}	3 deg.s^{-1}	5 deg.s^{-1}
1 deg	363 ms	360 ms	354 ms	320 ms
2 deg	267 ms	264 ms	256 ms	220 ms
3 deg	157 ms	153 ms	145 ms	106 ms

In the table, we observe that the maximum sampling period for which we can prove the stability is decreased by about 60%. Moreover, these results confirm that initial angular speed $\omega(0)$ has much less influence than the initial attitude $\theta(0)$. Here, initial speeds which are much larger than most of the aimed speed used for slew maneuvers lead to asymptotically stable trajectories.

We are now ready to perform the analysis of the full model by adding the torque uncertainties. By analogy with the method used for the soft IQC analysis, we assess the stability of the system with uncertain torque without threshold in the definition of the pulse-width τ_n of (6.13). It is the case $\Gamma_{min} = 0$ Nm i.e. $t_{min} = 0$ ms. The range of variations of δ_{PWM} is $[0, h]$ as specified in (6.41). As for the soft IQC

analysis, δ_Γ will be set to some value and we will look for the maximum sampling period h for which asymptotic stability of initial conditions in $\epsilon(P_0)$ can be proved. During this analysis, we will use two different ellipsoids $\epsilon(P_0)$ defined by $(\alpha(0), \omega(0))$ equal to $(1 \text{ deg}, 1 \text{ deg.s}^{-1})$ and $(2 \text{ deg}, 2 \text{ deg.s}^{-1})$. In such conditions, the region of the (δ_Γ, h) plane where the stability can be proved with theorem 10 is depicted in figure 6.20. In order to find similar stability maps as those found for the IQC analysis in section 6.4.3, we describe the feasibility region on the (δ_Γ, h) plane. Thus for a given relative uncertainty on the torque generated by the thrusters δ_Γ e.g. $\delta_\Gamma \in [-\delta, \delta]$, we searched for the largest h for which we could solve the constraints (6.62-6.76). The asymptotic stability regions are below the curves. The figure indicates that the regions of asymptotic stability of initial condition in $\epsilon(P_0)$ is dramatically reduced by the introduction of the torque uncertainty. Indeed, the stability cannot be proved for the $(1 \text{ deg}, 1 \text{ deg.s}^{-1})$ ellipsoid when the uncertainty is larger than $\pm 25\%$ for the case with no threshold.

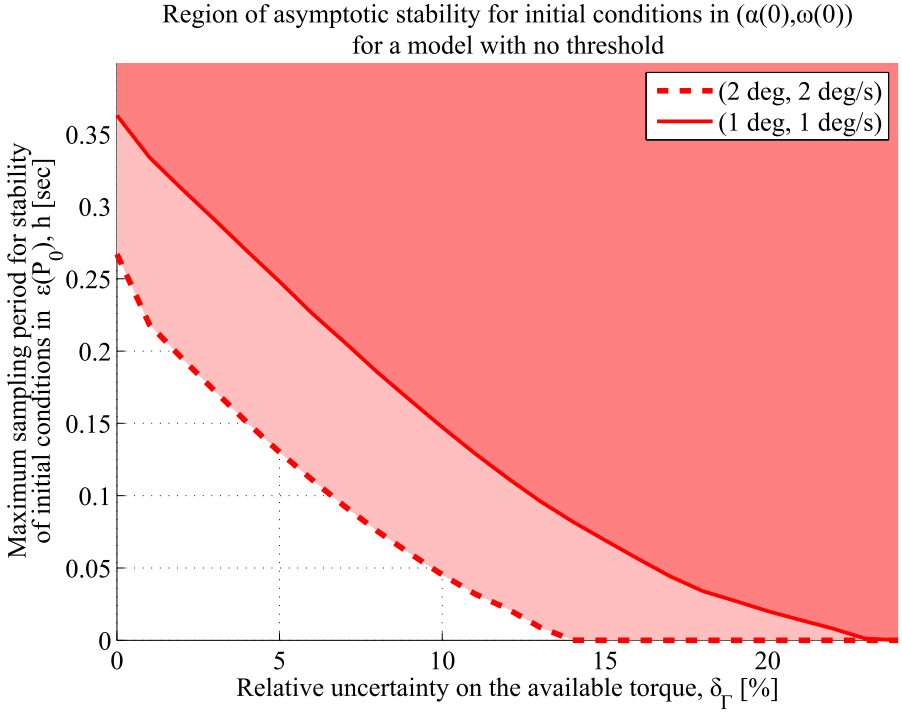

Figure 6.20: Asymptotic stability region found in the setup of table 6.2, $\Gamma_{av} = 380$ Nm

The results found with the method from [Seuret and Gomes Da Silva Jr, 2011] guarantee asymptotic stability for small sampling periods with respect to the actual sampling period of the current space launchers which is $1,000$ ms. In particular, the representation of Δ_{PWM} as an uncertain parameter and the extension of the original result to polytopic uncertainties leads to too much conservatism. Even though we intend to prove the stability over "small" ellipsoid of initial conditions, the results are not satisfying. The reason for this might be the natural tendency of the LMI solver to find P matrices that define ellipsoids of stable initial conditions that allow very large initial state for the controller and much lower values for the angular rate and attitude. Thus, the ellipsoid $\epsilon(P_0)$ that we defined as having semi-axis of similar size quickly does not "fit" in $\epsilon(P)$ anymore.

6.6 Stability analysis as a pulse-modulated system with hard IQC

Intensive research on the field of pulse-modulated systems by Russian mathematicians as Arkadii Kh. Gelig and Alexander N. Churilov in the mid-90's led to the results presented in [Gelig and Churilov, 1998]. They found several stability results developed from works by Vladimir Yakubovitch, Vasile Popov and others. As many of these results are based on the Kalman-Yakubovich-Popov lemma [Rantzer, 1996], the stability conditions and equations involved are similar to those found in IQC theory. These works show how Eastern scientists were developing IQC theory prior to the founding article [Megretski and Rantzer, 1997]. From our perspective of extension of IQC results to systems with PWM, we believe in the interest of pursuing these works. Their closeness to the classical IQC framework of chapter 4 could allow to build upon them and define a soft IQC that is satisfied by the transformed operator they define to represent the PWM. In such case, the analysis of systems with PWM would be facilitated as the PWM could be studied like any other perturbation block. To perform the stability analysis of systems with a pulse modulator, Arkadii Kh. Gelig and Alexander N. Churilov overcame the issue of unboundedness by a loop transformation. This loop transformation appears to be very similar to the one we performed in the study of section 6.4 although we did our study without knowing the existence of the works of Arkadii Kh. Gelig and Alexander N. Churilov. In facts, their loop transformation is nothing but a rigorous mathematical formulation of the loop transformations we did in section 6.4 to arrive at a system we could analyze with LPVMAD.
The framework defined by [Gelig and Churilov, 1998] relies on hard IQC. A first consequence of the later fact is that we will have to implement the method ourselves. In the frame of the study presented in [Chaudenson et al., 2013b], we introduced new quadratic constraints to the IQC description of the system by [Gelig and Churilov, 1998] and guaranteed asymptotic stability of the analysis model defined in section 6.2 over a widened range of sampling periods h. The following section presents these works. A few leads toward improvements of these advanced results can be found in appendix B.

6.6.1 Model Definition

As usual, the first step of the analysis consists in performing the transformations needed for the model to fall into the framework of the tool we aim to use. In this case, the result from [Gelig and Churilov, 1998] is an IQC-based stability result and the analysis of the system is done through the analysis of a LFR of the analysis model. For convenience, we start by depicting again the closed-loop of the analysis model, see figure 6.21, in which we use the generalized integrator $\mathcal{I}(s)$ from (6.4).

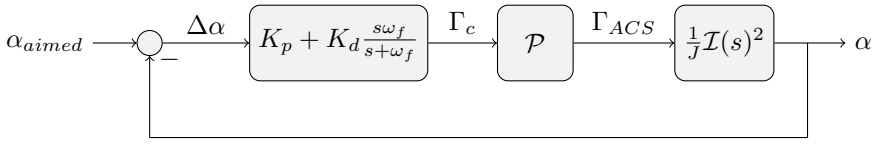

Figure 6.21: Closed-loop model for analysis as a pulse-modulated system

Contrary to the methods we used in the previous studies, we are going to try to analyze the asymptotic stability of the closed-loop by building IQC that are describing the perturbation blocks, no matter if they have a dedicated multiplier in the literature or not. As the perturbation operators we are going to define are not "usual" ones, we will have to build the IQC to describe them. The only condition we need to do so is that they have to be causal and $\mathcal{L}_2$ gain bounded. Hence we have an approach that is different from the one of the analysis based on soft IQC section 6.4. There, the transformations were driven by the fact that we wanted to include in the model operators that could be described with the multipliers from LPVMAD.

The transformation resulting in the LFR of the system is done as follow. Obviously, all the subsystems in the closed-loop figure 6.21 are LTI except the PWM. Thus we define the latter as the perturbation block of our LFR i.e. $\Delta = \mathcal{P}$ and gather the LTI transfer functions of the controller and the dynamic model in the nominal block $M_{iqc,h} \in \mathbb{RH}_\infty$. The subscript "$iqc, h$" is for "hard IQC". It results in the LFR of figure 6.22. In this figure and for the rest of this section, we will denote the torque command Γ_c by z and the torque delivered by the PWM actuator Γ_{ACS} by w. We make this choice for the sake of simplicity and to make the equations we are going to write more readable. On figure 6.22, the matrices (A, B, C) correspond to a state-space realization of the nominal LTI block $M_{iqc,h}$ of the LFR:

$$M_{iqc,h}(s) = -\left(K_p + K_d \frac{s\omega_f}{s+\omega_f}\right) \frac{1}{J} \mathcal{I}(s)^2. \tag{6.78}$$

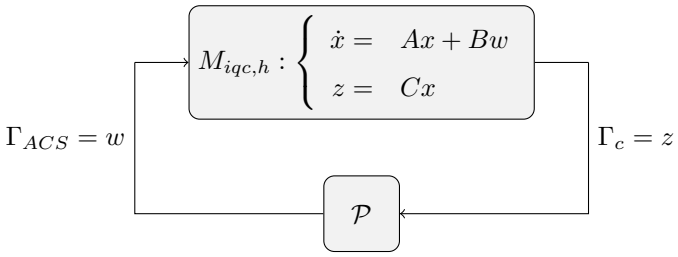

Figure 6.22: LFR of the analysis model for analysis as a pulse-modulated system

We will deal in this section with nominal parts $M_{iqc,h}$ that have a transfer function with a relative degree of at least 2 and a Hurwitz A matrix. Regarding the nominal system $M_{iqc,h}$ we defined in (6.78). We see that we needed to introduce the generalized integrator $\mathcal{I}$ in the analysis model and to set $\omega_d > 0$ in (6.4). Hence $M_{iqc,h}$ of (6.78) has all the above properties. A result for LFR with nominal part with relative degree of at least 1 is given in [Gelig and Churilov, 1998].

6.6.2 Loop transformations

To address the stability of the LFR on figure 6.22 using IQC, we need to ensure that both subsystems in the LFR verify some assumptions. In particular, the perturbation block, here $\mathcal{P}$, must be causal and have bounded $\mathcal{L}_2$-induced gain. Unfortunately, we saw in paragraph 6.2.3 that $\mathcal{P}$ is causal but it does not have bounded $\mathcal{L}_2$-induced gain. As said in the introduction, this issue led to the loop transformations of section 6.3. Here we are going to proceed to a very similar transformation with mathematically rigorous motivations and definitions. First of all, let us introduce the so-called equivalent nonlinearity.

Equivalent nonlinearity

To perform to the stability analysis of the pulse-modulated system we defined in paragraph 6.6.1 through its LFR on figure 6.22, we are going to use the method of [Gelig and Churilov, 1998] based on a technique called averaging method which has been investigated in [Gelig and Elkhimova, 1995]. This method is based on one simple observation. The PWM operator $\mathcal{P}$ produces a signal $w = \Gamma_{ACS}$ defined in (6.12) which has high amplitude high-frequency harmonics. Indeed, the time variations of $w = \Gamma_{ACS}$ are infinitely fast since the signal is piecewise constant e.g. figure 6.23.
Nevertheless, as all Hurwitz linear system, $M_{iqc,h}$ is essentially a low-pass filter. Thus the high-frequency components of the pulse-modulated signal $w = \Gamma_{ACS}$ are mostly filtered out by the low-pass nominal part $M_{iqc,h}$. This is even truer as the nominal part has relative degree of at least 2. It means that the high frequencies do not influence the behavior of the system very much even if they have large amplitude. Consequently, the motion of the launcher is more driven by low-frequency harmonics e.g. the average

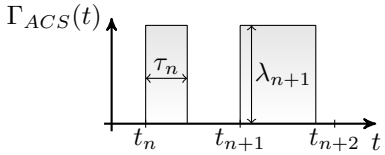

Figure 6.23: PWM output signal time-domain representation

value, of the pulse-modulated signal than by the abrupt time variations of the signal. This physical consideration is completed by the fact that it is easy to observe that the system behaves similarly to its actual configuration figure 6.21 when the pulse-modulator $\mathcal{P}$ is replaced by its so-called equivalent nonlinearity.
To take this into account and define the aforementioned equivalent nonlinearity, let us consider the sequence v_n of average values of w over a sampling period T_n:

$$\forall n \in \mathbb{N}, \quad v_n = \frac{1}{h} \int_{t_n}^{t_{n+1}} w(t)dt. \tag{6.79}$$

Then we define the equivalent nonlinearity Φ of the PWM which is also referred to as the static characteristic of the modulator. The nonlinearity Φ has the following property:

For all $n \in \mathbb{N}$, there exists a time instant $\tilde{t}_n \in T_n$ such that

$$\Phi\left(z\left(\tilde{t}_n\right)\right) = v_n. \tag{6.80}$$

In words, it means that the output of static characteristic of the PWM Φ takes the value v_n once in every sampling period T_n. This definition can be precised for the type of modulation we use. Our pulse-width modulation is defined by λ_n, τ_n from (6.13) and figure 6.23. It draws:

$$\tilde{t}_n = t_n. \tag{6.81}$$

This relationship is derived from the definitions of the modulated signal (6.12-6.13). From (6.81), Φ is defined over every sampling period T_n by

$$\Phi(z(\tilde{t}_n)) = \Phi(z(t_n)) = v_n. \tag{6.82}$$

For now, we just know that the output of Φ with input z is v_n at $t = t_n$. From the definition of the output signal of $\mathcal{P}$ (6.12) that involves λ_n and τ_n (6.13), we can define analytically the values taken by v_n:

$$\begin{aligned} v_n &= \tfrac{\tau_n \lambda_n}{h} \\ &= \begin{cases} 0, & \text{if } |z(t_n)| < \Gamma_{min} \\ z(t_n), & \text{if } \Gamma_{min} \leq |z(t_n)| < \Gamma_{av} \\ sign(z(t_n))\Gamma_{av}, & \text{if } |z(t_n)| \geq \Gamma_{av} \end{cases} . \end{aligned} \tag{6.83}$$

From the above definitions, we observe that the output of Φ is the result of the application of a threshold operator at Γ_{min} and a saturation operator at Γ_{av} with slope 1 to $z(t_n)$. This is depicted in figure 6.24 where we can set $x = z(t_n)$ to recover definition (6.83). The definitions presented above allow us to

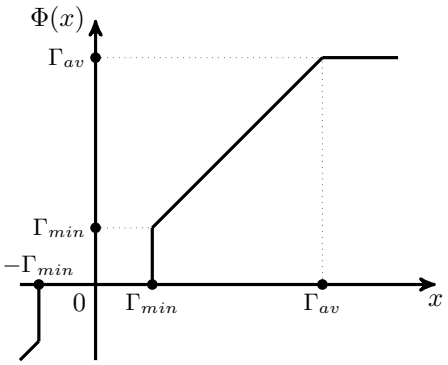

Figure 6.24: Characteristic of the equivalent nonlinearity (or static characteristic) of the PWM

claim that the equivalent nonlinearity Φ belongs to the sector $(0, 1)$. Moreover, the Lipschitz constant of the operator Φ i.e. the maximum slope of the plot in figure 6.24, is $L = \infty$. We will see later on that $L = \infty$ has consequences on the stability test. The Lipschitz constant of Φ can be seen as its maximum incremental gain. Another remark is important, it is that neither the sector bound 1, nor the Lipschitz constant L are depending on the value of h. This is a particular case due to the definition of the PWM we use to model the ACS behavior.
Finally, since Φ only considers the value of z at $t = t_n$ to generate its outputs over each sampling period T_n, we can write that the output of Φ is the output of $\Phi(\mathcal{SH}_h)$ where $\mathcal{SH}_h$ is the sample-and-hold operator with sample and hold functions synchronized at the sampling period h. $\mathcal{SH}_h$ defines a piecewise constant output signal which is defined over the nth sampling period by:

$$\forall z \in \mathcal{L}, \forall t \in T_n, \quad \mathcal{SH}_h(z(t)) = z(t_n).$$

Since the equivalent nonlinearity Φ is memoryless, the two operators Φ and $\mathcal{SH}_h$ commute. Thus we can define the piecewise constant signal v defined over the nth sampling period by the average value of the pulse-modulated signal w over T_n, that is:

$$\forall z \in \mathcal{L}, \forall t \geq 0, \quad v(t) = \Phi(\mathcal{SH}_h(z))(t) = \mathcal{SH}_h(\Phi(z))(t) = v_n. \tag{6.84}$$

Change of variables and loop transformation

The PWM has unbounded $\mathcal{L}_2$ gain and we need to represent it with other operators by the mean of loop transformations. The definition of the equivalent nonlinearity Φ aimed to prepare these loop transformations. Indeed, Φ is an operator that we know exactly. Its input-output relationship has been defined in the previous paragraph as the combination of a threshold and a saturation. Consequently, we can describe it precisely with IQC. We aim to introduce operators that we can describe accurately with IQC, an example of such operator would be the PWM equivalent nonlinearity Φ (6.80).
To integrate Φ into the initial model such that its characteristics can be taken into account for the analysis, we split the pulse-modulated signal w into two components v from (6.84) and f:

$$w = \mathcal{P}(z) = f + v \text{ for } \begin{cases} f = & (\mathcal{P} - \mathcal{SH}_h\Phi)(z), \\ v = & \mathcal{SH}_h\Phi(z). \end{cases} \tag{6.85}$$

f is the difference between the pulse-modulated signal and its average value over the current sampling period. Let us introduce the new definition of w (6.85) into the state-space representation of the nominal

system $M_{iqc,h}$. With the signals f and v, the state equation of $M_{iqc,h}$ from figure 6.22 reads as:

$$\begin{cases} \dot{x} &= Ax + Bf + Bv \\ z &= Cx. \end{cases} \tag{6.86}$$

This representation of the system does not solve our problem as f is defined by the $\mathcal{L}_2$-unbounded signal w we would like to remove from the state-space representation. To get rid of w, we take the integral of f from 0 to $t \in \mathbb{R}_+$ to define

$$u(t) = \int_0^t \left(\mathcal{P} - \mathcal{S}\mathcal{H}_h\Phi\right)(z(\tau))d\tau. \tag{6.87}$$

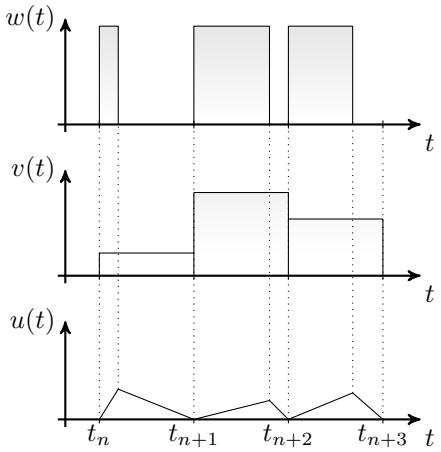

Figure 6.25: Signals w, u and v used for the loop transformation

A sketch of w, v and u is given in figure 6.25. With the definition of u we can recast the state-space equation (6.86) into

$$\begin{cases} \dot{x} &= Ax + B\dot{u} + Bv \\ z &= Cx. \end{cases} \tag{6.88}$$

Now to eliminate $\dot{u}$ from the state-space equation, we perform the state coordinate change

$$y = x - Bu. \tag{6.89}$$

With (6.89) we can reformulate the state-space equation (6.88) and obtain

$$\begin{cases} \dot{y} &= Ay + ABu + Bv \\ z &= Cy + CBu. \end{cases} \tag{6.90}$$

Here we can use the assumption on the relative degree of the transfer function of $M_{iqc,h}$ to set $CB = 0$. Furthermore, as a preparation for the use of the Popov criterion, we also consider $\dot{z}$ as an output of

(6.90), leading to the final state-space representation:

$$G_{iqc,h} : \begin{cases} \dot{y} = & Ay + ABu + Bv \\ z = & Cy \\ \dot{z} = & CAy + CABu. \end{cases} \quad \text{and} \quad \begin{cases} u = & \int (\mathcal{P} - \mathcal{SH}_h\Phi)(z)dt \\ v = & \mathcal{SH}_h\Phi(z) \end{cases} \tag{6.91}$$

For a better overview of the system resulting from the transformations, we represent the final LFR in figure 6.26. The PWM perturbation block $\mathcal{P}$ of figure 6.22 is replaced by two perturbation blocks which create v and u from z. The nominal system $M_{iqc,h}$ is replaced by $G_{iqc,h}$ which has inputs v and u and outputs z and $\dot{z}$. We consider that $\dot{z}$ inputs $\Delta_{iqc,h}$ as a preparation for the Popov criterion. From the state-space representation of $G_{iqc,h}$ given in (6.91), we can determine the transfer function from the input

$$\begin{bmatrix} v \\ u \end{bmatrix} \quad \text{to the output} \quad \begin{bmatrix} z \\ \dot{z} \end{bmatrix}. \tag{6.92}$$

It can be defined with the transfer function of $M_{iqc,h}$:

$$G_{iqc,h}(s) = \begin{pmatrix} M_{iqc,h}(s) & sM_{iqc,h}(s) \\ sM_{iqc,h}(s) & s^2M_{iqc,h}(s) \end{pmatrix}. \tag{6.93}$$

From (6.91), we can also define the state-space matrices of $G_{iqc,h}$:

$$G_{iqc,h} : \begin{cases} \tilde{A} = A & \tilde{B} = \begin{pmatrix} B & AB \end{pmatrix} \\ \tilde{C} = \begin{pmatrix} C \\ CA \end{pmatrix} & \tilde{D} = \begin{pmatrix} 0 & 0 \\ 0 & CAB \end{pmatrix} \end{cases}. \tag{6.94}$$

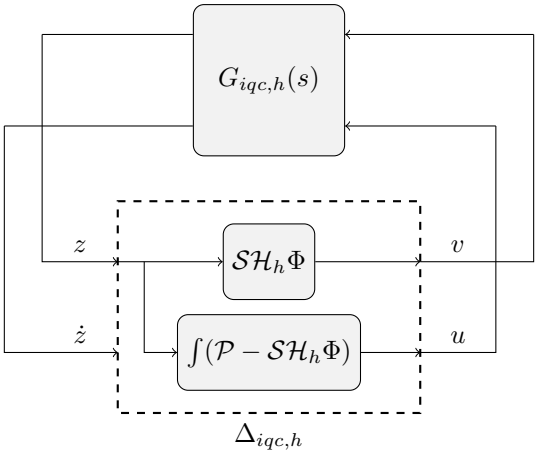

Figure 6.26: LFR of the model for analysis as a pulse-modulated system after coordinate change

The LFR model with PWM has been transformed into an equivalent LFR figure 6.26 with operators whose $\mathcal{L}_2$-gain can be bounded over a sampling period. Hence the PWM can be represented with the two new operators that define v and u from z. Since these operators are $\mathcal{L}_2$-gain bounded over T_n, we

will present in the next paragraph the IQC we built to describe them.

6.6.3 IQC description of the new LFR

Now that new perturbation operators have been defined, we need to study them in order to derive integral quadratic relations between the signals $z, \dot{z}, v$ and u of the interconnection figure 6.26. This LFR involves the nominal LTI system $G_{iqc,h}$ of (6.93) and the perturbation block $\Delta_{iqc,h}$ that generates v and u from z and $\dot{z}$. Some of the IQC relationships are from the works in [Gelig and Churilov, 1998] and others have been derived during the project. They are studied separately in the next two paragraphs. Furthermore, leads for new multipliers describing $\Delta_{iqc,s}$ have been gathered in appendix B.

Multiplier of A.Kh. Gelig and A.N. Churilov

First we study the equivalent nonlinearity Φ from (6.80) in the manner of [Gelig and Churilov, 1998]. As mentioned after its definition, Φ satisfies a sector condition. We alluded to this in paragraph 6.6.2 when we noticed that Φ is the combination of a threshold operator and a gain 1 saturation. The sector condition means that there exists a $z_* > 0$ such that

$$0 \leq \frac{\Phi(x)}{x} \leq \frac{1}{z_*} \quad \text{for } x \neq 0, \text{ and } \Phi(0) = 0 \tag{6.95}$$

holds. This condition can be recast into

$$\forall x \in \mathbb{R}, \quad (x - z_* \Phi(x))\Phi(x) \geq 0. \tag{6.96}$$

If we let the nonlinearity Φ operate on signal $x = \mathcal{SH}_h(z)$ i.e. if Φ and $\mathcal{SH}_h$ are in cascade in the system, the sector condition (6.96) can be reformulated into:

$$\forall t \geq 0, \quad (\mathcal{SH}_h(z)(t) - z_* \Phi(\mathcal{SH}_h(z))(t))\, \Phi(\mathcal{SH}_h(z))(t) \geq 0 \tag{6.97}$$

holds for any $z \in \mathcal{L}$. We notice that the definition of $v = \Phi(\mathcal{SH}_h(z))$ from (6.84) appears in the above equation so we rewrite it in the equivalent formulation

$$\forall z \in \mathcal{L}, \forall t \geq 0, \quad (\mathcal{SH}_h(z)(t) - z_* v(t))\, v(t) \geq 0 \tag{6.98}$$

Here we have a constraint that is very similar to a sector condition but slightly modified due to the presence of $\mathcal{SH}_h$ at the input of Φ. To recover a more classical sector condition similar to the one satisfied by Φ alone (6.96) but for the operator $\Phi(\mathcal{SH}_h(\bullet))$, we introduce the sampling error defined for all $z \in \mathcal{L}$ by

$$\xi = z - \mathcal{SH}_h(z). \tag{6.99}$$

Then we can recast (6.98), into

$$\forall z \in \mathcal{L}, \forall t \geq 0, \quad (z(t) - z_* v(t))\, v(t) \geq \underbrace{(z(t) - \mathcal{SH}_h(z)(t))}_{\xi(t)}\, v(t). \tag{6.100}$$

The right hand side of the inequality (6.100) is the product of the sampling error ξ and v. If we had considered $h = 0$, the right hand side would have been zero i.e. the sampling error would have been zero as no sampling would have occurred. In such a case, $\Phi(\mathcal{SH}_h) = \Phi$ and we already derived an IQC satisfied by the input and output of Φ in paragraph 4.4.2. It comes from the classical sector condition. Nevertheless, we need to take the fact that the right hand side is not zero into account to derive a valid

IQC for $\Phi(\mathcal{SH}_h(\bullet))$ from (6.100). The problem is that we don't know whether the right hand term in (6.100) is positive or not. To overcome this issue, we introduce two additional positive parameters ε_1 and ε_2 such that

$$\forall z \in \mathcal{L}, \forall t \geq 0, \quad (z(t) - z_* v(t))\, v(t) + \varepsilon_1 \dot{z}^2 + \varepsilon_2 v^2 \geq 0. \tag{6.101}$$

The reason for the introduction of $\varepsilon_1 > 0, \varepsilon_2 > 0$ will become clear shortly. For now, notice that for the first term in (6.101) we have a lower bound which is not necessarily larger than zero and that the two other terms $\varepsilon_1 \dot{z}$ and $\varepsilon_2 v^2$ are positive. Hence we can hope to find $\varepsilon_1 > 0, \varepsilon_2 > 0$ such that the integral quadratic constraint

$$\forall n \in \mathbb{N}, \quad \int_{t_n}^{t_{n+1}} \begin{pmatrix} z(t) \\ \dot{z}(t) \\ v(t) \end{pmatrix}^T \begin{pmatrix} 0 & 0 & \frac{1}{2} \\ 0 & \varepsilon_1 & 0 \\ \frac{1}{2} & 0 & \varepsilon_2 - z_* \end{pmatrix} \begin{pmatrix} z(t) \\ \dot{z}(t) \\ v(t) \end{pmatrix} dt \geq 0. \tag{6.102}$$

holds.
Before making sure that the IQC (6.102) is valid through the application of constraints on the parameters $\varepsilon_1 > 0, \varepsilon_2 > 0$, we are going to add other terms to the quadratic form. We know that a priori, new multipliers will add more information about $\Delta_{iqc,h}$ in the IQC and so can not increase the conservatism. To have a good characterization of $\Delta_{iqc,h}$ with the IQC we started to build with (6.102), we have to find other relations between the signals of the transformed LFR and put them into IQC form.

Popov parameter In addition to the multiplier defining the IQC (6.102), we add the multiplier of the classical Popov criterion with real parameter θ and arrive at the multiplier

$$P_1 := \begin{pmatrix} 0 & 0 & \frac{1}{2} \\ 0 & \varepsilon_1 & \frac{\theta}{2} \\ \frac{1}{2} & \frac{\theta}{2} & \varepsilon_2 - z_* \end{pmatrix} \tag{6.103}$$

With the multiplier defined above, we hope to define a valid IQC for $\Delta_{iqc,h}$. However, for now we only exploited relations between $z, \dot{z}$ and v and to have a good characterization of $\Delta_{iqc,h}$ by the IQC, we need to put more information inside and in particular, we have to involve u in the IQC.

Energy constraint on v and u One additional advantage of the introduction of u and v to define w is given by the following fact. There exist a bound on the energy norm of u in terms of the energy norm of v that is valid for all integer n:

$$\int_{t_n}^{t_{n+1}} |u(t)|^2 dt \leq \frac{h^2}{3} \int_{t_n}^{t_{n+1}} |v(t)|^2 dt. \tag{6.104}$$

A tedious proof of (6.104) can be found in [Gelig and Churilov, 1998], Lemma 3.1. This inequality easily translates into the IQC

$$\int_{t_n}^{t_{n+1}} \begin{pmatrix} v(t) \\ u(t) \end{pmatrix}^T \begin{pmatrix} 1 & 0 \\ 0 & -\frac{3}{h^2} \end{pmatrix} \begin{pmatrix} v(t) \\ u(t) \end{pmatrix} dt \geq 0. \tag{6.105}$$

Notice that, since (6.104) still holds if we multiply the whole equation by a non-negative parameter, we can introduce a $\lambda_1 \geq 0$ in the multiplier in (6.105). This parameter will give an additional degree of freedom in the constraints of the stability test. In facts, it takes the role of the τ_k factors of the conical combination of multipliers defined in paragraph 4.4.2. To combine the new multiplier of IQC (6.105) with the one of (6.103) we need to inflate the matrix to take the signal u into account. Thus we get

$$P_{GC} := \begin{pmatrix} 0 & 0 & \frac{1}{2} & 0 \\ 0 & \varepsilon_1 & \frac{\theta}{2} & 0 \\ \frac{1}{2} & \frac{\theta}{2} & \varepsilon_2 - z_* + \lambda_1 & 0 \\ 0 & 0 & 0 & -\frac{3\lambda_1}{h^2} \end{pmatrix}. \tag{6.106}$$

Considering the way we constructed the multiplier P_{GC}, we still have to make sure that its parameters are such that P_{GC} defines a valid IQC satisfied by $\Delta_{iqc,h}$. Thus we need to find a combination of parameters such that the inequality

$$\int_{t_n}^{t_{n+1}} \begin{pmatrix} z(t) \\ \dot{z}(t) \\ v(t) \\ u(t) \end{pmatrix}^T P_{GC} \begin{pmatrix} z(t) \\ \dot{z}(t) \\ v(t) \\ u(t) \end{pmatrix} dt \geq \theta \int_{t_n}^{t_{n+1}} \Phi(z(t))\dot{z}(t)\, dt \tag{6.107}$$

holds. We will later use the specific form of the right hand side for a Lyapunov type argument.
In order to get conditions on the parameters in P_{GC} such that inequality (6.107) holds, we use Wirtinger's inequality to get a bound on the energy norm of the sampling error $z - \mathcal{SH}_h(z)$ in each sampling interval in terms of $\dot{z}$,

$$\int_{t_n}^{t_{n+1}} |(z - \mathcal{SH}_h(z))(t)|^2 dt \leq K^2 h^2 \int_{t_n}^{t_{n+1}} |\dot{z}(t)|^2 dt, \tag{6.108}$$

where $K := 2/\pi$. Hence, for (6.107) to be valid it is sufficient to show that there exists a $\theta_0 \geq 0$ such that

$$(z - z_* v)v + \theta v\dot{z} + \varepsilon_1 \dot{z}^2 + \varepsilon_2 v^2 - \theta\Phi(z)\dot{z} - \theta_0[(Kh)^2\dot{z}^2 - (z - \mathcal{SH}_h(z))^2] \geq 0. \tag{6.109}$$

Here the role of $\varepsilon_1, \varepsilon_2$ becomes apparent. These parameters were introduced to take care of the non-negative right hand side in (6.100) by a completion of the squares. Condition (6.109) can be found in equations 17 and 18 in [Gelig and Churilov, 1993]. The way to make sure that the above condition holds will be investigated with more details in the next paragraph. For now, we use the condition of validity of the IQC defined by P_{GC} given by (6.112). If we can find $\varepsilon_1 > 0$, $\varepsilon_2 > 0$, $\theta_0 \geq 0$ and θ such that (6.109) holds it follows that (6.107) is valid. This motivates the following theorem.

Theorem 11 (Gelig and Churilov with fixed parameter) *Consider the interconnection of figure 6.26 with the definitions from (6.83-6.87-6.91), the matrix A to be Hurwitz and $CB = 0$. Suppose the equivalent nonlinearity Φ satisfies the sector condition (6.95) and the Lipschitz condition*

$$|\Phi(x_1) - \Phi(x_2)| \leq L|x_1 - x_2| \tag{6.110}$$

for any x_1, x_2 in $\mathbb{R}$. In addition to that, suppose there exist numbers $\lambda_1 \geq 0, \varepsilon_2 > 0$ and θ such that the

Frequency Domain Inequality (FDI)

$$\begin{pmatrix} G_{iqc,h}(j\omega) \\ I_2 \end{pmatrix}^* P_{GC} \begin{pmatrix} G_{iqc,h}(j\omega) \\ I_2 \end{pmatrix} \prec 0 \tag{6.111}$$

holds for all $\omega \in \mathbb{R}_+$. *Here* ε_1 *is given by formula*

$$\varepsilon_1 := \frac{h^2}{\pi^2 \varepsilon_2} + \frac{2|\theta| L h}{\pi}. \tag{6.112}$$

Then we have

$$\lim_{n\to\infty} v_n = 0, \quad \lim_{t\to\infty} z(t) = 0. \tag{6.113}$$

Brief sketch of the proof. By the KYP Lemma and (6.111) there exists a symmetric (not necessarily positive definite) X and a $\delta > 0$ such that

$$2y^* X(Ay + Bv + ABu) + \begin{bmatrix} z \\ \dot{z} \\ v \\ u \end{bmatrix}^* P_{GC} \begin{bmatrix} z \\ \dot{z} \\ v \\ u \end{bmatrix} \leq -\delta v^2, \tag{6.114}$$

along trajectories of the interconnection. Let us define the Lyapunov function

$$V(y) := y^* X y + \theta \int_0^{Cy} \Phi(z) dz.$$

From inequality (6.107) and (6.114) we get that

$$V(y(t_{n+1})) - V(y(t_n)) \leq -\delta h v_n^2 \leq 0. \tag{6.115}$$

We can then sum the terms for $n = 0$ to $n = N \in \mathbb{N}$:

$$V(y(t_{N+1})) - V(y(t_0)) \leq -\delta h \sum_{n=0}^{N} v_n^2 \leq 0. \tag{6.116}$$

Since v_n is bounded by definition, v is also bounded. Then the estimate

$$\forall t \in T_n, \quad |u(t)| \leq h|v(t)| \tag{6.117}$$

infers that u is bounded too. As A is assumed to be Hurwitz, y is bounded as well and so is $V(y)$. Thus, since h, δ are positive constants, from (6.116) we infer

$$\sum_{n=0}^{\infty} v_n^2 < \infty,$$

and hence $\lim_{n\to\infty} v_n = 0$. Again by (6.117) $\lim_{t\to\infty} u(t) = 0$. Since A is Hurwitz $y(t) \to 0$ for $n \to \infty$.□

It is shown in the proof given in [Gelig and Churilov, 1993] that the particular choice of ε_1 in (6.112)

guarantees the existence of a $\theta_0 \geq 0$ such that (6.109) and so (6.107) holds. As a disadvantage of this approach one has to fix one parameter (ε_1) and thus not all are available for optimization.

Improvements of stability condition and new multipliers

We are going to improve the result of A.Kh. Gelig and A.N. Churilov in two ways. First we will reformulate the validity condition of IQC (6.107) to ensure easier and more efficient implementation. Indeed, the result of the previous paragraph requires to fix the parameter ε_1 of the multiplier P_{GC} to ensure (6.107) to be valid. Nevertheless, this formulation is not easy to implement. To test the stability there is no other choice but to look for the validity of (6.107) over a grid of the free parameters. This is why we are going to look at the condition of validity of the IQC defined by P_{GC} into details. We will do this with the aim to recast the validity condition of (6.107) such that it is easily accessible for optimization e.g. by making it convex. Secondly we introduce an additional IQC satisfied by $\Delta_{iqc,h}$. It will improve its IQC description and reduce the conservatism of the stability test.

Convex IQC validity condition The goal of the present paragraph is to recast the condition on the parameters of the multiplier P_{GC} for (6.107) to be valid. For convenience, we give it again below:

$$\int_{t_n}^{t_{n+1}} \begin{pmatrix} z(t) \\ \dot{z}(t) \\ v(t) \\ u(t) \end{pmatrix}^T P_{GC} \begin{pmatrix} z(t) \\ \dot{z}(t) \\ v(t) \\ u(t) \end{pmatrix} dt \geq \theta \int_{t_n}^{t_{n+1}} \Phi(z(t))\dot{z}(t)\, dt \tag{6.118}$$

Now in the manner of the proof of lemma 3 in [Gelig and Churilov, 1993], we look for a conditions on the parameters of P_{GC} (6.106) that guarantees (6.118) to be valid. To get a clearer view of the problem, we expand the left hand term of IQC (6.118):

$$\int_{t_n}^{t_{n+1}} \lambda_1 \left(|v(t)|^2 - \frac{3}{h^2}|u(t)|^2 \right) dt + \int_{t_n}^{t_{n+1}} \left((z(t) - z_* v(t))v(t) + \varepsilon_1 \dot{z}(t)^2 + \varepsilon_2 v(t)^2 + \theta \dot{z}(t)v(t) \right) dt. \tag{6.119}$$

Since we know from (6.104) that the first integral in (6.119) is nonnegative, in order to get conditions on the parameters in P_{GC} such that inequality (6.118) holds, it is sufficient to find a condition on the parameters of P_{GC} such that the second integral in (6.119) is bounded by the right hand term of (6.118). It reduces the problem to the search for a condition on the parameters of P_1 (6.103) ensuring that

$$\int_{t_n}^{t_{n+1}} \left((z(t) - z_* v(t))v(t) + \varepsilon_1 \dot{z}(t)^2 + \varepsilon_2 v(t)^2 + \theta \dot{z}(t)v(t) \right) dt \geq \theta \int_{t_n}^{t_{n+1}} \Phi(z(t))\dot{z}(t)\, dt. \tag{6.120}$$

To prove (6.120), it is sufficient to show that there exists a parameter $\theta_0 \geq 0$ such that:

$$(z - z_* v)v + \varepsilon_1 \dot{z}^2 + \varepsilon_2 v^2 + \theta \dot{z} v \geq \theta \Phi(z)\dot{z} + \theta_0 \left[K^2 h^2 \dot{z}^2 - (z - \mathcal{SH}_h(z))^2 \right] \tag{6.121}$$

where the dependence on time t is dropped for clarity and $K := 2/\pi$. Indeed, if we integrate (6.121) from t_n to t_{n+1}, the second term of the right hand side is positive. This bound comes from Wirtinger's inequality see e.g. lemma 2 in [Gelig and Churilov, 1993] and (6.108). The inequality gives a bound on the energy norm of the sampling error $\xi = z - \mathcal{SH}_h(z)$ over each sampling interval in terms of $\dot{z}$,

$$K^2 h^2 \int_{t_n}^{t_{n+1}} |\dot{z}(t)|^2 dt \geq \int_{t_n}^{t_{n+1}} |(z - \mathcal{SH}_h(z))(t)|^2 dt,$$

which can also be recast into

$$\int_{t_n}^{t_{n+1}} (K^2h^2|\dot{z}(t)|^2 - |\xi(t)|^2)dt \geq 0.$$

Hence, for (6.121) to be valid it is sufficient to show that there exists a $\theta_0 \geq 0$ such that

$$(z - z_*v)v + \theta v\dot{z} + \varepsilon_1\dot{z}^2 + \varepsilon_2 v^2 - \theta\Phi(z)\dot{z} - \theta_0[(Kh)^2\dot{z}^2 - \xi^2] \geq 0, \tag{6.122}$$

where $\xi = z - \mathcal{SH}_h(z)$. First, by expansion of Wirtinger's term we recast (6.122) into

$$(z - z_*v)v + \theta(v - \Phi(z))\dot{z} + (\varepsilon_1 - \theta_0K^2h^2)\dot{z}^2 + \varepsilon_2 v^2 + \theta_0\xi^2 \geq 0. \tag{6.123}$$

Then we use two bounds derived from the assumptions. On the first hand, the sector bound modified by the sampling (6.100) gives

$$(z - z_*v)\, v \geq \xi v. \tag{6.124}$$

On the other hand, the assumption that Φ has finite incremental gain with bound L (6.110) with $x_1 = \mathcal{SH}_h(z)$ and $x_2 = z$ gives

$$|v - \Phi(z)| \leq L|\xi|. \tag{6.125}$$

Equations (6.124) and (6.125) give the following sufficient condition for (6.123) and so (6.122) to be true:

$$(\varepsilon_1 - \theta_0K^2h^2)\dot{z}^2 - |\theta|L|\xi||\dot{z}| + \varepsilon_2 v^2 + \xi v + \theta_0\xi^2 \geq 0. \tag{6.126}$$

This is done by bounding the first two terms of (6.123). From (6.126), we will obtain a quadratic form in $|\dot{z}|$ and $|\xi|$ by completion of the squares:

$$\varepsilon_2 v^2 + \xi v = \left(\sqrt{\varepsilon_2}v + \frac{1}{2\sqrt{\varepsilon_2}}\xi\right)^2 - \frac{1}{4\varepsilon_2}\xi^2 \geq -\frac{1}{4\varepsilon_2}\xi^2. \tag{6.127}$$

Indeed, the role of $\varepsilon_1, \varepsilon_2$ is now clear. The parameters $\varepsilon_1, \varepsilon_2$ were introduced to take care of the non-negative right hand side in (6.97) by the completion of the squares argument (6.127). If we insert the bound on $\varepsilon_2 v^2 + \xi v$ from (6.127) in (6.126) we get

$$(\varepsilon_1 - \theta_0K^2h^2)\dot{z}^2 - |\theta|L|\xi||\dot{z}| + \left(\theta_0 - \frac{1}{4\varepsilon_2}\right)\xi^2 \geq 0. \tag{6.128}$$

This gives us constraints on the parameters that capture the modulation and also links them to the Popov parameter θ. The left hand term in (6.128) is a quadratic form in $|\dot{z}|$ and $|\xi|$, we can determine the matrix defining it and ensure the positivity constraint through positiveness of the matrix:

$$\begin{pmatrix} \varepsilon_1 - \theta_0K^2h^2 & L\frac{\theta}{2} \\ L\frac{\theta}{2} & \theta_0 - \frac{1}{4\varepsilon_2} \end{pmatrix} \succeq 0. \tag{6.129}$$

If we can find $\varepsilon_1 > 0$, $\varepsilon_2 > 0$, $\theta_0 \geq 0$ and θ such that (6.129) holds it follows that (6.107) is valid. This is a reformulation of the condition on $\varepsilon_1 > 0, \varepsilon_2 > 0, \theta_0 \geq 0$ and θ given in by [Gelig and Churilov, 1993] in (6.112) to guarantee (6.107) to be valid. Since (6.129) is nonlinear in ε_2, we use Schur's complement

formula to come to the following LMIs with affine dependence on all parameters:

$$\begin{pmatrix} \varepsilon_1 - \theta_0(Kh)^2 & \frac{\theta L}{2} & 0 \\ \frac{\theta L}{2} & \theta_0 & 1 \\ 0 & 1 & 4\varepsilon_2 \end{pmatrix} \succeq 0, \qquad \theta_0 \geq 0. \tag{6.130}$$

Hence, for the IQC (6.118) to be valid it is sufficient to impose (6.130) on the involved parameters.

The condition of validity of IQC (6.107) is now convex so it is easily accessible for optimization when combined with the KYP lemma (see paragraph 4.4.3) LMI formulation of the FDI (6.111) in the stability theorem 11.
To complete the improvements brought to the result from [Gelig and Churilov, 1993], we now add a new quadratic constraint to better the IQC description of $\Delta_{iqc,h}$.

New multiplier We know that we can decrease the conservatism of a stability test with IQC by putting more information in the IQC multiplier. For now, P_{GC} contains information about the sector condition modified by the sampling satisfied by $\Phi(\mathcal{SH}_h)$ and also about the energy bound between u and v. Our goal here is to add more information in P_{GC} to eventually decrease the conservatism of the stability test. The usual method for the definition of valid IQC is to analyze the inputs and outputs of the operator $\Delta_{iqc,h}$. We notice that signals u and v have, by definition, the same sign. This is hinted by figure 6.25 and it can be derived from the definition of u and v as follows.
First, we observe from its definition that w does not change its sign in T_n for any n (see (6.12-6.13)). Thus $v(t)$ has the same sign as $w(t)$ for all $t \geq 0$. Let us consider an integer n such that $z(t_n) \geq \Gamma_{min}$. Remember that in this section, we have the original PWM definition with $\Gamma_{min} > 0$. For $t \in T_n$ we have

$$\begin{aligned} u(t) &= \int_0^t (w(\tau) - v(\tau))\, d\tau \\ &= \sum_{k=0}^{n-1} \left[\int_{t_k}^{t_{k+1}} w(\tau)\, d\tau - h\frac{1}{h} \int_{t_k}^{t_{k+1}} w(\sigma)\, d\sigma \right] \\ &\quad + \int_{t_n}^{t} (w(\tau) - v_n)\, d\tau. \end{aligned}$$

The sum vanishes and we only have to consider the second term. Since v_n is the average of w over the whole interval T_n the integral

$$r(t) := \int_{t_n}^{t} (w(\tau) - v_n)\, d\tau \tag{6.131}$$

vanishes only for $t = t_n$ and $t = t_{n+1}$. Moreover $r(t)$ is increasing for $t \in [t_n, t_n + \tau_n)$ and decreasing for $t \in [t_n + \tau_n, t_{n+1})$. Thus $u(t)$ has the same sign as $w(t)$ on T_n. The same arguments can be used when $z(t_n) \leq -\Gamma_{min}$ with the same conclusion. Finally, the case $|z(t_n)| < \Gamma_{min}$ is trivial since in this case $u(t) = 0, \forall t \in T_n$.

The fact that u and v have the same sign translates into

$$\forall t \geq 0, \quad u(t)v(t) \geq 0. \tag{6.132}$$

(6.132) can be put in matrix form to define the quadratic constraint

$$\forall t \geq 0, \quad \begin{pmatrix} v(t) \\ u(t) \end{pmatrix}^T \begin{pmatrix} 0 & \frac{1}{2} \\ \frac{1}{2} & 0 \end{pmatrix} \begin{pmatrix} v(t) \\ u(t) \end{pmatrix} \geq 0, \tag{6.133}$$

Of course if we take the integral of this quadratic constraint over a sampling period we arrive at a valid IQC. To incorporate multiplier (6.133) into P_{GC} we introduce a non-negative parameter λ_2 and add the resulting multiplier to P_{GC} to get

$$P := \begin{pmatrix} 0 & 0 & \frac{1}{2} & 0 \\ 0 & \varepsilon_1 & \frac{\theta}{2} & 0 \\ \frac{1}{2} & \frac{\theta}{2} & \varepsilon_2 - z_* + \lambda_1 & \frac{\lambda_2}{2} \\ 0 & 0 & \frac{\lambda_2}{2} & -\frac{3\lambda_1}{h^2} \end{pmatrix} \tag{6.134}$$

Note that the quadratic constraint (6.133) is always valid. Hence it does not change the LMI condition (6.130) guaranteeing the validity of the IQC defined by P_1 (6.103) that we determined in the previous paragraph. Furthermore, we added the parameters $\lambda_i \geq 0, i \in \{1, 2\}$ on the two positive IQC. These parameters are analogous to the τ_k we defined in paragraph 4.4.2. We are going to see next that as the stability conditions of the theorem can all be formulated as LMI constraints, the introduction of these parameters allow to have a wider set of parameters into which we can look for a combination that make constraints feasible. It is how the introduction of these parameters can result in conservatism reduction.

New theorem With the new elements from the two previous paragraphs, we can formulate a completely analogous result to theorem 11.

Theorem 12 *Consider the interconnection of the LTI stable system $M_{iqc,h}$ with the PWM operator $\mathcal{P}$ depicted figure 6.22. Assume that the matrix A is Hurwitz and the relative degree of $M_{iqc,h}$ is at least 2 where (A, B, C) is a state-space realization of $M_{iqc,h}$. Suppose the equivalent nonlinearity satisfies the sector condition (6.96) and the Lipschitz condition*

$$|\Phi(x_1) - \Phi(x_2)| \leq L|x_1 - x_2|$$

for any x_1, x_2 in $\mathbb{R}$. In addition to that, suppose there exist $\lambda_1 \geq 0, \lambda_2 \geq 0, \varepsilon_1 > 0, \varepsilon_2 > 0$, $\theta_0 \geq 0$ and a real θ such that the following conditions are fulfilled:

(1) The LMIs (6.130) hold.

(2) The FDI

$$\begin{pmatrix} G_{iqc,h}(j\omega) \\ I_2 \end{pmatrix}^* P \begin{pmatrix} G_{iqc,h}(j\omega) \\ I_2 \end{pmatrix} \prec 0 \tag{6.135}$$

with P in (6.134) and $G_{iqc,h}$ (6.91) holds for all $\omega \geq 0$.

Then we have

$$\lim_{n\to\infty} v_n = 0, \quad \lim_{t\to\infty} z(t) = 0. \tag{6.136}$$

Proof. It is easy to see that (6.133) implies (6.107) for P instead of P_{GC}. Thus theorem 12 follows from theorem 11. □

LMI implementation using KYP lemma For the problem to be efficiently tractable, we need to recast the FDI stability condition in theorem 12 above, into a finite set of LMI. The KYP lemma described in [Rantzer, 1996] gives the equivalence between the FDI (6.135) and the existence of a symmetric solution $X \in \mathbb{R}^{n\times n}$ of the LMI

$$\begin{pmatrix} \tilde{A} & \tilde{B} \\ I_n & 0_{n\times 2} \end{pmatrix}^T \begin{pmatrix} 0_{n\times n} & X \\ X & 0_{n\times n} \end{pmatrix} \begin{pmatrix} \tilde{A} & \tilde{B} \\ I_n & 0_{n\times 2} \end{pmatrix} + \begin{pmatrix} \tilde{C} & \tilde{D} \\ 0_{2\times n} & I_2 \end{pmatrix}^T P \begin{pmatrix} \tilde{C} & \tilde{D} \\ 0_{2\times n} & I_2 \end{pmatrix} \prec 0. \tag{6.137}$$

$(\tilde{A}, \tilde{B}, \tilde{C}, \tilde{D})$ is a realization of $G_{iqc,h}$ while n is the number of state variables and 2 the number of perturbation channel in the LFR figure 6.26.
Finally, stability of the pulse-modulated system figure 6.21 is guaranteed if we can find $\lambda_1 \geq 0, \lambda_2 \geq 0$, $\varepsilon_1 > 0, \varepsilon_2 > 0$, $\theta_0 \geq 0$, a real number θ and a real symmetric matrix $X \in \mathbb{R}^n$ such that (6.130) and (6.137) are valid. This problem can be readily implemented in Matlab® LMIlab using Yalmip interface developed by [Löfberg, 2004].

The previous paragraphs allowed to present the multiplier P_{GC} of [Gelig and Churilov, 1993] and improve it to obtain P. Further works resulted in a convex formulation of the validity of the IQC defined by P_{GC} and P. These IQC that are satisfied by the operator $\Delta_{iqc,h}$ from figure 6.26. The subsequent stability analysis compares the stability results found with the multipliers P and P_{GC}.

6.6.4 Stability analysis

To perform the stability analysis of the model presented in section 6.6.2 with the multipliers from the above paragraphs, we need to define the parameters of the static characteristic Φ introduced in (6.83). After the definition of Φ in paragraph 6.6.2, we have $z_* = 1$ and $L = \infty$. However, the computations are impossible with $L = \infty$ so we rely on a Lipschitz approximation of Φ.

Lipschitz approximation of the equivalent nonlinearity

To do a rigorous stability analysis of the space launcher model described in section 6.6.2, we have to avoid the use of $L = \infty$ in the LMI constraints that we need to solve to guarantee the feasibility of the IQC defined by our multipliers. Thus we are going to assume that the maximum slope of Φ from figure 6.24 is not infinite. We can see it on the sketch of the characteristic of a Lipschitz approximation of Φ presented in figure 6.27. It shows a possible representation of the characteristic plot of Φ with finite Lipschitz constant. Building upon this assumption, we perform the stability test with an incremental gain $L_{max} < \infty$. Thus, a trade-off has to be made between the maximum slope of the approximated equivalent nonlinearity L_{max} and the sampling period h of the PWM. Crudely, a large h ensures less thrusters activation while increasing L_{max} gives a more accurate representation of the threshold i.e. a better approximation of the analysis model. Consequently, our goal is to have a proof of the stability for a very large L with the largest sampling period h. We can also separate here the case when we have no threshold in the PWM definition. In this case, stability for $L_{max} = 1/z_* = 1$ corresponds to the case where $\Gamma_{min} = 0$.

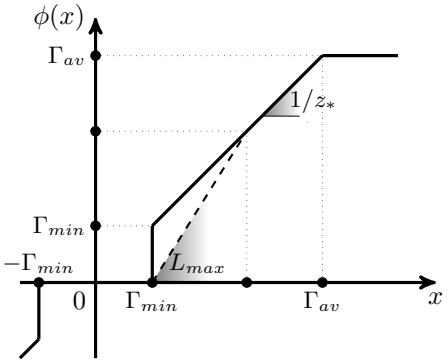

Figure 6.27: Characteristic plot of Φ, the solid line is the ideal characteristic ($L_{max} = \infty$) and the dashed line represents the approximated characteristic ($L_{max} < \infty$). L_{max} and $1/z_*$ are the slopes of the lines.

Stability domain, trade-off curve

Considering the facts exposed in the previous paragraph, we will present the trade-off curves of L_{max} versus h as results of the stability analysis. Here, L_{max} denotes the largest Lipschitz constant for which the LMI constraints (6.130) and (6.137) are feasible for a given h. If they are feasible, it means that we have a proof of the stability. During the analysis, the values of L_{max} are limited to the range $[0; 20]$.
First, the analysis has been performed with a multiplier derived from P_{GC} (6.106). We used the Popov criterion multiplier P_{GC} with $\theta = 0$. In such case, the IQC corresponds to the circle criterion applied to the nonlinearity $\mathcal{SH}_h(\Phi)$ associated to the norm constraint on u and v presented in (6.105). The stability could not be proved for the range of sampling periods we considered that is $[10^{-3}, 1]$ second. It means that this IQC description of $\Delta_{iqc,h}$ is too conservative to allow finding a proof of stability by fulfilling constraints (6.130) and (6.137). This result was expected. Indeed, we performed aside another quick analysis. It consisted in the application of the classical circle criterion (for instance in [Khalil, 1996]) to our initial LTI system $M_{iqc,h}$ in interconnection with the sector bounded nonlinearity Φ (6.80). It fits the framework of Lure's problem presented in chapter 4. Stability cannot be proved with the circle criterion in these conditions. Hence since when $\theta = 0$, our stability test is a circle criterion test modified by the sampling (so harder to satisfy) accounting for more perturbation (due to u) it could not lead to a feasible problem. The use of this method aimed to illustrate the similarities between Lure's problem and the problem we are dealing with for the analysis of a pulse-modulated system after loop transformations.
The other results are given in figure 6.28. To obtain them we used the multipliers P_{GC} and P defined in (6.106) and (6.134), respectively. The legend entries in figure 6.28 are to be read as follow:

- (Gelig-Churilov, P_{GC}) is obtained using the Popov criterion multiplier which is P_{GC}, i.e. P with $\lambda_2 = 0$;

- (ACA'13, P) is obtained using the Popov criterion combined with multipliers from IQC (6.133) which is P from (6.134). These results were presented at the 19^{th} IFAC Symposium on Automatic Control in Aerospace, [Chaudenson et al., 2013b].

Furthermore, the dashed horizontal line corresponds to the case $L = L_{max} = 1$ when there is no threshold in the definition of the pulse-width τ_n (6.13).

The stability analysis using the IQC defined by multiplier P to capture the PWM behavior showed an important reduction in the conservatism with respect to the results with P_{GC}. For the case $L_{max} = 1$, the maximum h for which stability can be proved is increased by an order of magnitude with P when compared to the maximum stable h obtained with the Popov multiplier P_{GC}. Note that this case also

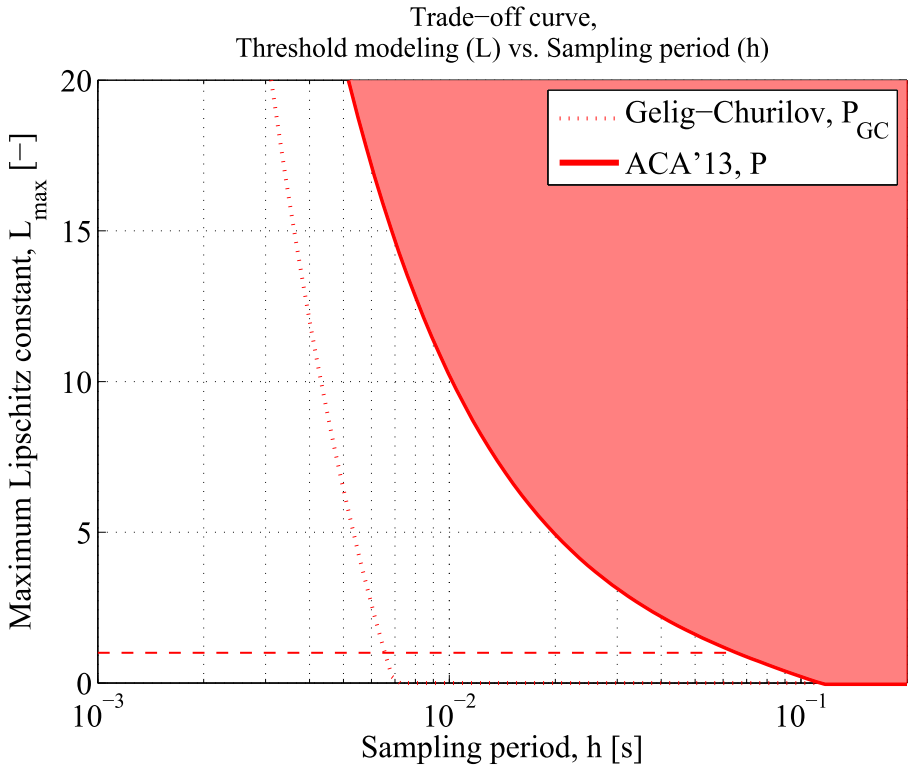

Figure 6.28: Trade-off curves for three multipliers, (h, L) combinations below the curves define stable systems.

corresponds to the case when there is no modeling of the threshold in the equivalent nonlinearity Φ and so that as we prove global asymptotic stability here, this result is comparable to the ones obtained in section 6.5 with the difference that the previous results were local. An explanation for this is that IQC (6.133) captures a very important feature of the PWM. In fact, v and u, can be seen as a torque input and an angular speed disturbance in $G_{iqc,h}$, respectively. Again, it confirms that it is the same kind of representation of the PWM as in section 6.4. Their main characteristic is that they have the same sign. Hence when v creates an angular acceleration of the launcher with a given sign, the speed perturbation u has the same sign and so the latter "helps" the rotation of the launcher in the direction indicated by v. This constraint causes the multiplier to capture the effect of the PWM that produces a torque which has the same sign as the torque command. That information was not contained in the multiplier P_{GC} and so it was a source of conservatism.

Despite the reduction of conservatism brought by the new multiplier P with respect to the analysis results with P_{GC} from [Gelig and Churilov, 1998], the maximum sampling period h for which we can prove stability is still below the nominal sampling period of ACS in current space launchers. One reason for these physical systems to fail the stability test is their theoretically infinite static gain. This feature appears when we proceed to the frequency-by-frequency validation of (6.135).

In the manner of the introduction analysis with the classical circle criterion, if we perform the analysis of the system as a Lure interconnection with only Φ in feedback with our initial LTI system $M_{iqc,h}$, the classical Popov criterion in [Khalil, 1996] can prove the stability for Φ with any positive maximum gain. It indicates that further improvement can be brought to the IQC description of the system and that they should result in conservatism reduction.

Another possible reason for the new stability test to remain too conservative could be that the characteristics of u used to define P in (6.134) are giving it too much influence on the system. This is in

contradiction with the fact that the system is mostly driven by the v and only perturbed by u. In the current multiplier, the information about u is only its sign and its norm bound with respect to the norm of v. It could be fruitful to relate u to the outputs of the system z and $\dot{z}$ as well in order to reduce the conservatism.

6.6.5 Conclusion

This last section focused on stability analysis of the simple but accurate space launcher model and its PWM-type actuator from section 6.2. On the basis of a result from [Gelig and Churilov, 1993], we defined a new multiplier and recast the stability conditions into convex stability conditions allowing to make the use of the result easier and to decrease the conservatism of this IQC based stability analysis method. The result can be applied to multi-input-multi-output systems and this is its main advantage over the method from section 6.3 which was dedicated to the analysis of single-input-single-output systems. It is also derived in the IQC framework so we can hope for further extensions of it toward the more classical soft IQC framework.
We intend to pursue the works presented here by the definition of new multipliers describing $\Delta_{iqc,h}$ presented in appendix B as we did not manage to implement the corresponding stability analyzes.

6.7 Conclusion

The present chapter aimed to show different stability and robust stability results for systems with PWM. It was intended to study pulse-modulation devices as they are commonly used to model the ON/OFF behavior of the thrusters used for attitude control. Therefore, the analysis of such systems is of high interest. We proposed three different methods. Two of them were based on IQC theory but relied on different approaches. The third one was used to find a different stability result with a tool using another theory. In this case, we used a Lyapunov theory based tool. As usual in robustness analysis, the first step of the process is to transform the model to be studied to fit it into the framework of the tool to be used. All the IQC-based methods rely on the fact that it is not the high frequency components of the PWM that drive the trajectories of the system but only the low-frequency components. The nominal actuator from section 6.3 and the so-called averaging method of section 6.6 clearly have this idea in common that induces the same type of loop transformation. Low-frequency harmonics are driving the motion of the launcher and the "other part" of the effect of the PWM (Δ_{PWM} or $\int(f-v)$) are only perturbations in the sense that they have little influence on the overall behavior.
During this study, we used the same representation for the analysis with soft IQC and the analysis with the result of [Seuret and Gomes Da Silva Jr, 2011]. The transformations we did in section 6.3 were essentially driven by the multipliers implemented in the LPVMAD toolbox and a pragmatic analysis of the effect of the PWM on the angular speed of the launcher. This speed was split into two components, one from a "nominal actuator", the other from a "perturbation operator". The goal of the construction of this representation was twofold: it allowed to bypass the issue of the $\mathcal{L}_2$ unboundedness of the PWM operator and it enabled us to use the multipliers of LPVMAD to perform a stability analysis of the system with soft IQC. As a result, we could use all the features of state-of-the-art multipliers to reduce the conservatism of the stability test. The approach of Arkadii Kh. Gelig and Alexander N. Churilov is similar to the one we used to build the model for soft IQC analysis but it is mathematically nicer. The loop transformations are performed as changes of variable and result in the analytical definition of two new operators. These operators when associated to a modified nominal system form a LFR equivalent to the initial model. From there, the definition of the operators enables to determine multipliers which are defining IQC satisfied by the new perturbation operators.
The three different analyses give different characterizations of stability and have pros and cons. The following points aim to sum up these features.

- The method based on pragmatic modeling of the effect of the PWM on the angular speed and soft IQC robust stability analysis could eventually be extended to multi-input multi-output PWM. Even if it may not be straightforward, we can think of a combination of this PWM representation with the factorization of the three degrees of freedom equations of motion defined in chapter 5. Furthermore, the representation of the operator Δ_{PWM} as a nonlinearity in a sector may be too conservative as it gives too much influence to Δ_{PWM} on the behavior of the launcher. However, the method is good to show the potential of the IQC tool and see how we can assess the stability of system with various perturbation operators and give results in a few minutes. In addition to that, the similarities between this method and the hard IQC based method gives leads for the improvement of the latter.

- The Lyapunov theory based tool was found once the modeling for soft IQC was finished. As the transformation we performed made the problem fall into sampled-data systems theory, we decided to address robustness properties by extending the result in [Seuret and Gomes Da Silva Jr, 2011] for uncertain systems. The main advantage of this technique is that it is specially developed for sampled-data systems and as this representation of PWM seems promising, such results will give input to further development of analytical tools for control law validation. The main drawback of the technique is that it guarantees only local stability of the system. Furthermore, we saw we managed to prove the stability over very small ellipsoids of initial conditions and for sampling periods that are small with respect to the one used for current space launchers.

- The method based on the works of Arkadii Kh. Gelig and Alexander N. Churilov is a rigorous formulation of the transformations done for the soft IQC analysis. As it is trying to build multipliers directly from the analytical definition of the perturbation operator, we can hope for very interesting developments to come. However, even with the improvement in conservatism reduction we brought with our works, the method is still too conservative. Nevertheless, it is the most promising of the three methods we used and several leads should be investigated in future works. In addition to that, leads can be given by the two other methods and reversely, we can think of improvements of the soft-IQC based stability analysis based on these works.

Concerning the perspectives of this study, clearly the method based on hard IQC presents lots of leads for improvements. The first one, is the extension of the framework to soft IQC. Such an extension would allow to use the multipliers we defined in section 6.6 directly with more classic multipliers as those of appendix A and perform analyzes of more complex systems. A second lead would simply be the search for new quadratic constraints on the inputs and outputs of $\Delta_{iqc,h}$. Finally, other loop transformations could help to improve the system description and so reduce the conservatism.

Chapter 7

Conclusion

In the aerospace domain, the trend is to introduce analytical tools during the development phase and Verification and Validation (V&V) processes of the construction of space launchers. Indeed, with the recent advances in control system theory, we hope that advanced analytical techniques will improve significantly the design, the controller tuning and the control law assessment of current and future space launchers.

The implementation of these new techniques would come as a complement on the popular methods used today for verification and validation. In most cases, these are based on time-domain simulations and provide stochastic guarantees. They could certainly be bettered with more rigorous tools. Among the numerous robustness analysis techniques that were developed in the second half of the XX^{th} century, one seems more appropriate than the others as it is well-suited for the analysis of large complex nonlinear systems. This analytical method is based on operator description with Integral Quadratic Constraints (IQC). Its main interest is that IQC descriptions can be found for almost any operators under mild assumptions causing very few exceptions. In the context of control law validation for space launchers, highly complex systems with subsystems which are not encountered regularly in control system theory, this feature is a huge advantage over the other techniques that could have been used. Furthermore, from a theoretical point of view, IQC based stability analysis happens to be a generalization of other well-known results from different stability theories. For instance, result from input-output theory as the small-gain theorem, from the robust control field as the μ-analysis or from absolute stability theory as Circle and Popov criteria can be recovered as particular cases of the general IQC stability theorem 4. This fact is crucial in the choice of the tool, it means that we can use very specific tools to describe each subsystems and it is a huge advantage that allows to study complex systems with reduced conservatism. For conventional subsystems, there are numerous multipliers in the literature. In addition to that, for subsystems which do not fall into the frame of classical results or classical IQC results, building new IQC to describe operators is possible and made easier by the good knowledge of the subsystem the engineers have. This is why the knowledge of the control system engineers at ESA and Astrium ST collaborating with the project was crucial.

As expected the IQC based tools allowed us to perform robustness analyzes with reduced conservatism. Consequently, we hope for the analysis of a complete representative model to be feasible in the near future and to have reduced conservatism too. To do so, we will take advantage of the fact that we can easily change the model configuration to improve the representativeness, or to analyze something else. In the applications, it is possible perform the analyzes gradually, including more and more details without having to redefine the analysis models. This feature is mostly due to the representation of the model used for the analysis. As it relies on Linear Fractional Representations (LFR) of systems, it benefits from the

flexibility of this representation and increasing the representativeness of the model from a simple one is easy.

These are the main reasons why the partners of the project chose IQC over other well-known methods as the formal tool to be used during this PhD. This choice has been comforted during the works by satisfying comparison with other analytical methods. Moreover, during an ESA project ended in 2008 and which aimed to implement the recent IQC analysis techniques, a toolbox was developed [Köroglu et al., 2008] and was ready to be used for the study.

In this framework, the goal of the project was to make use of IQC based robustness analysis methods in the context of control law validation for space launchers in ballistic flight.
First we defined a simplified but representative space launcher model. It was mostly formed of classical subsystems from the field of automatic control research. We based all the works on it. Through simplifications and transformations, we obtained analysis models that were fitting in the IQC framework and with which we could address the two key elements to be investigated during the study: the uncertain nonlinear equation of motion and the nonlinear PWM Attitude Control System (ACS). The models were defined with the engineers of Astrium ST and ESA and have the fundamental features of models currently used for Monte-Carlo based verification and validation. Every simplifications were done in agreement with the industrial partners to keep a model of the system that was as meaningful as possible to guarantee the representativeness of the analysis results.

After the model definition, we described the IQC framework for stability and performance analysis from simple considerations about signals, systems and system interconnections to the main IQC stability theorem. It also allowed us to determine the exact setup required for our analysis models to fall into the scope of IQC. Several examples have been given to show the many ways there exist to build IQC multipliers that define valid IQC for operators from widely used characterizations such as gain, sector bounds, spectral content, etc. Finally, the main stability theorem was given as well as a less known IQC result. We presented two different theorems with the aim to put the emphasis on the fact that IQC are a mean to describe operators and that it is not required to fit the main IQC theorem framework to guarantee stability and/or performance of a LFR with an IQC describing the perturbation block.

Once the model defined and the tool known, the issues caused by the two aforementioned key elements have been assessed. These issues were defined in accordance to the needs of the industrial partners and their current knowledge of the system. From the two problems emerged two separated studies. Of course, we would like to see them merged in future works. The first goal was to assess the effect of the nonlinear uncertain equation of motion on the stability and performance of space launchers. Indeed, as the current analyzes are generally done on very simplified models since the tools in use cannot account for the nonlinearity induced by the three-dimensional equation of motion, there is a great interest in performing robustness analysis of a system with static and dynamic couplings and uncertain inertia matrix. As a consequence, the study aimed to estimate the domains of stability and performance under inertia uncertainties. We addressed this issue by defining a factorization of the equation of motion that models inertia uncertainties and gyroscopic couplings generation with LFR. From the analyzes we obtained maps of feasibility regions of the stability test in the inertia uncertainty plane. The second problem we investigated was the effect of the ON/OFF behavior of the ACS thrusters on the stability of the closed-loop system. The description of the actuators resulted in the use of a PWM operator in the analysis model. This study had to be performed by the mean of loop transformations due to the PWM unboundedness. The two approaches used, our study of the effect of a pulse-modulated torque signal on the angular speed and the other one from [Gelig and Churilov, 1998] were finally very close in terms of physical meaning. They resulted in very similar system representations so it strengthened the

choice made in our works [Chaudenson et al., 2012]. Again, the goal was here to get readable results so we defined maps of feasibility regions.

For both applications, we applied other analysis methods which, even though they did not give comparable results, allowed to observe the influence of the modeling choices and the different types of stability we could prove for the models of our study. As the alternative methods were proving local asymptotic stability, it also enabled us to get a different view than the $\mathcal{L}_2$ stability we prove with the IQC-based analysis. Generally, the applications showed that IQC based methods were less conservative than the more classical methods we used to assess the robustness of launchers. The main advantage of IQC over other techniques is the possibility to analyze systems with various types of perturbation operators as parametric uncertainties, time-varying gains, nonlinearities and delays in one analysis and so to account for these different features simultaneously and specifically by diagonal augmentation of dedicated multipliers. This is rarely the case, except for very specific Lyapunov theory based stability results.

Concerning the analysis of the model with full equation of motion, the outcome of the modeling phase was a large 27-inputs 27-outputs perturbation operator gathering the uncertain inertia terms, the gyroscopic couplings over a very large flight envelope and the saturation actuator model with a dead-zone. Despite the size of the model, analyzes were performed and allowed to guarantee the stability of the closed-loop system for a large range of uncertain inertia terms depicted in figure 5.12. The performance analysis was done for a simpler perturbation operator but it also allowed us to illustrate the potential of IQC-based methods in the assessment of performance degradation due to uncertainties. The results are shown in figure 5.22. The analysis of the full nonlinear equation of motion also showed how the stability test resolution is currently limited. Indeed, for the robust stability analysis problem, the size of the LMI to be solved in the KYP lemma (lemma 6) caused some numerical inaccuracies to appear (see again figure 5.12). These were even more critical with the performance test results that we could not present as their reliability is still questioned. These issues appear as we were limited in computational power. Hence, we expect the future advances in resolution algorithm for large LMI problems and in computing power to make possible further investigations. Of course, that would also be made possible by the definition of smaller LFR to represent the equation on motion as it would reduce the computational burden. In particular, the polynomial definition of the equation of motion should be exploited, as well as smaller factorizations of the inertia and coupling matrices. Another lead should be fruitful to follow. It is the exploitation of the numerical structure of the LMI problem. Due to the structure of augmented multipliers (4.53), they are large (twice the size of LFR signals) but they have many zeros. We can find these large zero blocks in the expression of the KYP lemma (lemma 6) and maybe it is possible to reduce the problem size by looking at the problem structure. This would reduce the computational burden and hopefully the numerical inaccuracies too. Finally, to reduce the problem size by doing approximation we could consider to perform a sensitivity analysis to remove the parameters which have less influence on the stability and performance.

Regarding the analysis of the effect of the PWM on stability, our first work was to look into the works of other field to see if some were applicable to our aerospace application. Indeed, the PWM is a device that is extensively used in power electronics or energy systems but in very few aerospace studies. Consequently we took a more pragmatic approach. Our first idea was to determine the difference between the motion generated by a sample-and-hold actuator and one caused by a PWM. It allowed us to define a transformed representation of the PWM for which stability can be investigated with IQC as it bypasses the issue of PWM $\mathcal{L}_2$ unboundedness, see [Chaudenson et al., 2012]. Later, we observed the similarity between our observation based modeling and the loop transformations of [Gelig and Churilov, 1998]. The key point behind both methods is that the effect of a pulse-modulated signal on the output of a low-pass system is mostly due to the low-frequency components of the input signal. Hence the representations

we used combined a sort of first harmonic approximation of the PWM with a complementary operator aiming to keep the modulator representation exact. These approximations were represented by the nominal actuator in figure 6.5 and the operator $\Phi(\mathcal{SH}_h)$ from z to v in (6.91) whose definitions are almost identical. From this assumption, the analysis is done considering that the low-frequency approximation of the actuator "drives" the system and that the influence of the complementary operator on the system comes as a perturbation. It can be easily verified by simulation on a simple model as the one figure 6.1 by replacing the PWM by the saturation ϕ_{ACS} or by its equivalent nonlinearity Φ. The results were very different from one analysis method to another but the most promising one, based on the rigorous mathematical works of A.Kh. Gelig and A.N. Churilov, could lead to multipliers defining IQC dedicated to the study of pulse-modulated systems. This is without doubt a lead to follow in order to be able to take into account the nonlinear discrete-time behavior of the PWM during robustness analysis. Another advantage of this technique is that it can be applied to multi-input multi-output PWM and so be implemented in a model as the one from chapter 5. On these tracks, further loop transformations or an extension of the framework to soft IQC could be a major advances in the field, especially when thinking about the impact such tool could have on performance analysis and controller design. But before that the multiplier still has to be improved to cover the transformed LFR figure 6.26 in a better way and reduce the conservatism. To do so, merging the results of [Chaudenson et al., 2012] and [Chaudenson et al., 2013b] could help further investigations.

The introduction of analytical techniques along the steps of the development of a space launcher will allow significant reductions in terms of costs and manpower, and will enable, by a more systematical way of tuning and assessing control laws, to get flyable designs much faster. In this scope, IQC based tools already present promising result and show that they may be the most appropriate ones for the robustness analysis of large complex systems. They account for the system structure and allow to deal specifically with each subsystems, it means that we can improve the representation contained in the multipliers easily and reuse the set up to assess the improvements. We experimented this while building new multipliers in the last chapter. The flexibility of the method is a huge advantage. Moreover, the results obtained with IQC can go way beyond stability analysis with performance analysis with description of the particular performance criteria of the field with multipliers using the research of [Levant, 2010] or [Pittelkau, 2003]. Later on controller synthesis and merging of IQC method with worst-case search algorithms could extend greatly the frame of use of this analytical tool and give it the influence it deserves.

Chapter 8

Appendix: Leads for new multipliers

8.1 Introduction

A lead for the continuation of the works with the representation of the PWM operator of A.Kh. Gelig and A.N. Churilov presented in section 6.6 is to try to improve the multiplier

$$P := \begin{pmatrix} 0 & 0 & \frac{1}{2} & 0 \\ 0 & \varepsilon_1 & \frac{\theta}{2} & 0 \\ \frac{1}{2} & \frac{\theta}{2} & \varepsilon_2 - z_* + \lambda_1 & \frac{\lambda_2}{2} \\ 0 & 0 & \frac{\lambda_2}{2} & -\frac{3\lambda_1}{h^2} \end{pmatrix}$$

such that the IQC it defines guarantees a better representation of $\Delta_{iqc,h}$ from figure 6.26. Bettering the representation of $\Delta_{h,iqc}$ by the IQC defined with P means to put more information on how Δ maps z and $\dot{z}$ into v and u into P. Basically, we would like to replace the zeros in P by non zero terms. To do so, we looked for new constraints involving z, $\dot{z}$, v and u. To guide us, we observed the current structure of the multiplier P. We see for instance that there are no constraint linking u and z or $\dot{z}$. From a pragmatic point of view, such a constraint could be a way to materialize the fact announced before that the low-pass system $M_{iqc,h}$ is essentially driven by v, the sampled output of the modulator equivalent nonlinearity Φ. Thus we could expect u to be "small" with respect to z or at least to have a constraint involving u and z. With this goal, we derived some constraints on z, $\dot{z}$ and u using a similar method to [Gelig and Churilov, 1993] and derived from section 6.6.

8.2 Modified passivity condition

First we consider the definition of signal u (6.87) as a function of w and v:

$$u(t) = \int_0^t (w(\tau) - v(\tau))\, d\tau. \tag{8.1}$$

We saw that u is a piecewise affine function of the time which vanishes every $t_n,\ n \in \mathbb{N}$ (6.131). Its definition can be recast in (6.131) for all t in T_n:

$$u(t) = \int_{t_n}^t (w(\tau) - v_n)\, d\tau \tag{8.2}$$

The definition of $w - v$ over a sampling period T_n with the expressions from (6.12) reads as

$$(w-v)(t) = \begin{cases} \lambda_n - v_n, & t \in [t_n; t_n + \tau_n) \\ -v_n, & t \in [t_n + \tau_n; t_{n+1}) \end{cases}, \tag{8.3}$$

where λ_n is the pulse height and τ_n is the pulse width defined in (6.13) and given again below:

$$\lambda_n = sign\left(z(t_n)\right)\Gamma_{av},$$

$$\tau_n = \begin{cases} 0, & \text{if } |z(t_n)| < \Gamma_{min} \\ \frac{|z(t_n)|}{\Gamma_{av}} h, & \text{if } \Gamma_{min} \leq |z(t_n)| < \Gamma_{av} \\ h, & \text{if } |z(t_n)| \geq \Gamma_{av} \end{cases}.$$

Furthermore, over a sampling period we can determine the average value of the pulse-modulated signal:

$$v_n = \frac{\lambda_n \tau_n}{h}. \tag{8.4}$$

Integration of (8.3) from t_n to $t \in T_n$ gives the analytical definition of u thanks to (8.4):

$$u(t) = \begin{cases} \lambda_n \left(1 - \frac{\tau_n}{h}\right)(t - t_n), & t \in [t_n; t_n + \tau_n) \\ \lambda_n \frac{\tau_n}{h}\left(t_{n+1} - t\right), & t \in [t_n + \tau_n; t_{n+1}) \end{cases} \tag{8.5}$$

Considering the definition we gave to the pulse-modulated signal parameters λ_n and τ_n above, it appears that $u(t)$ is 0 over T_n when $|z_n| \leq \Gamma_{min}$ and $|z_n| \geq \Gamma_{av}$. We see again that for all integer n we have $u(t_n) = 0$. As a first step in the description of the mapping from z to u, we observe that when $\Gamma_{min} \leq |z_n| \leq \Gamma_{av}$ and as defined by (6.13) τ_n is always positive and the following sign constraints hold for all $t \in T_n$:

$$\begin{cases} 1 - \frac{\tau_n}{h} & \geq 0 \\ t - t_n & \geq 0 \\ t_{n+1} - t & \geq 0 \end{cases} \tag{8.6}$$

Thus, we can find out what is the sign of u compared to the sign of $z_n = \mathcal{SH}_h(z)$. As a consequence, u always has the sign of $\lambda_n = sign(z_n)\Gamma_{av}$ so it has the sign of z_n for $t \in T_n$. Finally, at any time instant t we have the constraint

$$u(t)(\mathcal{SH}_h z)(t) \geq 0 \tag{8.7}$$

drawn from the fact that the product of two terms with the same sign is positive. This passivity constraint on the operator from $(\mathcal{SH}_h z)$ to u can be recast into an IQC involving z, $\dot{z}$ and u. For this, let us remind the definition of the sampling error $\xi = z - (\mathcal{SH}_h z)$ to find that (8.7) is equivalent to

$$u(t)z(t) \geq u(t)\xi(t). \tag{8.8}$$

We observe here a classic passivity constraint for the transfer from z to u but with the sampling taken

into account with the non-zero right hand side of (8.8). This is the same type of constraint as for the modified sector condition (6.98). To build a valid IQC from this constraint, we introduce two positive parameters η_1 and η_2 in the manner of [Gelig and Churilov, 1993] and we obtain

$$\eta_1 \dot{z}(t)^2 + \eta_2 u(t)^2 + u(t)z(t) \geq \eta_1 \dot{z}(t)^2 + \eta_2 u(t)^2 + u(t)\xi(t). \tag{8.9}$$

By completion of the squares (see an example in (6.127)) the estimate

$$\eta_1 \dot{z}(t)^2 + \eta_2 u(t)^2 + u(t)z(t) \geq \eta_1 \dot{z}(t)^2 - \frac{1}{4\eta_2}\xi(t)^2 \tag{8.10}$$

holds. We would like to show that the integral of the constraint above is positive to use the same Lyapunov argument as in paragraph 6.6.3. For this, we first rewrite Wirtinger's inequality from lemma 2 in [Gelig and Churilov, 1993] or (6.108):

$$\int_{t_n}^{t_{n+1}} |(z - \mathcal{SH}_h(z))(t)|^2 dt = \int_{t_n}^{t_{n+1}} |\xi(t)|^2 dt \leq K^2 h^2 \int_{t_n}^{t_{n+1}} |\dot{z}(t)|^2 dt.$$

It allows us to establish the positivity of the integral of the right hand term in (8.10). The sufficient condition for (8.9) to hold is:

$$\eta_2 \geq \frac{(Kh)^2}{4\eta_1} > 0 \Leftrightarrow \begin{pmatrix} \eta_2 & 1 \\ 1 & \frac{4\eta_1}{(Kh)^2} \end{pmatrix} \geq 0. \tag{8.11}$$

The equivalence between the two conditions in (8.11) is given by Schur's lemma. (8.11) ensures that the IQC

$$\int_{t_n}^{t_{n+1}} \begin{pmatrix} z(t) \\ \dot{z}(t) \\ u(t) \end{pmatrix}^T \begin{pmatrix} 0 & 0 & \frac{1}{2} \\ 0 & \eta_1 & 0 \\ \frac{1}{2} & 0 & \eta_2 \end{pmatrix} \begin{pmatrix} z(t) \\ \dot{z}(t) \\ u(t) \end{pmatrix} \geq 0. \tag{8.12}$$

is valid.
Here by considering the analytical expression of u we built another IQC that is satisfied by the inputs and outputs of $\Delta_{iqc,h}$ of figure 6.26. The interest of building such new IQC is that we hope for conservatism reduction in the stability test of theorem 12. To implement this new multiplier, we need to elaborate a new version of theorem 12. First two parameters η_1 and η_2 are added. Then in condition (1) of theorem 12 we add that the parameters must satisfy the LMI

$$\begin{pmatrix} \eta_2 & 1 \\ 1 & \frac{4\eta_1}{(Kh)^2} \end{pmatrix} \geq 0 \text{ and } \eta_1, \eta_2 > 0. \tag{8.13}$$

Finally, we should look for the validity of (2) of theorem 12 with the multiplier changed in:

$$P' := \begin{pmatrix} 0 & 0 & \frac{1}{2} & \frac{1}{2} \\ 0 & \eta_1 + \varepsilon_1 & \frac{\theta}{2} & 0 \\ \frac{1}{2} & \frac{\theta}{2} & \varepsilon_2 - z_* + \lambda_1 & \frac{\lambda_2}{2} \\ \frac{1}{2} & 0 & \frac{\lambda_2}{2} & \eta_2 - \frac{3\lambda_1}{h^2} \end{pmatrix} \tag{8.14}$$

To go further and look for more improvements in the characterization of $\Delta_{iqc,h}$, we continue our investigations and look for another modified sector condition.

8.3 Modified sector condition

We already saw in the above paragraph that signals u and z are satisfying a kind of passivity constraint modified to take into account the sampling. We are going to observe that they also satisfy a sector condition which also has to be modified for the same reason. For this, we will use exactly the same method as in 6.6.3.
Let us consider that u is the output of a nonlinearity Ψ with input $\mathcal{SH}_h(z)$, that is

$$u = \Psi(\mathcal{SH}_h(z)). \tag{8.15}$$

That assumption makes the setup of the analysis look like the setup figure 8.1. Still in the manner of [Gelig and Churilov, 1993], we would like to show that Ψ fulfills a sector condition

$$0 \leq \frac{\Psi(x)}{x} \leq \frac{1}{y_*} \quad \text{for } x \neq 0, \text{ and } \Psi(0) = 0. \tag{8.16}$$

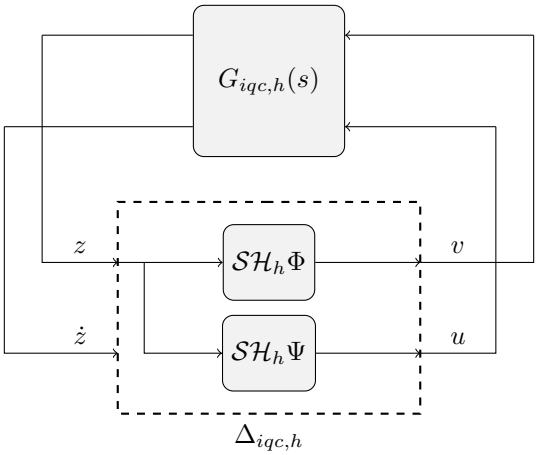

Figure 8.1: LFR of the model as we consider it when looking for new quadratic constraints

To find this condition, we observe the time-domain expression given in (8.5) for u. u is a piecewise affine function. Over each sampling interval T_n, we know that if $|z(t_n)| \leq \Gamma_{min}$ or $|z(t_n)| \geq \Gamma_{av}$, u is zero. For the other values of $|z(t_n)|$ the absolute value of $u(t)$ over a sampling period T_n reaches a maximum for $t = t_n + \tau_n$:

$$\forall t \in T_n, \quad |u(t)| \leq |u(t_n + \tau_n)| = |z(t_n)| \left(1 - \frac{|z(t_n)|}{\Gamma_{av}}\right) h. \tag{8.17}$$

From this observation and the fact that $u(t)$ and $\mathcal{SH}_h(z)(t)$ have the same sign (8.7), we have the following for any sampling interval T_n:

$$\text{If } \mathcal{SH}_h(z)(t) \geq 0, \text{ then } u(t) \geq 0 \text{ and } u(t) \leq \mathcal{SH}_h(z)(t)h(1 - \frac{\Gamma_{min}}{\Gamma_{av}}) \Leftrightarrow \beta\mathcal{SH}_h(z)(t) - u(t) \geq 0 \quad (8.18)$$

with $\beta = h(1 - \frac{\Gamma_{min}}{\Gamma_{av}})$. We also have:

$$\text{If } \mathcal{SH}_h(z)(t) \leq 0, \text{ then } u(t) \leq 0 \text{ and } u(t) \geq \mathcal{SH}_h(z)(t)h(1 - \frac{\Gamma_{min}}{\Gamma_{av}}) \Leftrightarrow \beta\mathcal{SH}_h(z)(t) - u(t) \leq 0. \quad (8.19)$$

The two conditions above can be recast into a single one valid for all sampling period and that is similar to (6.98)

$$\left(\mathcal{SH}_h(z)(t) - y_* u(t)\right) u(t) \geq 0 \quad (8.20)$$

where $y_* = 1/\beta$. Note that when $u(t) = 0$ the constraint also holds. Now to take the sampling into account we are going to use the sampling error signal $\xi = z - \mathcal{SH}_h(z)$ defined in (6.99) when we were looking for a convex constraint on the parameters of P_{GC}. Then the modified sector condition on Ψ given by (8.20) can be equivalently expressed as:

$$u(t)\left(z(t) - y_* u(t)\right) \geq u(t)\xi(t). \quad (8.21)$$

The above constraint (8.21) is tighter than the positivity constraint (8.7) and can be transformed into a hard IQC using exactly the same method with completion of the squares and Wirtinger's inequality as in paragraphs 6.6.3 and 6.6.3.
To reduce the conservatism of the representation of the mapping from z to u and as it fulfills a sector condition, we are going to use the Popov criterion to capture the mapping in a better way. Thus, we are going to introduce an extra real parameter θ_Ψ and consider the quadratic form F:

$$F(z(t), \dot{z}(t), u(t)) = \begin{pmatrix} z(t) \\ \dot{z}(t) \\ u(t) \end{pmatrix}^T \begin{pmatrix} 0 & 0 & \frac{1}{2} \\ 0 & \alpha_1 & \frac{\theta_\Psi}{2} \\ \frac{1}{2} & \frac{\theta_\Psi}{2} & \alpha_2 - y_* \end{pmatrix} \begin{pmatrix} z(t) \\ \dot{z}(t) \\ u(t) \end{pmatrix}. \quad (8.22)$$

The following is done in the manner of [Gelig and Churilov, 1993] and with the same method as for the definition of (6.130). Hence the proof is given with less details in this case and we invite the reader to refer to the construction of (6.130) for more precisions.

We are going to look for a condition for the IQC

$$\int_{t_n}^{t_{n+1}} F(z(t), \dot{z}(t), u(t))dt \geq \theta_\Psi \int_{t_n}^{t_{n+1}} \Psi(z)(t)\dot{z}(t)dt \quad (8.23)$$

to hold such that we can use exactly the same Lyapunov argument as in the brief proof of theorem 11. For this, it is sufficient to show that there exists a non-negative number α_Ψ such that

$$F(z(t), \dot{z}(t), u(t)) \geq \theta_\Psi \Psi(z)\dot{z} + \alpha_\Psi \left((Kh)^2\dot{z}^2 - \xi^2\right) \quad (8.24)$$

holds. Indeed, we can use Wirtinger's inequality (6.108) to show the positivity of the integral of the

second term on the right hand side of 8.24. The constraint (8.24) can be expanded in

$$(z - y_* u)u + \theta_\Psi(u - \Psi(z))\dot{z} + (\alpha_1 - \alpha_\Psi(Kh)^2)\dot{z}^2 + \alpha_2 u^2 + \alpha_\Psi \xi^2 \geq 0. \tag{8.25}$$

If we assume that the nonlinearity Ψ satisfies the Lipschitz condition

$$|\Psi(x_2) - \Psi(x_1)| \leq L_\Psi |x_2 - x_1| \tag{8.26}$$

for any x_1, x_2 in $\mathbb{R}$. We can express (8.26) with $x_1 = \mathcal{SH}_h(z)$ and $x_2 = z$ to find a bound on the second term in (8.25). Furthermore, as $(z - y_* u)u \geq \xi u$ from (8.21); a sufficient condition for (8.25) to hold is:

$$\xi u - \theta_\Psi L_\Psi |\xi||\dot{z}| + (\alpha_1 - \alpha_\Psi(Kh)^2)\dot{z}^2 + \alpha_2 u^2 + \alpha_\Psi \xi^2 \geq 0. \tag{8.27}$$

By completion of the squares for the terms in $u\xi$ and u^2 another sufficient condition is:

$$-\theta_\Psi L_\Psi |\xi||\dot{z}| + (\alpha_1 - \alpha_\Psi(Kh)^2)\dot{z}^2 + (\alpha_\Psi - \frac{1}{4\alpha_2})\xi^2 \geq 0. \tag{8.28}$$

(8.28) is a quadratic form in $|\xi|$ and $|\dot{z}|$. By writing its matrix, we have a condition of validity of (8.23) very similar to 25 in [Chaudenson et al., 2013b] thanks to the application of Schur's lemma. This condition reads as:

$$\begin{pmatrix} \alpha_1 - \alpha_\Psi(Kh)^2 & L_\Psi\theta_\Psi/2 & 0 \\ L_\Psi\theta_\Psi/2 & \alpha_\Psi & 1 \\ 0 & 1 & 4\alpha_2 \end{pmatrix} \succeq 0 \text{ and } \alpha_\Psi \geq 0. \tag{8.29}$$

We can now merge the quadratic form F from (8.23) with the quadratic form defined by the multiplier P to obtain a quadratic form defined by

$$P'' := \begin{pmatrix} 0 & 0 & \frac{1}{2} & \frac{1}{2} \\ 0 & \varepsilon_1 + \alpha_1 & \frac{\theta}{2} & \frac{\theta_\Psi}{2} \\ \frac{1}{2} & \frac{\theta}{2} & \varepsilon_2 - z_* + \lambda_1 & \frac{\lambda_2}{2} \\ \frac{1}{2} & \frac{\theta_\Psi}{2} & \frac{\lambda_2}{2} & \alpha_2 - y_* - \frac{3\lambda_1}{h^2} \end{pmatrix}. \tag{8.30}$$

Under the conditions (6.130) and (8.29), P'' defines a valid IQC satisfied by $\Delta_{iqc,h}$. We can now write another extension of theorem 11.

Theorem 13 *Consider the interconnection of the LTI stable system $M_{iqc,h}$ with the PWM operator $\mathcal{P}$ depicted figure 6.22. Assume that the matrix A is Hurwitz and the relative degree of $M_{iqc,h}$ is at least 2 where (A, B, C) is a state-space realization of $M_{iqc,h}$. Suppose the equivalent nonlinearity satisfies the sector condition (6.96) and the Lipschitz condition (6.110)*

$$|\Phi(x_1) - \Phi(x_2)| \leq L|x_1 - x_2|$$

for any x_1, x_2 in $\mathbb{R}$. Suppose that the nonlinearity Ψ in (8.15) satisfies the sector condition (8.16) and the Lipschitz condition

$$|\Psi(x_1) - \Psi(x_2)| \leq L_\Psi |x_1 - x_2|.$$

In addition to that, suppose there exist $\lambda_1 \geq 0, \lambda_2 \geq 0, \varepsilon_1 > 0, \varepsilon_2 > 0, \alpha_1 > 0, \alpha_2 > 0, \theta_0 \geq 0, \alpha_\Psi \geq 0$ *and real numbers* θ *and* θ_Ψ *such that the following conditions are fulfilled:*

(1) The LMIs (6.130) and (8.29) hold.

(2) The FDI

$$\begin{pmatrix} G_{iqc,h}(j\omega) \\ I_2 \end{pmatrix}^* P'' \begin{pmatrix} G_{iqc,h}(j\omega) \\ I_2 \end{pmatrix} \prec 0 \tag{8.31}$$

with P' *in (8.30) holds for all* $\omega \in \mathbb{R}_+$.

Then we have

$$\lim_{n\to\infty} v_n = 0, \quad \lim_{t\to\infty} z(t) = 0. \tag{8.32}$$

Proof. It is easy to see, that (8.29) implies (6.107) for P'' instead of P. Thus theorem 13 follows from theorem 12 and 11. □

Chapter 9

Appendix: Classical IQC multipliers

In this appendix the reader can find the description of the multipliers implemented in the IQC toolbox LPVMAD and that were not mentioned before to not overload the body of the text. More precisions can be found in [Köroglu et al., 2008] and the references therein. These multipliers cover perturbations commonly encountered in system analysis.

9.1 LTV parametric uncertainties

We now define a multiplier for the parametric LTV perturbation. For an engineer, such perturbations correspond to parameters of the system which are varying with time. The real parameter δ introduced earlier on in (4.78) is now considered to be time-varying. The rate of variation of $\delta(t)$ can eventually be bounded, in this case, we talk about "slowly" time-varying parameter. In this context, Δ belongs to $\mathcal{U}_{ltvs}$ defined as

$$\mathcal{U}_{ltvs} = \{\Delta(\delta(t)) = \delta(t)I_r, \forall t \geq 0, [\delta(t), \dot{\delta}(t)] \in \mathcal{D}' \subseteq \mathbb{R}^2\}. \tag{9.1}$$

Similarly to what has been done before to derive a multiplier defining an IQC covering an uncertain time-invariant parameter in chapter 4, we are going to consider the set of matrices S that define guarantee the inequality

$$\begin{pmatrix} I_{dr} \\ \Delta_{el}(\delta(t)) \end{pmatrix}^T S \begin{pmatrix} I_{dr} \\ \Delta_{el}(\delta(t)) \end{pmatrix} \geq 0 \tag{9.2}$$

to be valid for all $[\delta(t), \dot{\delta}(t)] \in \mathcal{D}'$ and with Δ_{el} to be defined soon. The problem with time-varying uncertain parameters is that we don't have a straightforward commutation identity as before in (4.80). Furthermore, we could directly use this constraint to define an IQC satisfied by $\Delta(\delta(t))$ with a static dynamic weighting i.e. $d = 1$; recall the definition of H in (4.79). However, we would loose the information about the rate of variation of δ. Consequently, we use the so-called swapping lemma already used in [Jönsson, 1996] and [Köroglu and Scherer, 2006]. This will require a few definitions given below.
First, we define $H \in \mathbb{RH}_\infty^{dr \times r}$ as in (4.79) and consider a state-space realization (A_H, B_H, C_H, D_H) of it with $A_H \in \mathbb{R}^{n_H \times n_H}$ a Hurwitz matrix. We define $H_{el} \in \mathbb{RH}_\infty^{(q+n_H)\times(r+n_H)}$, $H_{er} \in \mathbb{RH}_\infty^{(q+n_H)\times(r)}$,

$H_B \in \mathbb{RH}_\infty^{n_H \times r}$ and $H_C \in \mathbb{RH}_\infty^{q \times n_H}$:

$$H_{el} = \left[\begin{array}{c|cc} A_H & B_H & I \\ \hline C_H & D_H & 0 \\ 0 & 0 & I \end{array}\right], H_{er} = \left[\begin{array}{c|c} A_H & B_H \\ \hline C_H & D_H \\ I & 0 \end{array}\right], \tag{9.3}$$

$$H_B = \left[\begin{array}{c|c} A_H & B_H \\ \hline I & 0 \end{array}\right] \text{ and } H_C = \left[\begin{array}{c|c} A_H & I \\ \hline C_H & 0 \end{array}\right]. \tag{9.4}$$

Using these transfer functions, the swapping lemma reads in our framework as

$$H_{el} \underbrace{\begin{bmatrix} \delta I_r \\ \dot{\delta} I_{n_H} H_B \end{bmatrix}}_{\Delta_{er}} = \underbrace{\begin{bmatrix} \delta I_q & 0 \\ 0 & \dot{\delta} I_{n_H} \end{bmatrix}}_{\Delta_{el}} H_{er}. \tag{9.5}$$

From this, in a similar fashion as in chapter 4, we define the aforementioned set of matrices $\mathcal{S}'(\mathcal{D}')$ as

$$\mathcal{S}'(\mathcal{D}') = \left\{ S \in \mathbb{R}^{2(dr+n_H)\times 2(dr+n_H)} \;\middle|\; \forall [\delta, \dot{\delta}] \in \mathcal{D}', \begin{bmatrix} I \\ \Delta_{el}(\delta) \end{bmatrix}^T S \begin{bmatrix} I \\ \Delta_{el}(\delta) \end{bmatrix} \geq 0 \right\}. \tag{9.6}$$

The definition of $\mathcal{S}'(\mathcal{D}')$ ensures by right multiplying and left multiplying the quadratic inequality of (9.6) by H_{er} and H_{er}^*, respectively and by application of the swapping lemma that for all $S \in \mathcal{S}'(\mathcal{D}')$, the quadratic inequality

$$\begin{bmatrix} I \\ \Delta_{er} \end{bmatrix}^T \begin{bmatrix} H_{er} & 0 \\ 0 & H_{el} \end{bmatrix}^* S \begin{bmatrix} H_{er} & 0 \\ 0 & H_{el} \end{bmatrix} \begin{bmatrix} I \\ \Delta_{er} \end{bmatrix} \geq 0 \tag{9.7}$$

holds for all $\Delta \in \mathcal{U}_{ltvs}$.
Finally, the above quadratic inequality obviously define a valid IQC for the operator Δ_{er} by integration over frequency. Hence it allows proving the stability of the interconnection of Δ_{er} with the extended plant

$$M_e = \left[\begin{array}{c|ccc} A_M & B_M^{(1)} & 0 & B_M^{(2)} \\ \hline C_M & D_M^{(1)} & 0 & D_M^{(2)} \end{array}\right]. \tag{9.8}$$

Finally, since the stability of $(M, \Delta(t))$ is equivalent to the stability of $(M_e, \Delta_{er}(t))$, the multiplier $\Pi_{ltvs} \in \mathbb{RH}_\infty^{2(dr+n_H)\times 2(dr+n_H)}$ defined by $S \in \mathcal{S}'(\mathcal{D}')$, H_{el} and H_{er} as:

$$\Pi_{ltvs}(j\omega) = \begin{pmatrix} H_{er}(j\omega) & 0 \\ 0 & H_{el}(j\omega) \end{pmatrix}^* S \begin{pmatrix} H_{er}(j\omega) & 0 \\ 0 & H_{el}(j\omega) \end{pmatrix}. \tag{9.9}$$

allows to study the robust stability of a plant connected to a time-varying perturbation block.

9.2 Time-invariant, odd-monotone static nonlinearities

We consider now the sector bounded, slope restricted odd nonlinearity Δ. Δ belongs to $\mathcal{U}_{nlom}$ defined below:

$$\Delta \in \mathcal{U}_{nlom} = \{\Delta : \mathbb{R} \to \mathbb{R},\ \forall \xi, \xi_1, \xi_2, \Delta(-\xi) = -\Delta(\xi), \begin{cases} 0 \leq & \Delta(\xi)/\xi & \leq \beta, \\ 0 \leq & (\Delta(\xi_1) - \Delta(\xi_2))/(\xi_1 - \xi_2) & \leq \mu \end{cases} \}. \tag{9.10}$$

Δ is a nonlinear perturbation in the sector $(0, \beta)$ and with a maximum incremental gain μ. To build the multiplier that will define an IQC satisfied by such a Δ, we can proceed as in [Zames and Falb, 1968]. They introduced $x \geq 0$ and the SISO transfer function $G(s)$ satisfying:

$$G(s) = \int_{-\infty}^{+\infty} g(t) e^{-st} \mathrm{dt} \text{ and } \int_{-\infty}^{+\infty} |g(t)| \mathrm{dt} \leq g_0.$$

From this, they defined the multiplier:

$$\Pi_{nlom}(j\omega) = \begin{bmatrix} 0 & x + g_0 - G(j\omega) \\ x + g_0 - G(-j\omega) & -\frac{2}{\beta}x - \frac{1}{\mu}(2g_0 - G(j\omega) - G(-j\omega)) \end{bmatrix}. \tag{9.11}$$

9.3 Uncertain time-delays

The last perturbation to be considered is the time-delay. The multiplier implemented in the toolbox takes into account bounded time-varying time-delays in $\mathcal{D}_\tau := \{D_\tau : \mathcal{L}_2^r \to \mathcal{L}_2^r, D_\tau(\xi(t)) = \xi(t - \tau(t))\}$. The main issue with this element is that it cannot be seen as a perturbation block since it does not tend to the zero operator when the time-delay tends to zero. To face this, we introduce the perturbation operator $\Delta_\tau := (D_\tau - I) \circ \frac{1}{s}$. If the time-delay is bounded by τ_{max}, Δ_τ belongs to $\mathcal{U}_{nlom}$:

$$\mathcal{U}_{dmii} = \{\Delta = (D_\tau - I) \circ \frac{1}{s}, \tau : [0; \infty) \to [0; \tau_{max}]\}. \tag{9.12}$$

A multiplier that defines an IQC satisfied by $\Delta_\tau \in \mathcal{U}_{dmii}$ can be defined introducing $X = KK^T > 0, X \in \mathbb{R}^{r \times r}$ and writing:

$$\Pi_{dmii} = \begin{bmatrix} \tau_{max}^2 X & 0 \\ 0 & -X \end{bmatrix}. \tag{9.13}$$

This construction of multipliers describing Δ_τ comes form [Kao and Lincoln, 2004]. Refined multipliers for the cases when we have bounds on the rate of variation of the time-varying delay $\mathcal{D}_\tau$ are given in [Kao and Rantzer, 2007] but are not implemented in LPVMAD.

Chapter 10

Appendix: Equation of motion in angular momentum

The following paragraph presents briefly a new version of the works of chapter 5. By the mean of a change of variable in the state vector, we can avoid using the inertia matrix I_g twice and so reduce the size of the LFR derived from the modeling step from size 27 to size 18. For simplicity, we will only describe the reformulation with a new block diagram representing the equations of motion in the manner of figure 5.7 and give the state-space representation of the nominal system in the LFR.

First of all, let us remind to the reader the block diagram representing the equation of motion expressed with the coupling matrix from the cross-product definition, it is given figure 10.1.

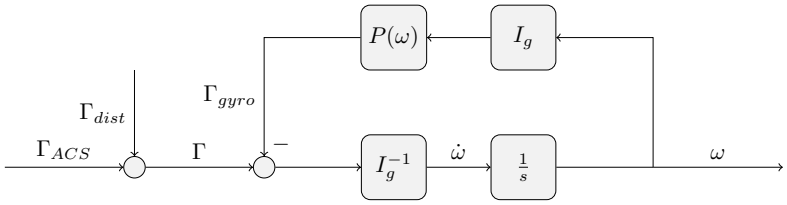

Figure 10.1: Original block diagram for Newton's equation of rotational motion

In this configuration, since the inertia matrix I_g is time-invariant, it is possible to move it from the left side of the first integrator to the right side. It gives the block diagram figure 10.2.

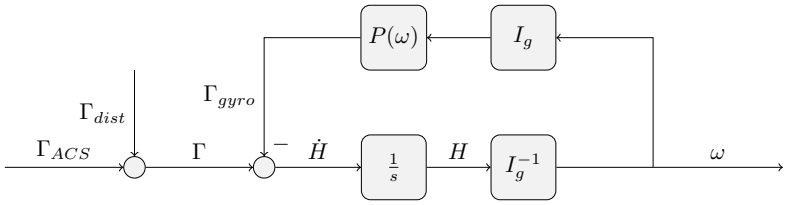

Figure 10.2: Change of variable, angular momentum H becomes a state of the model

In facts, moving the inertia matrix from one side of the integrator to another changes the variable to be integrated. It is now the derivative of the angular momentum denoted by $\dot{H}$. Finally, we can move the inertia matrix block one step further to the right, canceling the I_g^{-1} from the gyroscopic coupling path. The new representation of the equation of motion is given figure 10.3.
Inserting this new representation in the block diagram of the three degrees of freedom analysis model of figure 5.10, we obtain the new closed-loop representation of figure 10.4.

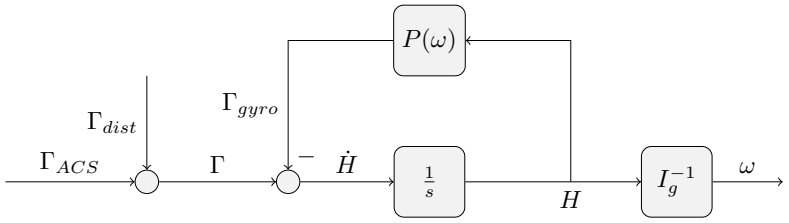

Figure 10.3: New representation of the equation of motion

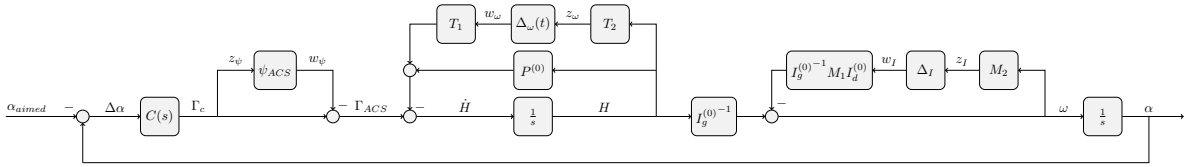

Figure 10.4: New block diagram for closed-loop LFR of chapter 5

After these simple manipulations of the representation, we have each one of the uncertain matrices from chapter 5 appearing only once in the model. This will give a boost to the stability analysis as it will make the computations less expensive. Indeed, the new LFR of the analysis model can be set up with the operators $M_{dyn}^{'}$ and $\Delta_{dyn}^{'}$ as follow.
First the nominal part $M_{dyn}^{'}$ is defined by its state-space realization as follow:

$$A = \begin{bmatrix} -P^{(0)} & -D_C & C_C \\ I_g^{(0)^{-1}} & 0_{3\times3} & 0_{3\times3} \\ 0_{3\times3} & -B_C & A_C \end{bmatrix},\ B = \begin{bmatrix} 0_{3\times9} & -T_1 & -I_3 \\ -I_g^{(0)^{-1}} M_1 I_d^{(0)} & 0_{3\times6} & 0_{3\times3} \\ 0_{3\times9} & 0_{3\times6} & 0_{3\times3} \end{bmatrix}, \tag{10.1}$$

$$C = \begin{bmatrix} M_2 I_g^{(0)^{-1}} & 0_{9\times3} & 0_{9\times3} \\ 0_{6\times3} & 0_{6\times3} & 0_{6\times3} \\ 0_{3\times3} & -D_C & C_C \end{bmatrix} \text{ and } D = \begin{bmatrix} -M_2 I_g^{(0)^{-1}} M_1 I_d^{(0)} & 0_{9\times6} & 0_{9\times3} \\ 0_{6\times9} & 0_{6\times6} & 0_{6\times3} \\ 0_{3\times9} & 0_{3\times6} & 0_{3\times3} \end{bmatrix}. \tag{10.2}$$

The new perturbation operator is defined as

$$\Delta_{dyn}^{'} = \begin{bmatrix} \Delta_I & 0 & 0 \\ 0 & \Delta_\omega(t) & 0 \\ 0 & 0 & \psi_{ACS} \end{bmatrix}. \tag{10.3}$$

These definitions determine the operators in the LFR figure 10.5 with the signals

$$v = \begin{bmatrix} v_I \\ v_\omega \\ v_\psi \end{bmatrix} \text{ and } w = \Delta_{dyn}^{'}(v) = \begin{bmatrix} \Delta_I v_I \\ \Delta_\omega(t) v_\omega \\ \psi_{ACS}(v_\psi) \end{bmatrix} = \begin{bmatrix} w_I \\ w_\omega \\ w_\psi \end{bmatrix}. \tag{10.4}$$

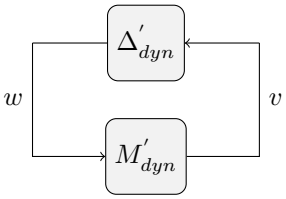

Figure 10.5: New LFR for robust stability analysis of the uncertain nonlinear equations of motion

Stability analysis Thanks to LPVMAD, stability domain computations were run in the manner of those paragraph 5.5.2. Differently from the previous study, calculations could be run on a laptop with the exact same configuration of table 5.1. It led to the stability domain estimate figure 10.6. The range of uncertainties in the terms of the inertia matrix for which stability can be proved is enlarged dramatically, it is now way beyond the "nominal" uncertainties. Furthermore, the computational effort needed is reduced so the full performance analysis should be feasible with this new model.

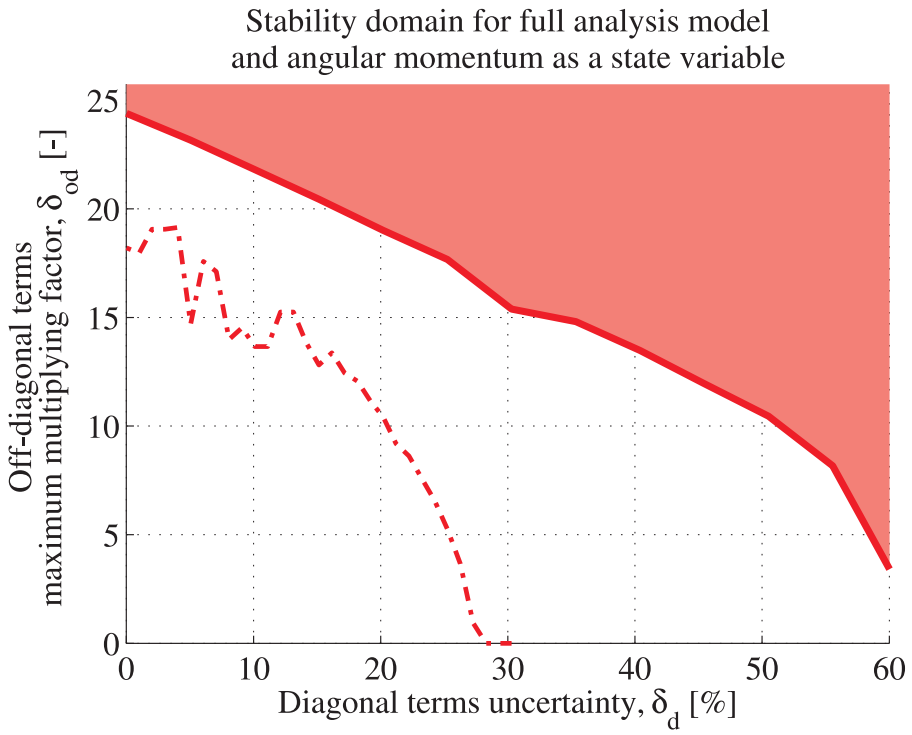

Figure 10.6: Stability region found in the setup of table 5.1, dynamic model with angular momentum as a state variable (solid), method of chapter 5 (dashed line).

References

[Ahmed et al., 1998] Ahmed, J., Coppola, V. T., and Bernstein, D. S. (1998). Adaptive asymptotic tracking of spacecraft attitude motion with inertia matrix identification. *Journal of Guidance, Control, and Dynamics*, 21(5):684–691.

[Balas et al., 2005] Balas, G., Chiang, R., Packard, A., and Safonov, M. (2005). *Robust Control Toolbox® 3*. Natick, MA: The MathWorks, Inc.

[Biannic et al., 2006] Biannic, J., Tarbouriech, S., and Farret, D. (2006). A practical approach to performance analysis of saturated systems with application to fighter aircraft controllers. In *5th IFAC Symposium on Robust Control Design, Toulouse, France*.

[Boyd et al., 2004] Boyd, S., El Ghaoui, L., Feron, E., and Balakrishnan, V. (2004). *Linear matrix inequalities in system and control theory*. Society for industrial and applied mathematics.

[Boyd and Yang, 1989] Boyd, S. and Yang, Q. (1989). Structured and simultaneous lyapunov functions for system stability problems. *International journal of Control*, 49(6):2215–2240.

[Chaudenson et al., 2013a] Chaudenson, J., Beauvois, D., Bennani, S., Frechin, C., Ganet-Schoeller, M., and Sandou, G. (2013a). Dynamics modeling and comparative robust stability analysis of a space launcher with constrained inputs. In *12th European Control Conference, Zurich, Switzerland.*

[Chaudenson et al., 2012] Chaudenson, J., Beauvois, D., Bennani, S., Frechin, C., Ganet-Schoeller, M., Sandou, G., and Scherer, C. W. (2012). Pwm modeling for attitude control of a launcher during ballistic phase and comparative stability analysis. In *7th IFAC Symposium on Robust Control Design, Aalborg, Denmark.*

[Chaudenson et al., 2013b] Chaudenson, J., Fetzer, M., Scherer, C. W., Beauvois, D., Sandou, G., Bennani, S., and Ganet-Schoeller, M. (2013b). Stability of pulse-modulated systems with an application to space launchers. In *19th IFAC Symposium on Automatic Control in Aerospace, Würzburg, Germany.*

[Churilov and Gessen, 2003] Churilov, A. N. and Gessen, A. V. (2003). Lmi approach to stabilization of a linear plant by a pulse modulated signal. *Internation Journal of Hybrid Systems*, 3:375–388.

[Costic et al., 2001] Costic, B., Dawson, D., De Queiroz, M., and Kapila, V. (2001). Quaternion based adaptative attitude tracking controller without velocity measurements. *Journal of Guidance, Control and Dynamics*, 24(6):1214–1222.

[Doyle, 1982] Doyle, J. C. (1982). Analysis of feedback systems with structured uncertainties. *IEE Proceedings, D*, 129(6):242–250.

[Doyle, 1985] Doyle, J. C. (1985). Structured uncertainty in control system design. *Proceedings of the IEEE 24th Conference on Decision and Control*, 24:260–265.

[Doyle et al., 1982] Doyle, J. C., Wall, J., and Stein, C. (1982). Performance and robustness analysis for strucutred analysis. In *21st IEEE Conference on Decision and Control*.

[El Ghaoui et al., 1995] El Ghaoui, L., Palopoli, L., Nikoukhah, R., Delebecque, F., and Commeau, J.-L. (1995). Lmitool: a package for lmi optimization in scilab, user's guide. Technical report, UC Berkeley.

[Falcoz et al., 2010] Falcoz, A., Henry, D., and Zolghadri, A. (2010). Robust fault diagnosis for atmospheric reentry vehicles: A case study. *Systems, Man and Cybernetics, Part A: Systems and Humans, IEEE Transactions on*, 40(5):886–899.

[Fan et al., 1991] Fan, M., Tits, A., and Doyle, J. (1991). Robustness in the presence of mixed-parametric uncertainty and unmodeled dynamics. *IEEE Transactions on Automatic Control*, 36(1):25–38.

[Fridman et al., 2005] Fridman, E., Shaked, U., and Suplin, V. (2005). Input/output delay approach to robust sampled-data h infinity control. *Systems and Control Letters*, 54:271–282.

[Fujita et al., 1995] Fujita, M., Namerikawa, T., Matsumura, F., and Uchida, K. (1995). μ-synthesis of an electromagnetic suspension system. *Automatic Control, IEEE Transactions on*, 40(3):530–536.

[Gahinet et al., 1996] Gahinet, P., Apkarian, P., and Chilali, M. (1996). Parameter dependent lyapunov functions for real parametric uncertainties. *IEEE Transactions on Automatic Control*, 41(3):436–442.

[Gahinet and Nemirovskii, 1993] Gahinet, P. and Nemirovskii, A. (1993). Lmi lab: A package for manipulating and solving lmis. In *INRIA*.

[Gelig and Churilov, 1993] Gelig, A. and Churilov, A. (1993). Popov-type stability criterion for functional-differential equations describing pulse modulated control systems. *Functionnal Differential Equations*, 1:95–107.

[Gelig and Churilov, 1998] Gelig, A. C. and Churilov, A. N. (1998). *Stability and oscillations of nonlinear pulse-modulated systems*. Birkhäuser.

[Gelig and Elkhimova, 1995] Gelig, A. C. and Elkhimova, Y. (1995). Stability of nonlinear impulse systems under random perturbations of the parameters. *Automatice Remote Control*, 56(11):1620–1626.

[Gomes da Silva Jr. and Tarbouriech, 2005] Gomes da Silva Jr., J. and Tarbouriech, S. (2005). Antiwindup design with guaranteed regions of stability. *Automatic Control, IEEE Transactions on*, 50(1):106–111.

[Hanson and Beard, 2010] Hanson, J. and Beard, B. (2010). Applying monte carlo simulation to launch vehicle design and requirements analysis. Technical report, NASA.

[Hughes, 1986] Hughes, P. (1986). *Spacecraft Attitude Dynamics*. J. Wiley, New-York.

[Jang et al., 2008] Jang, J.-W., Van Tassel, C., Bedrossian, N., Hall, C., and Spanos, P. (2008). Evaluation of ares i control system robustness to uncertain aerodynamics and flex dynamics. In *AIAA GNC Conference*, number 6621.

[Jönsson, 1996] Jönsson, U. (1996). *Robustness analysis of uncertain and nonlinear systems*. PhD thesis, Lund Institute of Technology, Lund, Sweden.

[Jönsson, 2001] Jönsson, U. (2001). Lecture notes on integral quadratic constraints. Technical report, Division of Optimization and Systems theory, Department of Mathematics, Royal Institute of Technology, Stockholm, Sweden.

[Kao and Lincoln, 2004] Kao, C. Y. and Lincoln, B. (2004). Simple stability criteria for systems with time-varying delays. *Automatica*, 40(8):1429–1434.

[Kao et al., 2004] Kao, C.-Y., Megretski, A., J$\acute{}$onsson, U., and Rantzer, A. (2004). Iqc-β, a matlab toolbox for robustness analysis. In *IEEE Symposium on Computer Aided Control Systems Design*.

[Kao and Rantzer, 2007] Kao, C. Y. and Rantzer, A. (2007). Stability analysis of systems with uncertain time-varying systems. *Automatica*, 43(6):959–970.

[Khalil, 1996] Khalil, H. K. (1996). *Nonlinear systems*. Prentice Hall.

[Köroglu et al., 2008] Köroglu, H., Farhood, M., and Scherer, C. W. (2008). Lpvmad, the iqc analysis tool. Technical report, Delft University of Technology, The Netherlands.

[Köroglu and Scherer, 2006] Köroglu, H. and Scherer, C. W. (2006). Robust stability analysis against perturbations of smoothly time-varying parameters. In *Proceedings of IEEE Conference on Decision and Control*, pages 2895 – 2900, San Diego, CA.

[Köroglu and Scherer, 2007] Köroglu, H. and Scherer, C. W. (2007). Robust performance analysis for structured linear time-varying parturbations with bounded rates of variations. *IEEE Transactions on Automatic Control*, 52(2):197–211.

[Levant, 2010] Levant, A. (2010). Chattering analysis. *IEEE Transactions on Automatic Control*, 55(6):1380–1389.

[Liu et al., 2010] Liu, K., Suplin, V., and Fridman, E. (2010). Stability of linear systems with general sawtooth delay. *IMA Journal of Mathematical Control and Information*, 27(4):419–436.

[Löfberg, 2004] Löfberg, J. (2004). Yalmip : A toolbox for modeling and optimization in MATLAB. In *Proceedings of the CACSD Conference*, Taipei, Taiwan.

[Lyapunov, 1892] Lyapunov, A. M. (1892). *General problem of the stability of motion*. PhD thesis, University of Moscow.

[Megretski et al., 2000] Megretski, A., Kao, C. Y., J$\acute{}$onsson, and Rantzer, A. (2000). *A guide to IQC-β: Software for robustness analysis*.

[Megretski and Rantzer, 1995] Megretski, A. and Rantzer, A. (1995). System analysis via integral quadratic constraints, part i. Technical report ISRN LUTFD2/TFRT-7531-SE, Department of Automatic Control, Lund University, Sweden.

[Megretski and Rantzer, 1997] Megretski, A. and Rantzer, A. (1997). System analysis via integral quadratic constraints. *IEEE Transactions on Automatic Control*, 42(6):819–830.

[Mirkin, 2007] Mirkin, L. (2007). Some remarks on the use of time-varying delay to model sample-and-hold circuits. *IEEE Transactions on Automatic Control*, 52(6):1109–1112.

[Naghshtabrizi et al., 2008] Naghshtabrizi, P., Hespanha, J., and Teel, A. (2008). Exponential stability of impulsive systems with application to uncertain sample-data systems. *Systems and Control Letters*, 57(5):378–385.

[Nesterov and Nemirovskii, 1994] Nesterov, Y. and Nemirovskii, A. (1994). *Interior-point polynomial algorithms in convex programming*. Society for industrial and applied mathematics.

[Packard and Doyle, 1993] Packard, A. and Doyle, J. C. (1993). The complex structured singular value. *Automatica*, 29(1):71–109.

[Paganini, 1995] Paganini, F. (1995). Robust stability under mixed time-varying, taime-invariant and parametric uncertainties. Technical report, Control and Dynamical Systems, California Institute of Technology.

[Peaucelle et al., 2012] Peaucelle, D., Tarbouriech, S., Ganet-Schoeller, M., and Bennani, S. (2012). Evaluating regions of attraction of lti systems with saturations in iqs framework. In *7th IFAC Symposium on Robust Control Design, Aalborg, Denmark*.

[Pereira and Vettori, 2006] Pereira, R. and Vettori, P. (2006). Stability of quaternionic linear systems. *Automatic Control, IEEE Transactions on*, 51(3):518–523.

[Pittelkau, 2003] Pittelkau, M. (2003). Definitions, metrics, and algorithm for displacement, jitter and stability. In *AAS/AIAA Astrodynamics Specialists conference*, volume 116, pages 901–920.

[Rantzer, 1996] Rantzer, A. (1996). On the kalman-yakubovich-popov lemma. *Systems and Control Letters*, 28:7–10.

[Seuret and Gomes Da Silva Jr, 2011] Seuret, A. and Gomes Da Silva Jr, J. (2011). Networwed control: taking into account sample period variations and actuator saturation. In *18th IFAC World Congress*.

[Sidi, 1997] Sidi, M. J. (1997). *Spacecraft dynamics and control*. Cambridge university press.

[Sturm, 1999] Sturm, J. (1999). Using sedumi 1.02, a matlab toolbox for optimization over symmetric cones. *Optimization Methods and Software*, 11:625–653.

[Summers et al., 2013] Summers, E., Arcak, M., and Packard, A. (2013). Delay robustness of interconnected passive systems: an integral quadratic constraint approach. *IEEE Transactions on Automatic Control*, 58(3):712–724.

[Tarbouriech and Gomes Da Silva Jr, 2000] Tarbouriech, S. and Gomes Da Silva Jr, J. (2000). Synthesis of controllers for continuous-time delay systems with saturating controls via lmiï¿œs. *IEEE Transactions on Automatic Control*, 45(1):105–111.

[Toh et al., 1999] Toh, K., Todd, M., and Tutuncu, R. (1999). Sdpt3 a matlab software package for semidefinite programming. *Optimization Methods and Software*, 11:545–581.

[Vandenberghe et al., 1998] Vandenberghe, L., Boyd, S., and Wu, S. (1998). Determinant maximization with linear matrix equality constraints. *SIAM Journal on Matrix Analysis and Applications*, 25(2):449–533.

[Wen and Kreutz-Delgado, 1991] Wen, J.-Y. and Kreutz-Delgado, K. (1991). The attitude control problem. *IEEE Transactions on Automatic Control*, 36(10):1148–1162.

[Willems, 1971] Willems, J. (1971). Dissipative dynamical systems, part i: General theory; part ii: Linear systems with quadratic supply rates. *Archive for Rational Mechanics and Analysis*, 45(5):321–393.

[Yakubovich, 1967] Yakubovich, V. (1967). Frequency conditions for the absolute stability of control systems with several nonlinear and linear non stationnary units. *Automation and Remote Control*, 28(6):857–880.

[Yakubovich, 1971] Yakubovich, V. (1971). S-procedure in nonlinear control theory. *Vestnik Leningrad University Mathematics*, 28:62–77.

[Yakubovich, 1982] Yakubovich, V. (1982). On an abstract theory of absolute stability of nonlinear systems. *Vestnik Leningrad University Mathematics*, 10:341–361.

[Zames, 1966] Zames, G. (1966). On the input-output stability of time-varying nonlinear feedback systems, parts i and ii. *IEEE Transactions on Automatic Control*, AC-11:228 and 465.

[Zames and Falb, 1968] Zames, G. and Falb, P. (1968). Stability conditions for systems with monotone and slope-restricted nonlinearities. *SIAM Journal on Control*, 6(1):89–108.

Résumé

Cette thèse considère l'analyse de stabilité robuste et de performance robuste de différents modèles de lanceurs spatiaux en phase balistique. Dans le contexte économique actuel, il est nécessaire d'accroître l'efficacité et de réduire les coûts de la phase de validation des lois de commande d'attitude des lanceurs. Pour cela, les méthodes analytiques d'étude de la robustesse semblent appropriées en proposant des résultats rigoureux ainsi que des garanties formelles sur les marges de stabilité et les niveaux de performance. En particulier, les méthodes fondées sur les contraintes intégrales quadratiques (IQC) ont prouvé leur capacité à compléter les résultats probabilistes obtenus par les méthodes de validation actuelles. Ainsi, la première étude de cette thèse propose une factorisation des équations du mouvement pour un solide rigide en rotation permettant de mettre en œuvre une analyse de robustesse par IQC sur un modèle dynamique représentatif. Dans un second temps, la principale contribution de cette thèse porte sur l'étude des systèmes régulés via un modulateur d'impulsion de type PWM (*pulse-width modulator*). Deux méthodes a priori différentes utilisant une représentation IQC de certains sous-systèmes du modèle conduisent à l'estimation du domaine de stabilité d'un modèle de lanceur pourvu d'actionneurs de type PWM.

Mots-clés : aérospatiale, phase balistique, analyse, robustesse, équation de la dynamique, modulateur de largeur d'impulsions, contraintes intégrales quadratiques.

Abstract

This thesis investigates stability and performance analysis of space launcher models. In the current context, the need for cost reduction and efficiency improvement of the verification and validation (V&V) industrial process leads toward the use of analytical techniques providing rigorous robustness guarantees. V&V tools based on Integral Quadratic Constraints (IQC) shall complement the stability and performance certificates yielded by the existing time-domain stochastic methods. The first study investigates the effect of the uncertain nonlinear equation for the rotating motion of a rigid launcher on the robust stability and robust performance of a representative three dimensional model. IQC are used to estimate the stability domain using a factorization of the equation of motion troublesome terms. The second contribution of this thesis addresses the stability analysis of pulse-modulated systems. Two a priori distinct IQC-based methods are implemented to obtain mathematical certificates on the stability of a space launcher model with a pulse-modulator used as a representative actuator.

Keywords: aerospace, ballistic phase, robustness, analysis, equation of motion, pulse-width modulator (PWM), integral quadratic constraints (IQC).